



The University of  
**Nottingham**

UNITED KINGDOM • CHINA • MALAYSIA

Al-Mosawe, Hasan (2016) Prediction of permanent deformation in asphalt mixtures. PhD thesis, University of Nottingham.

**Access from the University of Nottingham repository:**

<http://eprints.nottingham.ac.uk/38642/1/Al-Mosawe%2C%20Hasan%20PhD%20Thesis.pdf>

**Copyright and reuse:**

The Nottingham ePrints service makes this work by researchers of the University of Nottingham available open access under the following conditions.

This article is made available under the University of Nottingham End User licence and may be reused according to the conditions of the licence. For more details see:  
[http://eprints.nottingham.ac.uk/end\\_user\\_agreement.pdf](http://eprints.nottingham.ac.uk/end_user_agreement.pdf)

For more information, please contact [eprints@nottingham.ac.uk](mailto:eprints@nottingham.ac.uk)



The University of  
**Nottingham**

UNITED KINGDOM • CHINA • MALAYSIA

**PREDICTION OF  
PERMANENT DEFORMATION  
IN ASPHALT MIXTURES**

By

**Hasan Al-Mosawe**

Thesis submitted to the University of Nottingham

for the degree of Doctor of Philosophy

Department of Civil Engineering

**November 2016**

# ABSTRACT

An asphalt mixture is combined of different sizes of aggregate, filler, and bitumen for application on the most common road construction materials. In asphalt pavement material there are different types of distress such as permanent deformation (rutting), fatigue cracking, ravelling, potholes, stripping, etc. There are many reasons for these types of distress, some of them related to the pavement structure, e.g. whether the underlying layers are weak, others related to the mixture properties. Other causes could be related to external conditions such as high temperature, high axle load, long duration of load application, etc. This research has focused on the permanent deformation (rutting) as a function of aggregate gradation.

The aggregate gradations of more than twenty asphalt mixtures, manufactured with different gradations, were analysed by using the Bailey method of gradation analysis. The analysis was performed in relation to Repeated Load Axial Test (RLAT) testing results to study the performance of each mixture. The results showed that the Bailey method is not capable on its own to define the differences between the gradations of each mixture. Therefore, three more packing ratios were introduced to adequately describe the aggregate gradation. The aggregate particle

packing was extensively studied through these packing ratios and it was shown how the different particle sizes interact with each other. Images were taken for two mixtures to validate the theory behind the ratios. The five packing ratios (two of Bailey and three new ratios) were used in Artificial Neural Network (ANN) and Adaptive Neuro-Fuzzy Inference System (ANFIS) techniques for all the mixtures as input data to predict the mixture performance (RLAT permanent deformation and Indirect Tensile Stiffness Modulus ITSM stiffness modulus) and they showed good prediction capability.

After establishing the impact of aggregate packing on the performance, six mixtures were re-manufactured and re-tested with different variables; the selection of the mixtures was made to cover a range of different gradations (ratios). The aim of this step was to understand the effect of these variables on the asphalt mixture in the light of the packing ratios. The variables that were used were binder content, testing temperature and compaction effort. The binder content results showed an interesting effect on the permanent deformation and stiffness of the asphalt mixture. The packing of aggregate was very helpful in understanding the different mixture behaviour with different binder content. The effect of aggregate packing was not shown at relatively low testing temperature, but as the temperature rises the aggregate packing effect starts to appear. The effect of compaction which was represented by the number of gyrations in gyratory compactor was inconsistent; results show over-compaction can lead to poor performance.

Finally, a linear viscous method was introduced aiming to predict the rutting in an asphalt mixture. The method was based on using a multilayer linear pro-

gramme (BISAR) and using viscous parameters of the mixture as input. The non-linear properties of the material were incorporated by using the RLAT test. For this purpose, six mixtures were used and tested in a wheel tracking machine. The predicted results were compared with the wheel tracking rut depth in the laboratory and showed good agreement at different temperatures. However, at high temperature (50 °C) the material properties in the RLAT test did not behave as linear viscous, which resulted in a much poorer prediction. Trials were made to predict field rut but it was found that special requirements were needed for the approach which were not available at the time of the research. However, for the available field data, the method was found to be a good predictor.

# PUBLICATIONS

- Al-Mosawe, Hasan, Thom, Nick, Airey, Gordon, and Albayati, Amjad 2015.  
*Effect of Aggregate Gradation on the Stiffness of Asphalt Mixtures*, in the 14<sup>th</sup> Asphalt, Pavement Engineering and Infrastructure Conference, 11-12 February 2015, Liverpool, UK.
- Al-Mosawe, Hasan, Thom, Nick, Airey, Gordon, and Albayati, Amjad 2015.  
*Effect of Aggregate Gradation on the Stiffness of Asphalt Mixtures*. in the International Journal on Pavement Engineering & Asphalt Technology 16.2 pp. 39-49.
- Al-Mosawe, Hasan, Thom, Nick, Airey, Gordon, and Albayati, Amjad 2016.  
*Predicting Asphalt Mechanical Properties as a Function of Aggregate Packing*. in Transportation Research Board 95th Annual Meeting. No. 16-2225. 2016.
- Al-Mosawe, Hasan, Thom, Nick, Airey, Gordon, and Albayati, Amjad 2016.  
*Effect of different variables on asphalt mechanical properties* presented and published in the 4th International Chinese European Workshop (CEW), Delft University of Technology, Netherlands, from 29th June to 1st of July 2016 Proceeding.

- Al-Mosawe, Hasan, Thom, Nick, Airey, Gordon, and Albayati, Amjad 2016. *Predicting Mechanical Properties of Asphalt Mixtures Based on Aggregate Packing using Soft Computing Techniques* is submitted and is UNDER REVIEW in the Journal of Materials and Design.
- Al-Mosawe, Hasan, Thom, Nick, Airey, Gordon, and Albayati, Amjad 2016. *Linear Viscous Approach to Predict Rut Depth in Asphalt Mixtures* is submitted and is UNDER REVIEW in the Construction and Building Materials.

# ACKNOWLEDGEMENTS

The author would like to acknowledge some people and organisations without whose contributions this thesis would not have been possible. Firstly, I would like to express my sincere thanks to my first supervisor Dr Nick Thom for his guidance and suggestions for this research. He is a person that I learnt a lot from, not only in research; I am very grateful to him. I would also like to thank my second supervisor Prof. Gordon Airey for his help and support throughout the research. Dr Amjad Albayati, who was acting as a third supervisor, has always provided me with knowledge and encouragement.

Special thanks are due to the University of Baghdad / Ministry of Higher Education in Iraq who sponsored the research and funded me for the study period, and to AECOM (especially Dr Iswandaru Widyatmoko) for providing the field data.

Warm hearted thanks go to my parents, brothers and sister for their encouragements and kindness, and I ask God to bless them all. My thanks to the researchers and the team of the technicians at NTEC who were very helpful and friendly in my laboratory work: Jon Watson, Richard, Lawrence and Martyn.

Big thanks also go to my friends and their families in Nottingham who made



staying in Nottingham enjoyable especially: Dr Mohammed Alasadi, Saad Alatrany, Ashraf Al-Hadethe, Ammar Alatta and Mohammed Al-Najjar.

Finally, but most importantly, I owe a debt of thanks to my wife Zena for her patience and help.

# DECLARATION

This is to declare that the contents of this thesis are my own work and were performed at the University of Nottingham from 2013 to 2016. This thesis has not been submitted to any other institution for another degree.

Hasan Al-Mosawe

Nottingham, November 2016

Email: [evxhmal@nottingham.ac.uk](mailto:evxhmal@nottingham.ac.uk), [almosawe88@gmail.com](mailto:almosawe88@gmail.com)

# DECLARATION

We declare that the contents and the work described in this thesis were performed at the University of Nottingham, Faculty of Engineering from June 2013 to November 2016 under our supervision.

**Nick Thom**

**Assistant Professor**

**Faculty of Engineering**

**Email: [nicholas.thom@nottingham.ac.uk](mailto:nicholas.thom@nottingham.ac.uk)**

**November, 2016**

**Gordon Airey**

**Professor**

**Faculty of Engineering**

**Email: [gordon.airey@nottingham.ac.uk](mailto:gordon.airey@nottingham.ac.uk)**

**November, 2016**

# Contents

<b>ABSTRACT</b>	<b>i</b>
<b>PUBLICATIONS</b>	<b>iv</b>
<b>ACKNOWLEDGEMENTS</b>	<b>vi</b>
<b>List of Figures</b>	<b>xvii</b>
<b>List of Tables</b>	<b>xxiii</b>
<b>1 Introduction</b>	<b>1</b>
1.1 Background . . . . .	1
1.2 Problem Statement . . . . .	4
1.3 Why Aggregate Gradings? . . . . .	7
1.4 Aims and Objectives . . . . .	8
1.5 Thesis Organisation . . . . .	10
1.6 Research Implications . . . . .	11
<b>2 Permanent Deformation in Asphalt Mixtures</b>	<b>13</b>
2.1 Introduction . . . . .	13

2.2	Performance Evaluation . . . . .	14
2.2.1	Binder Behaviour . . . . .	14
2.2.2	Aggregate Behaviour . . . . .	17
2.2.3	Asphalt Mixture Behaviour . . . . .	19
	Resistance to Permanent Deformation . . . . .	21
	Aggregate Gradings . . . . .	25
	Volumetric Properties . . . . .	26
	Compaction Methods . . . . .	27
2.3	Laboratory Tests for Measuring Permanent Deformation . . . . .	28
2.3.1	Static Uniaxial and Triaxial Test . . . . .	29
2.3.2	Cyclic uniaxial and triaxial test . . . . .	30
2.3.3	Wheel Tracking Test . . . . .	32
2.4	Packing of Aggregate . . . . .	33
2.4.1	Theory of Packing in Particles . . . . .	35
2.4.2	Aggregate Gradation . . . . .	38
	Coarse vs Fine Aggregate . . . . .	41
2.4.3	Bailey Method of Gradation Analysis and Asphalt Mix Design	42
	Control Sieves . . . . .	43
	Evaluation Ratios . . . . .	45
2.4.4	Dominant Aggregate Size Range (DASR) . . . . .	48
2.5	Prediction of Permanent Deformation . . . . .	52
2.5.1	Elastic Model . . . . .	52
	Layer-Strain Approach . . . . .	54

2.5.2	Viscoelastic Methodology . . . . .	58
	Applications to Viscoelastic Models . . . . .	60
2.5.3	Comparison of Layer-Strain and Viscoelastic Methodologies	63
2.5.4	Linear Viscous Approach . . . . .	64
2.6	Summary and Research Needs . . . . .	65
<b>3</b>	<b>Soft Computing Techniques</b>	<b>68</b>
3.1	Introduction . . . . .	68
3.2	Artificial Neural Network (ANN) . . . . .	69
3.2.1	Applications of ANN in Pavement Field . . . . .	70
3.3	Adaptive Neuro-Fuzzy Inference System (ANFIS) . . . . .	74
3.3.1	Fuzzy Logic System . . . . .	74
	Concept . . . . .	74
3.3.2	ANFIS . . . . .	77
	Applications of ANFIS in the Pavement Field . . . . .	80
<b>4</b>	<b>Effect of Aggregate Packing on Permanent Deformation</b>	<b>82</b>
4.1	Introduction . . . . .	82
4.2	Material Selection . . . . .	83
4.2.1	Bitumen . . . . .	83
4.2.2	Aggregate . . . . .	84
4.2.3	Volumetric Properties . . . . .	86
4.3	Repeated Load Axial Test (RLAT) . . . . .	88
4.4	Bailey Method . . . . .	90

4.4.1	Control Sieves and Evaluation Ratios . . . . .	90
4.4.2	Limitations to Bailey Ratios . . . . .	91
4.4.3	New Ratios . . . . .	92
4.5	Image Analysis . . . . .	95
4.5.1	Image Processing . . . . .	95
4.6	Prediction Modelling . . . . .	98
4.6.1	Linear Regression Model . . . . .	99
4.6.2	Artificial Neural Network (ANN) . . . . .	103
	Construction of ANN Model . . . . .	103
	ANN Model Results and Discussion . . . . .	107
	Sensitivity Analysis . . . . .	109
4.6.3	Adaptive Neuro-Fuzzy Inference System (ANFIS) . . . . .	110
	Construction of ANFIS Model . . . . .	110
	ANFIS Results and Discussion . . . . .	112
4.7	Conclusions . . . . .	115
<b>5</b>	<b>Effect of Different Variables on Mechanical Properties of Asphalt</b>	
	<b>Mixtures</b>	<b>118</b>
5.1	Introduction . . . . .	118
5.2	Effect of Aggregate Packing on Stiffness Modulus . . . . .	119
5.2.1	Prediction of Stiffness . . . . .	120
	Regression Analysis . . . . .	121
	Artificial Neural Network ANN . . . . .	123

5.3	Material Selection and Testing . . . . .	126
5.3.1	Testing . . . . .	127
5.4	Binder Content . . . . .	128
5.5	Temperature . . . . .	133
5.6	Compaction Effort . . . . .	134
5.7	Prediction Modelling for Different Variables . . . . .	137
5.7.1	Artificial Neural Network ANN . . . . .	138
	Sensitivity Analysis . . . . .	140
5.7.2	Adaptive Neuro-Fuzzy Inference System ANFIS . . . . .	144
5.8	Conclusions . . . . .	147
<b>6</b>	<b>Rut Depth Prediction</b>	<b>151</b>
6.1	Introduction . . . . .	151
6.2	Formulation of Theoretical Model . . . . .	152
6.3	Material and Testing Programme . . . . .	154
6.3.1	Material . . . . .	154
6.3.2	Testing Programme . . . . .	154
	Wheel Tracking Test . . . . .	154
	Repeated Load Axial Test (RLAT) . . . . .	155
6.4	Methodology . . . . .	157
6.5	Analysis of Results . . . . .	163
6.5.1	Temperature . . . . .	164
	Prediction at 30 °C . . . . .	165



Prediction at 50 °C . . . . .	167
6.6 Field Rut Depth Prediction . . . . .	177
6.6.1 Data Collection . . . . .	177
6.6.2 Use of Field Data . . . . .	177
6.6.3 Prediction Results and Discussion . . . . .	179
6.6.4 Limitations and Specific Data Required . . . . .	182
6.7 Conclusions . . . . .	183
<b>7 Conclusions and Recommendations</b>	<b>186</b>
7.1 Introduction . . . . .	186
7.2 Conclusions . . . . .	187
7.2.1 Aggregate Packing . . . . .	187
7.2.2 Rut Depth Prediction . . . . .	189
7.3 Recommendations for Future Work . . . . .	190
<b>References</b>	<b>194</b>
<b>Appendices</b>	<b>213</b>
<b>A Matlab Code for ANN</b>	<b>214</b>
<b>B Weights and Biases for ANN and ANFIS</b>	<b>218</b>
B.1 ANN . . . . .	218
B.2 ANFIS . . . . .	224

Source codes, Functions and System files for All Packing Ra-  
tios Model . . . . . 224

# List of Figures

1.1	Schematic Diagram showing Telford and McAdam Different Construction Practices (Read, 1996) . . . . .	2
1.2	Change in Pavement Layer Thickness during Centuries (Pavement Interactive, 2008) . . . . .	2
1.3	A Typical Flexible Pavement . . . . .	3
1.4	Rutting in road pavements [Google Images] . . . . .	5
1.5	Hydroplaning problems in road pavements [Google Images] . . . . .	6
2.1	Van der Poel Nomograph . . . . .	16
2.2	Behaviour of Shear Loading in Aggregate, Asphalt Institute (1996)	17
2.3	Aggregate Stone Skeleton, Asphalt Institute (1996) . . . . .	18
2.4	Structural and Non-Structural Rutting, Gibb (1996) . . . . .	20
2.5	Accumulation of Permanent Deformation under Repeated Wheel Loading, Taherkhani (2006) . . . . .	21
2.6	Stresses induced in a Pavement due to a Moving Load (Mallick and El-Korchi, 2013) . . . . .	22

2.7	Typical Strain Results from Creep Testing (Mallick and El-Korchi, 2013) where $\varepsilon_T$ : Total strain; $\varepsilon_e$ : Elastic Strain; $\varepsilon_p$ : Plastic strain; $\varepsilon_{ve}$ : Viscoelastic Strain; $\varepsilon_{vp}$ : Viscoplastic Strain. . . . .	30
2.8	Sample Setting in Uniaxial Cyclic Test . . . . .	31
2.9	Typical Repeated Axial Load Test Result . . . . .	32
2.10	Wheeltracking Apparatus (Gibb, 1996) . . . . .	33
2.11	Densest Arrangement of spherical particles, Yideti (2014) . . . . .	36
2.12	Types of layers. A) Square layer; B) Rhombic layer (Lira Miranda, 2012) . . . . .	36
2.13	Top and Panoramic view of regular packing arrangements. A) Simple cubical, B) Hexagonal loose, C) Face-centred cubical, D) Orthorhombic, E) Tetragonal, F) Hexagonal close. . . . .	37
2.14	Average Void size Calculation . . . . .	39
2.15	Schematic Diagram of Control Sieves, Vavrik (2000) . . . . .	45
2.16	Dominant Aggregates and Interstitial Volume, Kim (2006) . . . . .	49
2.17	Local Disruption to DASR . . . . .	50
2.18	Disruption Factor Representation, Guarin (2009) . . . . .	51
2.19	Maxwell Model and its Behaviour, Rabbira (2002) . . . . .	59
2.20	Kelvin Model and its Behaviour, Rabbira (2002) . . . . .	59
2.21	Burger's Model, Antes et al. (2003) . . . . .	60
2.22	Schematic Response of Different Mechanical Models and Real Behaviour, Taherkhani (2006) . . . . .	61

3.1	An Artificial Neuron . . . . .	69
3.2	Predicted vs experimental results of Flow number ( $F_n$ ) (Mirzahosseini et al., 2013) . . . . .	73
3.3	Representation of a crisp (classical) set (Selvi, 2009) . . . . .	74
3.4	Representation of a fuzzy set (Selvi, 2009) . . . . .	75
3.5	Example of Membership Function Forms . . . . .	75
3.6	Schematic diagram of fuzzy inference system . . . . .	76
3.7	Adaptive Neuro-Fuzzy Inference System (ANFIS) (Jang, 1993) . . . . .	79
4.1	Aggregate Gradations for the Thirteen Mixtures . . . . .	85
4.2	Number of Gyration vs Densities for different mixtures . . . . .	86
4.3	Air Voids of the 13 different asphalt mixtures . . . . .	87
4.4	VMA of the 13 different asphalt mixtures . . . . .	87
4.5	The three Stages of RLAT Test . . . . .	89
4.6	Accumulated Permanent Strain resulted from RLAT . . . . .	90
4.7	Determination of the Packing Ratios . . . . .	94
4.8	The Steps of Image Processing . . . . .	96
4.9	Difference between the aggregate structure of the two mixes . . . . .	98
4.10	Regression Prediction Model . . . . .	101
4.11	Predicted Strains for the large data set . . . . .	102
4.12	Differences in Residuals of the Predicted strains . . . . .	103
4.13	Structure of ANN . . . . .	104
4.14	Processing of Backpropagation Algorithm . . . . .	106

4.15	ANN Prediction Results . . . . .	108
4.16	Structure of ANFIS . . . . .	112
4.17	Membership function of $C_f/E_c$ . . . . .	112
4.18	ANFIS Prediction Results . . . . .	114
4.19	Relationship Surface between the Inputs and Output . . . . .	115
5.1	Effect of Density on the Stiffness . . . . .	120
5.2	Measured and predicted stiffness for Brown's model . . . . .	121
5.3	Measured and Predicted Stiffness for Aggregate Packing Regression Model . . . . .	123
5.4	ANN Prediction Results of ITSM Stiffness based on the Aggregate Packing Ratio . . . . .	125
5.5	Aggregate gradation of the Six Mixtures . . . . .	127
5.6	Effect of Binder Content on Density . . . . .	129
5.7	Effect of Binder Content on Permanent Strain; NOTE: Numbers shown in figure are the number of cycles reached at 8% strain . . . .	130
5.8	Effect of Binder Content on Stiffness . . . . .	132
5.9	Effect of Temperature on Permanent Strain, (NOTE: Numbers shown in the figure are the number of cycles reached to the corresponding strain.) . . . . .	134
5.10	Effect of Number of Gyration on %Air Voids . . . . .	135
5.11	Effect of the Number of Gyration on Performance of Asphalt Mixtures	137
5.12	Different Variables ANN Prediction Results of RLAT Strain . . . . .	139

5.13	Results of the ANN Prediction Model for ITSM Stiffness . . . . .	141
5.14	ANN Sensitivity Model for Packing Ratios, Binder Content, and Testing Temperature . . . . .	143
5.15	ANN Sensitivity Model for Packing Ratios, Binder Content, and Compaction Effort . . . . .	143
5.16	ANN Sensitivity Model for Packing Ratios, Testing Temperature, and Compaction Effort . . . . .	144
5.17	Results of the ANFIS Prediction Model for RLAT Strain . . . . .	146
6.1	Aggregate Gradations for Asphalt Mixtures . . . . .	155
6.2	Wheel Tracking Machine . . . . .	156
6.3	RLAT Testing Machine . . . . .	157
6.4	Schematic diagram of slab coring (dimensions in mm) . . . . .	158
6.5	Typical Plot of Viscosity vs Strain for an asphalt mixture . . . . .	159
6.6	Slab Model Layers divided in BISAR . . . . .	160
6.7	Methodology Flow Chart . . . . .	162
6.8	(a) Viscosity-Strain Curve. (b) Rut Depth Prediction. For Mix 1 . .	164
6.9	(a) Viscosity-Strain Curve. (b) Rut Depth Prediction. For Mix 3 . .	165
6.10	(a) Viscosity-Strain Curve. (b) Rut Depth Prediction. For Mix 5 . .	166
6.11	(a) Viscosity-Strain Curve. (b) Rut Depth Prediction. For Mix 7 . .	167
6.12	(a) Viscosity-Strain Curve. (b) Rut Depth Prediction. For Mix 10 .	168
6.13	(a) Viscosity-Strain Curve. (b) Rut Depth Prediction. For Mix 13 .	169

6.14 (a) Viscosity-Strain Curve. (b) Rut Depth Prediction. For Mix 1 at 30 °C . . . . .	170
6.15 (a) Viscosity-Strain Curve. (b) Rut Depth Prediction. For Mix 3 at 30 °C . . . . .	171
6.16 (a) Viscosity-Strain Curve. (b) Rut Depth Prediction. For Mix 5 at 30 °C . . . . .	172
6.17 (a) Viscosity-Strain Curve. (b) Rut Depth Prediction. For Mix 7 at 30 °C . . . . .	173
6.18 (a) Viscosity-Strain Curve. (b) Rut Depth Prediction. For Mix 10 at 30 °C . . . . .	174
6.19 (a) Viscosity-Strain Curve. (b) Rut Depth Prediction. For Mix 13 at 30 °C . . . . .	175
6.20 (a) Viscosity-Strain Curve. (b) Rut Depth Prediction. For Mix 13 at 50 °C . . . . .	176
6.21 Shifting RLAT data to 40 °C . . . . .	179
6.22 Viscosity-Strain curve of Core 4 in Field . . . . .	180
6.23 Field Prediction Results . . . . .	182



# List of Tables

2.1	Factors affecting Permanent Deformation in Asphalt Mixtures, Sousa et al. (1991) . . . . .	24
2.2	Standard Sieve sizes and Associated Primary Control Sieves, Vavrik (2000) . . . . .	44
4.1	Particle Densities of Bardon Hill Aggregate . . . . .	84
4.2	Bailey Ratios for the 13 Mixtures . . . . .	91
4.3	The New Ratios for each Mixture . . . . .	94
4.4	Round one of Multicollinearity Analysis in Minitab 17 . . . . .	100
4.5	Round three of Multicollinearity Analysis in Minitab 17 . . . . .	100
4.6	Performance of ANN Model . . . . .	107
4.7	ANN Sensitivity Analysis . . . . .	110
4.8	Performance of ANFIS Model . . . . .	113
5.1	Performance of Brown's and Packing Ratios Stiffness Models . . . . .	122
5.2	Performance of the ANN Stiffness Model . . . . .	124
5.3	Packing Ratios for each Mixture . . . . .	128
5.4	Performance of ANN Model for the Different Variables . . . . .	140

5.5	ANN Sensitivity Analysis for the Different Variables . . . . .	142
5.6	Performance of Permanent Strain ANFIS Model for the Different Variables . . . . .	145
5.7	Brief Summary of the Different Variables Results . . . . .	150
B.1	Strain ANN Weights for Packing Ratios Model . . . . .	219
B.2	Strain ANN Biases for Packing Ratios model . . . . .	220
B.3	Strain ANN Weights for Packing Ratios and Different Variables Model	221
B.4	Strain ANN Biases for Packing Ratios and Different Variables Model	222
B.5	Stiffness ANN Weights for Packing Ratios and Different Variables Model . . . . .	223
B.6	Stiffness ANN Biases for Packing Ratios and Different Variables Model	224

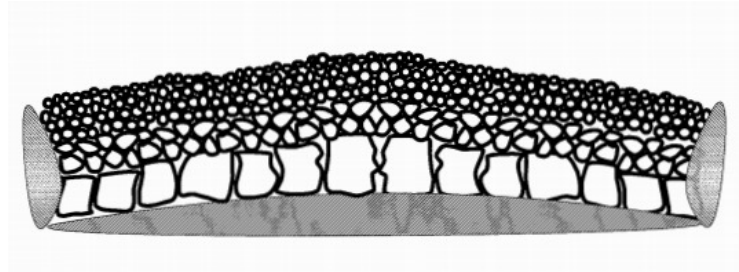
# Chapter 1

## Introduction

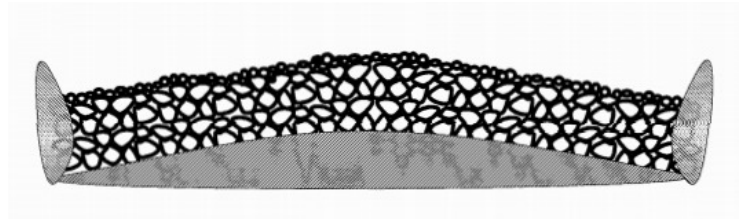
### 1.1 Background

It is essential to provide an efficient transport system for economic and quality-of-life reasons. Roads are one of the important elements of the transportation system. Early roads were made for wagons; therefore, most were not well paved and had an inadequate drainage system. In the 18<sup>th</sup> century further developments in constructing roads were made in France by Tresaguet and in the UK by Thomas Telford (1757-1834) and John Loudon McAdam (1756-1836) (Figure 1.1) in response to the increase in traffic volume and weight (Read, 1996). Telford focused on providing a solid base to the pavement while McAdam emphasized the provision of thinner pavement layers by using small angular material (Croney and Croney, 1991). Figure 1.2 shows the change in pavement layer thickness during the different centuries (Pavement Interactive, 2008).

At the end of the 19<sup>th</sup> century asphaltic materials became more popular when



(a) Telford's



(b) McAdam's

Figure 1.1: Schematic Diagram showing Telford and McAdam Different Construction Practices (Read, 1996)

more vehicles were used on the road, and dust free roads were required (Taherkhani, 2006). Tar was used in the beginning, but later bitumen refined from petroleum became most commonly used in pavement field.

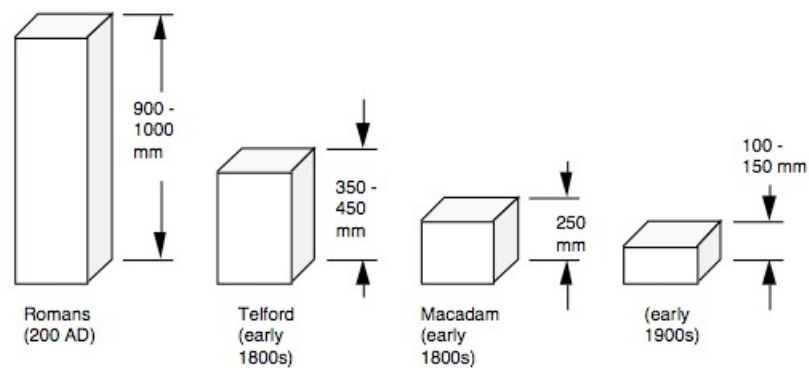


Figure 1.2: Change in Pavement Layer Thickness during Centuries (Pavement Interactive, 2008)

In general, roads are built to carry traffic safely and economically throughout their design life. The structure of a road pavement comprises a number of layers

to provide a dry, skid resistant, stiff and even surface for vehicles. There are three types of pavement depending on the material used to construct it: flexible pavement, rigid pavement, and composite. A flexible pavement is composed of asphaltic materials while a rigid pavement includes a concrete slab; a composite is a combination of both types. A typical flexible pavement is shown in Figure 1.3, where individual asphalt layers are named surface course, binder course, and base coarse (Read, 1996).

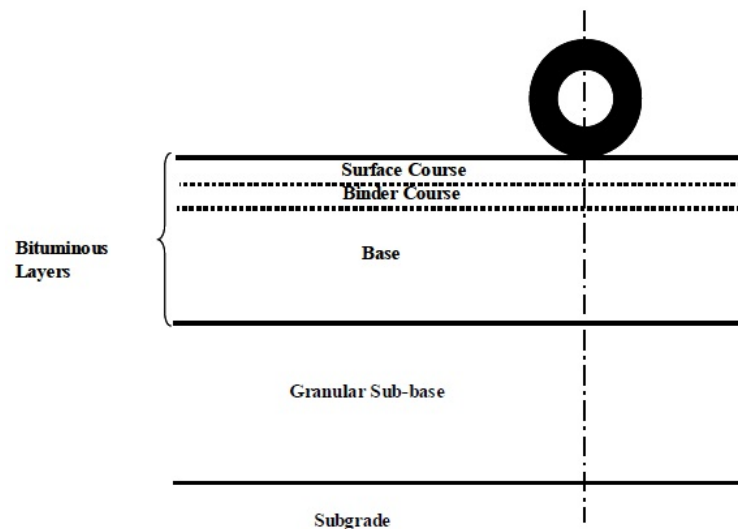


Figure 1.3: A Typical Flexible Pavement (Taherkhani, 2006)

### Surface Course

The duty of the surface course is to give a protected and smooth surface for vehicles with sufficient skid resistance. It additionally shields the sub-layers from the entrance of water. Skid resistance relies upon the microtexture and macrotexture of the surface layer. This layer is designed to be resistant to permanent deformation

and fatigue cracking.

### **Binder Course**

The binder course provides a level laying substrate to the surface course layer and ensures that the traffic loads are distributed to the sub-layers. It is also designed to resist permanent deformation and fatigue cracking caused by traffic load.

### **Base Layer**

This layer is considered as the main structural layer, and it prevents the sub-layer from being overstressed. The layer should also be designed to resist permanent deformation and fatigue cracking. It provides the pavement a protection from moisture and it provides stable construction platform

### **Sub-Base**

This is composed of granular material only and is part of the road foundation. The layer is well compacted to distribute the traffic load to the subgrade and to give a foundation on which to construct the asphaltic layers. This layer is also used to provide a drainage system to prevent excessive water from reaching the subgrade.

## **1.2 Problem Statement**

An asphalt pavement has the function of carrying traffic safely, smoothly, and economically between locations. However, there are certain factors that can negatively

affect the performance of asphalt such as construction quality control, traffic and environment, and material properties. These factors can cause a reduction to the pavement's original smoothness and serviceability, which leads to either failure or severe damage. The two primary forms of failure caused by the load applied to a flexible pavement are cracking and rutting. Rutting is defined as a longitudinal depression in the wheel path (as shown in Figure 1.4), with or without transverse displacement. It prevents the drainage of water to the sides of the road making it accumulate in the ruts which increases the possibility of accidents related to hydroplaning (as shown in Figure 1.5). A 0.5 in. (12.5 mm) rut depth is considered by Mallick and El-Korchi (2013) as rutting failure, although, this value is dependent on the type of road and design speed. Therefore, each country or specifications may have their own judgement, not following to a specific failure value.



Figure 1.4: Rutting in road pavements [Google Images]



Figure 1.5: Hydroplaning problems in road pavements [Google Images]

In addition, deep rutting causes difficulties in steering for vehicles. This may cause loss of car control which then leads to an accident (Khanzada, 2000). In hot countries, asphalt pavements can rut after about one year following construction due to high temperature (e.g. pavement temperature over  $50\text{ C }^{\circ}$ ) and heavy axle loads.

One of the main factors that affects rutting is aggregate gradation. There is a lack of knowledge on how aggregate gradation affects the rutting of asphalt mixtures and how a change in the gradation will cause a change in the performance of the asphalt mixture.



### 1.3 Why Aggregate Gradings?

As Aggregate gradations are strongly affecting the performance of the asphalt mixture, specifications allow some limits for the gradations. These limits are based on either field experience or from the behaviour achieved from laboratory testing. Each layer in the pavement has gradation limits and it depends on the performance required for that layer. The limits are found because it is not possible to force the contractor to develop an asphalt mixture with exact particle distribution in the field to achieve a particular behaviour.

In practice, the contractors use these limits to design their mixtures with, therefore there are indefinite possibilities of aggregate gradations within specification limits. Gradations that lie beyond lower limit will have high amount of coarse particles and low amount of fine particles and this will lead to segregation and difficulties in mixing, aggregate surface coating, and compaction. Gradations that lie above the upper limit will have high amount of fine material and low amount of coarse particles and this will require high amount of binder content which results in poor performance. It is beneficial to have these gradation limits to allow flexibility in designing the mixture, however, not any combination of aggregate size particles resulting in good behaviour. Contractors usually success in designing the mixture according to the specifications but it is noticed that some roads gain permanent deformation (rutting) after a short period of construction. After the evaluation of the asphalt mixture, it is usually found that the contractor followed the specifications required; therefore, they recommend to resurface the road.

In the same manner, Superpave specification introduced areas in the gradation limits that are recommended not to pass the gradation curve through it. There are a plenty amount of research showed that there is no negative effect of passing the restricted zone. Sánchez-Leal (2007) studied the effect of aggregate gradation and suggested that the gradation limits make no sense, and developed gradation charts for designing asphalt mixtures. All these limitations can lead to the fact that the use of aggregate gradation limits are controversy.

## 1.4 Aims and Objectives

The aim of this research is to extend the understanding of the effect of aggregate gradation on asphalt mixture performance and to predict the permanent deformation caused by repeated load in laboratory test. The analysis is based on the aggregate gradation as the main variable and other variables will also be discovered. The research also aims to predict the rut depth caused by wheel loading on an asphalt mixture by using a linear viscous analysis. To achieve these aims the following steps were taken:

- Conduct a survey of the literature on the causes of permanent deformation and packing of aggregate particles. The review focuses on the effect of aggregate packing on asphalt mixtures and investigates the Bailey method of gradation and the Dominant Aggregate Size Range (DASR) method. These two methods concern the arrangement and packing of aggregate particles.
- Select a broad range of asphalt mixtures with different aggregate gradations

to cover the whole range of asphalt concrete mixtures and the combination of upper and lower limit of the specification.

- Test the mixtures in the laboratory to determine the permanent deformation of each.
- Use the Bailey method of analysis to evaluate the mixtures' performance based on the results from the Repeated Load Axial Test (RLAT). The benefit of using the RLAT test is that it is simple, available, and it represent the frequent passage of vehicles in the road by applying repeated load. The Bailey method was established to provide a high quality mix design by providing good aggregate interlock and at this stage, more analysis ratios were added.
- Use image processing to distinguish and prove the theoretical principles of the new and Bailey ratios. The images were used to help the understanding of aggregate interlock and there was no calculations obtained from the images.
- Include more testing variables in the laboratory testing to investigate their effects in the light of aggregate packing. The variables that were found important are the binder content, testing temperature, and compaction effort.
- Use soft computing techniques (ANN and ANFIS) to predict the permanent deformation of asphalt mixtures.
- Perform wheel tracking tests for six mixtures to measure their rut depth, and use a linear viscous approach to predict the rut depth by making use of multi-layer linear viscous analysis.

## 1.5 Thesis Organisation

This thesis consists of seven chapters. Chapter 2 presents a review of permanent deformation and the role of each component in the asphalt mixture. The chapter also presents a review of the packing theory of aggregate particles, and how the coarse and fine aggregate particles are specified. Finally, the chapter reviews rutting prediction methods used in the past by using elastic, viscoelastic, and viscous approaches.

Chapter 3 briefly explains the principle of the two soft computing techniques which are used in later chapters. The chapter also reviews the applications of these techniques in the pavement field.

Chapter 4 investigates the effect of aggregate packing on permanent deformation of asphalt mixtures. In this chapter, different mixtures were selected to cover a wide range of aggregate gradations, and the Bailey method of analysis was used to understand the behaviour of each mixture. At this stage, more analysis ratios were added, and soft computing techniques used to predict the permanent deformation of each mixture.

Chapter 5 shows the effect of binder content, testing temperature, and compaction effort on different asphalt mixtures in the light of packing ratios. The results are also analysed using ANN and ANFIS to predict the permanent deformation of these mixtures.

Chapter 6 introduces a linear viscous approach to predict the rut depth of wheel tracked slabs. The approach uses the non-linear properties of the asphalt mixture

taken from the repeated load axial test (RLAT); field data are then used to validate the approach. Finally, Chapter 7 states the conclusions achieved from this research and gives recommendations for future work.

## 1.6 Research Implications

This study has focused on the impact of aggregate gradation on the permanent deformation of asphalt mixtures. The research also introduced a linear viscous method to predict the rut depth of the asphalt mixtures. The implications of this research are summarised as follows:

- In most cases, when field investigations are required to explore the failure reasons in road pavements it is recommended to resurface the road. Investigations require material analysis (aggregate gradation, binder content) to check if specifications were followed. Sometimes no reason appear (after pavement structure analysis) to be the cause of failure and they resurface the road and the same problem occurs in a period of time. Using the method presented in this thesis helps to understand the packing of aggregate particles and to judge if an adjustment to the gradation is required, and no other resurfacing is required.
- The method of packing ratios presented in this thesis could also be used in designing the asphalt mixture to expect what performance will be achieved. Certain distribution of aggregate particles might be accepted to be within the specification limits but not necessarily to be of good performance when using

the packing ratios concept. The soft computing techniques model could also be used in predicting the mixture performance.

- The linear viscous approach presented in this research is ready to use in predicting the rut depth in road pavement especially it incorporates the non-linear properties of the material. The method could also be used in assessing pavement layers and see which one of them is more susceptible to rutting when field investigations are required.

# Chapter 2

## Permanent Deformation in Asphalt Mixtures

### 2.1 Introduction

This chapter presents a review of different issues related to permanent deformation. The first section discusses the performance evaluation of the binder, aggregate, and asphalt mixture. The asphalt mixture behaviour was evaluated in terms of the resistance to permanent deformation, aggregate gradings, and volumetric properties. The following section will review the laboratory tests that are most commonly used to evaluate permanent deformation in the asphalt mixture. In the third section, the theory of packing will be introduced and it will be shown how it has been employed in the asphalt mixture characterisation. The Bailey method and Dominant Aggregate Size Range (DASR) will be reviewed in this section as well. Finally, stress-strain behaviour of asphalt mixture will be considered and the different con-

stitutive model theories and applications will also be presented.

## 2.2 Performance Evaluation

### 2.2.1 Binder Behaviour

In general, bitumen behaves as visco-elastic material. Early understanding attempts showed that the mechanical performance of asphalt mixtures is highly dependent on the binder properties (Lee, 2006). Research on bitumen mechanical properties started around the 1960's when Van der Poel proved that the stiffness of an asphalt mixture could be related to the binder properties (penetration and softening point) (Poel and Der, 1954; Van der Poel, 1955), as shown in Figure 2.1.

Van der Poel (1954) condensed his findings of bitumen mechanical behaviour as a function of loading time and temperature into the 'Van der Poel nomograph'. Following his findings, researchers tried to simulate the conduct of the bitumen as linear viscoelastic using rheological models, (Jongepier et al., 1969; Hall, 1972). However, their assumptions were only applicable for small strains and stresses. The stress-strain behaviour of pure bitumen has been described as very complex by several researchers, Ossa (2005); Cheung (1995); Cheung and Cebon (1997a,b,c). Bitumen behaves as an elastic solid at low temperature and high loading time, and as a viscous liquid at high temperature and low loading time, Brown and Sparks (1958); Gaskins et al. (1960); Moavenzadeh and Stander Jr (1967). Visco-elastic behaviour has been observed in the transition zone. So the temperature plays



a vital role in the consistency of the bitumen and this phenomenon is known as viscosity.

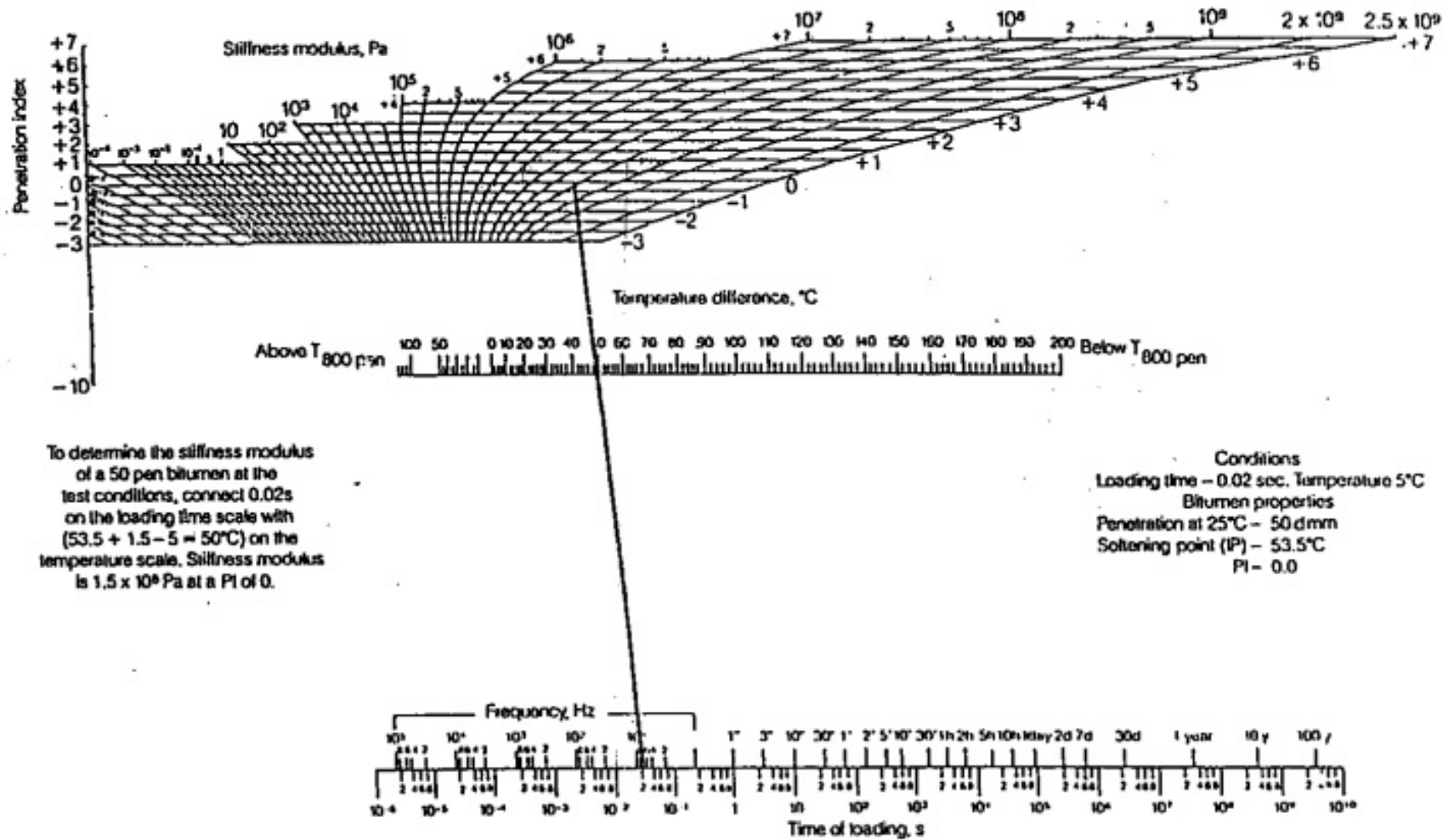


Figure 2.1: Van der Poel Nomograph

## 2.2.2 Aggregate Behaviour

Many types of aggregate are used to produce asphalt mixtures. There are three categories of aggregate depending on its origin: natural aggregate, processed aggregate, and synthetic aggregate. The primary aim of the aggregate in asphalt mixtures is to resist shear stresses that develop from repeated traffic load. Permanent deformation is related to the resistance of aggregate particles in the mixture to the applied load. If the aggregate is overloaded then shear planes will form in the aggregate structure and allow permanent deformation to develop in the mixture, as shown in Figure 2.2. This happens when the shear stress in the shear plane is greater than the shear strength of the aggregate. Because there is zero cohesion in dry aggregate, shear strength depends on the movement, packing, and internal friction of aggregate particles. Cubical aggregate is preferred more than the rounded particles because they tend to lock together resulting in a stronger mass, while rounded aggregate particles slide over each other, as shown in Figure 2.3.

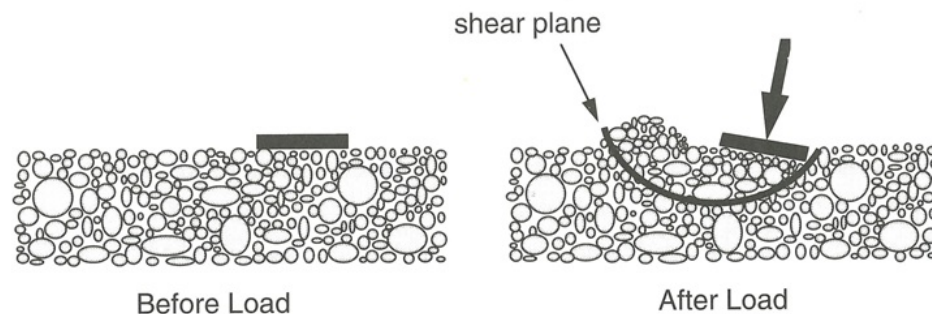


Figure 2.2: Behaviour of Shear Loading in Aggregate, Asphalt Institute (1996)

The effect of aggregate on asphalt mixtures is a matter of study by researchers. Aggregate particle size distribution plays an important role in influencing the per-

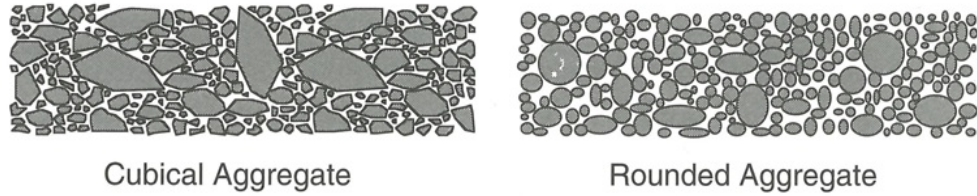


Figure 2.3: Aggregate Stone Skeleton, Asphalt Institute (1996)

manent deformation of hot mix asphalt. Golalipour et al. (2012) studied the effect of aggregate gradation on the performance of rutting in asphalt pavements. They selected aggregate gradations with a nominal size of 19mm, and used three different gradations, the upper limit, the lower limit, and a middle gradation according to The Asphalt Institute. They tested the three different gradations with two tests, Marshall test, and Dynamic Creep test. The results from the Marshall test showed that the upper limit of the gradation had the highest value of stability, and the lower limit of gradation had the lowest. For the dynamic creep test, the results showed that the asphalt mixture at the upper limit had the lowest permanent deformation and cumulative strain. This was because the upper limit had more fine particles than the two other gradations and it had higher density, and fewer air voids. However, Ahmed and Attia (2013) showed that coarser aggregate resists permanent deformation better than fine aggregate by using four types of aggregate gradation and conducting a wheel tracking test. The mixtures used named coarse gradation, fine gradation, open graded, and dense gradation according to the Egyptian specifications.

### 2.2.3 Asphalt Mixture Behaviour

Permanent deformation is considered as one of the main types of distress that occurs in flexible pavements when subjected to traffic load. It is caused by a combination of densification (volume change) and shear deformation. Concerning densification, poor compaction while constructing the layers may cause the aggregate skeleton to become more closely packed during the early life of the structure. Shear deformation is the main subsequent cause of rutting and it can result in the formation of shoulders on either side of the rut; it occurs because of the viscous behaviour of the material. Many factors can cause permanent deformation to occur in asphalt mixtures, such as aggregate gradation, type of aggregate, binder type and content, compaction level, compaction method, and temperature, Cai (2013). There are two broad types of rutting in pavements namely structural rutting and non-structural rutting, as shown in Figure 2.4. Structural rutting is caused by a weak material under the asphalt layer (generally the subgrade) even if the surface layer is very stiff. The second form of rutting (which this thesis focuses on) is the type that concerns asphalt mixture designers; it is related to the properties of the mixture, and it occurs because of the lack of shear strength to withstand the vertical repeated load.

When a wheel load is applied to an asphaltic pavement, it creates a deformation in the material elements. The properties of the material, temperature, load level and loading time are factors that determine the magnitude of the deformation. As the load is removed, some of this deformation will be recovered but a part will

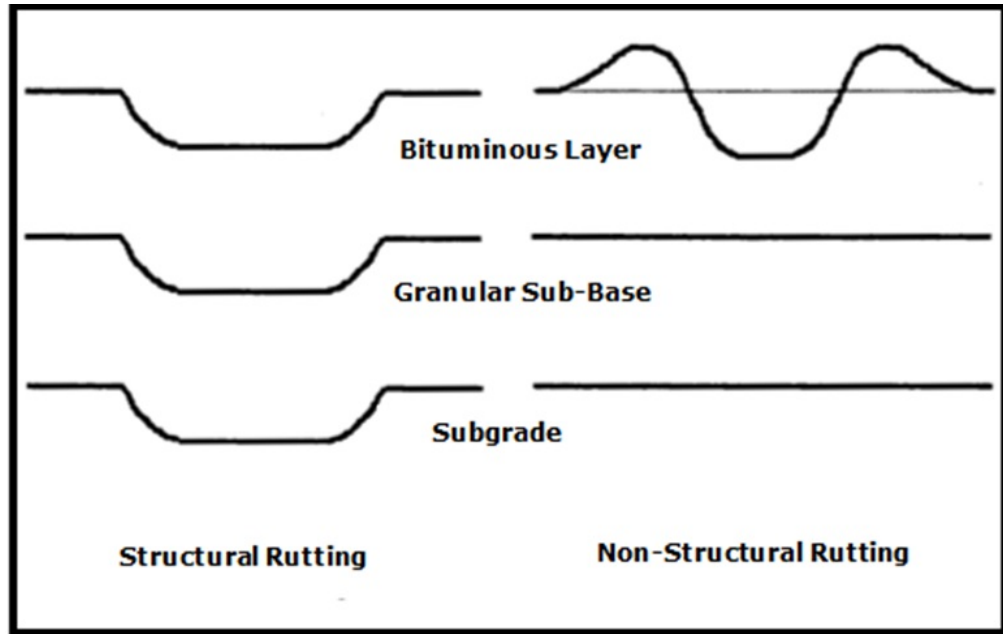


Figure 2.4: Structural and Non-Structural Rutting, Gibb (1996)

remain in the material. The recovered part is due to the elastic and delayed elastic components of the material while the remainder is due to the plastic and viscous components. The accumulation of deformations for each load applied can result in high deformation in asphaltic material, as shown in Figure 2.5. Hofstra and Klopman (1972) measured the densities of asphalt mixture samples under a rutted wheel track and outside the wheel track, and they found that both sets of samples had equal densities. They concluded that the deformation accumulated due to the shear flow of material, not densification.

Asphalt mixtures carry three main types of load in the field: vertical compressive load on the pavement surface and transmitted through the asphalt layers, tensile stresses acting horizontally in the bottom of the asphalt layer, and shear stresses, see Figure 2.6. The asphalt mixture should be designed to withstand the vertical compressive stresses within the asphalt layers and prevent permanent deformation

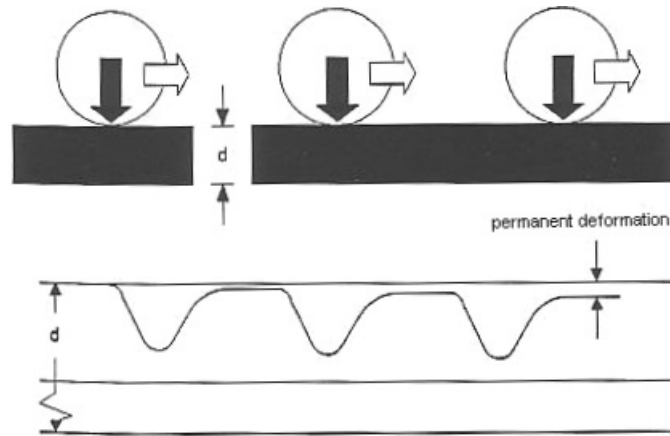


Figure 2.5: Accumulation of Permanent Deformation under Repeated Wheel Loading, Taherkhani (2006)

taking place; it should also be designed to resist the tensile stresses at the bottom of the layer (prevent fatigue cracking). The asphaltic layers are also subjected to temperature change stresses and it should be designed for these stresses (prevent thermal fatigue cracking), Asphalt Institute (1996).

### Resistance to Permanent Deformation

As mentioned earlier, the permanent deformation of asphaltic mixtures is influenced by the properties of binder and aggregate, their proportions, compaction level and environmental conditions. The resistance to permanent deformation is very dependent on the type of mixture. In some types of mixture such as Hot Rolled Asphalt (HRA), the deformation resistance relies on the stiffness of binder and mortar, while in Asphalt concrete (Dense Bitumen Macadam (DBM)) or Stone Mastic Asphalt (SMA), the resistance to deformation relies on the particle interlock and is less dependent on the bitumen. Brown and Cooper (1984) tested DBM mixtures in the repeated load triaxial test at 30 °C and found that the binder grade had

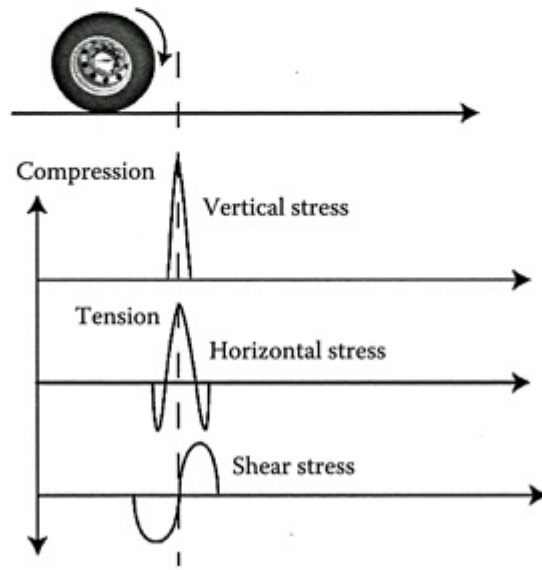
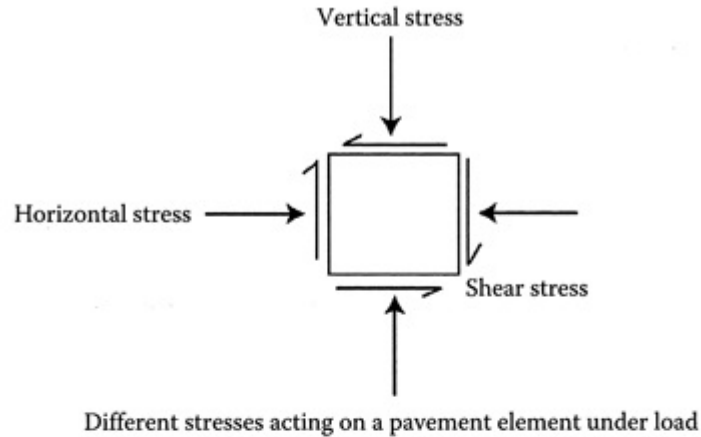


Figure 2.6: Stresses induced in a Pavement due to a Moving Load (Mallick and El-Korchi, 2013)

no effect on the deformation of asphalt mixtures. To give more understanding of this, Gibb (1996) performed a fascinating study on which component of the asphalt mixture material resists the permanent deformation. He selected two types of asphalt mixture, DBM and HRA, and conducted compressive cyclic uniaxial tests at different temperatures; two types of binder were used (40/60 and 160/220) for the two mixtures. He found that at conditions where the binder has low stiffness (high



testing temperatures) the aggregate structure provided the resistance to permanent deformation more than the binder and the DBM showed better resistance than the HRA. On the other hand, at higher binder stiffness (low testing temperatures), the HRA resisted the deformation better than the DBM. The large permanent deformation that occurred in the dense mixture (DBM) was due to the plastic strain that came from the movement of aggregate particles when repeated load was applied. He concluded that the permanent deformation resistance is dominated by the binder to a certain level of binder stiffness; if the binder stiffness is below that level then it will have less contribution to the deformation resistance, and the role of aggregate structure starts to be more dominant.

Brown and Snaith (1974) also found that the role of binder viscosity in resisting permanent deformation is dependent on the contribution of aggregate resistance. They also found that at high temperatures the aggregate structure is more dominant in providing permanent deformation resistance. Therefore, under such conditions the binder content in the mix plays a significant role affecting the packing of aggregate structure. The more the binder in the mix the less the aggregate interlock resulting in less resistance to deformation, while a lower binder content in the mix leads to more aggregate interlock, therefore, resistance increases. They also found that at lower temperatures, a medium bitumen content (4.0 %) will maximise the contribution of both aggregate interlock and binder viscosity in resisting the permanent deformation. However, an optimum binder content needs to be judged to give a reasonable performance at different temperatures in the field.

Brown and Cooper (1984) concluded that aggregate gradation plays an important role in resisting the permanent deformation of asphalt mixtures by testing continuous and gap-graded mixtures at 30 °C. They also found that continuously graded mixtures had more resistance to permanent deformation than gap-graded mixtures. However, gap-graded mixtures with a proportion of coarse aggregates, such as SMA, can give good resistance to permanent deformation due to their greater particle interaction. Gibb (1996) also compared the results of permanent deformation resistance between rounded and angular aggregate particles in asphalt mixtures. He found that mixtures with spherical particles achieved higher deformation than those with angular particles under repeated loading test.

Sousa et al. (1991) summarised the factors that affect permanent deformation in asphalt mixtures, as shown in Table 2.1.

Table 2.1: Factors affecting Permanent Deformation in Asphalt Mixtures, Sousa et al. (1991)

	<b>Factor</b>	<b>Change in Factor</b>	<b>Effect of Factor change on Rutting Resistance</b>
<b>Aggregate</b>	Surface texture	Smooth to rough	Increase
	Gradation	Gap to continuous	Increase
	Shape	Rounded to angular	Increase
	Size	Increase in maximum size	Increase
<b>Binder</b>	Stiffness	Increase	Increase
<b>Mixture</b>	Binder content	Increase	Decrease
	Air void content	Increase	Decrease
	VMA	Increase	Decrease
<b>Test Field Conditions</b>	Temperature	Increase	Decrease
	State of stress/strain	Increase in tire contact pressure	Decrease
	Load repetitions	Increase	Decrease
	Water	Dry to wet	Decrease if mix is water

## Aggregate Gradings

Gradation of aggregate is the particle size distribution of an asphalt mixture and is determined in terms of percent of passing each standard sieve. Designers are concerned with aggregate gradation since they are looking for certain performance requirements. The Superpave mix design specifies band within gradation named as the 'restricted zone'; it recommends that the gradation should not violate the restricted area to achieve good resistance to permanent deformation. The restricted zone lies along the maximum density line and between the intermediate particle size (4.75 or 2.36 mm, depending on the nominal maximum particle size) and the 0.3 mm, Kandhal and Cooley Jr (2001). Although the restricted zone was recommended by Superpave, there is some research that has showed that passing the gradation through the zone can result in better mixture performance. Kandhal and Cooley Jr (2001) conducted laboratory testing for different gradations and nominal maximum particle sizes to investigate the effect of the restricted zone on permanent deformation of dense-graded Hot Mix Asphalt (HMA) mixtures. They used two nominal maximum sizes (9.5 and 19.0 mm) and five gradations; three of the gradations passed through the restricted zone and the others did not. They used three tests to evaluate the permanent deformation, namely the Asphalt Pavement Analyzer (APA), Superpave shear tester, and repeated load confined test. They found that mixtures with gradations passing through the restricted zone performed similarly to or better than those falling outside the restricted zone for both nominal maximum sizes. Another study was done by Kandhal and Mallick (2001) to

compare asphalt mixtures made up of different gradations but of a similar type of aggregate and also mixtures with similar aggregate mineralogy but with different gradations. The asphalt mixtures were composed of granite, limestone, and gravel passing below, through, and above the Superpave restricted zone. Results showed that for the granite and limestone aggregate type mixtures, gradations that passed below the restricted zone had the highest amount of rutting, with a better performance for gradations passing through the zone, while the best performance was found when a grading passed over the restricted zone. The behaviour of the mixtures with gravel particles showed exactly dissimilar performance. In later chapters of this thesis, an extensive study of aggregate gradation and how the particles are packed together will be presented and interpreted by using selected packing ratios.

### **Volumetric Properties**

The volumetric properties of an asphaltic mixture play a crucial role in the performance of the mixture. Percentage air voids and voids in mineral aggregate (VMA) are the main two factors that determine the volumetric properties of the mixture. Mixtures with low VMA are good at resisting permanent deformation because the aggregate particles (especially large sizes) have enough room to be in contact with each other. However, very low VMA will tend to make the mixture susceptible to permanent deformation because the mortar (binder and filler) will have a chance to lie in between particles and will reduce the contact points between particles, (Gibb, 1996); very low VMA might be a result of high binder content in the mixture. The high bitumen content will result in a thick film thickness around the aggregate par-

ticles and this will decrease the resistance to permanent deformation, Taherkhani (2006).

## **Compaction Methods**

**Marshall Compaction** Marshall compaction was developed in 1939 by Bruce Marshall. The method is usually used for mixtures with high amount of fine graded aggregate with a maximum aggregate size of 25 mm, Swiertz et al.. The specimen is compacted by using compressive impact load by a loading hammer on each side of the sample and for several number of blows. The main disadvantage of Marshall compaction is that it focuses on getting the optimum values of air voids, binder content, strength, and durability of the mixture when using a mix design. Currently, Marshall compaction is not widely used in the pavement work because it does not simulate the compaction in field precisely.

**Roller Compactor** The purpose of a roller compactor of asphalt mixtures is to ensure that the compaction is representing the compaction in the field. Although the roller compactor simulates the field compaction, the use of it is limited due to several reasons: the size of the compactor is relatively large, the compactor is not portable, and it is expensive. Moreover, there are some difficulties in controlling the air voids of the sample, and the compaction process is time consuming.

**Superpave Gyrotory Compactor** The gyrotory compactor was developed in response to the need for a portable and easy to use device. There are some design principles need to be applied to achieve the required compaction: angle of gyra-

tion is one of the important factors that help to create vertical and shear forces which results in better compaction. Vertical pressure is another factor of gyratory compaction and is recommended by the Superpave to be 600 kPa as an estimate to field loading conditions. The gyratory compactor is currently very widely used because of its simplicity and efficiency among other compaction methods. For this reason it is used in this research as the compaction method for the samples.

## **2.3 Laboratory Tests for Measuring Permanent Deformation**

Generally, the aim of testing asphalt mixtures is to simulate the field performance as closely as possible to understand the behaviour of the material. Figure 2.6 presented earlier showed the different stresses induced in a pavement, and it is not easy to find a laboratory test to represent all these loading types. Over the years, several simplified tests have been developed to investigate the permanent deformation behaviour of asphalt mixtures and also used towards the development of constitutive models. The main laboratory tests are listed below:

- Static uniaxial and triaxial test
- Cyclic uniaxial and triaxial test
- Wheel tracking test

### 2.3.1 Static Uniaxial and Triaxial Test

The static uniaxial test is considered as the simplest test used for evaluating the deformation behaviour of viscoelastic materials such as asphalt mixtures. It was developed by the Shell organisation in Amsterdam for testing bituminous mixtures in the 1970's (Hills, 1973). The test can be conducted either by applying a constant stress (creep test) or constant strain rate in tension or compression. The sample used for this test is usually cylindrical in shape and a friction reduction system between the specimen and loading plates is used. Figure 2.7 shows a typical test result for loading and unloading phases; the figure shows the initial strain which comprises elastic and plastic behaviour which is known as time independent strain and occurs when the load is applied. This stage is followed by the time dependent strain which is also known as delayed elastic and viscous strain.

Although the creep test is used to estimate the performance properties of asphalt mixtures there are some differences between static loading and real load in the field. The main and most important differences are that the actual loading condition is cyclic while in a creep test it is static, and the pavement in the field is confined and in the creep test, it is unconfined (uniaxial). Many researchers in the past have shown that the cyclic loading of the sample produces greater permanent deformation than static load (Gibb, 1996; Bolk and Van de Loo, 1979; Graham et al., 1980; Monismith and Tayebali, 1988). The triaxial test was found to be an acceptable simulation of confined pavement elements in the field. Brown and Foo (1994) compared the results of unconfined to confined creep test for a dense-graded HMA mixture, and

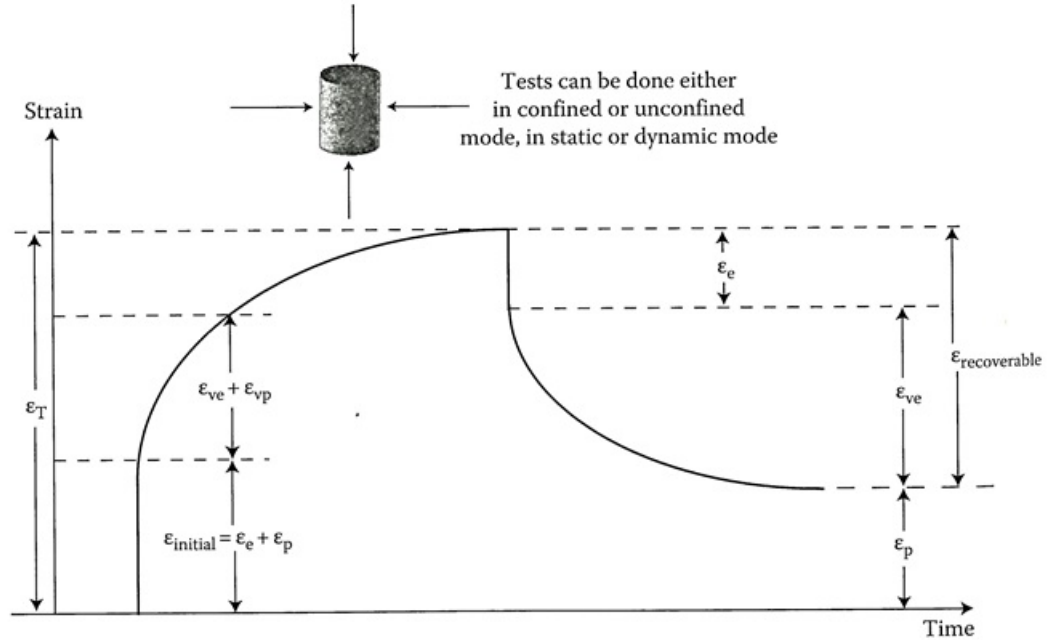


Figure 2.7: Typical Strain Results from Creep Testing (Mallick and El-Korchi, 2013)

where  $\varepsilon_T$ : Total strain;  $\varepsilon_e$ : Elastic Strain;  $\varepsilon_p$ : Plastic strain;  $\varepsilon_{ve}$ : Viscoelastic Strain;  $\varepsilon_{vp}$ : Viscoplastic Strain.

they concluded that the confined creep test represents the field more accurately.

### 2.3.2 Cyclic uniaxial and triaxial test

The cyclic uniaxial creep test or Repeated Load Axial Test (RLAT) was developed to investigate the behaviour of asphalt material under more realistic loading conditions (see Figure 2.8 for sample setting). The load is repeatedly applied for a particular loading time and a rest period may also be implemented after each loading pulse. The loading can be carried out in different waveforms such as sinusoidal, square, triangular, and trapezoidal. Brown (1976) found that the sinusoidal shape of loading is most simulative of field loading; Loulizi et al. (2002) had the same finding. Researchers usually select the loading time to correspond to the desired



speed of the vehicle. Although the frequency of load on the sample is an essential element in the laboratory test, there are few researchers who have investigated the correlation of loading time to vehicle speed in the field (Al-Qadi et al., 2008).

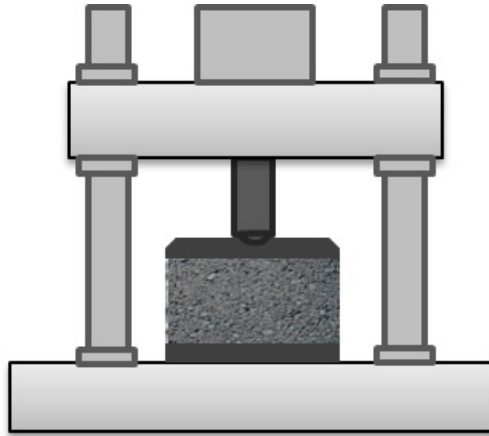


Figure 2.8: Sample Setting in Uniaxial Cyclic Test

A finite element model using elastic theory was used by Barksdale (1971) to estimate the pulse width of compressive stress as a function of speed and depth. He found that the pulse shape varies with the depth of pavement, and that it is sinusoidal in the surface layers, triangular in the bottom layers. Finally, he produced a chart to relate the loading time to vehicle speed and depth of pavement. Following this, Brown (1973) also found a relationship to correlate loading time to vehicle speed and pavement depth; his calculated loading time was about half of that calculated by Barksdale (1971). Although the cyclic uniaxial test does not exactly simulate the real load in field, Gibb (1996) suggested that it gives more reliable permanent deformation behaviour than static creep when comparing different asphalt mixtures.

Permanent vertical and horizontal strain can be measured by Linear Variable Dif-

ferential Transformers (LVDTs) which are located on the loading ram and lateral strain gauges are glued to the specimen if a triaxial test is conducted. Typical RLAT test results are shown in Figure 2.9.

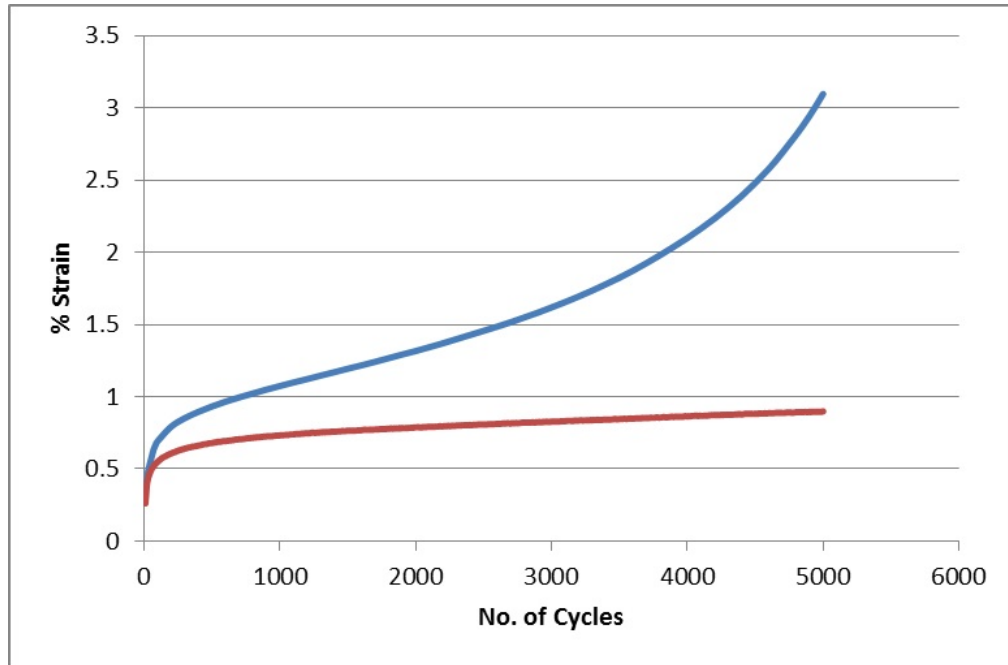


Figure 2.9: Typical Repeated Axial Load Test Result

### 2.3.3 Wheel Tracking Test

The wheel tracking test is widely used to simulate the field conditions in the pavement. There are different types of wheel tracking test that have been established for various purposes, such as Georgia loaded wheel tester, asphalt pavement analyser (APA), the Hamburg wheel tracking machine, the French wheel tracker, the Nottingham pavement testing facility, etc. The test is conducted at full scale, medium scale, or small scale. The specimen is loaded through either a real tyre or a small scale pneumatic or solid rubber tyre depending on which test is to be considered.

The specimen is repeatedly loaded by moving the loaded wheel on the specimen at large, or medium scale, or at small scale, the specimen is moved forward and backwards under the loaded pneumatic tyre; a schematic of the test apparatus is shown in Figure 2.10.

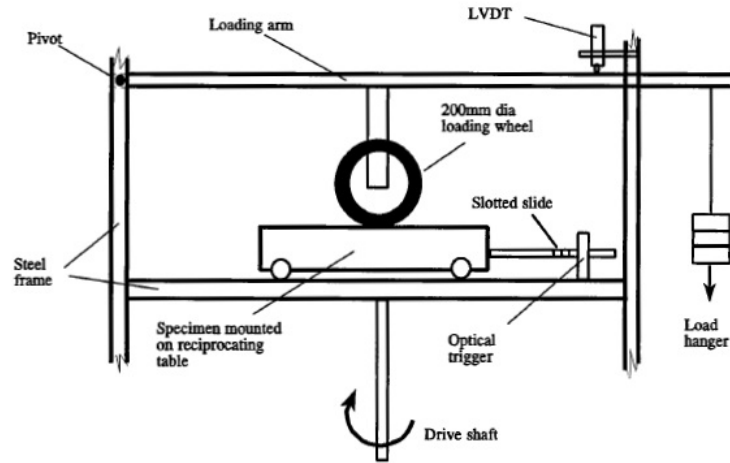


Figure 2.10: Wheeltracking Apparatus (Gibb, 1996)

The specimen size at small scale varies depending on which standard is followed. The test can be conducted at a desired temperature by placing the apparatus in a temperature controlled chamber. The wheel is loaded along the centre of the slab specimen for a predetermined number of passes or cumulative rut depth. As the wheel tracking test is considered as simulative of the field, researchers have used it to validate their rutting prediction methods (e.g (Taherkhani, 2006)).

## 2.4 Packing of Aggregate

According to Lira Miranda (2012), a good gradation of an asphalt mixture is typically one that gives the densest packing of particles, which leads to increasing the

stability by increasing the number of contact points between particles and by reducing air voids. Many attempts have been made in the past to understand the best gradation of particles to achieve the densest possible packing. Mixing various combinations of stones and sand particles to give the densest concrete was first examined by Fuller and Thompson (1907). The aim of their study was to relate the sand particle size to the coarse particle size and they proposed that the sand particle diameter should not exceed one-tenth of the coarse particle diameter to achieve a dense mixture. They concluded that the coarser the aggregate that was used, the coarser the sand particle that was required. Following their work, Talbot and Richart (1923) studied the gradation (size distribution) of aggregate to achieve the maximum density of a mixture. A slope of 0.5 on a straight line when plotting percent passing a sieve versus the particle size on logarithmic scales was considered to give maximum density. The formula for obtaining the maximum density line was:

$$P = 100 \left( \frac{d}{D} \right)^n \quad (2.1)$$

where P is the percentage of material by weight passing a specific sieve with an opening size d; D is the maximum particle size; and n is a parameter affecting the coarseness or fineness of the gradation.

Nijboer (1948) studied the effect of particle size and shape in asphalt mixtures. He confirmed the idea of the maximum density line given by a straight line on logarithmic scales of percent passing a sieve versus sieve size. He empirically proved that with typical crumbed rock particles the maximum density line has an approximate

slope of 0.45.

### 2.4.1 Theory of Packing in Particles

The arrangement of aggregate particles in a certain volume influences the interaction strength between them. In the past several years, researchers have studied the packing of granular materials by using computer simulation algorithms (Tory et al., 1968; Powell, 1980; Suzuki and Oshima, 1985; Isola, 2008). In most cases previous researchers used solid spheres to simulate the packing of particles and to model the behaviour of contacts between them, Isola (2008).

It is necessary to understand how the arrangements of spherical particles are organised to help to understand the packing of real particles. The packing of spheres was firstly investigated by Kepler in 1611 (mentioned in Yideti (2014)). He suggested that there is no arrangement of equally sized spheres filling a space with a greater average density than that of cubic close packing; this occupies 74% of a particular volume. The density is defined as the ratio of the volume of space filled by spheres to the whole volume of space. The three-dimensional arrangement can be expressed by placing the spheres in layers and the densest possible packing is achieved by placing the second layer of spheres in the dimples of the bottom layer (Szpiro, 2003). Figure 2.11 shows the densest possible packing arrangement of spheres called hexagonal close packing (HCP) (cubical close) and its packing density reaches about 74%.

Generally, by looking at a two dimensional view there are two different types of

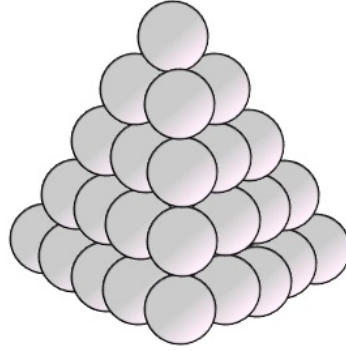


Figure 2.11: Densest Arrangement of spherical particles, Yideti (2014)

layers, a square and rhombic layer (Figure 2.12)

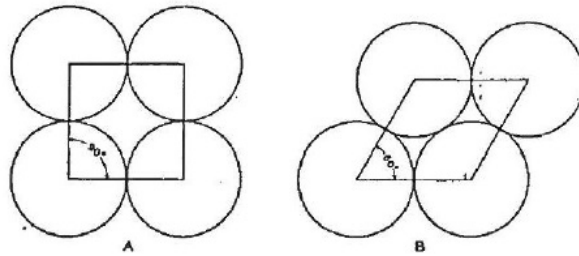


Figure 2.12: Types of layers. A) Square layer; B) Rhombic layer (Lira Miranda, 2012)

By combining these two layers in a three-dimensional space, six arrangements can be achieved; Guarin (2009) showed the shape of these arrangements by using single sized spheres; see Figure 2.13. The void structure is dependent on the shape of packing arrangement rather than the size of the spheres. It is then significantly important to fit particles in the voids between large spheres to obtain maximum packing density and this will be explained later.

Two-dimensional analysis of aggregate shape and contact between particles is based on four combinations of possible geometries, and the dimensional relationships are as follows (Vavrik, 2000):

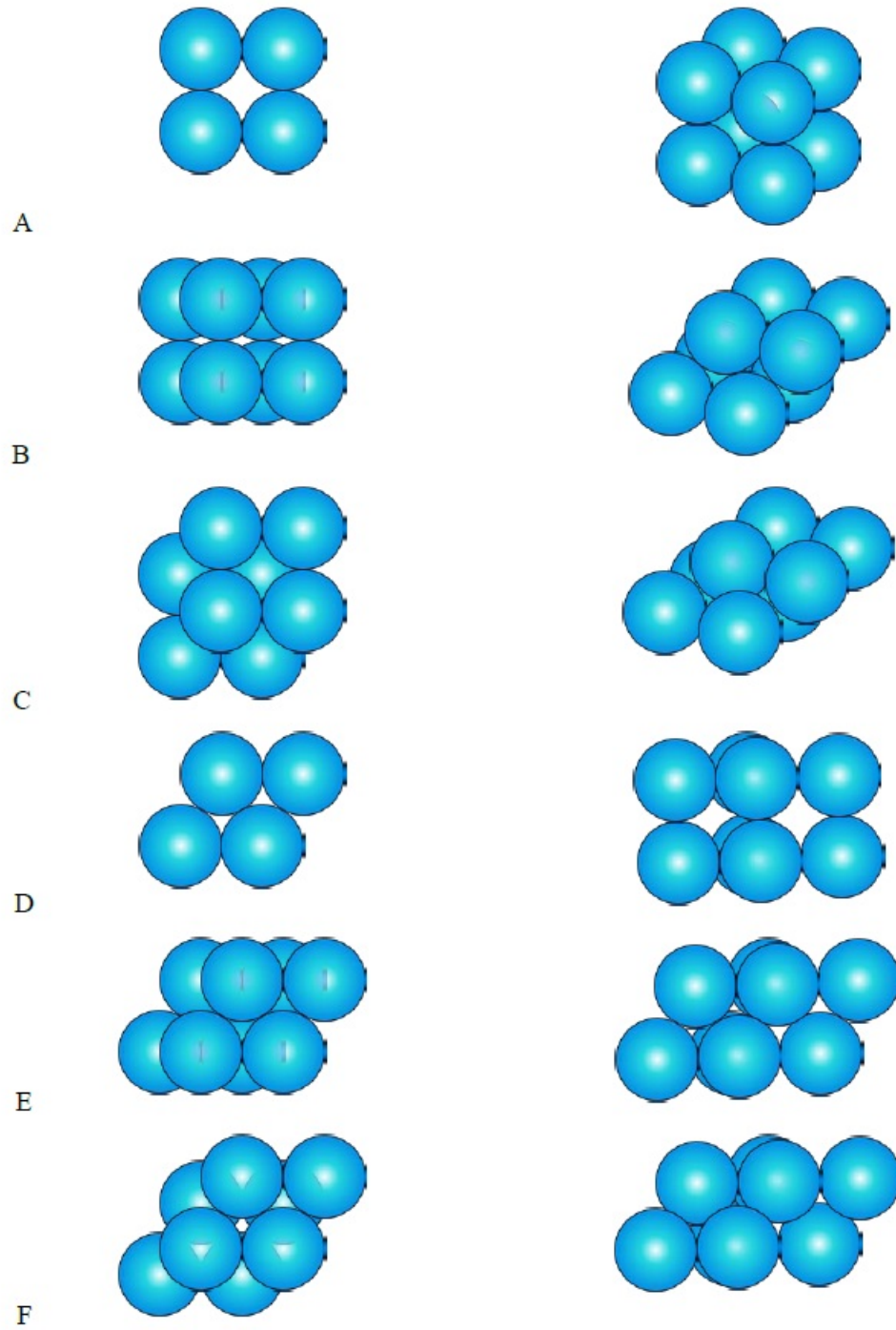


Figure 2.13: Top and Panoramic view of regular packing arrangements. A) Simple cubical, B) Hexagonal loose, C) Face-centred cubical, D) Orthorhombic, E) Tetragonal, F) Hexagonal close.

- All particle faces are round, shown in Figure 2.14a, this produces a ratio of 0.15

- Two particles have round faces and one has a flat face, shown in Figure 2.14b, this produces a ratio of 0.2
- One particle is round-faced and two have flat faces, presented in figure 2.14c, this provides a ratio of 0.24.
- All particle faces are flat, shown in Figure 2.14d, this produces a ratio of 0.29

These particle shape combinations are used to characterise the void size between three adjacent particles. The average value (0.22) of the four cases has commonly been taken as the void size between particles and many researchers have confirmed that it is a good representation of the average conditions (Lira Miranda, 2012; Guarin, 2009; Vavrik, 2000; Mamat, 2008; Alshamsi, 2006; Kim, 2006; Kim et al., 2006). In reality, there are different possible void sizes based on the shapes of particles used. However, the value of 0.22 is reasonable to cover a broad range of cases.

## 2.4.2 Aggregate Gradation

In general, aggregate properties in a mixture are defined by its particle size distribution. In soil mechanics, designers usually look for the best particle size distribution to achieve a required performance level such as resistance to permanent deformation, shear strength, and hydraulic properties. The requirement of aggregate gradation differs from one country to another based on the properties of the local available unbound material. Therefore, specifications usually require the gradation to lie in between two limits to achieve a certain level of performance. The aggregate



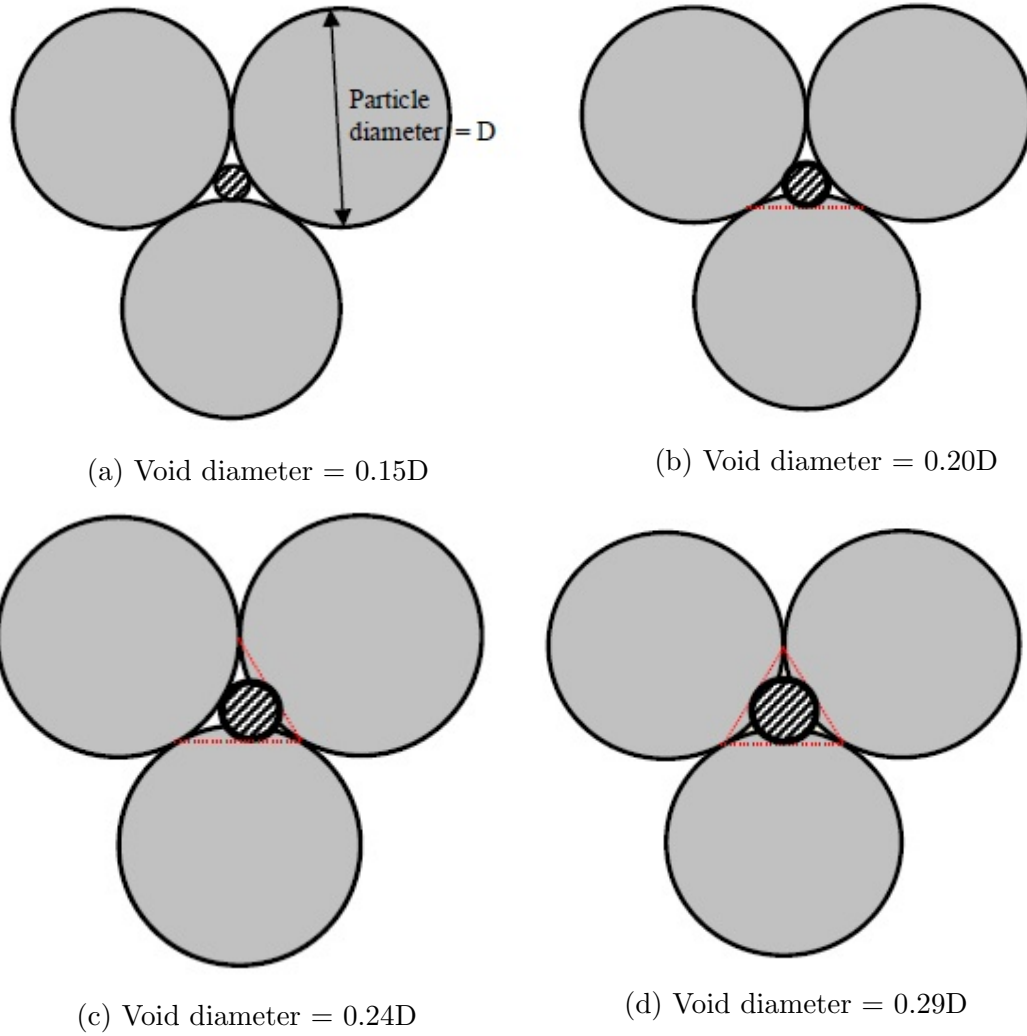


Figure 2.14: Average Void size Calculation

is sifted through standard sieves ranging from large opening sizes (20 or 32 mm) to small (0.063 mm), and the percentage passing each sieve is then determined. Different combinations of aggregate gradation produce different mixture classifications; the most common classifications are summarised below, Yideti (2014):

- Dense or well-graded: a gradation that has a broad range of particle sizes and all sizes are represented.
- Poorly-graded: a gradation that does not have a proper representation of all

particle sizes.

- Uniform-graded: a gradation in which the majority of the particles are of similar size.
- Gap-graded: a gradation that has, at least, one particle size missing.
- Open-graded: a gradation that contains only very few particles of small size aggregate.

The aggregates used in asphalt mixtures are naturally occurring and they can not be packed together to fill a unit volume completely; voids will exist between the particles. The aggregate packing to fill a certain volume depends on:

- Shape of aggregate particles: the shape of aggregate particles plays an important role in the density of the mixture. Rounded particles tend to form a more dense arrangement than elongated particles.
- Compactive energy: several compaction methods are used to compact a blend of an aggregate mixture such as Marshall hammer, gyratory compactor, kneading, and static pressure. The more compaction energy is applied, the denser the mixture becomes; however very high compaction energy may result in particle breakdown.
- Surface texture of aggregate particles: this can also affect the final density of the mixture because of the friction between particles. Smooth particles will tend to be reconfigured to the densest arrangement while rough particles resist the sliding of one particle on another resulting in low density.

- Aggregate particle gradation: the different types of aggregate gradation have a considerable impact on the density of the mixture. Single-sized gradations will not be packed as dense as gradations with two sizes.

### **Coarse vs Fine Aggregate**

The coarse aggregate particles are considered as the main component that resists deformation in the asphalt mixture. When a load is applied to the pavement, the aggregate particle interlock forms a path for the load to be transmitted to the underlying layers. Therefore, it is necessary to provide a good aggregate interlock to obtain good resistance to deformation. Mixtures with low aggregate interlock would resist low load levels only. The fine aggregate particles in the mixture complete the aggregate structure by filling the voids between coarse particles. If the fine particles were not present in the mixture, then the mixture would remain open and contain a high percentage of air voids. The fine particles need to be in a compacted state to minimise the permanent deformation due to shear flow and to prevent any densification from occurring. Mineral filler is included in a mixture to develop mastic and the mastic contributes to the properties of the mixture. Mineral filler as part of the aggregate blend is considered as filling the voids created by fine aggregate particles. These combinations of aggregate particles filling each other were described by Vavrik (2000) and developed into a design method known as *The Bailey Method*. The concept of the Bailey method will be explained in the following section.

### 2.4.3 Bailey Method of Gradation Analysis and Asphalt Mix Design

One of the methods developed to analyse HMA gradations is the Bailey method. The method is based on selecting an appropriate volume of coarse and fine particles to provide aggregate interlock. The method was presented by Vavrik (2000) and it aims to provide a high-quality mix design and this requires understanding of two concepts:

1. A more fundamental approach to distinguish between coarse and fine particles needs to be developed.
2. The aggregate particles need to be combined by volume to ensure good aggregate interlock coarse particles.

Traditions identify the coarse particles as particles larger than 4.75 mm and fine particles are those smaller than that (Vavrik, 2000). Vavrik (2000) suggested to change this definition to ensure that the mixture was properly analysed and to determine the aggregate interlock of the mixture. The role of coarse and fine particles presented in the previous section is mainly suggested by him to develop the concept. He defined the coarse and fine particles as:

- Coarse Aggregate: Large particles that when placed in a unit volume create voids.
- Fine Aggregate: Aggregate particles that fill the voids created by coarse aggregate.

It can be seen from the definition that there is no absolute size associated with the definition of coarse and fine aggregate. This could lead to some of the particles traditionally defined as coarse being considered as fine and vice versa.

### **Control Sieves**

Vavrik (2000) used control sieves to design a mixture and then used the control sieves to find ratios to evaluate the performance of the asphalt mixture. This study focuses on the ratios for evaluating mixture performance.

**Primary Control Sieve (PCS):** this is the sieve that identifies the range of particles sizes considered as coarse aggregate. Vavrik et al. (2001) introduced the definition of PCS as the break point between the coarse and fine aggregate. The PCS can be determined by multiplying the closest standard sieve to the Nominal Maximum Particle Size (NMPS) by 0.22. The value of 0.22 was presented in the previous section where it was shown that it is the size of the void that is created between three particles in two-dimensional space. Therefore, each asphalt mixture has its own PCS according to the NMPS of the aggregate blend. The NMPS is defined in Superpave as one sieve larger than the first sieve that retains more than 10%. PCS can be calculated by:

$$PCS = NMPS \times 0.22 \quad (2.2)$$

Vavrik (2000) presented a list of the PCS's that correspond to the US standard sieves and particle sizes as shown in Table 2.2.

Table 2.2: Standard Sieve sizes and Associated Primary Control Sieves, Vavrik (2000)

Particle Size		Particle Size $\times$ 0.22	Primar Control Sieve	
US Std.	mm	mm	US Std.	mm
1-1/2"	37.5	8.25	3/8"	9.5
1"	25	5.5	#4	4.75
3/4"	19	4.18	#4	4.75
1/2"	12.5	2.75	#8	2.36
3/8"	9.5	2.09	#8	2.36
#4	4.75	1.05	#16	1.18
#8	2.36	0.52	#30	0.600
#16	1.18	0.26	#50	0.300
#30	0.600	0.13	#100	0.150
#50	0.300	0.07	#200	0.075

The PCS separates the particle gradation curve into two fractions (fine and coarse) and by a similar process the fine fraction is also divided into two further fractions.

**Secondary Control Sieve (SCS):** this provides a further breakdown of the fine fraction of a combined gradation. The PCS is multiplied by 0.22 to obtain the closest standard sieve in order to fully define the structure of the gradation.

$$SCS = PCS \times 0.22 \quad (2.3)$$

**Tertiary Control Sieve (TCS):** this gives a further breakdown to the very fine particles filling the voids.

$$TCS = SCS \times 0.22 \quad (2.4)$$

Figure 2.15 shows a schematic diagram explaining the divisions of the aggregate blend.

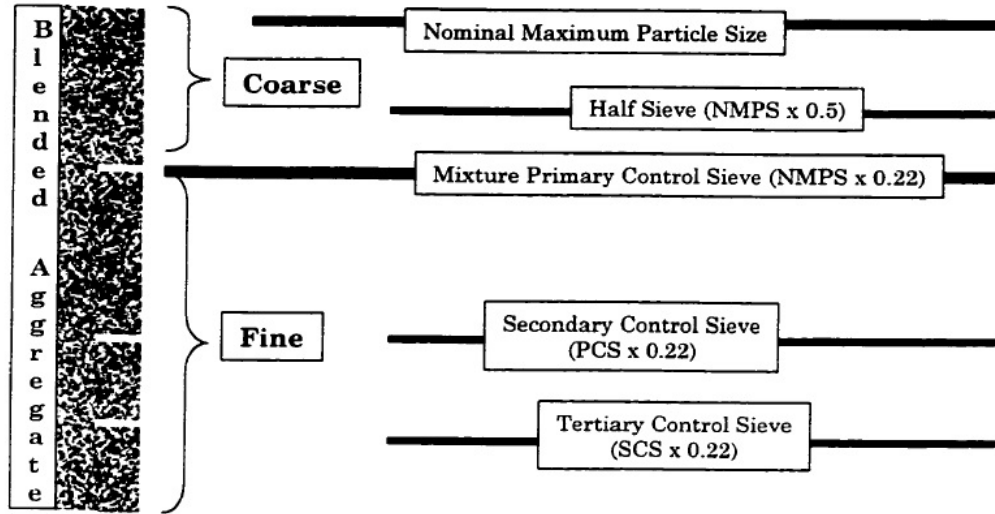


Figure 2.15: Schematic Diagram of Control Sieves, Vavrik (2000)

### Evaluation Ratios

Certain ratios are then introduced to evaluate the performance of the asphalt mixture. These ratios are based on the control sieves presented in the previous section.

**Coarse Aggregate Ratio (CA):** this ratio is used to evaluate the coarse portion of the aggregate gradation, to evaluate the void structure in the coarse aggregate.

For this purpose, a Half Sieve is introduced (Vavrik, 2002). The Half Sieve (HS) is defined as half of the NMPS ( $\text{NMPS} \times 0.5$ ). Those particles smaller than the HS and larger than the PCS are termed “interceptors”. Interceptors play an important role in mixture volumetric properties. By changing the proportions of interceptors, the VMA will be modified. Interceptor particles do not fill the voids created by the larger particles because of their relatively large size compared to the voids created.

However, the shape, elongation and orientation of the particles are all factors affecting the filling of the voids between coarse particles and interceptors. The CA

ratio is given by:

$$CA = \frac{\%PassingHS - \%PassingPCS}{100\% - \%PassingHS} \quad (2.5)$$

The packing of coarse aggregate has an important impact on the performance of the mixture. Vavrik (2000) suggested a range of values for the CA ratio between 0.40 to 0.80 for a dense graded mixture to ensure “balance” in the coarse portion of the aggregate structure. He also stated that a CA ratio below 0.40 allows the fine aggregate in the mixture to be over-compacted because of the smaller voids created in the coarse aggregate. Therefore, mixtures with low CA ratio require a larger amount of fine material to maintain sufficient mixture volumetric properties. He also reported that higher values of CA ratio imply excessive amounts of interceptor particles which might lead to segregation of the particles larger than the PCS. This would lead to a non-compactible mix. However, it will be proven in the following chapters that definite conclusion cannot be drawn on how the mixture will behave unless other factors are taken into account.

**Coarse Portion of Fine Aggregate ( $FA_c$ ):** this ratio describes the fine aggregate, which are particles smaller than the PCS. The fine particles of the aggregate gradation can also be presented as a blend of aggregate containing coarser and finer materials. The coarser portion of the fine aggregate will also create voids between particles and the finer particles will fill these voids.  $FA_c$  describes the interlock of the coarse portion in the fine aggregate. A very low value of this ratio (less than 0.40) gives an indication that the coarse portion of the fine aggregate is gap graded,



Vavrik (2000). He suggested a reasonable value of this ratio to be less than 0.50 because if this ratio increases the fine portion of the fine aggregate tries to push apart the coarse portion of the fine aggregate. He also reported that if this ratio reaches 0.55, the mixture will be ‘tender’, have over-compaction, and would suffer early failure under traffic. This ratio has a considerable effect on the VMA of the mixture, and can be determined from the equation below:

$$FA_c = \frac{\%PassingSCS}{\%PassingPCS} \quad (2.6)$$

**Fine Portion of Fine Aggregate ( $FA_f$ ):** this ratio represents the content of the very finest material (including filler) in the mix and is important for certain aspects of mixture behaviour (e.g. voids in fine fraction, binder demand). However, this ratio will not be considered here as this study has focused on coarse aggregate effects on permanent deformation.

Researchers have investigated the effect of changing the evaluation ratios on the performance of asphalt mixtures. Thompson (2006) studied the effect of the ratios on the rut depth, and he found that decrease in CA and  $FA_c$  ratio would result in a reduction in rut depth resistance of an asphalt mixture. Mohammad and Shamsi (2007) also investigated performance by using eight different mixtures. The aggregate structure was designed using the Bailey method of aggregate gradation evaluation. They found that the CA ratio has the strongest correlation with mixture volumetric properties while  $FA_c$  was less sensitive to them. The CA ratio was found to be correlated with the result of the Hamburg wheel tracking test.

Khosla and Sadasivam (2005) studied the effect of permeability of asphalt mixtures on their performance. The permeability was investigated in the light of Bailey ratios of gradations and it was shown that it is highly affected by certain aggregate sizes (#4, #8 and #16). Bailey guidelines recommended low proportion of #4 size aggregate and high of #8 and #16 to give low permeability mixture. They validated the the permeability guidelines by permeability test in the laboratory.

#### **2.4.4 Dominant Aggregate Size Range (DASR)**

In 2006 a conceptual and theoretical approach was introduced by Kim (2006) to investigate the coarse aggregate structure based on the gradation. The method was developed to identify which size range (DASR) of aggregate in the asphalt mixture is carrying the load. He used the porosity of the mixture as a criterion for aggregate interlock, and it was concluded from soil mechanics that the porosity of granular material in a loose state is approximately constant between 45% and 50% regardless of the size and distribution of particles, Lambe and Whitman (1969). He concluded that this applies to the aggregate material in an asphalt mixture and that as long as the porosity was no greater than 50% the particles would still be in contact with each other. He found a theoretical approach to determine the DASR; the DASR must have coarse enough particles with porosity smaller than 50% to achieve a mixture with good resistance to deformation and cracking. Particles which are smaller than the DASR were considered to fill the voids created by the DASR (these particles were named as Interstitial Components IC and their volume

is Interstitial Volume IV). Particles larger than the DASR will float in a DASR matrix and will not have a significant role in the aggregate structure. This concept is shown in Figure 2.16 for different mixture types.

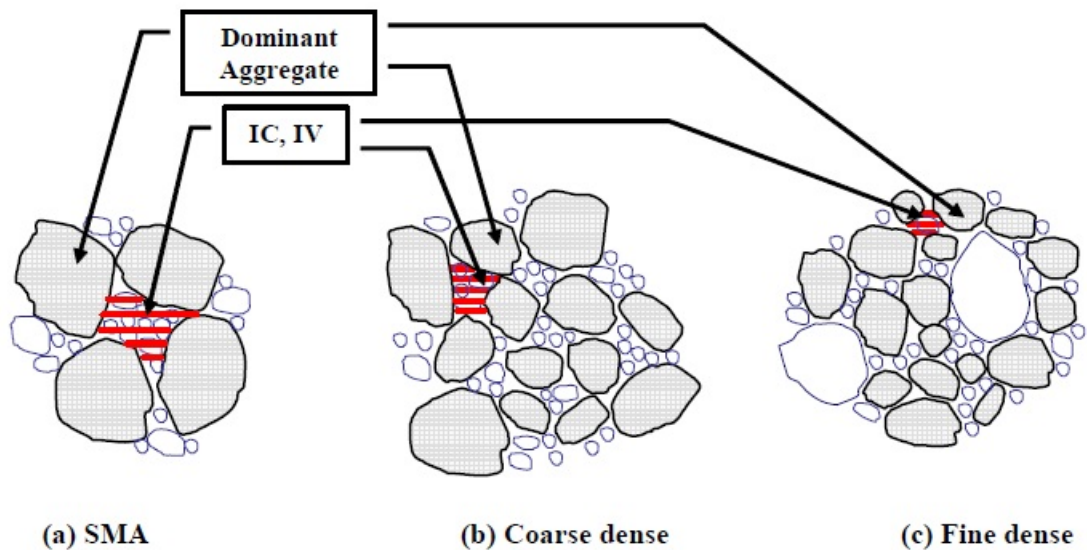


Figure 2.16: Dominant Aggregates and Interstitial Volume, Kim (2006)

The DASR could either be composed of single sized particles such as in SMA or of multiple sizes. The determination of DASR was less clear for dense graded mixtures because no single size of particles is dominant in the mixture. Therefore, a system was developed by Kim (2006) to estimate which contiguous sizes are interacting as a unit to form the DASR. Although he developed the system for contiguous sizes and it was applicable he reported that the system needs more data to prove the reasonableness of the approach, and more study is required.

Guarin (2009) studied the effect of changing the IC on the performance of asphalt mixtures. He conducted laboratory tests to evaluate the rutting and cracking

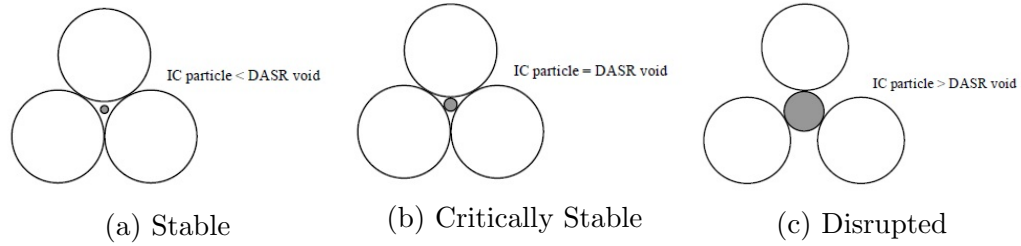


Figure 2.17: Local Disruption to DASR

of asphalt mixtures and showed that the IC have a significant impact on the results. Based on particle packing theory, he introduced a factor named Disruption Factor (DF) to evaluate the potential of IC to disrupt the DASR. The disruption factor is simply the ratio of IC volume to DASR volume (volumes are calculated theoretically). He classified the DASR disruption into two categories: local and global disruption. Local disruption is related to the effect of one IC particle being bigger than the DASR void and, in a close packed configuration of equal spheres, this is illustrated in Figure 2.17. Global disruption concerns the evaluation of the overall stability of the DASR structure.

The concept of determining the DF is to find an optimal DF range to obtain better performance of the asphalt mixture regarding rutting and cracking. If the DF is low, then the IC particles will not participate in transferring the load between DASR particles. However, if DF is in an optimal range, then better performance of the mixture will be achieved because the IC particles are engaging in transferring the load to the DASR. Finally, if the DF is very high then the DASR particles will be disrupted and this will have negative impact on the performance of the asphalt mixture, these three cases are shown in Figure 2.18.

Although the DASR approach has been used by several researchers, it will not be

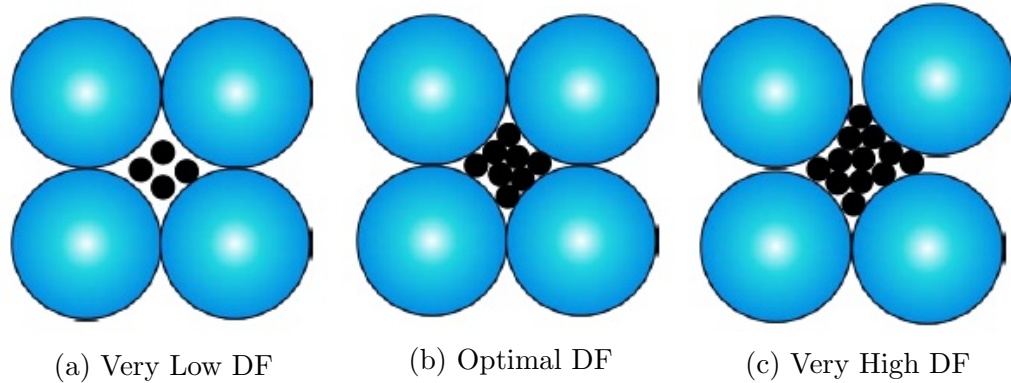


Figure 2.18: Disruption Factor Representation, Guarin (2009)

used in this study because the approach is mainly based on theoretical calculations and theoretical sphere packing assumptions, and also its applicability to dense graded mixtures is not as clear as to more open-graded mixtures. However, the principle of the DASR and disruption factor will be used to explain the different aggregate gradations in subsequent chapters.

There are some researchers that have used these concepts to analyse aggregate gradations of asphalt mixtures. Denneman et al. (2007) assessed the potential benefits of these two techniques for HMA performance in South Africa. They stated that the main difference of the studied mixtures are lie in the coarse aggregate portion and this defines the performance of the mixture. They found that there is an advantage of DASR method over the Bailey method because the analysis in DASR is independent on the control sieves. However, they did not show why the change in Bailey ratios are affecting the performance, and they stated that the mixtures with coarser particles did not mean they have better resistance to rutting, however this needs evidence.

## 2.5 Prediction of Permanent Deformation

Generally, it is well known that the response of an asphaltic mixture depends on loading time and temperature. Asphalt concrete mixtures behave as linear visco-elastic materials under low temperature conditions (or short loading times), while they behave as non-linear elasto-viscoplastic materials under high temperature conditions (or long loading times). When asphaltic mixtures behave as linear visco-elastic materials, they can be modelled using one of the physical models in which the model components are arranged as springs and dampers either in parallel or in series to best fit test results. Some of these physical models and their applications will be introduced in this section. This type of modelling supposes that the rutting in asphalt mixtures forms primarily from shear flow, and the permanent deformation is dependant on the viscous properties and independent of the elastic properties in the pavement materials (Khaznada, 2000).

### 2.5.1 Elastic Model

The elastic model is considered as the simplest constitutive model. Burmister (1943) introduced the theory of elasticity for a two layer pavement which was later developed to three and more layers. The material is identified as elastic and the loading curve is identical to the unloading curve and all of the strain is recovered when the applied load is removed. The stress and strain relationship can

be expressed by means of Hooke's law as:

$$\{\sigma\} = [D] \times \{\varepsilon\} \quad (2.7)$$

where  $\{\sigma\}$  and  $\{\varepsilon\}$  are stress and strain tensors, respectively, and  $[D]$  is the stiffness matrix that includes two material constants (Young's modulus,  $E$ , and Poisson's ratio,  $\nu$ ) and it is expressed as:

$$[D] = \frac{E}{(1 + \nu)(1 - 2\nu)} \begin{bmatrix} 1 - \nu & \nu & \nu & 0 & 0 & 0 \\ 0 & 1 - \nu & \nu & 0 & 0 & 0 \\ 0 & 0 & 1 - \nu & 0 & 0 & 0 \\ 0 & 0 & 0 & 0.5 - \nu & 0 & 0 \\ 0 & 0 & 0 & 0 & 0.5 - \nu & 0 \\ 0 & 0 & 0 & 0 & 0 & 0.5 - \nu \end{bmatrix} \quad (2.8)$$

In the use of asphaltic material, Young's modulus is replaced by "stiffness modulus" (Lee, 2006; Lu, 1998). The elastic model can be used to simulate asphalt mixture behaviour at low temperature and short loading times, and it gives an accurate prediction of real behaviour. A computer programme designed by Shell has been extensively used for elastic analysis of pavement structures, the programme being named Bitumen Stress Analysis in Roads (BISAR). Several researchers have applied the linear elastic approach in flexible pavement design and behaviour evaluation in the past (Eisenmann et al., 1977; Peutz et al., 1968; Ullidtz et al., 1987).

## Layer-Strain Approach

Many of the permanent deformation models developed in the 1970s were based on the Layer-Strain approach (Khanzada, 2000). This consists of predicting the rutting depth by using the permanent deformation characteristics which are determined from laboratory tests and the analysis procedure for the structure of the pavement uses either linear or non-linear elastic theory, Sousa and Weissman (1994). The general principle of this approach was first proposed by Barksdale (1972) and Romain (1972). The prediction of rut depth in the pavement for a given number of wheel load applications can be obtained by dividing the pavement into sub-layers directly beneath the wheel load. An assumption of linear or non-linear relationships between the elastic stress field and permanent deformation allows calculation of the permanent deformation. Obviously, non-linear elastic theory should give more accurate results (Brown and Bell, 1979). However, non-linear analysis has not been very widely used because of its added complexity (Albayati, 2006). Knowing the average stress state at the centre of each sub-layer, the corresponding axial plastic strain can be derived from laboratory results. After that the total rut depth can be calculated by summing up the plastic strains obtained at the centre of each sub-layer, considering the sub-layer thickness, by using the equation:

$$\Delta P = \sum_{i=1}^n [(\varepsilon_{pi})(\Delta Z_i)] \quad (2.9)$$

where:  $\Delta P$ : total rut depth;  $\varepsilon_{pi}$ : average plastic strain in the centre of the  $i^{th}$  sub-layer;  $\Delta Z_i$  : thickness of the  $i^{th}$  sub-layer; n: the total number of sub-layers.



Using layer-strain is a good approach for rut depth prediction as it permits the use of linear and non-linear elastic analysis. However, it has the disadvantage that this approach suggests that the permanent deformation is dependent on the elastic stress only while it is independent of the material viscosity (Khazada, 2000). The following paragraphs present a review on the use of the layer-strain approach.

Romain (1972) developed a computer programme for prediction of permanent deformation based on the layer-strain method. The layers of the pavement were divided into sublayers, and he produced model elements sufficiently thin to be considered as homogeneous in terms of vertical stress state. The stresses in each element were calculated by elastic theory and were then used with experimental stress-strain data to calculate the deformation in each element by applying a number of vehicle passages. He summed up the elemental deformation to produce the total surface deformation.

McLean and Monismith (1974) also used elastic theory to estimate the permanent deformation of a two layer system consisting of an asphalt layer and subgrade. They assigned a constant stiffness modulus for each layer and they subdivided the asphalt layer at 25 mm intervals. They calculated the stresses at the centre of each sublayer underneath the axle load based on the theory of elasticity. The stresses were then used to obtain the permanent deformation by using an empirical equation derived from the triaxial repeated load test, and they then summed up the permanent deformation for each sublayer to obtain the total permanent deformation. They compared their results with test track data obtained by Hofstra and Klopff (1972) and they found that the distribution of permanent strain were dif-

ferent from their results. The main reason for this difference was considered to be the assumption of constant stiffness with depth; in reality by increasing the loading time the stiffness is reduced.

Morris et al. (1974) developed a rutting model for the asphaltic layers where the characteristics of permanent deformation were determined from triaxial tests. Tension and compression stress modes were applied to the samples to evaluate the behaviour of the bituminous material. Comparison of the predicted rut depths with real measured values from Brampton Test Road in Canada were carried out by plotting a relationship between the total yearly permanent deformations over a period of 7 years. The model predicted that the permanent deformation occurred in the tension zone due to the lateral distortion of the material, which was the same as in the test section. Based on their model prediction they concluded that if the tensile stresses exist in the field the mechanism of rutting is due to the lateral distortion in the tension zone and the resistance to the stresses is provided by the binder only.

Monismith et al. (1977) developed a model to predict the rut depth in asphalt mixtures under repeated traffic loading. They used triaxial compression test to derive a constitutive relationship. They found that the time of loading in the triaxial test was a very sensitive factor affecting rut prediction. They computed the stresses and strains by using the elastic multi-layer system ELSYM (computer programme) and they calculated the total rut depth by summing up strain from

each layer. The plastic deformation was also calculated using the following equation:

$$\varepsilon = R \left[ \sigma_z - \frac{1}{2(\sigma_x \sigma_y)} \right] \quad (2.10)$$

where:  $\sigma_x$ ,  $\sigma_y$ , and  $\sigma_z$ : Normal Stress Components; R: Total effective strain ratio to equivalent stress.

They assumed the Poisson's ratio to be 0.5 for the asphaltic layers. The predicted rut depths were verified with real data from road sections in San Francisco, and the difference between the predicted and measured rut depth was approximately 2.5 mm.

Meyer and Haas (1977) developed a rutting model based on the approach in Morris et al. (1974). They included unbound granular materials into the model to make it more realistic. They characterised the permanent deformation characteristics for asphalt and unbound layers by carrying out dynamic triaxial tests to simulate field conditions with a variety of temperatures, densities, and loading rates. The model was verified against field results, and they used the same material as that used to construct Brampton Test Road in Canada. Based on the stresses obtained from finite element analysis, rut depths were calculated in some typical pavements. From the results they had, they found that the primary cause of rutting comes from the stiffness of subgrade material, thickness and stiffness of the bituminous layers, and the number of wheel repetitions.

## 2.5.2 Viscoelastic Methodology

The term viscoelastic is applied to material that exhibits time-dependent behaviour in a stress-strain relationship. Van der Poel (1954) defined the stiffness modulus of asphalt mixture as a function of loading time and temperature. After that researchers started to describe the behaviour of asphalt using linear viscoelastic models. The models have two main elements, a spring (which is purely elastic) and a dashpot (which is purely viscous), combined to form a mechanical model and to produce a stress-strain relationship as a function of time. By combining these two elements in series, a Maxwell model is formed, and by combining them in parallel, a Kelvin model is produced. Ossa et al. (2005) proved that these mechanical models can simulate the experimental results at low-stress level. The Maxwell model is shown in Figure 2.19 and the stress-strain relationship of each element is described as:

$$\sigma = R\varepsilon_2 \quad (2.11)$$

$$\sigma = \eta\dot{\varepsilon} \quad (2.12)$$

The strain-time relationship with different stress conditions is achieved by:

$$\varepsilon(t) = \frac{\sigma_0}{R} + \frac{\sigma_0}{\eta}t \quad (2.13)$$

where:  $\sigma$ : stress;  $R$ : linear spring constant;  $\varepsilon$ : strain;  $\eta$ : coefficient of viscosity;  $\dot{\varepsilon}$ : strain rate;  $t$ : time.

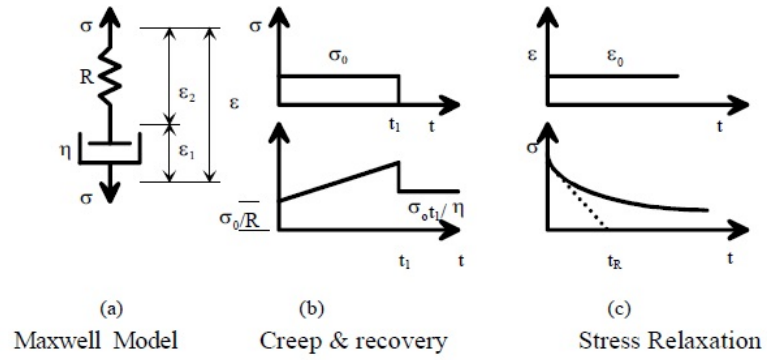


Figure 2.19: Maxwell Model and its Behaviour, Rabbira (2002)

By using the equation 2.13, it can be noticed that by applying  $\sigma_0$  at time  $(t) = 0$ , the model will behave as elastic only. The Kelvin model is shown in Figure 2.20, and the stress-strain relationship for each element presented in Maxwell is applicable.

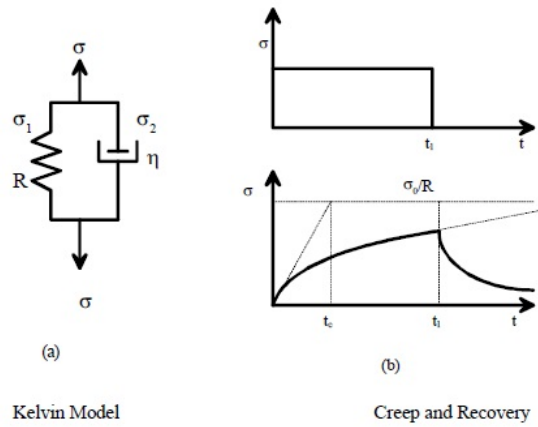


Figure 2.20: Kelvin Model and its Behaviour, Rabbira (2002)

The strain obtained from this model is described by:

$$\varepsilon = \frac{\sigma_0}{R} \left(1 - e^{-R\frac{t}{\eta}}\right) \quad (2.14)$$

The initial response of the Kelvin model when applying a stress value is that the whole stress value will be carried by the viscous element,  $\eta$ , but as the dashpot elongates the load will be transferred to the elastic element, R. Therefore, at the end of the load application the entire stress will be carried by the elastic element and this behaviour is called delayed elasticity, Rabbira (2002). The combination of Maxwell and Kelvin models connected in series produces the four-element Burger's model shown in Figure 2.21. Figure 2.22 shows the response of different mechanical model with real behaviour.

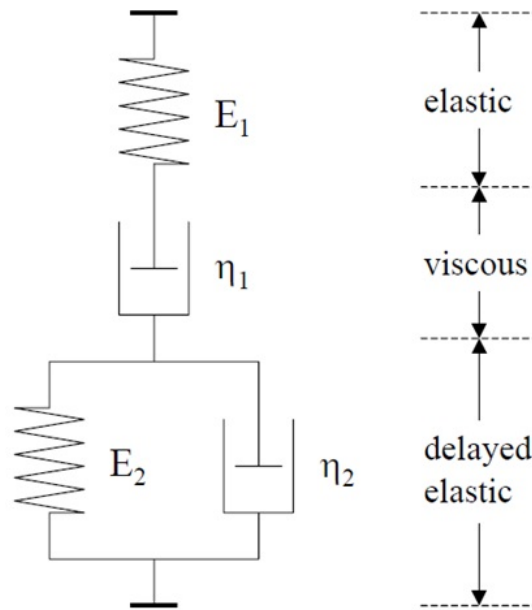


Figure 2.21: Burger's Model, Antes et al. (2003)

### Applications to Viscoelastic Models

In the last few decades, the time and temperature dependence of the mechanical properties of asphalt mixtures have been attempted to be characterised within the work frame of linear viscoelasticity. This type of model assumes that the primary

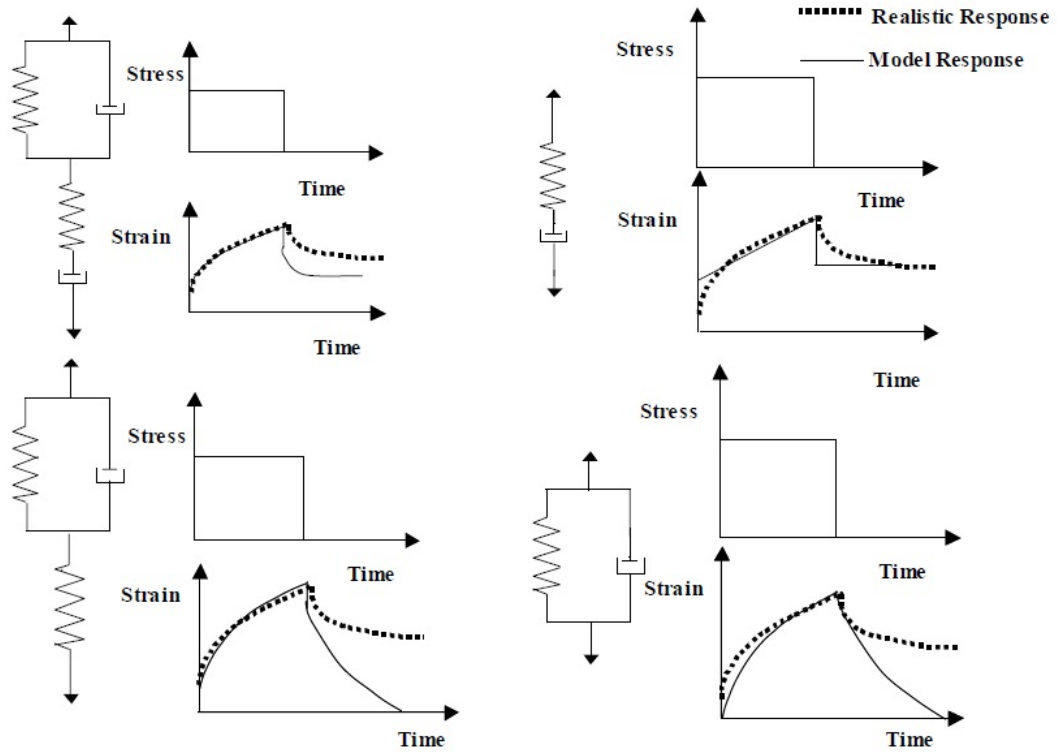


Figure 2.22: Schematic Response of Different Mechanical Models and Real Behaviour, Taherkhani (2006)

cause of rutting comes from the shear flow of the pavement materials (Khanzada, 2000). In this section, some of the past researchers work will be presented.

Monismith and Secor (1962) conducted their research on the viscoelastic behaviour of asphalt mixtures, which shows the time dependence of the stress-strain relationship. They used a Burgers model (four-element model) to fit the results of triaxial tests. They found that the four-element mechanical model was inadequate in predicting the actual results, but it was useful for identifying the properties of the mixture up to a point. The poor prediction result might have been because the model did not incorporate plastic deformation.

Gardner and Skok (1967) used the viscoelastic concept to evaluate laboratory test results and field performance. They incorporated the same Burger's model that was used by Monismith and Secor (1962) and they tested asphalt concrete samples under static and dynamic stress in the laboratory. From the static creep result, they found that the strain was not directly proportional to the stress at any time. They concluded from the dynamic load test results that the strain was dependent on the frequency of the load (the higher the frequency, the smaller the strain) and the lateral confining pressure. The main conclusion drawn from their research was that the four-element viscoelastic model can be used to predict the response of the material under given loading conditions. However, because the four-element viscoelastic theory does not incorporate the plastic behaviour of the material, it might not be able to predict under a very wide range of loading.

A two layer viscoelastic model was proposed by Battiatto et al. (1977) to predict permanent deformation in asphalt mixtures. They assumed that the subgrade is elastic and the asphaltic layers were simulated with a Maxwell model (spring and dashpot in series). They used the Unconfined Creep Test to find the material properties to fit to the model. The ridge formed adjacent to the wheel path can be accounted for in this model. Their results showed that the assumption of elastic behaviour of the subgrade led to the result of the permanent deformation due to the passage of a single wheel being independent of the stiffness of the subgrade.

A linear viscoelastic theory for permanent deformation calculation in a layered pavement system was proposed by Huschek (1977). He assumed that the unbound material is elastic and the bituminous layers have time-dependent material prop-



erties which he modelled by using the Maxwell model. Conventional and cyclic unconfined compression creep tests were used to estimate the material properties. Four factors were considered in material property estimation in the laboratory test: the distribution of temperature, the magnitude and number of repetitions of wheel loads, the transverse passage of wheel loads and the vehicle speed. He also reported that the specimen was confined to better include the influence of internal friction of aggregate. The stress and strain distribution in the material were calculated by using BISAR (elastic multi-layer computer programme) under a standard wheel load (600 kPa pressure). The rut depth was obtained by summing up the permanent deformation values through the different viscoelastic layers. The theoretical results were evaluated against real rutting data from a test road in Switzerland and good agreement was achieved between the two approaches.

### **2.5.3 Comparison of Layer-Strain and Viscoelastic Methodologies**

The layer-strain method is considered to be a “reasonable” approach to predict rut depth in asphalt mixtures because of its flexibility in incorporating linear or non-linear elastic analysis. Although the viscoelastic theory is more attractive, it is more complex to apply and results often showed poor agreement with measured rut depths; therefore, it does not have a significant advantage over the layer-strain method (Sousa et al., 1991). Concerning characterising the longitudinal ridge formed adjacent to the wheel path, the layer-strain approach is not able to predict

it while the viscoelastic approach does. The material properties are usually determined from triaxial testing in the layer-strain method while they are calculated from confined or unconfined creep test in the viscoelastic method (Khanzada, 2000).

#### 2.5.4 Linear Viscous Approach

Permanent deformation in asphalt mixtures is due to the movement between adjacent particles, surrounded by a thin layer of bitumen. The rheological properties of this binder film govern the deformation in the mixture (Hills et al., 1974). Nunn (1986) presented a viscous method to predict the permanent deformation in an asphalt mixture. The method was based on the use of the viscous part of the material behaviour; steps to predict the rut depth were as follows:

1. A plot of mixture stiffness ( $S_m(t)$ ) against loading time was derived from creep testing.
2. The binder properties (softening point and penetration) were used to produce binder stiffness ( $S_b(t)$ ) against loading time by using Van der Poel Nomograph (as shown previously in Figure 2.1).
3. The two curves were then combined to generate a plot of  $S_m(t)$  versus  $S_b(t)$ .
4. An equivalent loading time for a given number of commercial vehicle passes was then calculated at an effective temperature and used to derive the  $S_m(t)$ , and then the axial viscosity.
5. The axial viscosity was then utilised in a multi-layer linear viscous analysis to

calculate the permanent deformation accumulated in each increment of the number of commercial vehicles passes (new loading time).

The equation to determine the axial viscosity of the mixture ( $\lambda$ ) was as follows:

$$\lambda_m(t) = \frac{\sigma}{\dot{\epsilon}} = \frac{1}{\frac{d}{dt} \left( \frac{1}{S_m(t)} \right)} \quad (2.15)$$

He used the axial viscosity with the deformational Poisson's ratio in a multi-layer linear viscous analysis to determine the average rate of permanent strain and the accumulated permanent deformation in the whole pavement layer. A uniaxial creep test was conducted at 30 °C to measure the deformation of the mixture and a constant stress of 100 kPa was used. The predicted results showed an accuracy of  $\pm 30$  % compared to the measured deformation.

A new modified approach based on this analysis will be shown in a subsequent chapter to estimate the axial viscosity of the mixture in a more reliable approach. The modified method gave reasonable prediction as will be shown later.

## 2.6 Summary and Research Needs

The permanent deformation of asphalt mixtures in the top layers of a pavement can make a significant contribution to rutting. Many factors were shown to significantly affect the asphalt mixture and decrease the resistance to permanent deformation. Therefore, developing approaches to predict permanent deformation needs a good understanding of the deformation performance and the most important contributing

factors.

Laboratory tests that are used intensively to measure the resistance of asphalt mixtures to rutting were presented. There are different test protocols and conditions to measure the permanent deformation depending on what is required from the test.

The theory of aggregate packing was presented and studied extensively and it was shown how the different aggregate particle orientations and structures can affect the performance of the mixture. The Bailey method for asphalt mixture design and evaluation was presented and it was shown how the ratios were used to evaluate the mixture. More research and investigation into these evaluation ratios was found to be required to describe precisely the aggregate gradation and its real effect on the performance of the mixture. The literature showed that the evaluation ratios were mainly used for compactibility issues.

The DASR method was also presented and it was shown that it is a theoretical approach to define which size range of aggregate is carrying the load. The method has been extended by researchers to investigate how the dominant particles are disrupted by the interceptors and how this will affect the performance negatively.

The stress-strain behaviour of asphalt mixtures shows different performance at different temperatures and loading conditions. The elastic and viscoelastic behaviour were introduced and it was shown how their constitutive models perform. A review of the use of the two approaches (layer-strain and viscoelastic approaches) was presented and their advantages and disadvantages were discussed. The linear viscous approach is based on incorporating the viscous behaviour of the material into the analysis; it has shown reasonable results. An easy, efficient, and practical

way of predicting rut depth is required and this is one of the tasks of this research that will be developed in subsequent chapters.

# Chapter 3

## Soft Computing Techniques

### 3.1 Introduction

Soft computing techniques are information processing tools, and they are usually used for performance prediction and evaluation. Human type processing comprises logical and intuitive information processing while conventional computer processing is suitable for logical information only (Chattopadhyay, 2006). Soft computing techniques are developed to include human-like information processing by adding more features compared to conventional techniques, and they are used to solve complex problems. There are two main soft computing techniques: Artificial Neural Networks (ANN) and Adaptive Neuro-Fuzzy Inference Systems (ANFIS). The behaviour of asphalt mixtures is very sensitive to the change of variables such as aggregate gradation, binder content, temperature, etc. This chapter presents a brief explanation of how ANN and ANFIS work. Furthermore, the chapter will present applications of both techniques in the pavement field.

## 3.2 Artificial Neural Network (ANN)

Artificial neural networks (ANN) are considered as effective tools to solve complex problems. This section gives a brief summary of the ANN concept; information presented is mostly summarised from Gershenson (2003). The ANN model comprises *inputs* which are multiplied by *weights* (representing the strength of the relevant input). The inputs are then processed by a mathematical function which calculates the *activation* of the neuron. Another computational function is required to determine the *output* of the artificial neuron; the ANN combines artificial neurons to process information.

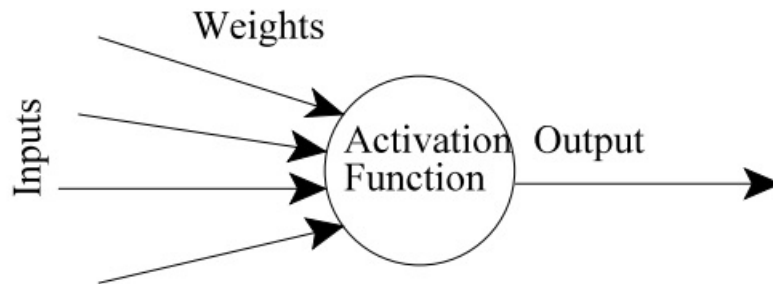


Figure 3.1: An Artificial Neuron

The weights are considered as an important part of the network describing the strength of the input. The higher the weight of a single artificial network, the more influential the input, which is multiplied by it, will be. The weights affect the computation of the neurons; therefore, the weights of an artificial network need to be adjusted until a required output is obtained. The process might be easy when only one or two neurons are used in the network, but when a large number

of neurons are used the process of adjusting the weights will be very complicated. Therefore, algorithms are required to perform the adjustment process; this process is called *learning* or *training*.

Backpropagation is the most regularly utilized algorithm type, used in training the neurons' weights (Rumelhart et al., 1986). It is used when the ANN network is organised in layers; it sends a signal “forward”, and the error is then propagated backwards. The inputs are supplied to the network by neurons in the *input layers*, and the output by neurons in *output layers*; there will be one or more than one *hidden layer* between input and output layers. The process of backpropagation uses supervised learning, which means that the users provide the network with examples of inputs and outputs they want the network to determine. The error is then computed (which is the difference between real and predicted results). The principle of backpropagation is to minimize this error until the ANN has learnt fully from the training data. The training process usually starts with random values of weights, and then these random values will be adjusted and the error reduced. ANNs are designed to learn from information supplied to them (Zaman et al., 2010; Ceylan et al., 2009).

### **3.2.1 Applications of ANN in Pavement Field**

In the past few years, several researchers have been successful in using the ANN techniques to simulate complex problems in the pavement engineering field (Demircan et al., 2010; Kutay et al., 2010; Xiao et al., 2011; Xiao and Amirkhanian, 2009;



Far et al., 2009). Lacroix et al. (2008) used previous prediction method results that predicted dynamic modulus from resilient modulus and implemented them in an ANN training model. The results showed that the ANN was an excellent tool for predicting the dynamic modulus, and the model was verified with four 12.5 mm surface course mixtures with different binder and aggregate types, and one 25.0 mm base mixture. Far et al. (2009) and Ceylan et al. (2008) similarly found that ANN is a useful tool for predicting the dynamic modulus of asphalt mixtures by using a four-layer neural network to construct the system and a backpropagation algorithm to train the data.

Xiao and Amirkhania (2009) used an ANN to predict the stiffness behaviour of rubberised asphalt concrete mixtures with reclaimed asphalt pavement (RAP). They also used statistical regression analysis to predict the stiffness via seven input variables, and they found that by using ANN the input variables were reduced to five only and better prediction results were achieved. They used a three-layer neural network to construct the system, and a backpropagation algorithm was used to train the experimental data.

Xiao et al. (2011) developed a series of ANN models to predict the viscosity values of crumb rubber-modified (CRM) binders. They used four input variables which were: the type of binder, the size of rubber crumb, mixing duration, and rubber content. Their results indicated that the ANN-based models were able to predict the viscosity of CRM binders, and also, the models are applicable for other types of rubber. The ANN models were constructed with a three-layer feedforward neural network, and a backpropagation algorithm was used to train the experi-

mental data. They performed a sensitivity analysis and showed that the mixing duration is relatively less important than other input factors.

Singh et al. (2012) predicted the dynamic modulus of asphalt mixtures based on the shape of aggregate parameters by using ANN tool. The aggregate shape parameters were determined by an automated aggregate image measurement system for coarse and fine aggregates; the shape parameters included angularity, texture, and sphericity. They constructed the model with a four-layer feedforward neural network and used a backpropagation algorithm to train the data. The shape parameters were used with loading frequency, asphalt viscosity, and air voids as input variables to the ANN.

Mirzahosseini et al. (2013) investigated the applicability of using ANN modelling to predict the rutting performance of dense asphalt mixtures. They used six input parameters to the network: percentage of coarse aggregate, filler, bitumen, air voids, VMA, and Marshall Quotient. They used statistical measures to evaluate the efficiency of the predictive tool. The ANN-based prediction model was found to be an excellent tool for predicting the flow number (a measure of repeated load permanent deformation) of asphalt mixtures. Figure 3.2 shows their predicted results compared to measured.

An ANN technique was also used by Shafabakhsh et al. (2015) to predict the permanent deformation of asphalt concrete mixtures modified by Nano-additives, and good results were achieved. Tapkın et al. (2010) used ANNs to predict Marshall test results for polypropylene modified dense bituminous mixtures, and Ozgan (2011) used it to predict the Marshall stability of asphalt concrete under different

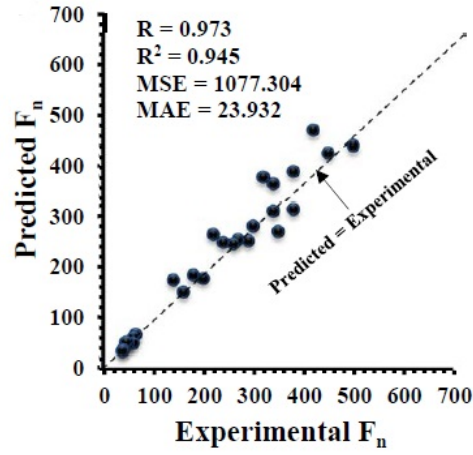


Figure 3.2: Predicted vs experimental results of Flow number ( $F_n$ ) (Mirzahosseini et al., 2013)

temperatures. The indirect tensile strength of different asphalt mixtures containing anti-stripping agents was well predicted by Gandhi et al. (2009) using an ANN.

In 1999 an equation to ease the process of using an ANN model was used by Juang and Chen (1999). They transferred their successfully trained three-layer ANN data to a spreadsheet, and the predicted output was calculated by using the following equation (Jang, 1993):

$$Output = f_2 \left\{ B_0 + \sum_{j=1}^n \left[ W_j \times f_1 \left( B_{Hj} + \sum_{i=1}^m W_{ij} P_i \right) \right] \right\} \quad (3.1)$$

where  $B_o$  = bias for the output layer;  $W_j$  = weight of connections between neuron  $j$  of the hidden layer and the output layer neuron;  $B_{Hj}$  = bias at neuron  $j$  of the hidden layer ( $j=1,n$ );  $W_{ij}$  = weight of connection between input variable  $i$  ( $i = 1, m$ ) and neuron  $j$  of the hidden layer;  $P_i$  = input parameter  $i$ ;  $f_2$  = transfer function for the output layer;  $f_1$  = transfer function for the hidden layers.

### 3.3 Adaptive Neuro-Fuzzy Inference System (ANFIS)

An ANFIS is a combination of a Fuzzy inference system and an ANN; therefore, a brief introduction to Fuzzy inference systems is required.

#### 3.3.1 Fuzzy Logic System

##### Concept

A fuzzy set is known as the extension to the crisp (classical) set which allows either complete membership or no membership to its elements (see Figure 3.3).

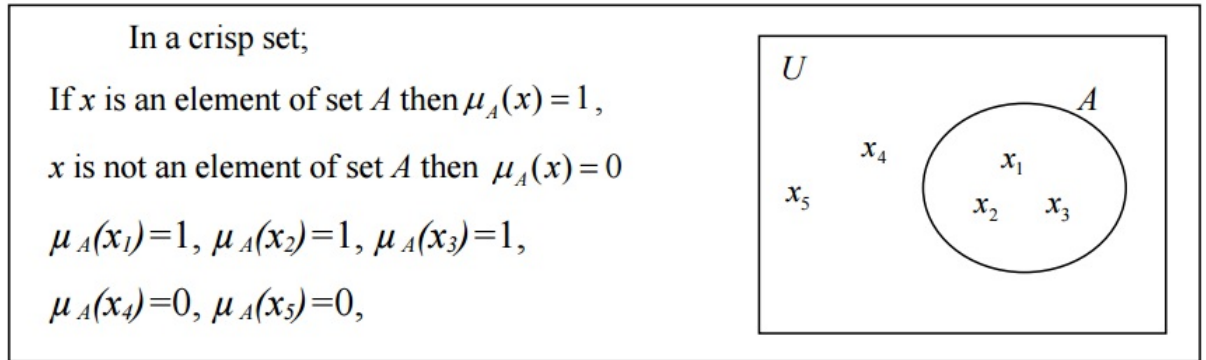


Figure 3.3: Representation of a crisp (classical) set (Selvi, 2009)

The fuzzy concept defined partial membership, a fuzzy set  $A$  on a universe  $U$  is represented by a membership  $\mu_A(x)$  which takes values between  $[0,1]$  as shown in Figure 3.4 (Selvi, 2009).

There are different forms of fuzzy membership functions, however triangular and trapezoidal are considered practical and preferred as simple linear functions (Tayfur et al., 2003). Figure 3.5 shows examples of different forms of membership

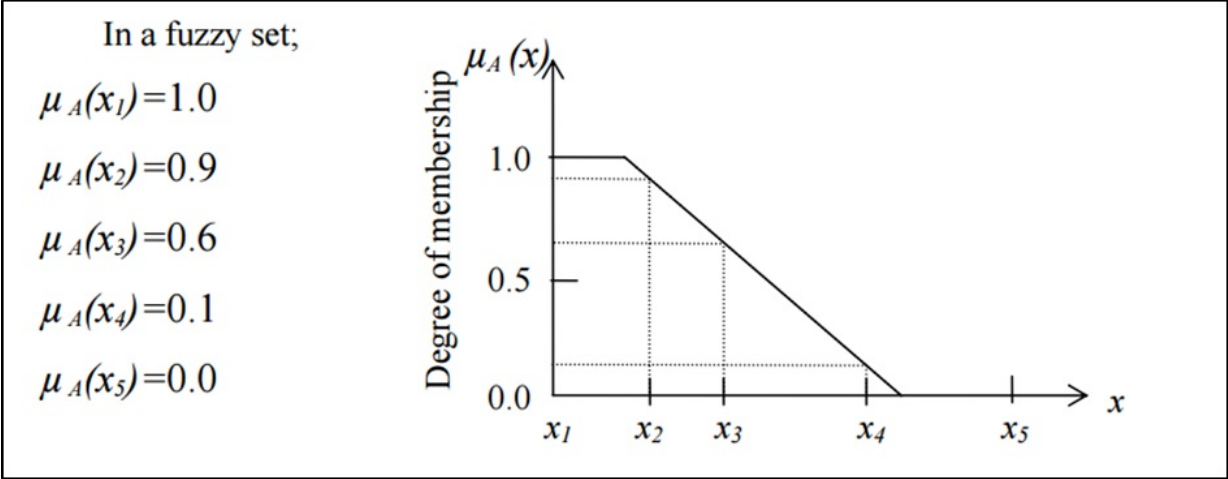


Figure 3.4: Representation of a fuzzy set (Selvi, 2009)

function.

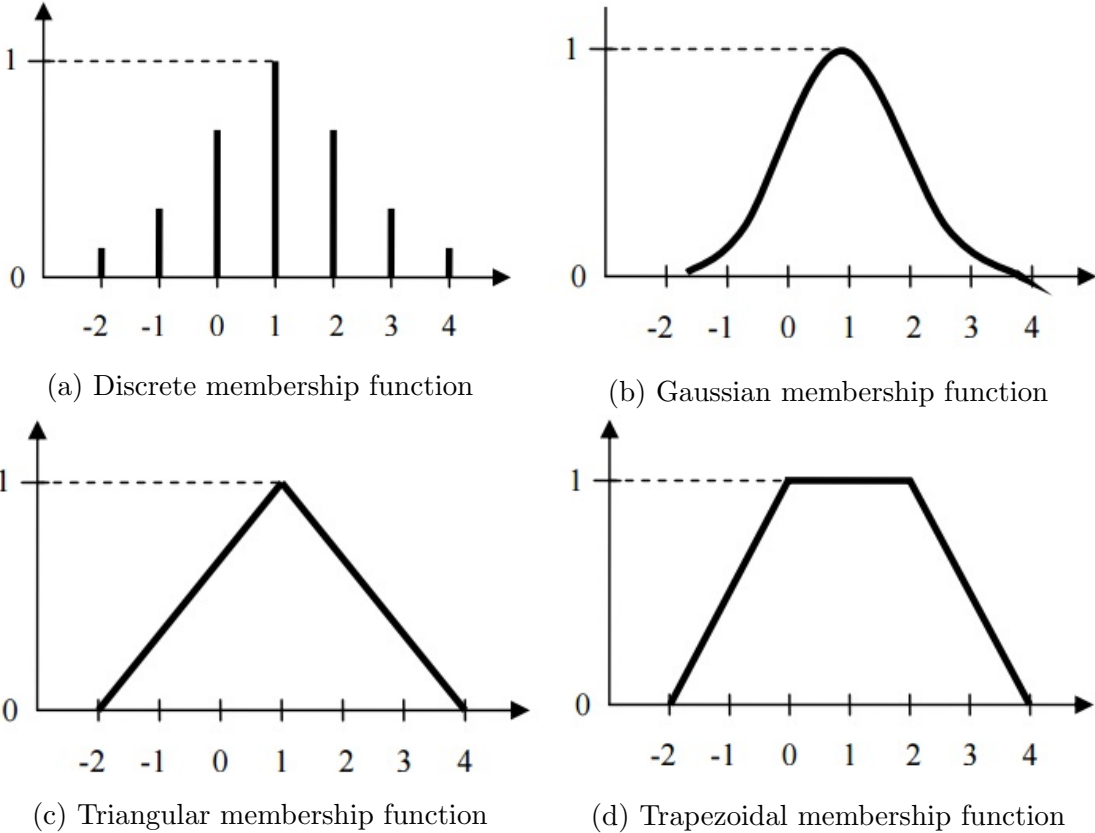


Figure 3.5: Example of Membership Function Forms

To utilize a fuzzy logic technique, the following steps are required to be per-

formed (also see Figure 3.6):

- Fuzzification: convert classical data to Membership Functions (MFs).
- Production of Rules: truth value of each rule is computed.
- Fuzzy Inference Process: combine MFs with control rules to derive the output.
- Defuzzification: convert each aggregated fuzzy output set into a single value.

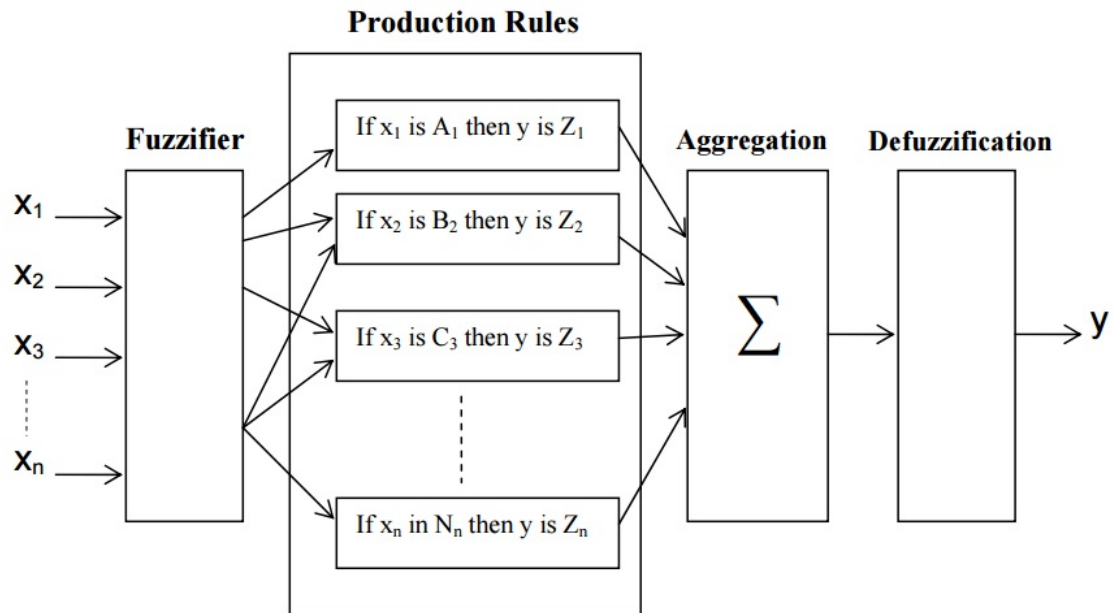


Figure 3.6: Schematic diagram of fuzzy inference system

In general two processes represent the fuzzification step: create MFs for input and output data, and represent them in linguistic labels. Fuzzy sets usually represent common sense linguistic labels such as low-medium-high, cold-warm-hot, poor-good-excellent, etc.

Fuzzy rules are represented as a sequence of IF-THEN form of the input parameters and leading to algorithms defining what the output label is (low-medium

high). There are two main types of fuzzy rule, namely, Mamdani fuzzy rules and Takagi-Sugeno fuzzy rules (Mehran, 2008). Takagi-Sugeno (called Sugeno) is widely used because it defines the output in the rule as a function of all input variables as expressed in the equation below:

If  $x_1$  is  $M_1$  AND  $x_2$  is  $M_2$  AND  $x_3$  is  $M_3$  THEN  $u_1 = f(x_1, x_2, x_3)$ ,  $u_2 = g(x_1, x_2, x_3)$

where  $x_1, x_2, x_3$ : input parameters;  $u_1, u_2$ : Outputs;  $M_1, M_2, M_3$ : fuzzy sets;  $f()$  and  $g()$  are functions of any type.

### 3.3.2 ANFIS

Jang (1993) used the advantages of artificial neural networks (which can self-learn the data and self-improve the output) and the fuzzy inference system (which uses a linguistic expression) and combined them in one technique named *Adaptive Neuro-Fuzzy System* (ANFIS). The idea behind developing ANFIS is to design a network that uses a fuzzy system to represent information in an interpretable way, and is also capable of learning from the data provided from the ANN and can adjust membership functions and linguistic rules to minimize the error between predicted and measured data (Wang et al., 2006). ANFIS is a hybrid system which uses Sugeno (uses type-3 fuzzy reasoning<sup>1</sup> as shown in Figure 3.7a) fuzzy inference system to generate fuzzy rules from the provided input and output data (Negnevitsky, 2005).

The ANFIS architecture involves a five-layer feedforward neural network shown in Figure 3.7b which includes two inputs  $x$  and  $y$  and one output  $f$ . The functions

---

<sup>1</sup>Type-3 fuzzy reasoning is also called Takagi-Sugeno type fuzzy system and is preferred for modelling linear and non-linear system (Mehran, 2008)

of the nodes in each layer are similar and defined by Jang (1993) as:

- **Layer 1:** This layer is know as the *input* layer where each node  $i$  is represented as a square node with a node function

$$O_i^1 = \mu A_i(x) \quad (3.2)$$

where  $x$  is the input to node  $i$ ;  $A_i$  is the logical label (low, medium, or high) of the membership function;  $O_i^1$  is the membership function of  $A_i$  and it specifies the degree to which the given  $x$  satisfies the quantifier  $A_i$ .

- **Layer 2:** In this layer each node is represented as a circle and labelled as  $\Pi$  which multiplies the received signals and sends the product out to the next layer:

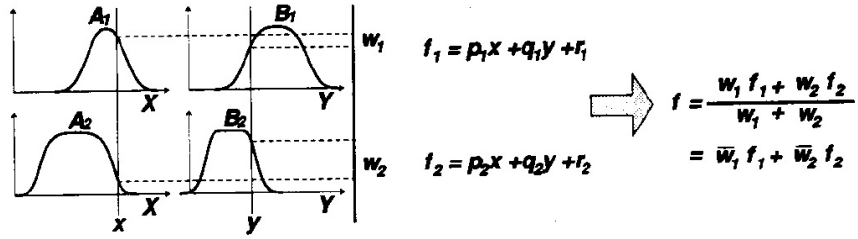
$$w_i = \mu A_i(x) \times \mu B_i(y), i = 1, 2 \quad (3.3)$$

Each output from nodes in this layer represents the firing strength ( $w_i$ ) of a rule.

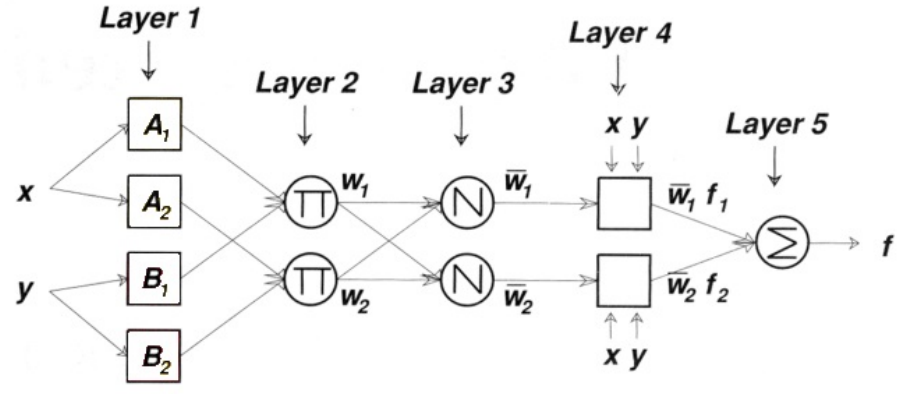
- **Layer 3:** This layer is represented as circles and labelled as  $N$ . The output of layer 2 needs to be normalized in this layer to give *normalized firing strength* ( $\bar{w}_i$ ). This can be achieved by determining the ratio of the  $i^{th}$  firing strength ( $w_i$ ) to the sum of all firing strengths:

$$\bar{w}_i = \frac{w_i}{w_1 + w_2}, i = 1, 2 \quad (3.4)$$





(a) Type-3 Fuzzy Reasoning



(b) Equivalent type-3 ANFIS

Figure 3.7: Adaptive Neuro-Fuzzy Inference System (ANFIS) (Jang, 1993)

- **Layer 4:** Nodes in this layer are represented as square nodes with a membership function ( $O_i^4$ ):

$$O_i^4 = \bar{w}_i f_i = \bar{w}_i (p_i x + q_i y + r_i) \quad (3.5)$$

where  $\bar{w}_i$  is the output of layer 3, and  $(p_i, q_i, \text{ and } r_i)$  are the parameter set referred to as *consequent parameters*

- **Layer 5:** This layer contains a single circle node labelled as ( $\Sigma$ ) which determines the overall output ( $O_1^5$ ) as the summation of all received signals:

$$O_1^5 = \sum_i \bar{w}_i f_i \quad (3.6)$$

### **Applications of ANFIS in the Pavement Field**

In the last ten years, the ANFIS technique has been used by researchers to model and predict the performance of pavement material (Moghaddam et al., 2015; Shafabakhsh and Tanakizadeh, 2015; Bianchini and Bandini, 2010; Özgan et al., 2012; Gopalakrishnan and Ceylan; Pourtahmasb et al., 2015). It was used by Moghaddam et al. (2015) to predict the rutting performance of asphalt mixtures modified with Polyethylene Terephthalate (PET). They constructed the system with three input variable: PET percentage, stress level, and temperature. They selected three bell-shaped membership functions for each input. They used fuzzy IF-THEN rules of a Takagi-Sugeno type. The evaluation of the system was based on RMSE (Root Mean Squared Error), and they found that ANFIS could learn and predict the accumulated permanent strain of PET modified asphalt mixtures.

Shafabakhsh and Tanakizadeh (2015) used ANFIS to investigate the effect of loading features on the resilient modulus (mr) of asphalt mixtures. The mr of asphalt mixtures was determined in the laboratory by using the indirect tensile test at four different temperatures. The load was applied in two forms, haversine and square, and loading time was taken at five levels, and three ratios of the rest period to loading time (R/L) were considered. Therefore, the input layer to the ANFIS included temperature, loading time, and R/L ratio; resilient modulus was in the output layer in constructing the ANFIS model. A Sugeno IF-THEN rule type was

used, and results showed that ANFIS is a very useful tool in predicting resilient modulus. In the same manner but by using a triangular membership function, Özgan et al. (2012) predicted stiffness of asphalt concrete mixtures at different temperatures and exposure time, and the ANFIS also showed good agreement with the measured stiffness.

Tapkin et al. (2012) investigated the potential of using the ANFIS technique to predict rutting in polypropylene modified asphalt mixtures by using dynamic creep test results. The test was carried out at different load values and certain temperature. They found that the Sugeno fuzzy rule system adequately predict the rutting of the modified mixture. Serin et al. (2013) used the ANFIS to predict the Marshall stability of lightweight asphalt concrete containing clay. They used bitumen content, transition speed of ultrasound and unit weight of mixtures as input variables to the model. They found that the constructed ANFIS model has a strong potential to predict the Marshall stability.

Kandil (2013) developed an ANFIS model to predict the Marshall stability and flow of the asphalt mixture based on the aggregate gradation and binder content. The model was constructed by using Sugeno type fuzzy inference system and a Gaussian function was selected to build the membership functions. He used the percent of passing of each sieve and binder content as input variables and he found that the ANFIS is a very good tool to predict the Marshall stability and flow. There are a considerable number of researchers that have used ANFIS as a prediction tool in the pavement field and found that it is useful to simulate the performance of asphalt mixtures (Tabatabaei et al., 2013; Yilmaz et al., 2011).

# Chapter 4

## Effect of Aggregate Packing on Permanent Deformation

### 4.1 Introduction

Aggregate gradation plays a vital role in the performance of an asphaltic mixture. Many researchers have examined the packing of particles, to understand how the aggregate can be structured. Starting with the maximum density of a single sized aggregate, studies have been made on the effect of particle gradation and calculation of maximum density. Regarding asphalt mix design, aggregate gradation will affect all mechanical properties. However, permanent deformation is critically affected by gradation, and this chapter will, therefore, focus on the effect of changing aggregate gradation on the permanent deformation of an asphalt mixture. The Bailey method of gradation analysis is used in this chapter to characterize asphalt mixtures. New gradation ratios are introduced to adequately describe the aggregate gradation. For

this purpose, several asphalt mixtures were selected and tested in the Repeated Load Axial Test (RLAT). This chapter aims to show how the different particle distributions affect on the permanent strain of the mixtures.

An imaging analysis will also be presented to clarify the interaction between the sizes of different aggregate particles, mainly coarse particles. After that regression analysis will be performed and it will be shown whether it is a suitable tool to predict the strain based on the aggregate gradation of the mixture or not. Following that, a model will be built using an artificial neural network (*ANN*) to make the prediction. Finally, an Adaptive Neuro-Fuzzy Inference System (*ANFIS*) will be used for more accurate prediction results. This chapter aims to make a prediction of asphalt mixture RLAT permanent strain based on the aggregate gradation of the mixtures.

## **4.2 Material Selection**

### **4.2.1 Bitumen**

In this study, a conventional 40/60 penetration grade binder was used because it is widely used in asphalt pavement engineering. According to EN (2007a) and EN (2007b), the penetration grade and softening point were found to be 44 *dmm* and 54.70 °C respectively.

### 4.2.2 Aggregate

The only type of aggregate used in this study was Bardon Hill Granite. The aggregate found in five batches named 20mm, 14mm, 10mm, 6mm, and dust. The dust is defined as range of particles sizes smaller than 4 mm and the filler used was limestone filler and was defined as passing sieve 0.063 mm ( $63\mu\text{m}$ ). The particle densities are shown in Table 4.1

Table 4.1: Particle Densities of Bardon Hill Aggregate

Aggregate Size	Particle density of aggregate
20mm	2.78
14mm	2.81
10mm	2.83
6mm	2.84
dust	2.80
filler	2.660

The gradation of aggregate was mostly selected to be within the asphalt concrete British standard EN (2005) limits of 14mm maximum aggregate size. Thirteen different aggregate gradations, most of them were chosen to cover variable ranges of Bailey ratios, were selected to understand the different particle structures in the mixtures (see figure 4.1). The British standard recommends a binder content of 5.1% for this range of aggregate gradations, so this percentage was used. Following EN (2004), the aggregate mixtures were heated up to  $160 \pm 5$  °C for a minimum period of 8 hours; at the same time, the binder was also heated up to  $160 \pm 5$  °C but for 3 – 5 hours only. The aggregate blends and binder were then mixed in the mechanical mixer at  $160 \pm 5$  °C for approximately 3 minutes. After the mixing process was completed and the aggregate particles were well coated with binder, the

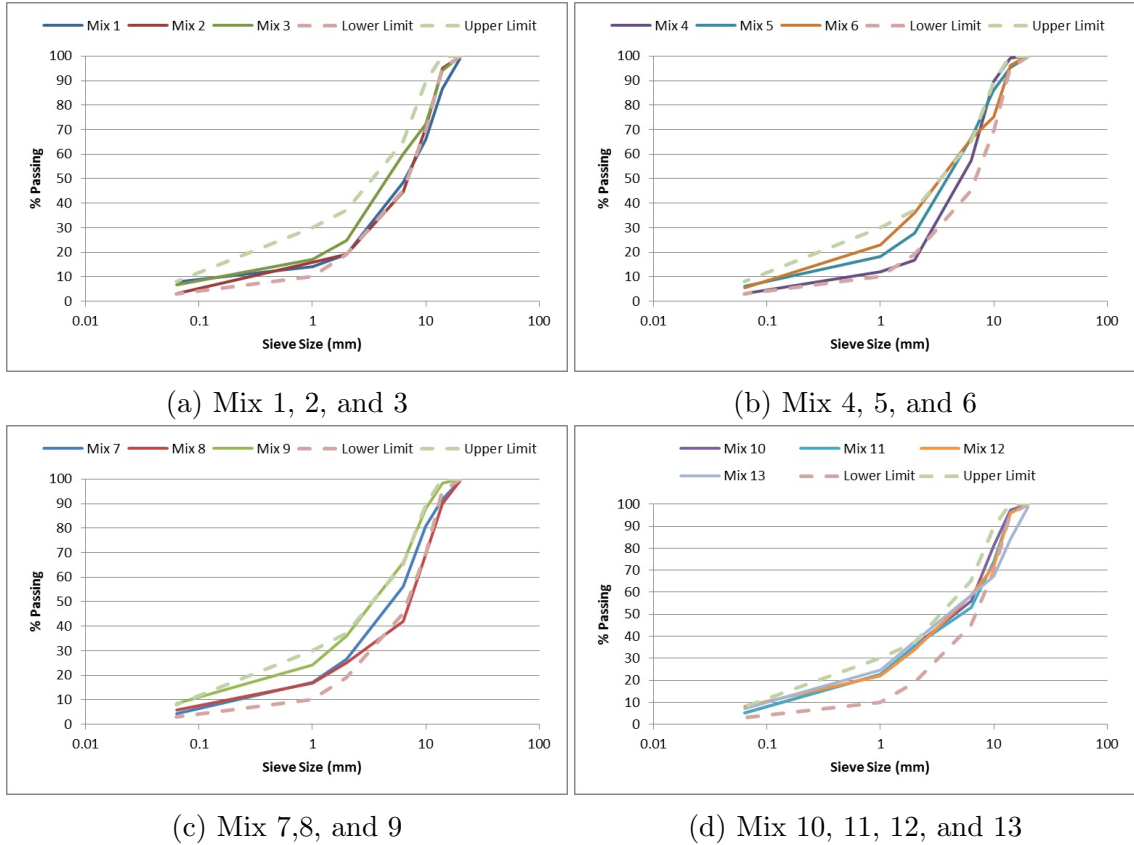


Figure 4.1: Aggregate Gradations for the Thirteen Mixtures

loose mixture was placed in the 100 mm diameter gyratory mould and compacted by the gyratory compactor at 150 °C. The mould was initially heated up, and the internal faces were lubricated with silicone grease. The compaction was performed at 0.6 MPa vertical pressure and the internal angle 1.25°. Target air voids of 5% were selected for all the mixtures. Most of the mixtures did not reach the target void content (height) so the gyratory compactor was stopped after 300 gyrations. None of the samples had a large increase in density after 200 gyrations (as shown in Figure 4.2). Three samples of each gradation were manufactured for repeatability. The samples were trimmed to a height of 60 mm so the resulting samples were 100mm diameter  $\times$  60mm height.

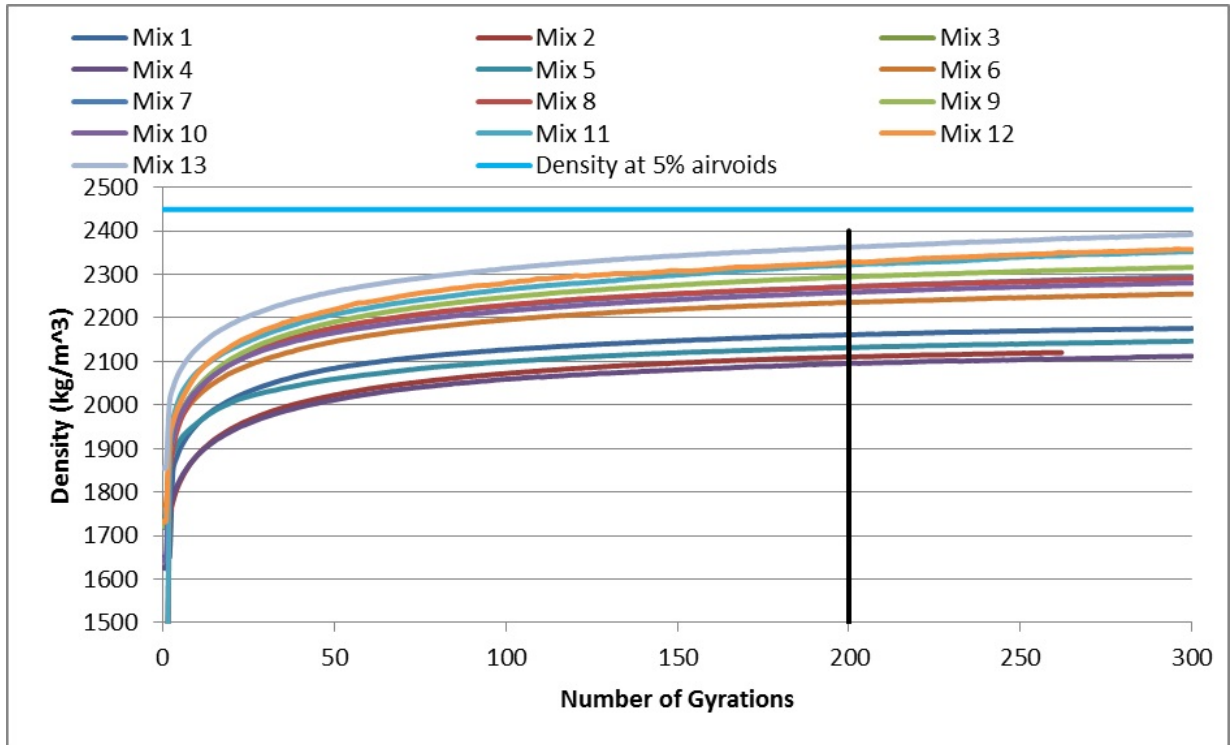


Figure 4.2: Number of Gyration vs Densities for different mixtures

### 4.2.3 Volumetric Properties

The samples were then weighed and wrapped in foil to determine their air voids content. The air voids and VMA are shown in Figure 4.3 and 4.4



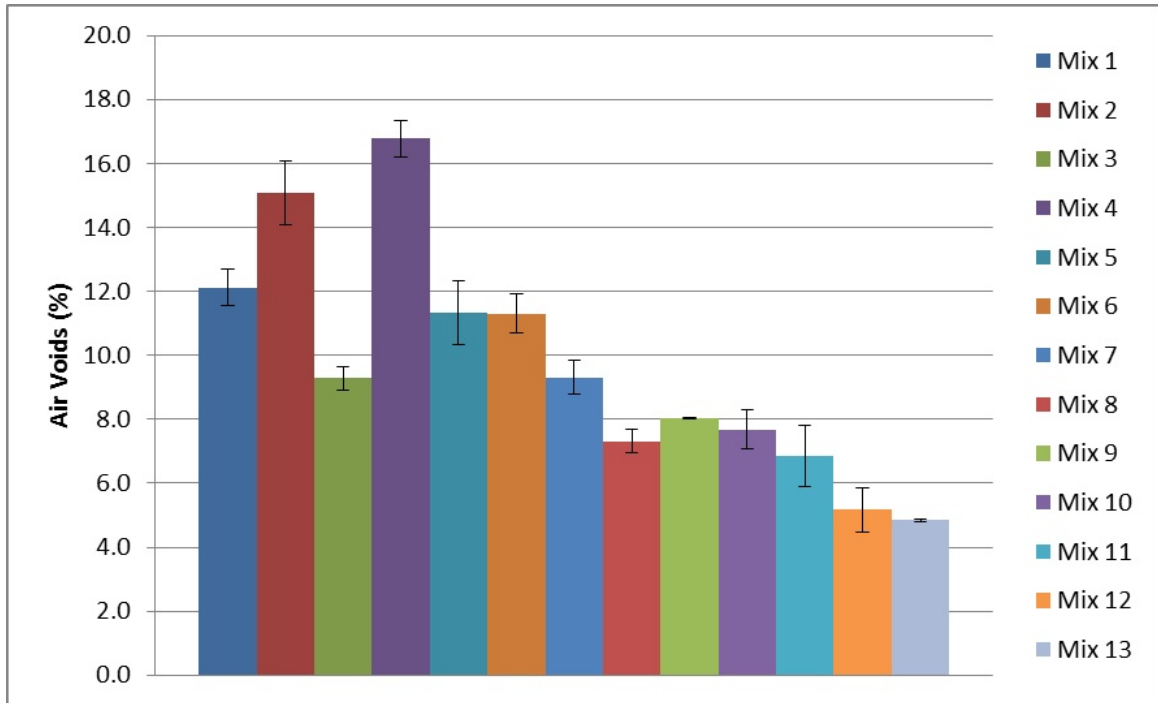


Figure 4.3: Air Voids of the 13 different asphalt mixtures

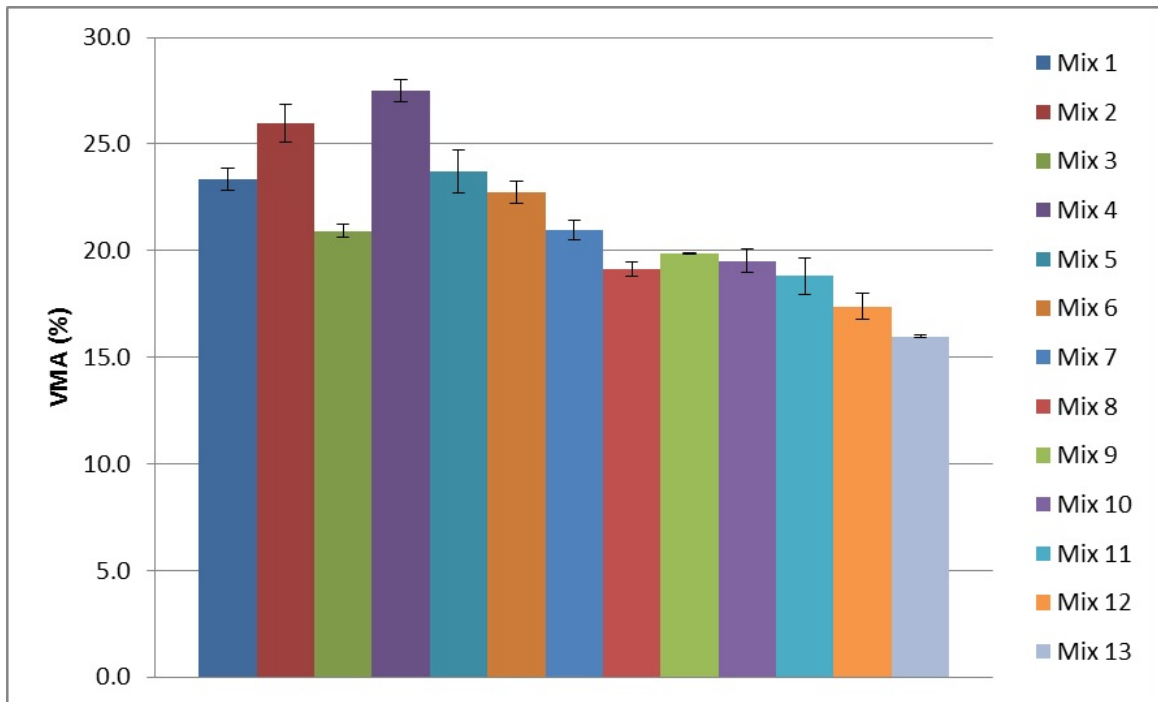


Figure 4.4: VMA of the 13 different asphalt mixtures

### 4.3 Repeated Load Axial Test (RLAT)

The RLAT test measures the permanent deformation that occurs in a sample after applying a certain stress and frequency. The test was initially conducted with standard test stress conditions of 100 kPa and 1800 cycles. The results showed little differences between the deformations which made evaluation difficult. To overcome these small differences and to better simulate the high stresses in the field, the axial stress and the number of cycles were increased to 300 kPa and 5000 cycles respectively. Each cycle comprised a 1-second load application and 1-second rest period; the testing temperature was fixed at 40 °C. The selection of 40 °C was based on the recommendation by the standards and also it is an estimate of an average yearly temperature in hot countries which the rutting is sensitive in. Both ends of each sample were coated with a thin layer of silicone grease and then with graphite powder. A typical test result, which is a relationship between total cumulative permanent strain and number of cycles, consists of three stages: primary stage, secondary stage, and tertiary stage, as shown in Figure 4.5. In the primary stage, the permanent strain accumulates rapidly and then the rate of increase in permanent strain per cycle starts to decrease until it reaches a constant value; this will be the starting point of the secondary stage. After that, the sample begins to gain strain again and the rate of strain accumulation starts to increase rapidly; this is considered to be the onset of the tertiary stage (Zhou et al., 2004). There is considerable research focusing on modelling these three stages, but it is beyond the scope of this research. Some of the samples had good resistance to permanent

deformation and did not reach the tertiary stage. The final accumulated strain is the parameter that this research will consider; Figure 4.6 shows the results of the 13 asphalt mixtures.

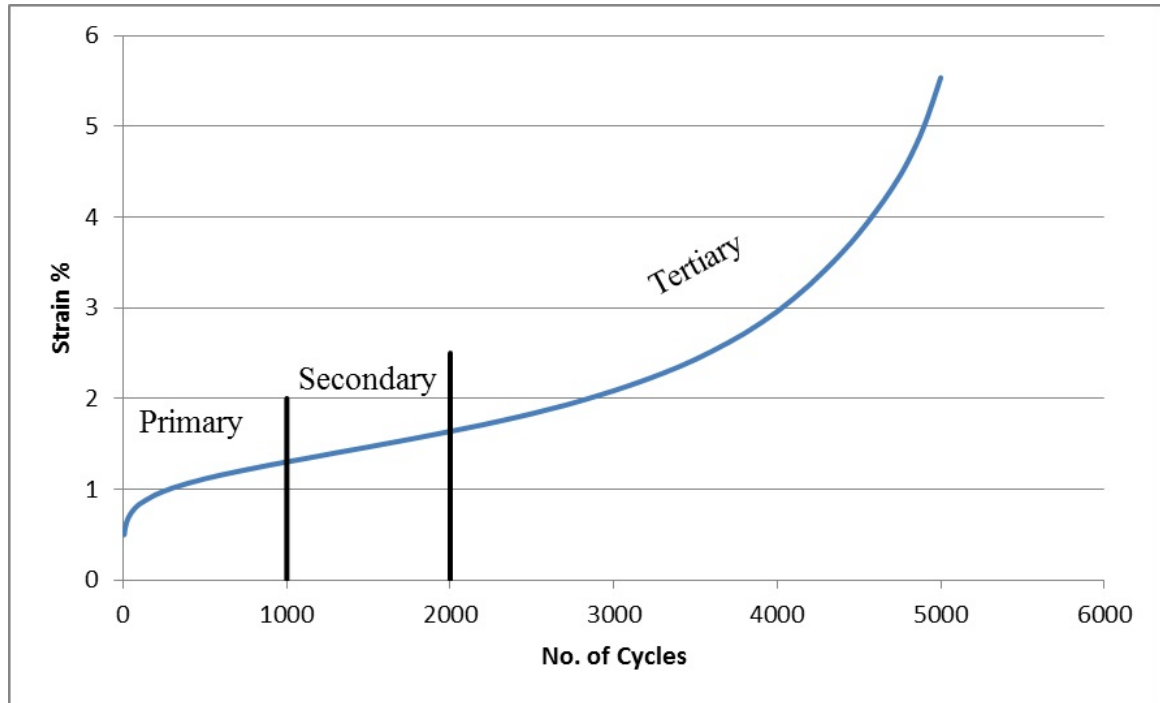


Figure 4.5: The three Stages of RLAT Test

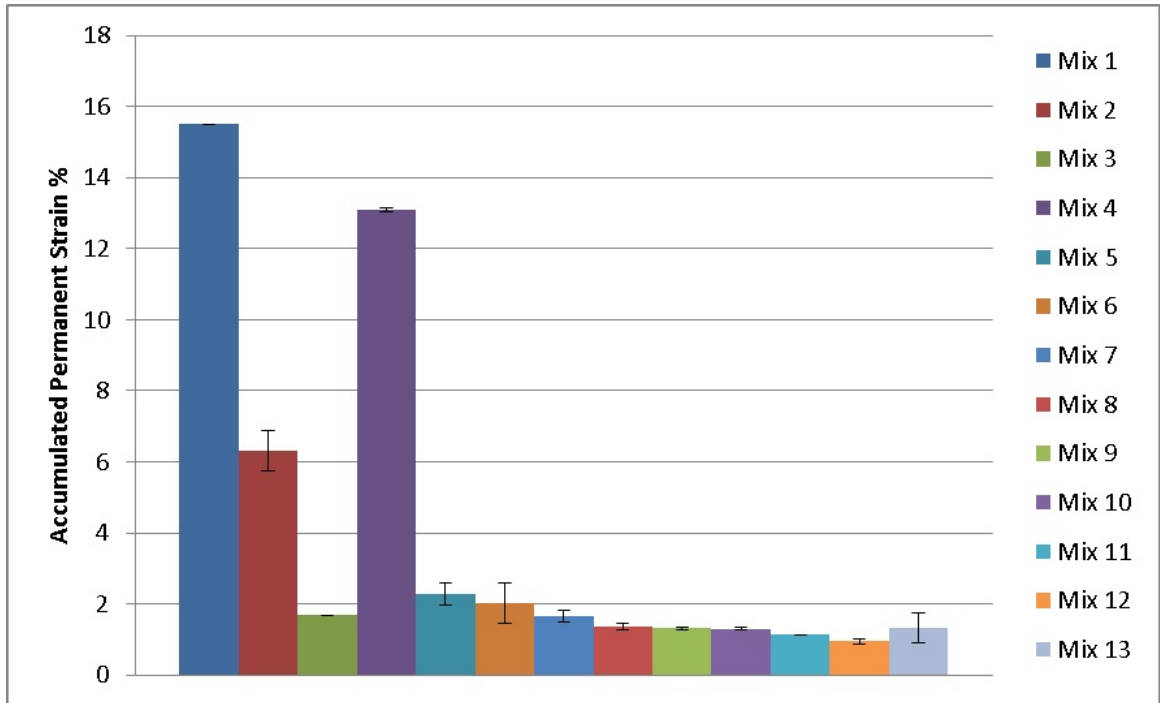


Figure 4.6: Accumulated Permanent Strain resulted from RLAT

## 4.4 Bailey Method

As mentioned earlier in chapter 2, the Bailey method introduces certain ratios to evaluate aggregate gradation. These ratios have been used in this research to assess the mixture performance in terms of mechanical properties. Permanent deformation is the main mixture property that will be evaluated by using these ratios; however, stiffness will also be assessed in the following chapter.

### 4.4.1 Control Sieves and Evaluation Ratios

Bailey control sieves are dependent on the Nominal Maximum Particle Size (NMPS), which is defined by Superpave as one sieve larger than the first sieve on which more than 10% of the aggregate is retained. Since all the mixtures have an NMPS of

14mm, then all the mixes have the same control sieves. After the calculation of the control sieves and using the factor of 0.22, the closest standard sieve was selected to be the control sieve.

$$PCS = NMPS \times 0.22 = 3.08, \text{ sieve size } 2.8mm \text{ was selected.}$$

$$SCS = PCS \times 0.22 = 0.616, \text{ sieve size } 0.5mm \text{ was selected.}$$

$$TCS = SCS \times 0.22 = 0.11, \text{ sieve size } 0.125mm \text{ was selected.}$$

$$HalfSieve(HS) = 0.5 \times NMPS = 7, \text{ sieve size } 8mm \text{ was selected.}$$

This research is not focusing on the effect of fine particles, so the TCS was not used in the analysis. The two Bailey ratios were calculated based on the selected control sieves, see Table 4.2. The third ratio ( $FA_f$ ) represents the content of the very finest material (including filler) in the mix and is important for certain aspects of mixture behaviour (e.g. voids in fine fraction, binder demand). However, this ratio will not be considered here as this study has focused on coarse aggregate effects on permanent deformation.

Table 4.2: Bailey Ratios for the 13 Mixtures

Bailey Ratio	Mix 1	Mix 2	Mix 3	Mix 4	Mix 5	Mix 6	Mix 7	Mix 8	Mix 9	Mix 10	Mix 11	Mix 12	Mix 13
$CA$	0.82	0.66	1.06	2.23	2.01	0.84	1.22	0.58	1.58	0.81	0.52	0.53	0.44
$FA_c$	0.49	0.49	0.40	0.43	0.37	0.34	0.34	0.39	0.39	0.34	0.34	0.35	0.37

#### 4.4.2 Limitations to Bailey Ratios

The  $CA$  ratio represents the interaction of the interceptor particles with the coarse aggregate (larger than 8mm) to evaluate the voids structure in the large particles. The  $FA_c$ , in turn, represents the interlock between particles in the fine fraction. These two ratios, however, do not show the interlock of fine to coarse particles,

in other words, how the interceptor particles are supported by the finer material. They also do not show the amount of coarse particles that the interceptors are supporting. For instance, in Table 4.2 Mix 1 and 6 have similar values of  $CA$ , so they both have the same level of interaction between the interceptors and large particles. However, it is not clear if this ratio is achieved from a high or low content of either interceptors or large particles. Another example is seen in Mix 1 and 10, which also have close values of  $CA$  but with different  $FA_c$ . Figure 4.6 shows entirely different deformation behaviour between the two mixes and one cannot explore the particle packing of these two mixtures to know the reason behind it simply by using Bailey ratios. For these omissions, it has been found that it is necessary to add more packing ratios to give a full understanding of the particle structure.

### 4.4.3 New Ratios

To overcome this inability to understand the full gradation curve, three ratios have been introduced based on the theory of Bailey. Firstly it was necessary to define the fine-coarse particles interlock, so a ratio has been developed as:

$$C_f/F_c = \frac{\%PassingPCS - \%PassingSCS}{\%PassingHS - \%PassingPCS} \quad (4.1)$$

where  $C_f$  : the coarse particles of the fine fraction;  $F_c$ : the fine particles of the coarse fraction.

This ratio plays a vital role in understanding the performance of the mixture. For instance, by evaluating the previous example of mix 1 and 10 one can find that

the main reason for such a difference in deformation results is that this ratio ( $C_f/F_c$ ) shows a large difference between the two mixes, 0.35 and 1.19 respectively, as shown in Table 4.3. The values of this ratio mean that the interceptor particles in Mix 1 are not well supported by the finer particles while they are in Mix 10. Up to this point, it is known the degree of which Mix 1 and 10 have interlock between large particles, fine particles, and fine-coarse particles. However, additional information is required to see the amount of large particles within these two mixtures. The reason for this is that if Mix 10 was taken as an example, it has an excellent fine-coarse particle interlock but two options are present themselves: either it has only a small amount of large particles in which case the interceptors and fine particles are carrying the load and high deformation is expected; or it has a large amount of large particles so that the mixture has a good interlock between all particle sizes. This needs the introduction of another ratio representing the percentage of coarse portion of coarse aggregate in the mix ( $CC$ ). The coarse portion is defined as particles larger than the Half Sieve (sieve size 8mm).

Finally, the ratio between the whole fine fraction to the whole coarse fraction ( $F/C$ ) was calculated to understand what the particle size range of the majority of the mixture is. These three new ratios (shown in Table 4.3) and the Bailey ratios (Table 4.2) will be used to define the full gradation curve and to predict the performance of the asphalt mixture in terms of permanent deformation (in this chapter) and stiffness modulus (later chapters). Figure 4.7 shows schematic diagram explaining the calculation of each ratio.

The understanding of aggregate structure will be further explored by assessing

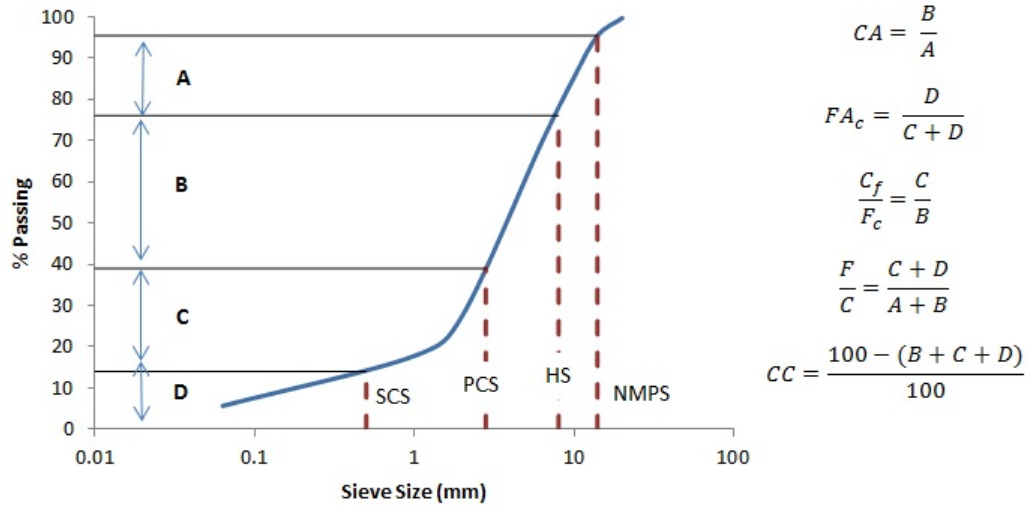


Figure 4.7: Determination of the Packing Ratios

Table 4.3: The New Ratios for each Mixture

New Ratio	Mix 1	Mix 2	Mix 3	Mix 4	Mix 5	Mix 6	Mix 7	Mix 8	Mix 9	Mix 10	Mix 11	Mix 12	Mix 13
$C_f/F_c$	0.35	0.56	0.53	0.25	0.51	1.22	0.62	0.74	0.80	1.19	1.54	1.59	1.81
$F/C$	0.37	0.47	0.50	0.31	0.58	0.90	0.58	0.52	0.83	0.84	0.85	0.91	1.23
$CC$	0.42	0.42	0.33	0.24	0.22	0.29	0.30	0.44	0.21	0.31	0.37	0.36	0.37

three mixtures. The results showed that those mixtures with higher values of  $C_f/F_c$  have better resistance to permanent deformation. However, all five ratios should be considered first to explain and define the behaviour of each gradation. For instance, by comparing Mix 1, Mix 8 and Mix 13 it can be noticed that Mix 1 has a  $CA$  value of 0.82 which means that the coarser part of the gradation (larger than the  $HS$ ) is filled with more interceptors (particles smaller than the  $HS$  and larger the  $PCS$ ) than Mix 8 or 13, which have  $CA$  ratios of 0.58 and 0.44 respectively. From this ratio one can predict that Mix 1 has fewer voids in the coarser part of the gradation than the others. However, by examining the other ratios one can observe that the  $C_f/F_c$  ratio in Mix 1 is significantly lower than in the other two mixes. As a result, Mix 1 has insufficient fine material to fill the voids between larger particles



and there will be a lack of fine particle to coarse particle interaction. The same phenomenon can be seen concerning the  $F/C$  ratio. According to such analysis, it can be predicted that Mix 8 and 13 are denser and more permanent deformation resistant than Mix 1.

## 4.5 Image Analysis

To examine the arrangement of the large particles in asphalt mixtures, x-ray scanning has been carried out for two mixtures (Mix 1 and Mix 13). This process was aimed at building a 3D analysis of the mixtures but, after taking the x-ray scans, it was found that dealing with slices in a 2D mode is adequate. Therefore, x-ray images near the top, bottom, and in the middle of each mixture were used. These images were taken to demonstrate the phenomena of ratios related to the coarse particles. The images were then processed through Avizo Fire 8.1 software. This software is used to visualize and analyse 2D and 3D material science images, Avizo (2014).

### 4.5.1 Image Processing

The images were processed with the software by using the following steps:

- Feed Avizo with the raw image.
- Apply the *Non-Local Means* Filter (if required depending on the image). This filter is considered to be very efficient for noisy data and is used in 2D mode.

The only drawback is that it is time-consuming, (Avizo, 2014).

- *Edit New Label Field* and choose a proper threshold value, (minimum value 70 maximum value 120 for an image resolution of  $600 \times 600$  pixels). The threshold range was used for separating aggregate particles from air and mastic.
- Use the *Separate Object* function: it is a module used to separate connected particles when the image is noisy, and the threshold is not able to distinguish the boundaries of each particle. The principle is to compute watershed lines on a distance map, (Avizo, 2014).
- Label the particles with different colours by applying the *Labelling* function.

The above steps are visualized in Figure 4.8. This process was applied to Mix 1 and

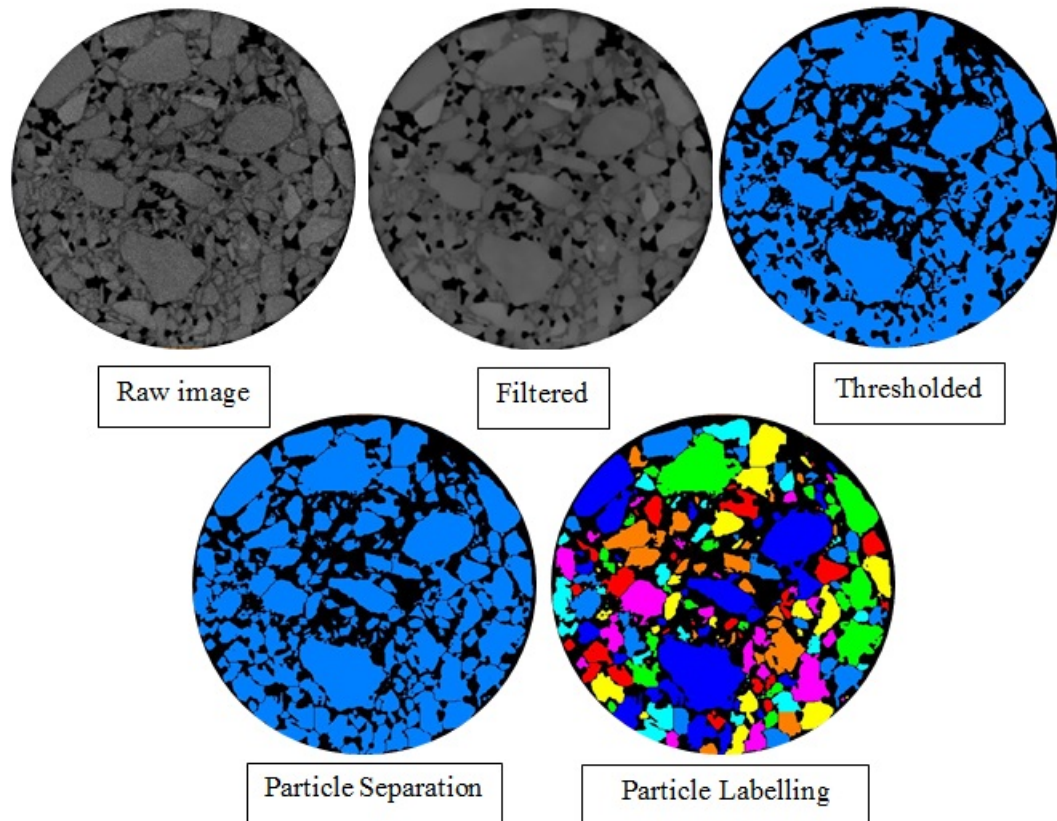


Figure 4.8: The Steps of Image Processing

13, and the resulting images clearly support the explanation made earlier in the previous section. Figure 4.9 shows the difference in aggregate structure between Mix 1 and 13. Mix 1 has large particles, and they are supported by the interceptors; however, there is little fine material visible between the interceptors. It can be seen in Figure 4.9 that Mix 13 has radial segregation. The large particles accumulated towards the outer part of the sample and a small area in the middle has more fine material. This segregation might be due to the method of compaction which pushes the large particles aside through the fine material. This did not happen in Mix 1 due to the dominance of the interceptors.

Consequently, Mix 1 has more voids than Mix 13 and most of these voids are located between the interceptors and the large particles. On the other hand, Mix 13 has a broad range of particle sizes forming a good aggregate structure. If one can imagine applying a load on both mixes, the voids in Mix 1 will tend to be filled as the material deforms and also the load will be mainly carried by the interceptors rather than the large particles as there are few direct contacts between them. Mix 1 will, therefore, develop high permanent deformation. Meanwhile, in Mix 13 the large particles are dominating and there are fewer voids between the particles so it will develop less permanent deformation.

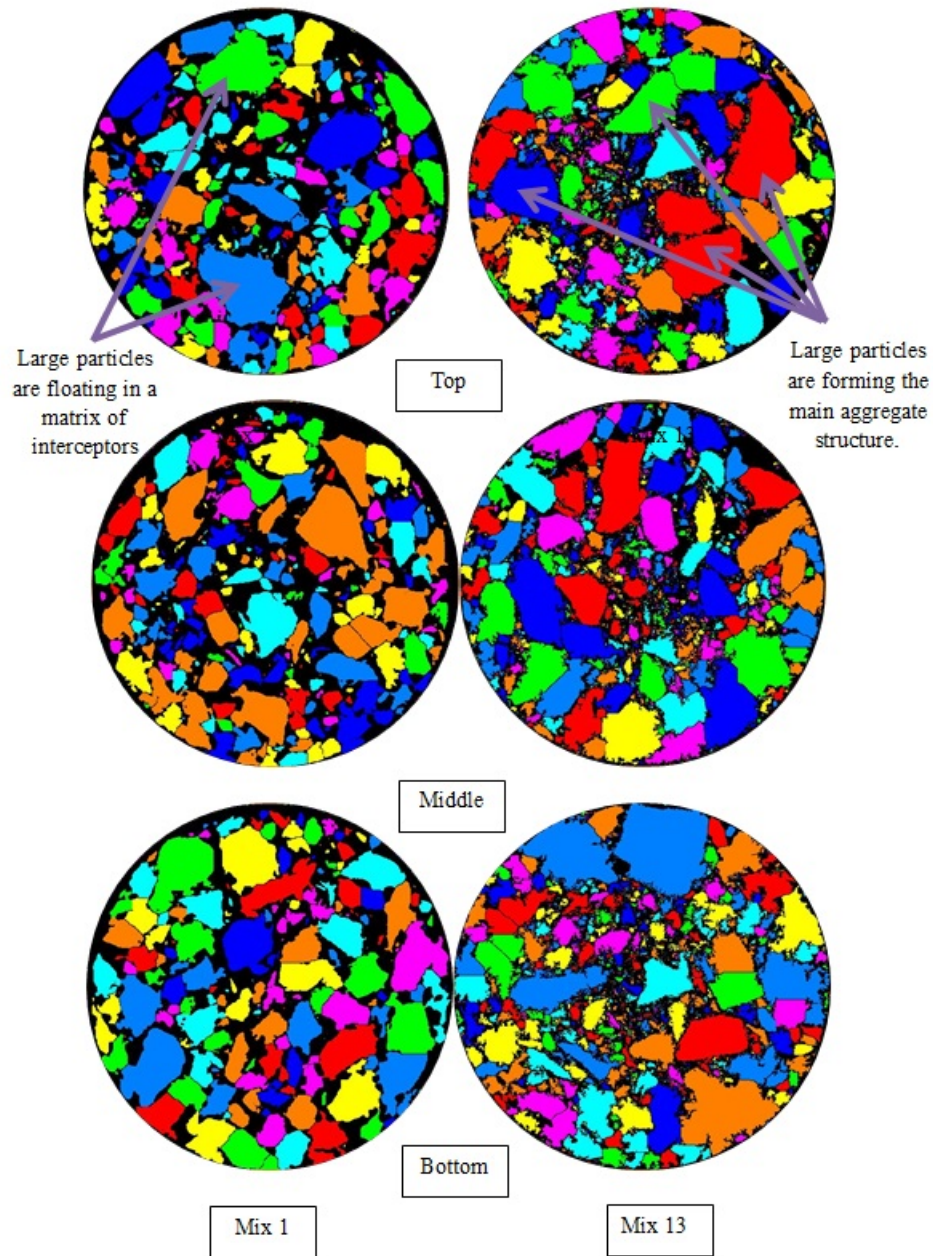


Figure 4.9: Difference between the aggregate structure of the two mixes

## 4.6 Prediction Modelling

The results obtained from the RLAT test were used to establish a model which can predict the behaviour of the mixtures. The modelling started with linear regression and then moved to the more advanced tool of intelligent networking, due to the

limitations of regression analysis.

#### 4.6.1 Linear Regression Model

The thirteen asphalt mixtures were firstly used in regression analysis aiming to predict the value of their permanent strain when 300 kPa is applied for 5000 cycles by using Minitab 17 statistical software based on the packing ratios. To achieve the most accurate results, each sample with a high strain value in the RLAT test, which may be considered to have failed, was assigned a 5.0 % permanent strain in building the statistical model. Therefore, if the model output results showed permanent strain close to 5.0 %, this means the sample is expected to have high deformation. Before the regression modelling, a multicollinearity analysis between the input variables, the five packing ratios, was performed to check if there is any correlation between them. The main parameter used in evaluating this analysis was the *Variance Inflation Factor* (VIF)<sup>1</sup>. A first round was performed by considering the five ratios as input parameters and the permanent strain as the output. It was found that there is collinearity between  $CA$  and  $CC$  and also between  $C_f/F_c$  and  $F/C$  because they have VIF values more than 5.0 and have values close to each other. Table 4.4 shows this analysis in detail.

Therefore, a second round was carried out by excluding  $CC$ , the results showed a better VIF value for  $CA$ , but the VIFs for the other pair remained high. A third round was conducted by eliminating both  $CC$  and  $F/C$ , and the final VIF values

---

<sup>1</sup>VIF measures the seriousness of multicollinearity in regression analysis. It gives a record that measures how much the variance of an expected regression coefficient is increased due to collinearity (Kutner et al., 2004).

Table 4.4: Round one of Multicollinearity Analysis in Minitab 17

Term	Coef	SE Coef	T-Value	P-Value	VIF
Constant	-6.62	6.85	-0.97	0.366	
CA	0.50	1.93	0.26	0.802	19.74
Fac	26.86	8.97	3.00	0.020	3.63
CF/Fc	1.97	2.00	0.98	0.357	16.40
F/C	-3.58	3.84	-0.93	0.383	16.12
CC	-4.0	14.6	-0.27	0.793	19.23

for all the input variables were then less than 5.0 (Table 4.5) which indicates that there is no correlation between them and that each is therefore independent.

Table 4.5: Round three of Multicollinearity Analysis in Minitab 17

Term	Coef	SE Coef	T-Value	P-Value	VIF
Constant	-8.51	3.70	-2.30	0.047	
CA	0.713	0.623	1.14	0.282	2.30
Fac	25.58	6.74	3.80	0.004	2.30
CF/Fc	0.205	0.919	0.22	0.829	3.86

After running this last regression analysis the statistical model gives an  $R^2$  of 79.23%, and the model equation was as follows:

$$\varepsilon = -8.51 + 0.713CA + 25.58FA_c + 0.205C_f/F_c \quad (4.2)$$

Figure 4.10 shows the predicted strain from the regression model. Some of the mixtures were relatively poorly predicted, suggesting limitations of linear regression analysis. To enlarge the database, some of the thirteen mixtures were re-manufactured but with a slight change (within 1-2 %) in the gradation due to changes in the laboratory aggregate stocks. Because of the very small change in density when the number of gyrations increased above 200 (see Figure 4.2), some of these samples were also compacted with only 200 gyrations. Their air voids and

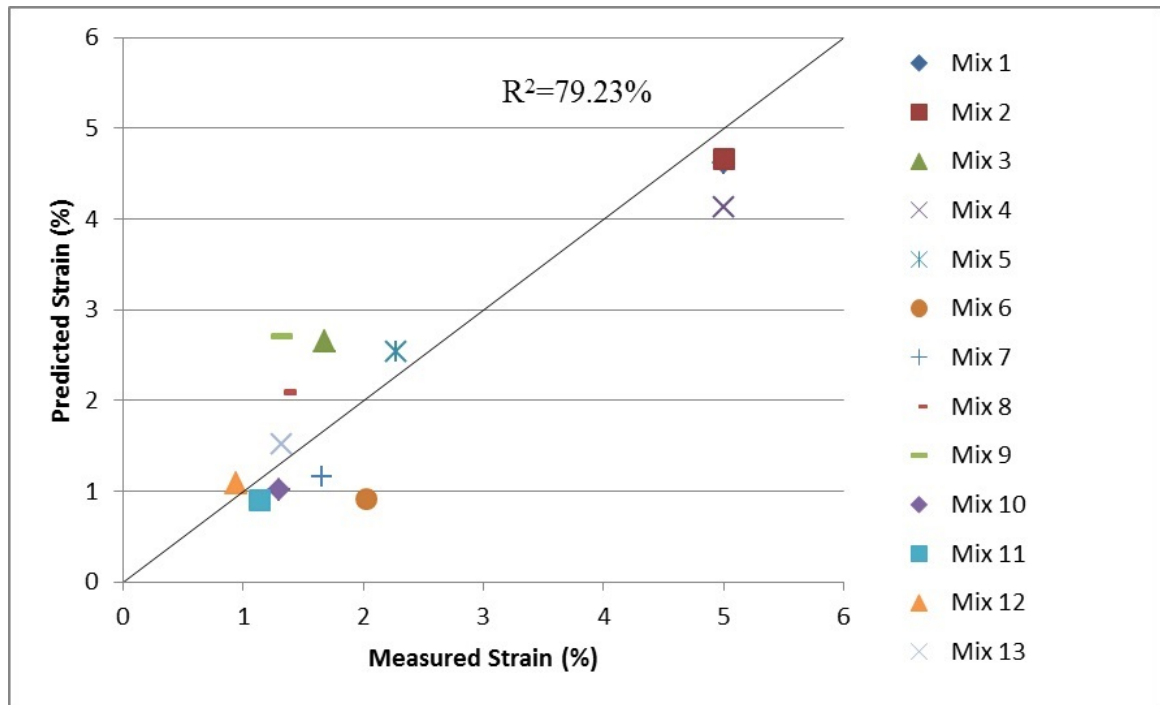


Figure 4.10: Regression Prediction Model

permanent deformation results were close to but not the same as those from the original sample set, mainly because of the slight change in aggregate gradation and the new batch of aggregate may have different aggregate shape. Two other mixtures were also added to create a proper understanding of mixtures other than asphalt concrete; these mixtures were Stone Mastic Asphalt (SMA) and Porous Asphalt. Data from all of these samples were firstly used in a standard regression model, and it was found that the model was not able to predict the results of the enlarged data set satisfactorily. These samples were then used to build a new regression model to check whether linear regression was a suitable tool for further consideration. Unfortunately, it was found not to give satisfactorily good prediction as can be seen in Figure 4.11. This is seen in the large residuals of the new set of data compared to the previous (see Figure 4.12), where the residual ( $e$ ) is the difference between

the observed and predicted values.

$$e = \varepsilon_{observed} - \varepsilon_{predicted} \quad (4.3)$$

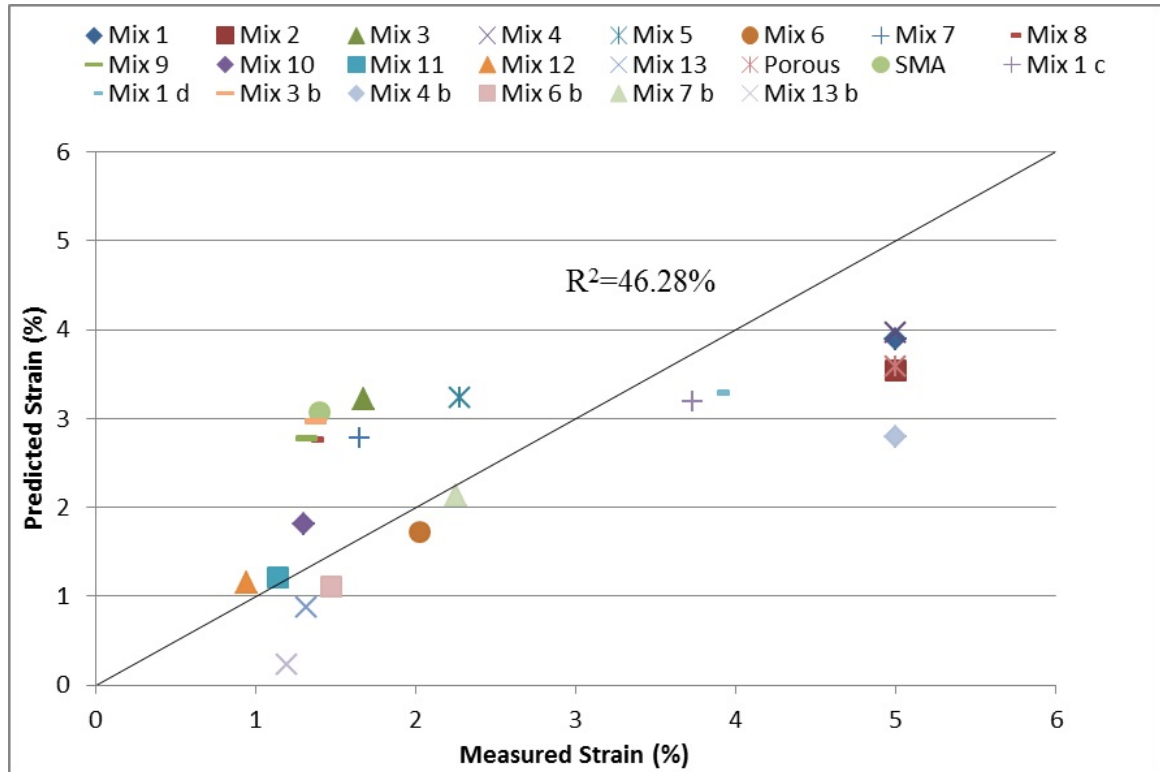


Figure 4.11: Predicted Strains for the large data set

It could be concluded that linear regression is not the right tool for building a model to predict the permanent deformation of asphalt mixtures. Therefore, other options should be considered.



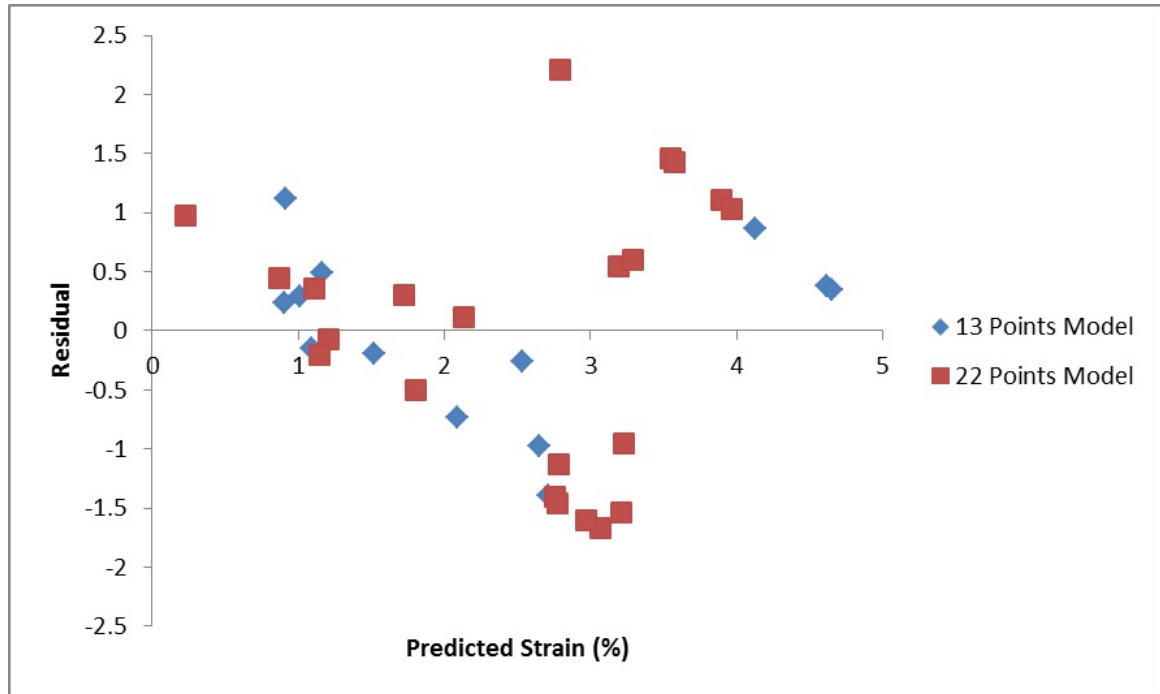


Figure 4.12: Differences in Residuals of the Predicted strains

## 4.6.2 Artificial Neural Network (ANN)

An artificial neural network is considered as a good intelligent network that is used in training data to build a model in various fields. An ANN was utilised in this study to overcome the limitations of regression modelling. Initially, the three ratios that the regression analysis recommended were used but this failed to give a good model of prediction after several ANN trials. Therefore, all five ratios were used once more to get a full understanding of the gradation details.

### Construction of ANN Model

The structure of the network used consisted of 1 layer of input with 5 nodes (5 ratios), 1 output layer with 1 node (strain), and three hidden layers with 5, 15, and 5 nodes respectively, see Figure 4.13. Each of the neurons in the hidden and

output layers has two functions: the first is to deal with assembling the weights and the second is to develop a transfer function to process the output. The accuracy of the ANN depends on the network structure; however there is no definite rule for choosing the number of hidden layers and number of neuros in each hidden layer, Tarefder and Zaman (2005). Trial iterations were made with single hidden layer, but good results were not achieved. Therefore, the number of hidden layers and neurons in each layer were selected not according to any rule but because they gave reasonable results; a different combination may also have given consistent results. Juang and Chen (1999) have produced an equation to represent the three-layer

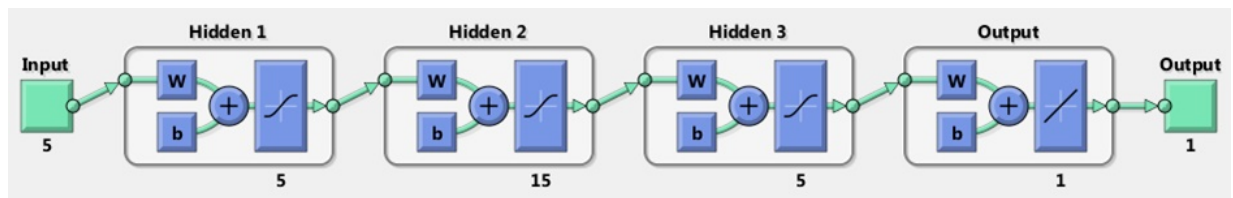


Figure 4.13: Structure of ANN

neural network. Their equation was used to ease the process of using the model by implementing it in a spreadsheet. In the same process, a four-layer neural network equation has also been derived by Lacroix et al. (2008). The output is a function of an aggregation of weights, transfer function and biases. In the same manner, an equation for a five-layer neural network has been derived following the previous two equation models. The network output is RLAT permanent strain and can be calculated by using Eq 4.4 and 4.5. A hyperbolic tangent sigmoid transfer function (tansig) function was used as a transfer function for the hidden and output layer. This function was considered to be best to simulate the network shown in Figure

4.14.

$$\varepsilon = f_o \left\{ B_o + \sum_{l=1}^r W_l f_h \left[ B_l + \sum_{k=1}^q W_{kl} f_h \left[ B_k + \sum_{j=1}^n W_{jk} f_h \left( B_j + \sum_{i=1}^m W_{ij} P_i \right) \right] \right] \right\} \quad (4.4)$$

$$f_{o,h}(T) = 2/(1 + e^{-2T}) - 1 \quad (4.5)$$

where  $B_o$  = bias for the output layer;  $l$  = subscript for hidden layer 3;  $k$  = subscript for hidden layer 2;  $j$  = subscript for hidden layer 1;  $i$  = subscript for the input layer;  $r$  = number of nodes in hidden layer 3 (i.e., 5);  $q$  = number of nodes in hidden layer 2 (i.e., 15);  $n$  = number of nodes in hidden layer 1 (i.e., 5);  $m$  = number of nodes in the input layer (i.e., 5);  $W_l$  = weight factors for the output layer (size:  $1 \times q$ );  $W_{kl}$  = weight factors for hidden layer 3 (size:  $r \times q$ );  $W_{jk}$  = weight factors for hidden layer 2 (size:  $k \times j$ );  $W_{ij}$  = weight factors for hidden layer 1 (size:  $j \times i$ );  $B_l$  = bias for hidden layer 3 (size:  $r \times 1$ );  $B_k$  = bias for hidden layer 2 (size:  $q \times 1$ );  $B_j$  = bias for hidden layer 1 (size:  $n \times 1$ );  $f_o$  = transfer function for the output layer;  $f_h$  = transfer function for the hidden layers.

Backpropagation is a supervised learning algorithm which allows for training and adjusting the network by minimizing the error between the network and target output. Random numbers of weights and biases are used to initiate the network training process, after which the inputs will be introduced to the system. The error is calculated as the difference in values of network output and target output and then propagated backwards through the neural network. The weights and biases of

each layer are adjusted to minimize the error for the next round of calculation. This is an ongoing process until a target error is reached. For this study, the training algorithm used was the Levenberg-Marquardt backpropagation algorithm (named “trainlm”) which is one of the most efficient and fastest, and 75% of the data were selected for training and 25% for testing. The ANN code (shown in Appendix A) was produced using an academic version of MATLAB 2015.

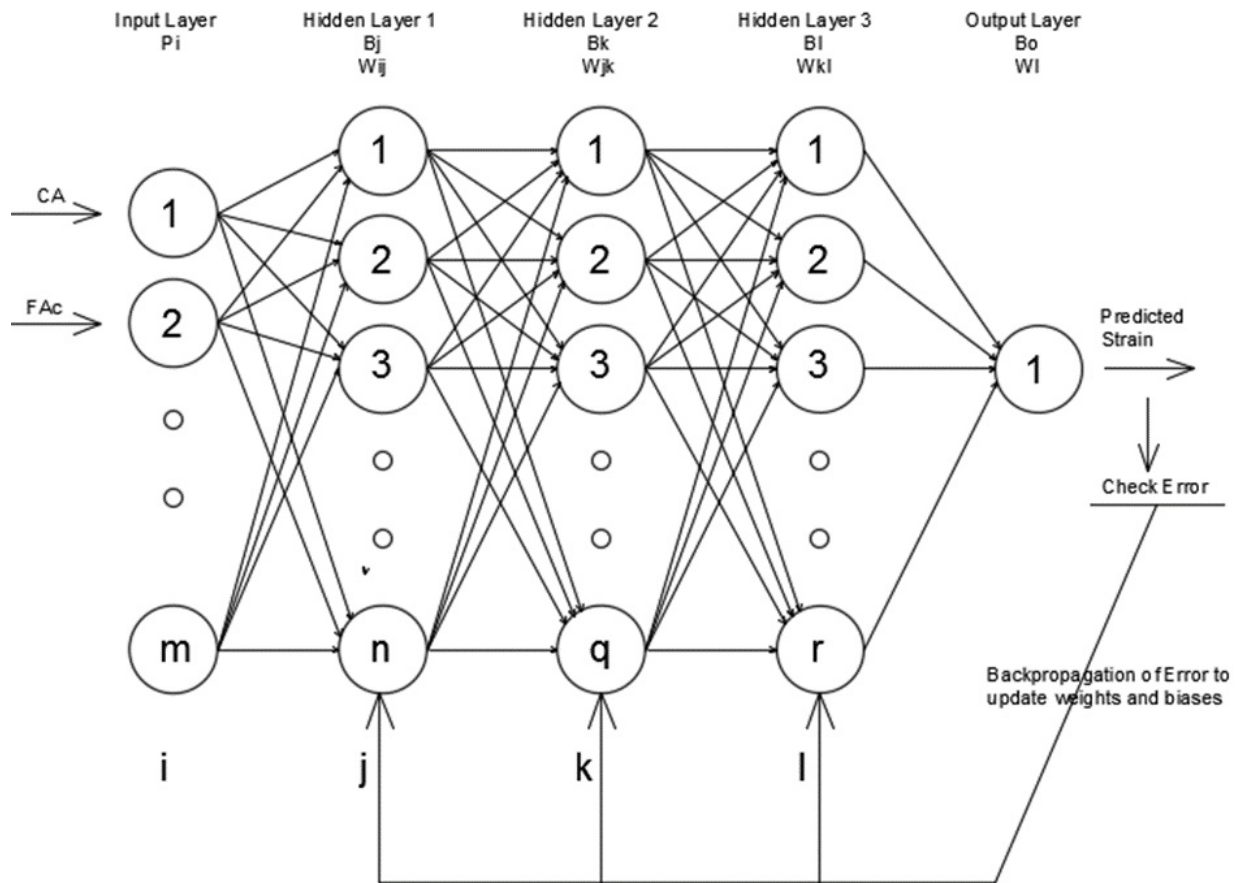


Figure 4.14: Processing of Backpropagation Algorithm

## ANN Model Results and Discussion

The performance of the model was evaluated by using an  $R^2$  value and the Root Mean Squared Error (RMSE). An  $R^2$  value, which is a measure of correlation between predicted and measured values, close to 1 reflects a good agreement between the predicted values from the ANN model and measured values. The lower the  $RMSE$  value the lower the error in the prediction; therefore good prediction is achieved with higher  $R^2$  and lower  $RMSE$ .

$$R^2 = \frac{\sum(o - t)^2}{\sum(o - o_{mean})^2} \quad (4.6)$$

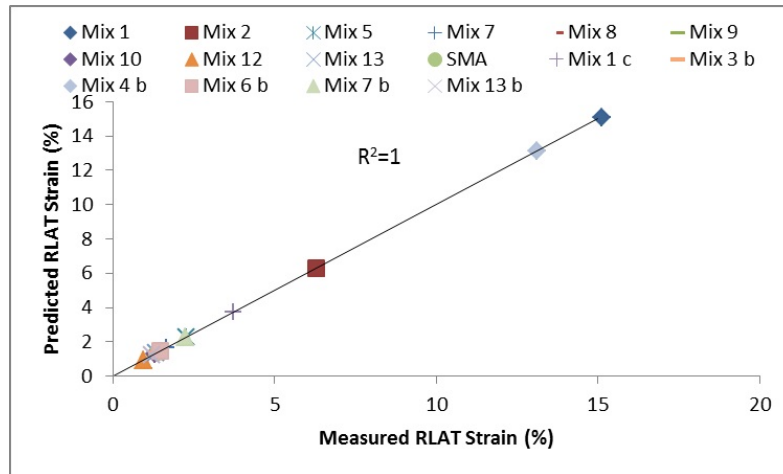
$$RMSE = \sqrt{\frac{\sum_{i=1}^n (o_i - t_i)^2}{n}} \quad (4.7)$$

where:  $n$ = total number of data points,  $o$ = network output,  $t$ = target output,  $o_{mean}$ = average of network output. The ANN model showed good agreement between the predicted and the measured strains. The predicted values are shown in Figure 4.15.

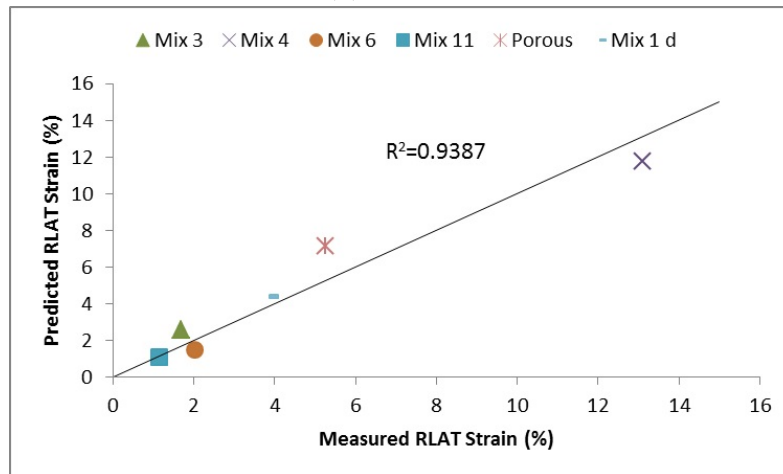
Figure 4.15 shows that the ANN predictions were very close to the line of equality (LOE), and it was evident that the ANN tool was better at predicting the strain values than regression modelling. The  $R^2$  and  $RMSE$  values for the model are shown in Table 4.6

Table 4.6: Performance of ANN Model

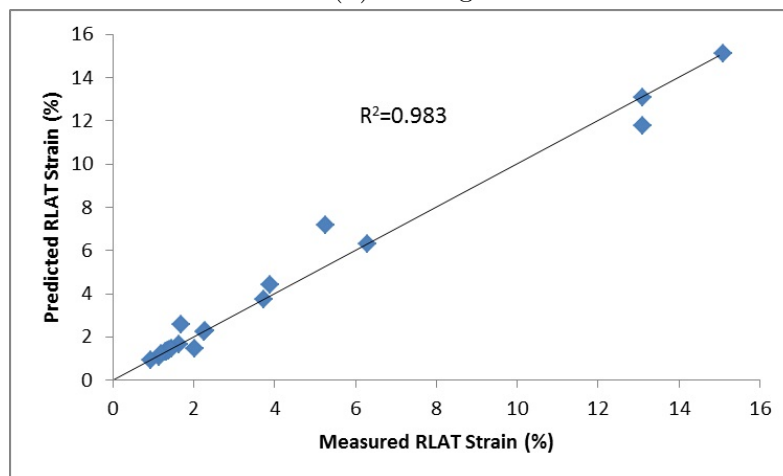
	Training	Testing	All Data
$RMSE$	1.86E-10	1.059	0.553
$R^2$	1	0.938	0.983



(a) Training



(b) Testing



(c) Training and Testing

Figure 4.15: ANN Prediction Results

It is expected that the error for the testing data will be larger because the model did not train itself on these data. Figure 4.15b shows that the porous mixture strain was overpredicted, and Mix 4 was under-predicted. However these two mixtures had high values of strain in the RLAT test, taking them into so-called ‘tertiary stage’ of strain accumulation, where a specimen approaches failure. This region is inevitably much harder to predict with confidence, and the  $R^2$  and  $RMSE$  values were highly affected by these two mixtures.

### **Sensitivity Analysis**

A sensitivity analysis for the input parameters was conducted by establishing a network for each parameter with the permanent strain.  $R^2$  and  $RMSE$  were used to evaluate the degree of correlation strength between each input and the strain. A new ANN model was made for each input variable, and it was trained and tested. The structure of each network was the same structure as for the previous ANN model (one input layer, three hidden layers, and one output layer). Table 4.7 summarizes the statistics of each ANN model for the training and testing phases. The large aggregate particles related ratio,  $CC$ , was found to have the strongest correlation with the strain with the highest  $R^2$  and lowest  $RMSE$  compared to other ratios. The ratios that are related to the fine-coarse material,  $C_f/F_c$  and  $F/C$  were found to have the poorest correlation with strain according to their  $R^2$  and  $RMSE$  values. However, when one of these ratios ( $C_f/F_c$ ) was combined with one of the others ( $CA$ ), it gave a strong correlation, better than either individually. It is therefore concluded that all the ratios are significant and important to build

a proper understanding of the aggregate particle structure and, in turn, to develop a good understanding and prediction of the performance.

Table 4.7: ANN Sensitivity Analysis

Input Parameter	ANN Model	$R^2$		$RMSE$	
		Training	Testing	Training	Testing
$CA$	1-5-15-5-1	1	0.965	2.54E-11	1.255
$FA_c$	1-5-15-5-1	1	0.947	9.64E-12	1.234
$C_f/F_c$	1-5-15-5-1	1	0.64	1.5E-13	1.171
$F/C$	1-5-15-5-1	1	0.869	1.95E-11	2.265
$CC$	1-5-15-5-1	1	0.979	1.3E-10	1.220
$CA, C_f/F_c$	2-5-15-5-1	1	0.972	3.11E-12	1.080

### 4.6.3 Adaptive Neuro-Fuzzy Inference System (ANFIS)

It is always desirable to look for a more accurate way to predict permanent strain. ANFIS is a multi-layer adaptive neural network-based fuzzy inference system which was developed by Jang (1993). This method was used in parallel with the ANN aiming to provide a more accurate prediction. As in the ANN, all the five ratios were used to build the model, but each ratio has a membership function that defines the range of each input value.

#### Construction of ANFIS Model

The structure of the model consisted of five input parameters, the inference system, and the output, as shown in Figure 4.16. In constructing the ANFIS model, the training and testing data selection is not random as in ANN. The input parameters need to be defined as membership functions (MF), so each input parameter was defined to have three membership functions named low, medium, and high. The



range of MFs is based on the range of each input value, so the mixtures with the minimum and maximum values of each ratio were included in the training process, and its membership functions were defined accordingly. This allows the model to train itself on all the critical values. Therefore, the training and testing data are not necessarily the same sets as in the ANN. The membership functions for  $C_f/F_c$  are shown in Figure 4.17 as an example. The membership functions that are used are a triangular function, and the ANFIS model was based on a Sugeno type fuzzy inference system which is widely used in asphalt mixture related analysis. The output membership function could be either constant or linear. A typical Sugeno type fuzzy inference system rule is: *If Input 1 = x and Input 2 = y, then output  $z = ax + by + c$* , for a linear membership function; if constant MF is used then ( $a = b = 0$ ). For simplicity and to reduce running time the constant function was employed in this analysis. The number of rules generated by this model was 243 based on the if-then system. In this system the input variables are fuzzified, and the fuzzy rules are then applied. After that, the weights are determined for each corresponding rule, and then the average weights for all output membership functions are calculated to evaluate the final output value (strain).

Sixteen data sets were used to train the system, and six datasets were used to test the model. In the training phase, initial values of fuzzy inference parameters (which are associated with layer 1 in the ANFIS system and are also called *premise* parameters) are assumed to predict the strain after being processed through the rules. The initially predicted strain is then compared with the actual value, and if the error is high, then the system will restart the process with adjusted values

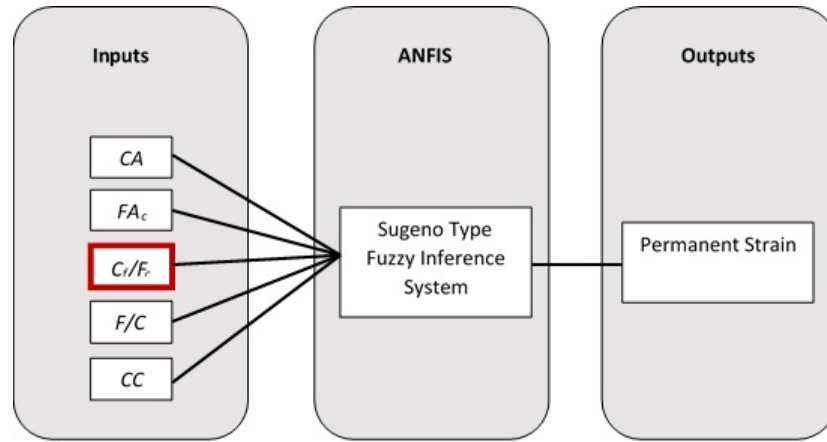


Figure 4.16: Structure of ANFIS

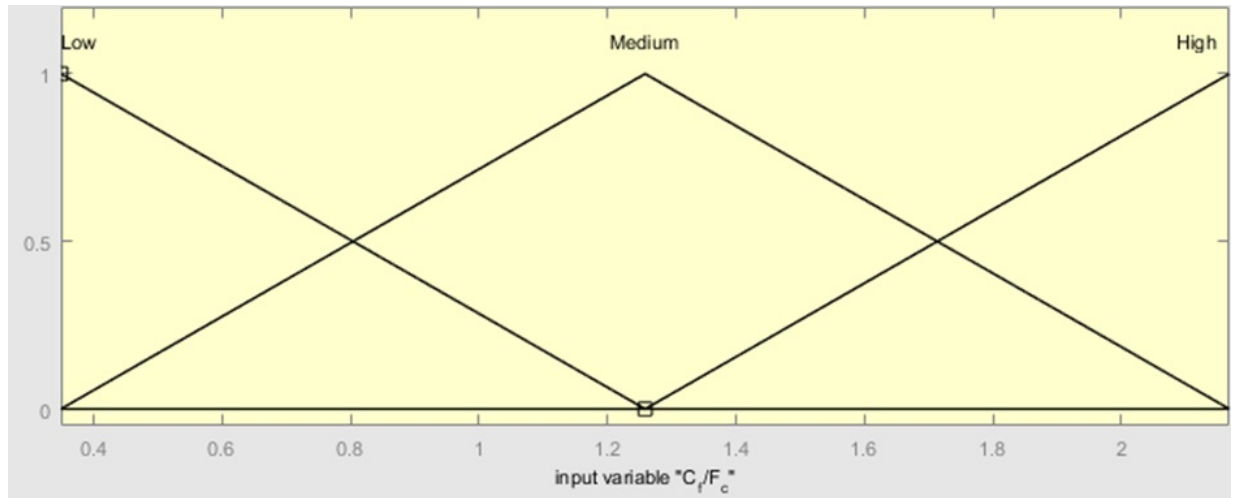


Figure 4.17: Membership function of  $C_f/F_c$

of fuzzy inference parameters until the error is minimized. The parameters are adjusted by a hybrid technique which uses the least square estimate and the gradient descent method.

### ANFIS Results and Discussion

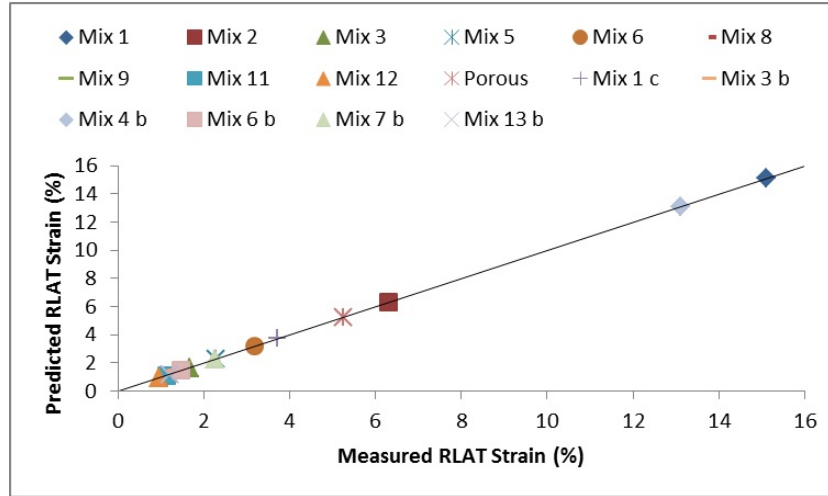
The model performance was also evaluated by using the  $R^2$  and  $RMSE$  values. The ANFIS model produced excellent and more precise predictions of the permanent strain of the mixtures. The main reason behind this is that an ANFIS generates

logical rules to understand the output. Figure 4.18 shows the network output for the training and testing data respectively. The  $R^2$  and  $RMSE$  values are presented in Table 4.8 which shows that the ANFIS network is better at predicting the permanent strain than the ANN, seen in the lower  $RMSE$  and the higher  $R^2$ .

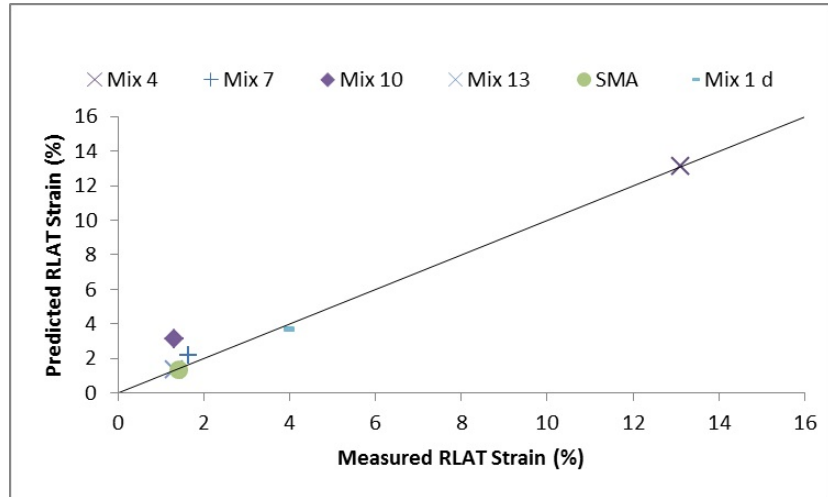
Table 4.8: Performance of ANFIS Model

	Training	Testing	All Data
$RMSE$	6.48E-5	0.786	0.411
$R^2$	1	0.974	0.991

The analyses also include the relationship between the input parameters and the output. Figure 4.19 shows the relationship surface between the inputs and output. Firstly Figure 4.19a displays the effect of  $CA$  and  $C_f/F_c$  on the strain; generally, it can be seen that when both ratios are maximized the strain will be minimized. This proves what has been explained earlier in this chapter; a higher  $CA$  ratio means healthy interaction between interceptors and coarse aggregate. So the combination of good coarse aggregate interaction (high  $CA$ ) and real fine-coarse aggregate interaction ( $C_f/F_c$ ) results in small values of permanent strain. It can also be seen that as the  $CA$  decreases with a constant high value of  $C_f/F_c$ , the strain starts to increase; however vice versa (when  $C_f/F_c$  decreases and  $CA$  is constant) is not the same performance. On the other hand, if both ratios are low then the mixture is voided (from an earlier discussion) so the resistance to permanent deformation will be poor. Figure 4.19b shows the relationship with the two coarse aggregate related ratios  $CA$  and  $CC$ , it shows that the higher the  $CA$ , the lower the strain regardless of the  $CC$  ratio value. However, as both ratios decrease the



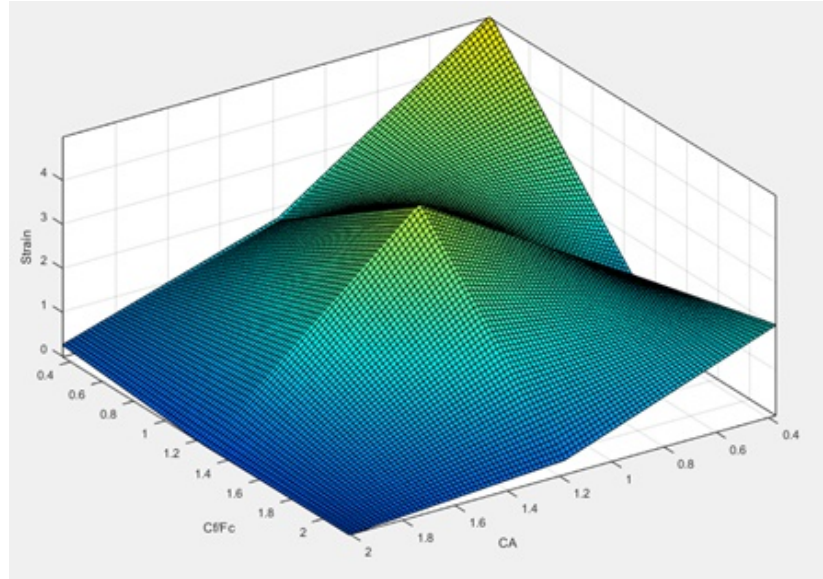
(a) Training



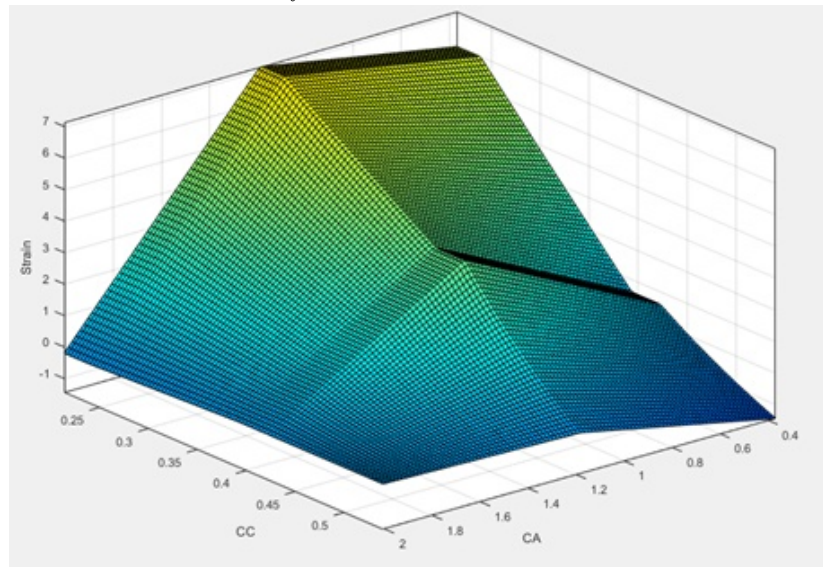
(b) Testing

Figure 4.18: ANFIS Prediction Results

resistance to permanent deformation will also start to fall. This is because the mixture will have little coarse aggregate and the main load is maintained by the finer materials, (note: negative values in this figure are related to the model training process and are not applicable to the results). The shapes of the surfaces in Figure 4.19 are clearly not uniform, and this is because it is not possible to use only one or two ratios to understand the performance of the mixture.



(a)  $C_f/F_c$  and  $CA$  vs Strain



(b)  $CC$  and  $CA$  vs Strain

Figure 4.19: Relationship Surface between the Inputs and Output

## 4.7 Conclusions

The permanent strain of asphalt mixtures has been evaluated in this chapter by using the Repeated Load Axial Test (RLAT). The primary variable which was investigated is the aggregate gradation of each mixture to discover how the change

in aggregate particle distribution will alter the packing of the particles and affect the performance. An extension to the Bailey method was used in the analysis. Several conclusions can be drawn:

- The aggregate gradations were firstly evaluated using Bailey ratios which represent the interaction between different coarse fractions and the interaction between different fine fractions. It was found that these ratios do not give a full understanding of particle interaction for the whole gradation curve. For example, it was shown that two mixtures may have a similar value of Bailey ratios, but they do not behave similarly in the laboratory. Therefore, it was necessary to introduce new ratios to fully understand the gradation curve. Three new ratios were added to cover the interaction between the coarse-fine particles and to give an indication of the percentage of coarse aggregate in the mix.
- Image analysis was performed by taking images from three slides in two mixtures and by using image analysis software. The analysis helped to investigate how well the ratios describe the particle arrangement in the mix. The images showed good agreement with the concept of the ratios, and they contributed to an understanding of mixture performance.
- The test results for thirteen mixtures were analysed through these ratios and a linear regression analysis used to predict the strain. A multicollinearity analysis for the input parameters showed a correlation between two pairs of ratios; therefore, two ratios were omitted from the regression analysis accord-

ingly. The regression model showed reasonable prediction of strain, but when the number of mixtures increased and small changes in aggregate gradation were included, the regression analysis resulted in relatively poor prediction.

- Artificial intelligence techniques were used to predict the permanent strain from the packing ratios. An artificial neural network (ANN) was used first, and it showed good prediction when using all five packing ratios. Sensitivity analysis between input parameters and output showed that some of the ratios were strongly correlated with the strain and others less. However, it indicated the importance of all ratios in the analysis.
- The second intelligence technique was an adaptive neuro-fuzzy inference system (ANFIS) which uses certain rules to process the output. This technique provided the best prediction compared to other techniques (ANN and regression) and gave a lowest error.

# Chapter 5

## Effect of Different Variables on Mechanical Properties of Asphalt Mixtures

### 5.1 Introduction

The aggregate packing ratios gave real ability to understand and predict the behaviour of asphalt mixtures within certain conditions as presented in chapter 4. This chapter will investigate whether these ratios have the power to predict the stiffness of asphalt mixtures. In the next section, the theory of aggregate packing ratios will be used in the same manner as presented in the previous chapter but in relation to stiffness. The stiffness will be evaluated by making use of the packing ratios in linear regression modelling and artificial neural networks and a comparison with an existing stiffness prediction model will also be shown. The effects of



different variables on the performance of asphalt mixtures will also be presented in the light of packing ratios. The variables include binder content, testing temperature, and compaction effort; all these variables will be used with the packing ratios to predict the stiffness and permanent deformation of asphalt mixtures. Artificial Neural Network (ANN) and Adaptive Neuro-Fuzzy Inference System (ANFIS) tools will be used for this purpose.

## **5.2 Effect of Aggregate Packing on Stiffness Modulus**

As the packing of aggregate particles showed a significant effect on the permanent strain in the previous chapter, their effect on stiffness will also be studied. The reason for presenting such analysis is to establish the importance of using the packing ratios in understanding and predicting the stiffness of the asphalt mixtures. Therefore, the same mixtures as presented in chapter 4 (including SMA, Porous asphalt and several repeated mixtures) will be evaluated in this section. The results of the ITSM test showed agreement with the explanation of ratios detailed in the previous chapter, in that the more packed the aggregate particles, the stiffer the asphalt mixture. Mix 13 which shows a dense packing of aggregate had a higher stiffness value than Mix 1. Figure 5.1 shows the ITSM results for all the mixtures related to their densities. There is a good correlation between the density of most of the mixtures and the stiffness, although Mix 12 is an outlier.

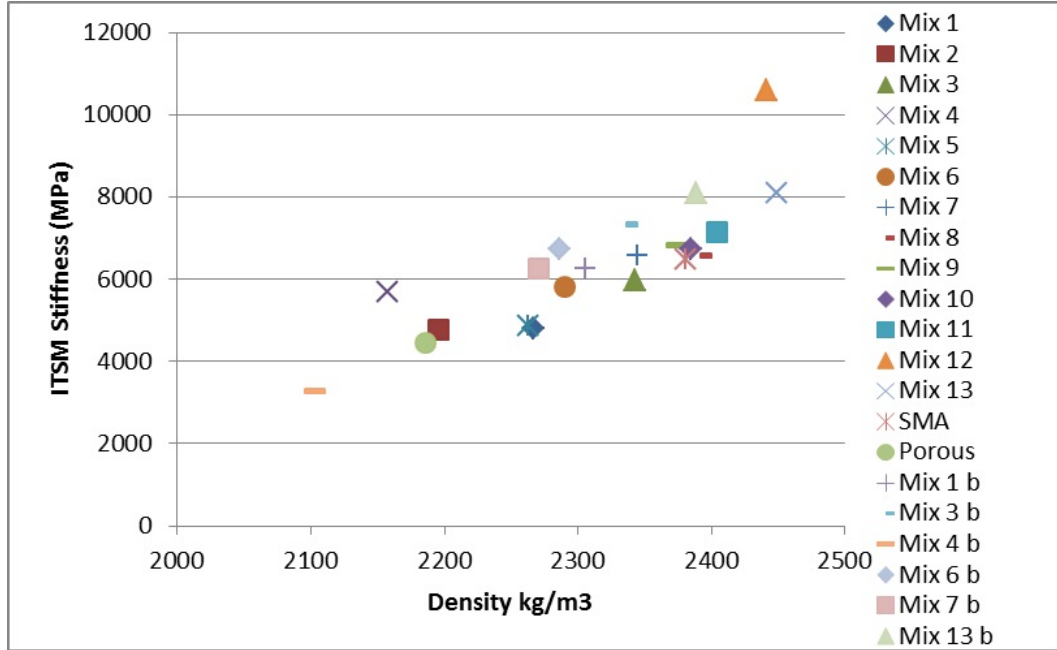


Figure 5.1: Effect of Density on the Stiffness

### 5.2.1 Prediction of Stiffness

Researchers in the past have found that the *Voids in Mineral Aggregate (VMA)* is the most influential parameter in relation to stiffness. For example, a stiffness model related to VMA was proposed by Brown (1978):

$$E_{mix} = E_{binder} \left[ 1 + \frac{257.5 - 2.5VMA}{n(VMA - 3)} \right]^n \quad (5.1)$$

where

$$n = 0.83 \log \left[ \frac{4 \times 10^4}{E_{binder}} \right] \quad (5.2)$$

Brown's model (Equation 5.1 and 5.2) was fitted to the mixture stiffness data by assuming the binder stiffness to be 140 MPa (the value that best matched the data set as a whole). Figure 5.2 shows the predicted and measured stiffness using

Brown's model.

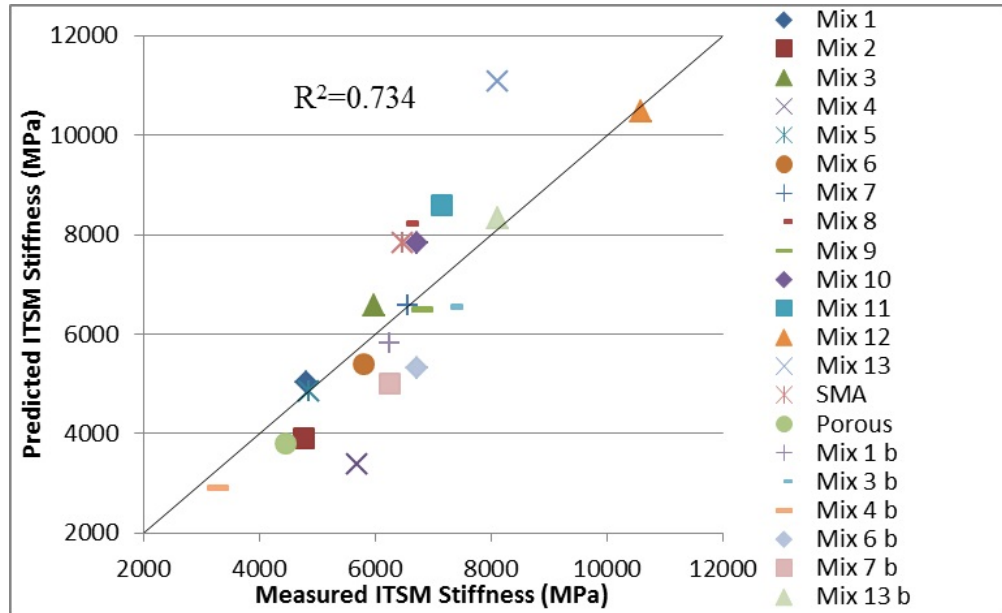


Figure 5.2: Measured and predicted stiffness for Brown's model

Brown's model depends mainly on the VMA of the blend. However, the VMA does not represent the proportions of the particles in the mixture. For instance, Mix 12 and 13 have a small difference in the values of VMA, 17.4 and 16.0 (Figure 4.4) respectively, and they gave close values of predicted stiffness as shown in Figure 5.2. However, in reality, the two mixes have quite different measured stiffness values. The VMA can be reached with various particle distributions as can be seen from Mixes 12 and 13, so it may not be the best parameter to depend on. Moreover, Brown's model also showed poor stiffness prediction for Mix 4.

### Regression Analysis

A statistical analysis was performed on the five ratios and the stiffness, and it was concluded that the same correlation between input variables as shown in Table

4.4 and 4.5 applied. Therefore, the same final three ratios were used in the linear regression analysis in Minitab 17 and the regression model is shown in Eq 5.3.

$$E_{mix} = 9181 - 765CA - 8464FA_c + 1401C_f/F_c \quad (5.3)$$

where  $E_{mix}$ : ITSM stiffness of the asphalt mixture (MPa).

The regression model showed some improvements in the prediction of Mix 13 and 4, but it predicted Mix 12 poorly. In general, the model was a useful tool for prediction apart from Mix 12 as shown in Figure 5.3. The reason that Mix 12 is stiffer than Mix 13 is because the fine material of Mix 13 is supporting much coarser material than that of Mix 12 (as shown in gradation curves in Figure 4.1 in the previous chapter). For this reason, the interlock of particles in Mix 12 is better, and they have nearly same permanent deformation resistance (as shown in the previous chapter). These details of comparison did not appear clearly in the ratios which make Mix 12 poorly predicted. To compare the performance of Brown's model and this regression model, the  $R^2$  and  $RMSE$  were calculated and these showed that Brown's model has a higher  $R^2$  but also higher  $RMSE$  than the packing ratio model. The performance of the two models is shown in Table 5.1.

Table 5.1: Performance of Brown's and Packing Ratios Stiffness Models

Parameter	Brown's	Packing Ratios
$RMSE$	1163	916
$R^2$	0.734	0.647

It can be noticed from the equation that the coarse-fine aggregate ratio ( $C_f/F_c$ ) and the proportions of the fine particles in the fine aggregate ( $FA_c$ ) are dominant

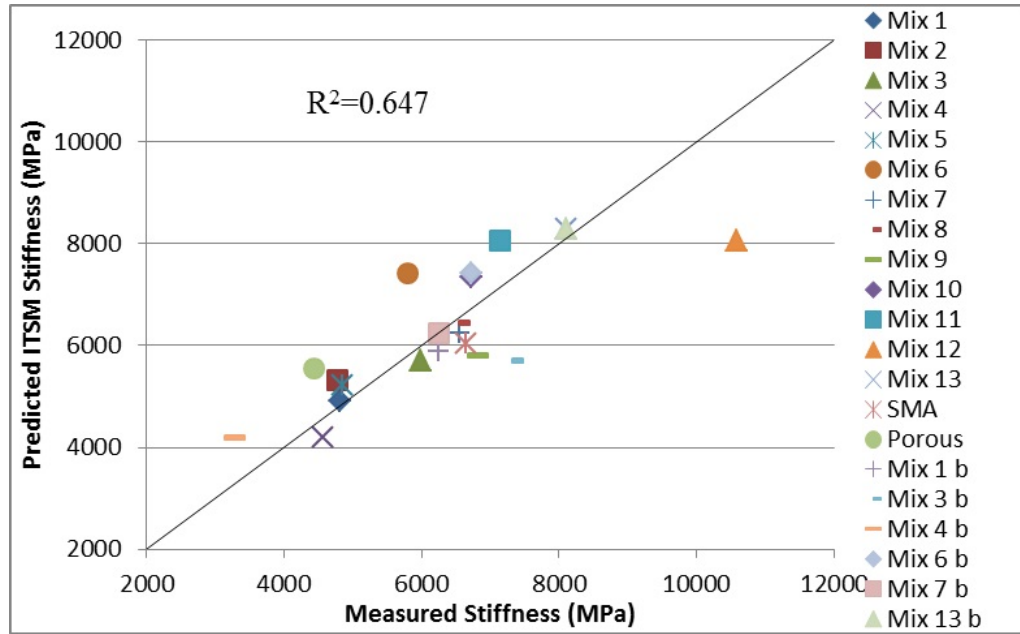


Figure 5.3: Measured and Predicted Stiffness for Aggregate Packing Regression Model

and make the greatest contribution to the result. However, these two ratios have opposite effects on the stiffness. The  $C_f/F_c$  has a *+ve* sign which indicates that as the interceptors are more supported by the finer particles, the stiffness increases. In contrast, the  $FA_c$  has a *-ve* sign which indicates that as the fine material increases the stiffness decreases. The excluded two ratios are also still needed (although not in the regression model) to describe and understand the interlock between particles.

### Artificial Neural Network ANN

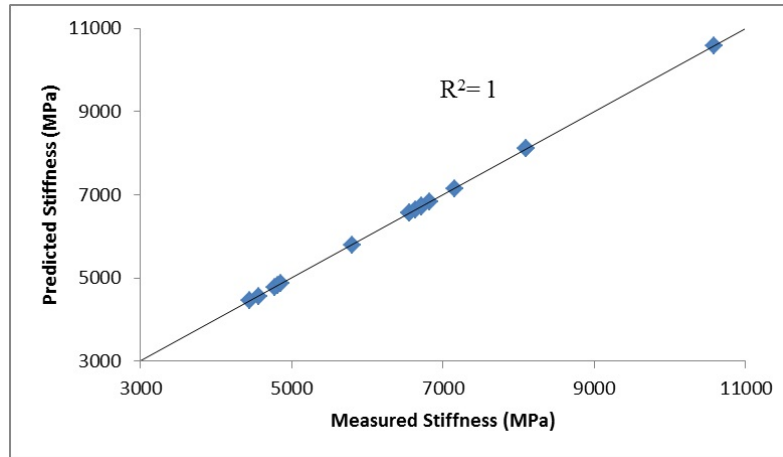
An artificial neural network was used to train the stiffness data with the packing ratios. The five ratios were used for this purpose, and the same ANN construction model presented in the previous chapter for permanent deformation were utilized in this section. The model results are shown in Figure 5.4. The model was trained on 75% of the data and tested on 25%; the results showed a good ability of the

packing ratios to predict the stiffness of the mixtures. The performance of the ANN stiffness model is presented in Table 5.2

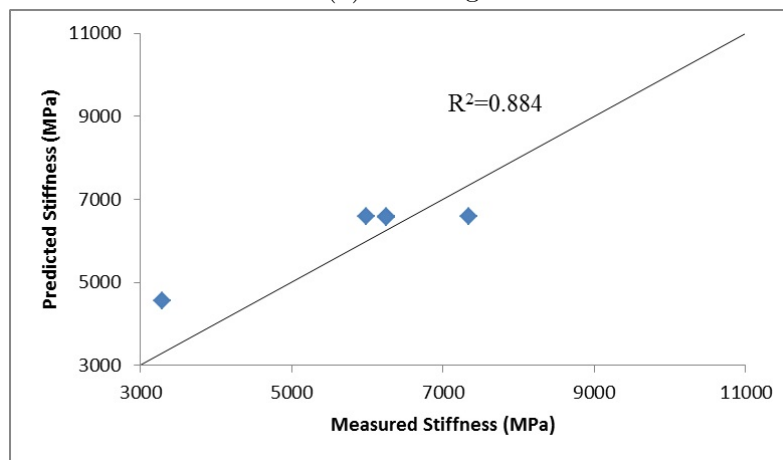
Table 5.2: Performance of the ANN Stiffness Model

	Training	Testing	All Data
<i>RMSE</i>	8.62E-07	744.2	363
<i>R</i> <sup>2</sup>	1	0.884	0.95

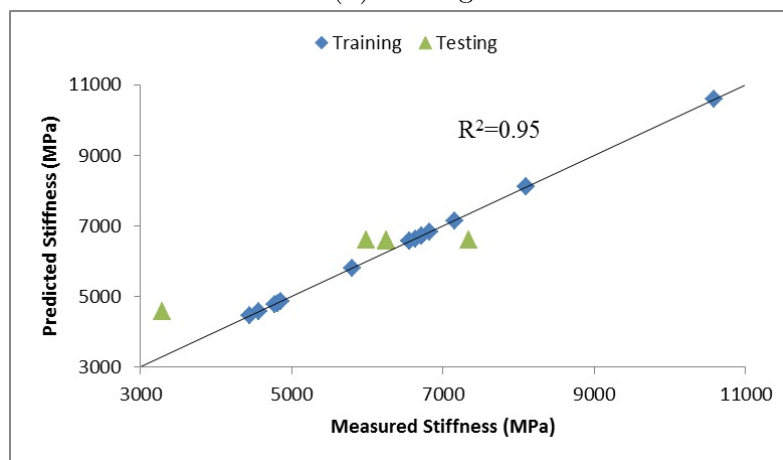
This section has showed that the aggregate packing ratios presented in chapter 4 are also significant for the prediction of mixture stiffness and the ANN model showed better performance than either Brown’s model or regression analysis. A further study will now be presented to evaluate the effect of different variables on both permanent deformation and stiffness of asphalt mixtures in the light of aggregate packing ratios.



(a) Training



(b) Testing



(c) Training and Testing

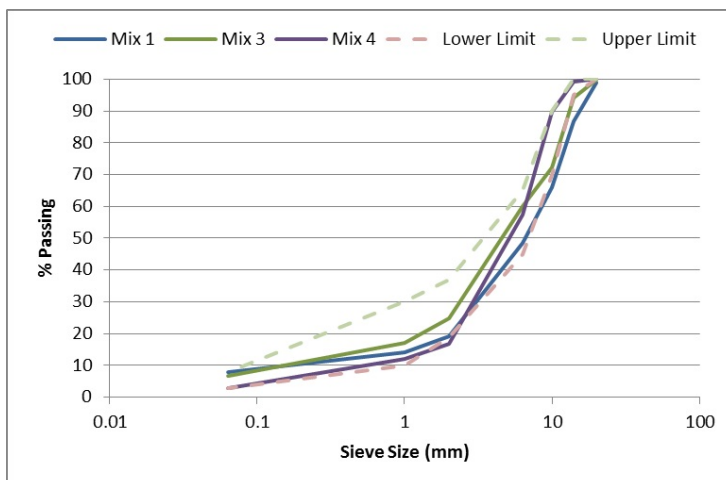
Figure 5.4: ANN Prediction Results of ITSM Stiffness based on the Aggregate Packing Ratio

### 5.3 Material Selection and Testing

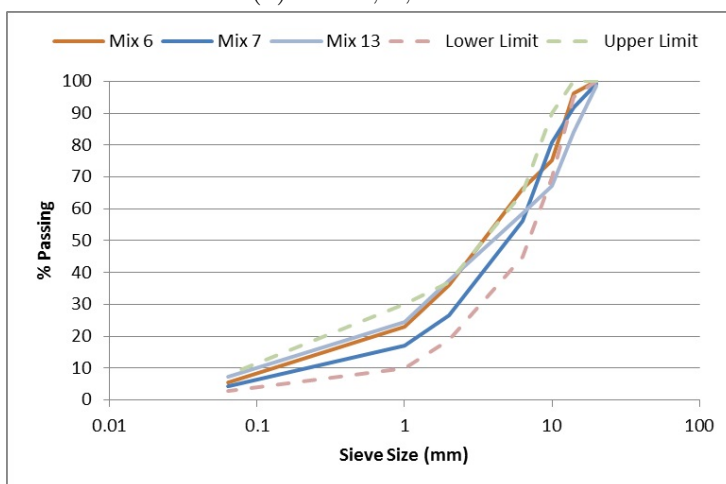
Asphalt mixture mechanical properties were evaluated using different variables that are believed to be influential on mixture performance. The mechanical properties were investigated for six mixtures which were chosen (to cover the range of different aggregate gradation) from the thirteen asphalt mixtures presented in chapter 4. The mixtures that were selected are Mix 1, 3, 4, 6, 7, and 13; their gradations are shown in Figure 5.5, the mixture blending procedure was the same as presented in chapter 4.

Obviously, the six mixtures have different aggregate packing characteristics according to the ratios presented in Table 5.3. Some of the mixtures, such as Mix 1, were slightly changed in their aggregate gradations in this phase of testing due to changes in some of the aggregate stocks, and the packing ratios therefore changed accordingly. The new gradation for Mix 1 also has good interaction between the interceptors and the coarse aggregate, and the interceptors are slightly better supported by the finer particles than the old mixture. Mix 4 has a very high ratio of interceptors ( $CA=2.23$ ) to support the low amount of coarse particles, and also the interceptors are not well maintained by the fine material ( $C_f/F_c=0.25$ ). This combination of ratios makes the mixture voided and influences negatively on its performance. On the other hand, the interceptors in Mix 13 are well supported by finer material ( $C_f/F_c=1.81$ ) and in their turn, they support a reasonable amount of coarse aggregate. This combination makes Mix 13 denser than Mix 4, and better performance is expected. To evaluate the asphalt mixtures in the light of these





(a) Mix 1, 3, and 4



(b) Mix 6, 7, and 13

Figure 5.5: Aggregate gradation of the Six Mixtures

packing ratios, three further variables were considered: binder content, testing temperature, and compaction effort.

### 5.3.1 Testing

Two main tests were carried out on these asphalt mixtures: the Repeated Load Axial Test (RLAT) for measuring the permanent deformation and Indirect Tensile Stiffness Modulus (ITSM) for measuring the stiffness. The RLAT test was

Table 5.3: Packing Ratios for each Mixture

Packing Ratio	Mix 1	Mix 3	Mix 4	Mix 6	Mix 7	Mix 13
$CA$	0.77	1.06	2.23	0.84	1.22	0.44
$FA_c$	0.41	0.40	0.43	0.34	0.34	0.37
$C_f/F_c$	0.53	0.53	0.25	1.22	0.62	1.81
$F/C$	0.48	0.50	0.31	0.90	0.58	1.23
$CC$	0.41	0.33	0.24	0.29	0.30	0.37

conducted under the same test conditions as presented in the previous chapter (stress level, conditioning period, sample preparation). However, the effect of testing temperature on permanent strain was explored by expanding the range of test temperatures (30, 40, and 50 °C).

The ITSM test was conducted on all the asphalt mixtures (three for each gradation) at 20 °C different variables (number of gyrations and binder content). The test was carried out according to *BS EN 12697-26, 2004* and the samples were conditioned for at least 7 hours at 20 °C. Standard test conditions were used: 5 $\mu$ m target horizontal deformation, 124 ms rise time and a Poissons ratio of 0.35 was assumed. In the next sections, the results of ITSM and RLAT test will be presented and evaluated.

## 5.4 Binder Content

Binder content is known to be one of the key factors that affects the performance of asphalt mixtures. In the light of the aggregate packing ratios, the behaviour of the six mixtures was studied using different binder contents. Three binder contents were used (4.1%, 5.1%, and 6.1%) which represent the standard binder content  $\pm$

1.0% to represent the extreme behaviour of mixtures by making this high increment of binder content. The six mixtures were tested in the Repeated Load Axial Test (RLAT) and Indirect Tensile Stiffness Modulus test (ITSM). Firstly, Figure 5.6 shows how the air voids content changed with binder content for the different mixtures. It can be seen that the increase in binder content leads to a lower air voids content in the asphalt mixtures. This is expected because the excess binder in the mix will fill the voids between aggregate particles. The decrease in air voids content does not necessarily mean a good mixture performance, and Figure 5.7 shows the effect of binder content on the permanent deformation (RLAT strain).

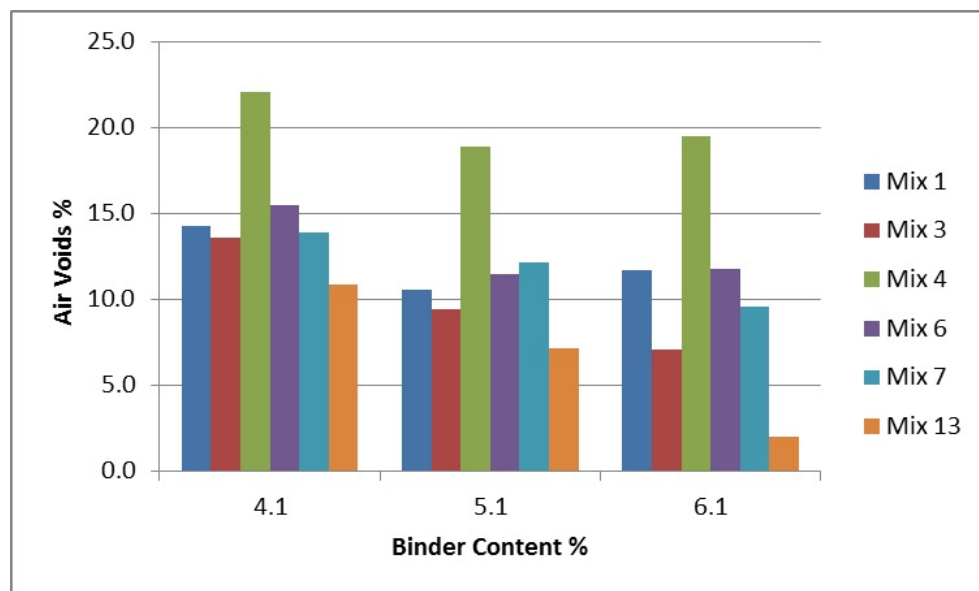


Figure 5.6: Effect of Binder Content on Density

The permanent deformation of asphalt mixture was evaluated in the same manner as presented in Chapter 4 by using the RLAT test for 5000 cycles and at a testing temperature of 40 °C.

The effect of binder content on the strain can be classified into four categories

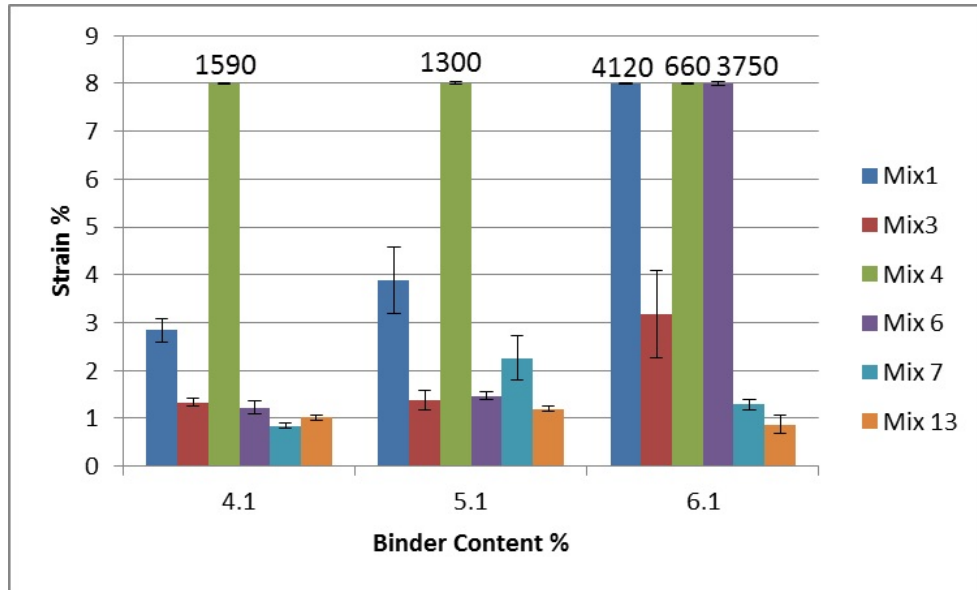


Figure 5.7: Effect of Binder Content on Permanent Strain; NOTE: Numbers shown in figure are the number of cycles reached at 8% strain

(see Figure 5.7 ):

1. Some of the mixtures were not greatly affected by the change in binder content. Mixes 7 and 13 have a good aggregate interlock based on the explanation of the aggregate packing ratios. Mix 7 has a reasonable amount of large aggregate, and it is over supported by the interceptors ( $CA=1.22$ ). However, because of the medium percentage of dust in the mix ( $C_f/F_c$ ), the excess amount of interceptors is supported by the dust. Meanwhile, Mix 13 also has a good amount of large particles, but they are less supported by the interceptors ( $CA= 0.44$ ); however the proportion of dust in the mixture is enough to form proper interaction and fill voids between large particles. The increase in binder content in both mixtures causes no substantial change in the permanent strain because the extra binder has plenty of room i.e. does not disturb the large aggregate packing. However, in both cases, the increase in binder

content decreased the stiffness of the mixtures.

2. Some of the mixes showed a vast increase in permanent strain when the percentage of binder increased from 5.1% to 6.1%. Mixes 3 and 6 exhibited a high permanent strain after increasing the binder content. The reason behind this is that both mixes have reasonable support from interceptors to the large particles ( $CA$ ), but they both have a high amount of fine material ( $FA_c$  for Mix 3 and  $F/C$  for Mix 6). The excess amount of fine material is mixed with the excess amount of binder (when the binder is 6.1%) and forms the mastic. This excess mastic will impact negatively on the resistance to permanent deformation and the stiffness of the mix. It can be noticed that Mix 6 has much greater increase in the permanent strain than Mix 3 because it has fewer large particles and more fine material.
3. Some of the mixes are poor whatever the binder content. Mix 4 suffered from poor deformation resistance over the range of binder content from 4.1% to 6.1% because the aggregate interlock in the mixture is poor. Mix 4 has a very high proportion of interceptors supporting a small percentage of large aggregate particles ( $CA$  and  $CC$  respectively). Moreover, it has a small amount of fine material, so this mixture is made up mainly of the interceptors with inadequate support by the fine material.
4. Some mixtures show a gradual increase in permanent strain as the binder content increases. Mix 1 has a good interlock between interceptors and large particles, and the amount of smaller particles is not very large compared

to Mix 13 for instance. However, the percentage of filler is high, so that the increase in binder content increases the percentage of mastic which will increase the strain and decrease the stiffness.

With regard to the ITSM stiffness of the mixtures, as a general behaviour, the increase in binder content decreased the stiffness of the mixtures, see Figure 5.8. The reason behind this is mainly that as the binder content increases in the mixture there will be an excess amount of binder (mastic), so the deformation will be higher.

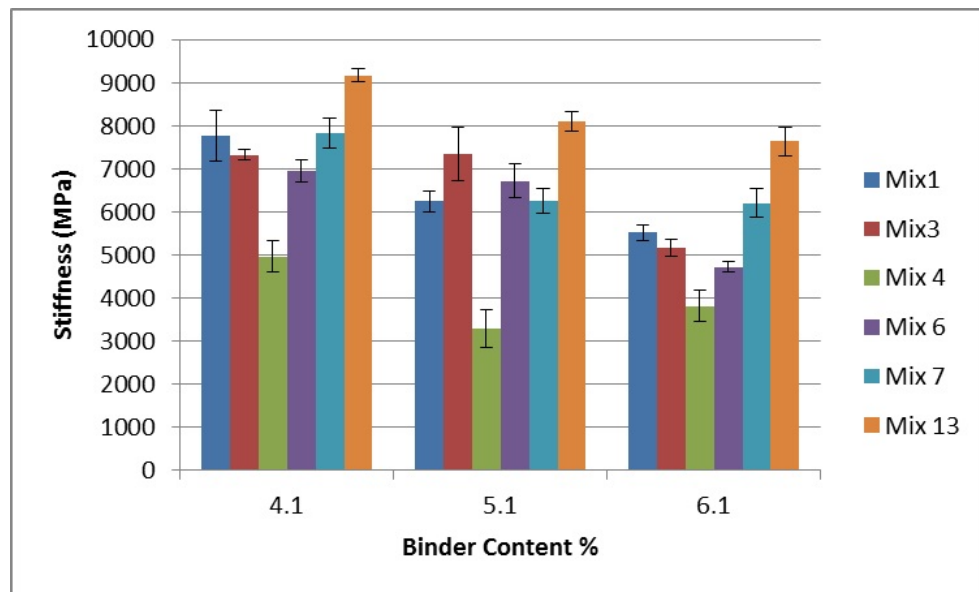


Figure 5.8: Effect of Binder Content on Stiffness

The 4.1 % binder content showed small improvement performance for some mixes than 5.1 %. However, the air voids content of the mixes that have 4.1 % binder content is higher than the other two binder content. Meanwhile, the mixtures that contain 6.1 % binder content performed poorly for most of the mixtures. As a balanced evaluation to have reasonable performance and air voids and also from the economical point of view, 5.1% binder content is considered to be relatively the

optimum value for all the mixes.

## 5.5 Temperature

The effect of temperature was studied in relation to the permanent deformation only. In general, the change in temperature will change the viscosity of the binder used, so when the temperature increases the viscosity of the binder decreases. Three different temperatures were used, 30, 40, and 50 °C and the results are shown in Figure 5.9. In general, the resistance to permanent deformation decreased as the temperature was increased. Because of the low stiffness of binder at 50 °C, the aggregate is dominant in maintaining the load applied, and all the mixtures reached maximum strain when tested in the RLAT except Mix 13. Mix 13 has an excellent aggregate interlock as explained in the previous section. At lower temperature (30 °C), although there are huge differences in aggregate packing between the mixtures, there were no substantial differences in resistance to permanent deformation. In other words, all mixtures performed similarly, and this supports the fact that the permanent deformation resistance is governed by the binder to a certain level of binder stiffness. As the temperature increased to 40 °C, the differences in aggregate packing started to appear in the performance of the mixtures; because it is believed that in this stage both the binder and aggregate are contributing in resisting the permanent deformation. Mix 4 showed very apparent poor behaviour, compared to the other mixes, by obtaining higher strain in RLAT test and Mix 1 also showed a significant increase in permanent strain.

This section showed the importance of aggregate interlock on the performance of asphalt mixtures at high testing temperature.

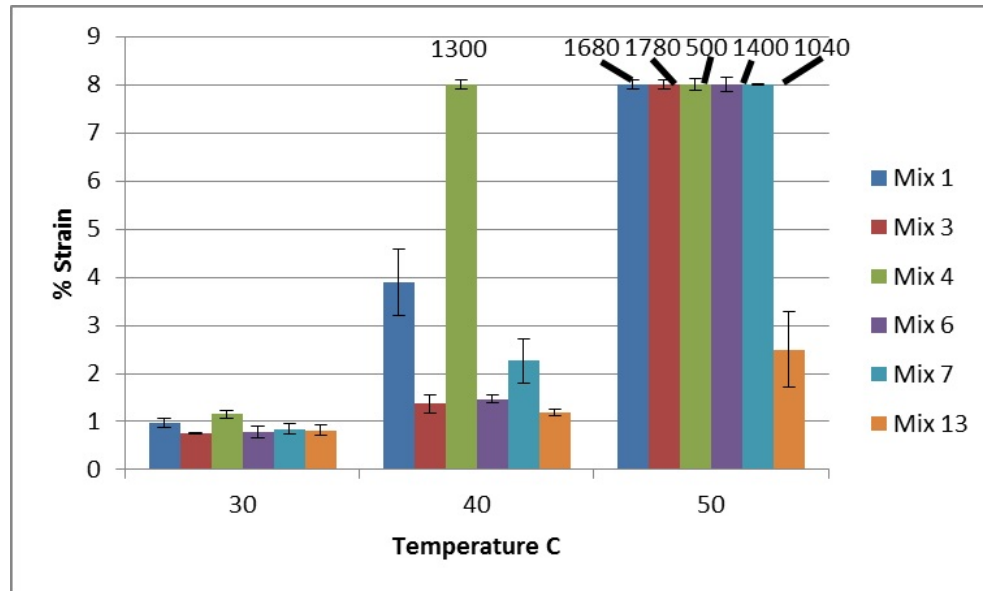


Figure 5.9: Effect of Temperature on Permanent Strain, (NOTE: Numbers shown in the figure are the number of cycles reached to the corresponding strain.)

## 5.6 Compaction Effort

Asphalt mixture properties are highly affected by compaction effort. Compaction effort affects the density of the mixture and how the particles are packed together. For this reason, it was necessary to understand its effect on performance in the light of aggregate packing ratios. Three levels of compaction were considered 100, 200, and 300 gyrations.

It can be seen in Figure 5.10 that most of the mixtures had lower air voids when the number of gyrations in the gyratory compactor increased. Mix 1 had lower air voids when the number increased from 100 to 200, but interestingly it increased



again when the number of gyrations was 300. It is not very clear why this happened to Mix 1 but, may be because it has a high proportion of coarse aggregate ( $CC$ ), and these are well supported by interceptors ( $CA$ ), but the interceptors are not very well supported by the finer particles ( $C_f/F_c$ ). This makes the increase in the number of gyrations cause a high contact pressure between interceptors and large particles, and this might result in particle breakdown. Other mixtures such as Mix 3 and 6 were not highly affected by the change in the number of gyrations.

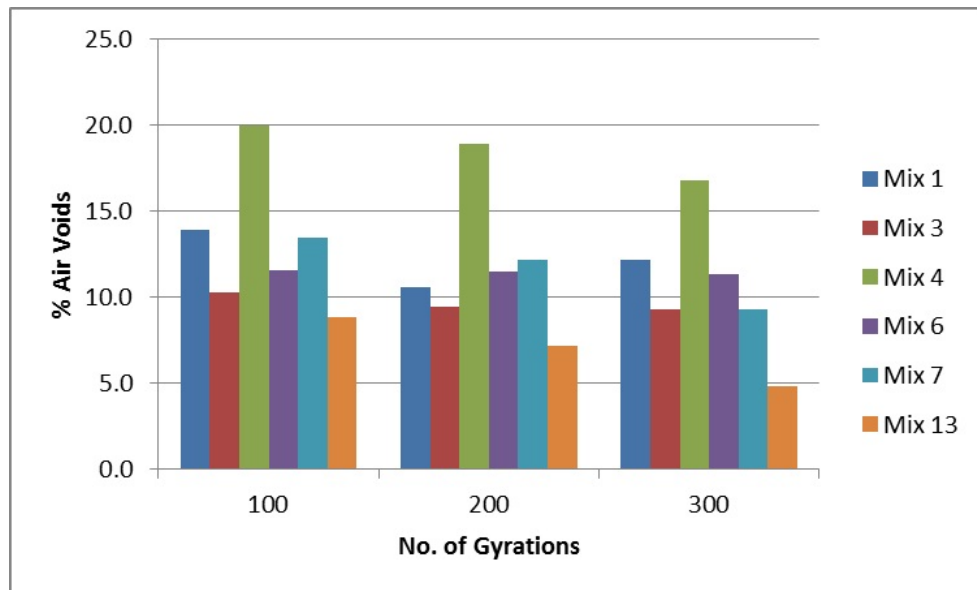
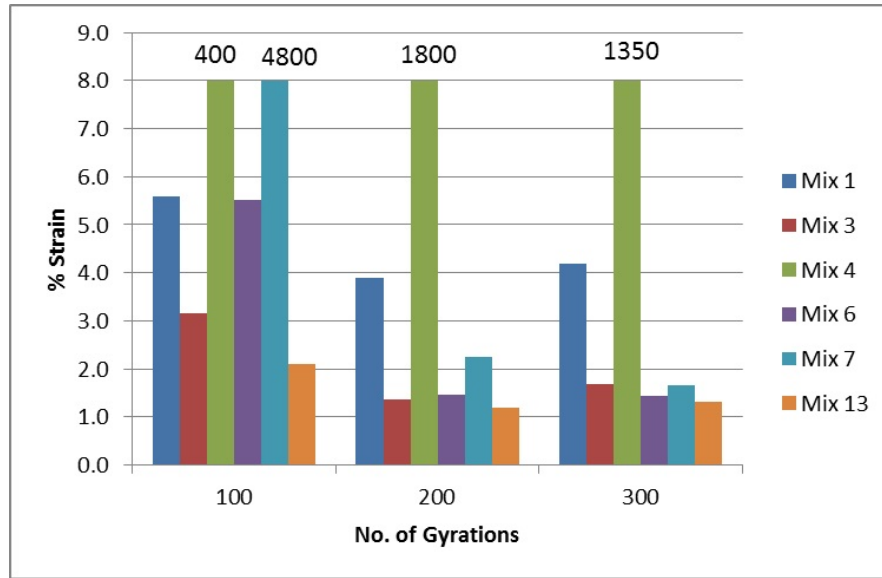


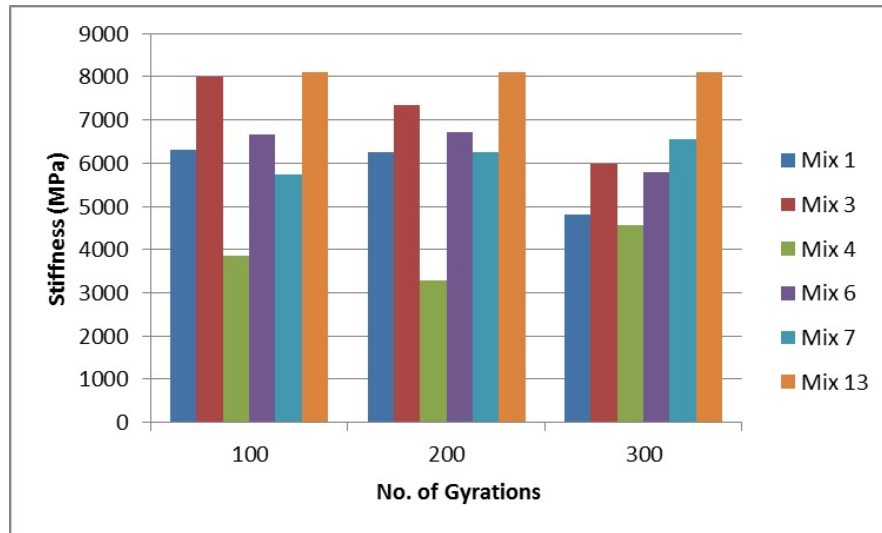
Figure 5.10: Effect of Number of Gyrations on %Air Voids

The effect of different numbers of gyrations on mixture performance is shown in Figure 5.11. It can be seen from the figures that the increase from 100 to 200 gyrations noticeably improved the resistance to permanent deformation. However, for all the mixtures the increase from 200 to 300 gyrations did not to any significant extent further increase the resistance to permanent deformation. This gives an indication that the samples had reached their optimum compaction at or before

200 gyrations. Two things could influence the optimum number of gyrations; the first is the packing of aggregate and the second is the compaction temperature. Concerning the packing of aggregate, the well-graded mixtures could reach their target density in relatively few gyrations. However poorly graded mixtures could not achieve the target density, and aggregate lock will have occurred. Consequently, the increase in the number of gyrations will have little effect on the mixture. Regarding the compaction temperature, when the sample was left in the compactor for 300 gyrations, the mixture will have cooled down and will therefore not improve its performance or density. However, there is no direct evidence on how much the temperature decreased. The stiffness was also measured for mixtures with a variable number of gyrations. By increasing the number of gyrations from 100 to 200, there was no large effect on the stiffness results. However, there was no clear pattern to how the different mixtures performed when changing the number of gyrations from 200 to 300.



(a)



(b)

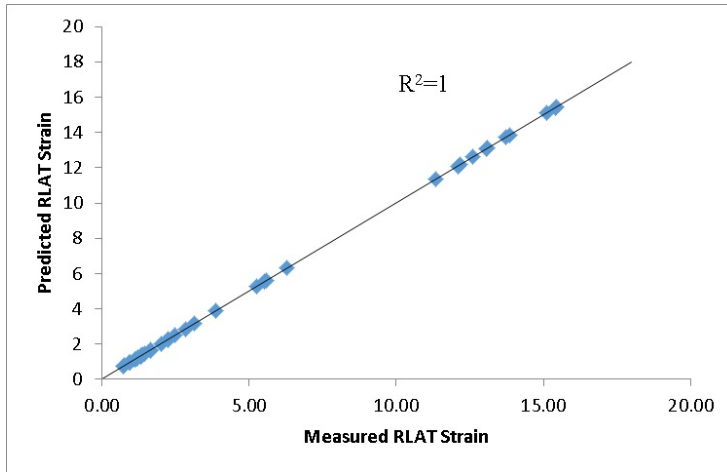
Figure 5.11: Effect of the Number of Gyration on Performance of Asphalt Mixtures

## 5.7 Prediction Modelling for Different Variables

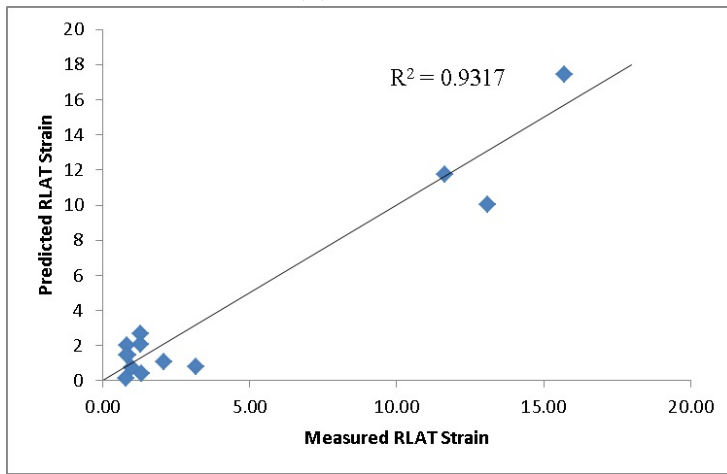
The permanent strain and ITSM data were also used to build a prediction model by using the ANN and ANFIS methods as explained in earlier chapters.

### 5.7.1 Artificial Neural Network ANN

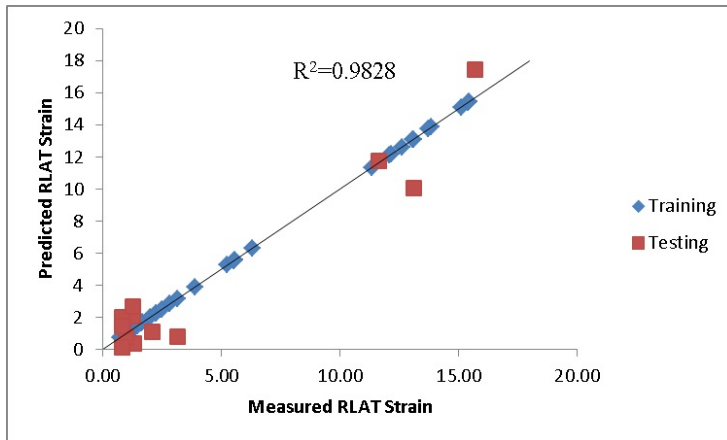
An artificial neural network was used to train the data presented in this chapter. The ANN model was aimed at predicting the permanent strain obtained from the RLAT by using several inputs. The inputs used were the packing ratios of each mix, binder content, testing temperature, and the number of gyrations in the gyratory compactor. The model construction parameters used were similar to those presented in Chapter 4, and 51 mixtures were used. The ANN model prediction results are shown in Figure 5.12; the testing results in 5.12b cover all the input variables. The results showed good agreement with the measured values in the laboratory for some of the mixtures; for others, the model poorly predicted the strain. The performance of the model was evaluated by using the  $R^2$  and  $RMSE$  values as shown in Table 5.4. The ITSM stiffness data for the mixtures were also used to build an ANN model based on the packing ratios, binder content and the number of gyrations. The number of mixtures that were used for this purpose was 33, and each measured ITSM value is the average of 3 mixtures; 75% of the data were used for training the network and 25% for testing. Figure 5.13 shows the model results, and it can be noticed that the ANN model has a real ability to perform the prediction, and the performance of the model is shown in Table 5.4. By comparing the performance of this ANN permanent strain model (Table 5.4) with that developed in Chapter 4 (Table 4.6), it can be seen that adding these new input parameters does impact negatively on some of the predicted strains in the model.



(a) Training



(b) Testing



(c) Training and Testing

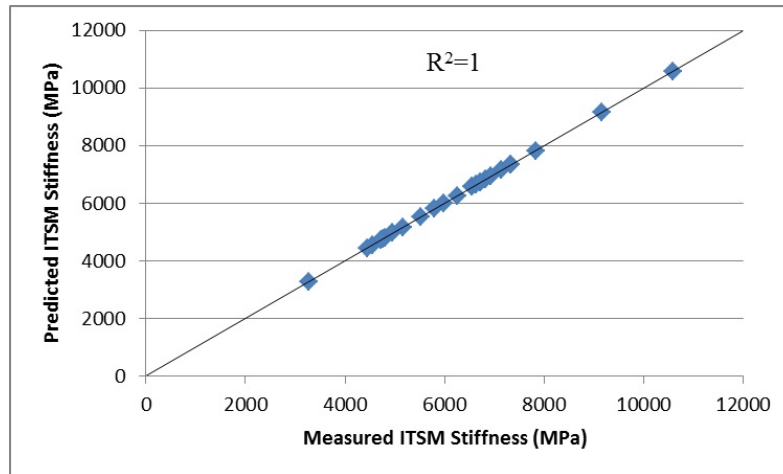
Figure 5.12: Different Variables ANN Prediction Results of RLAT Strain

Table 5.4: Performance of ANN Model for the Different Variables

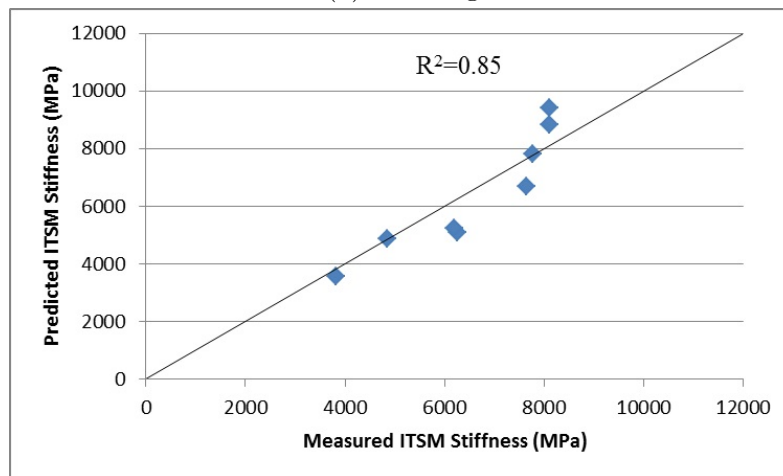
Strain			
	Training	Testing	All Data
<i>RMSE</i>	2.66E-03	1.38	0.699
<i>R</i> <sup>2</sup>	1	0.931	0.983
Stiffness			
<i>RMSE</i>	7.086E-07	829.6	408.5
<i>R</i> <sup>2</sup>	1	0.85	0.941

### Sensitivity Analysis

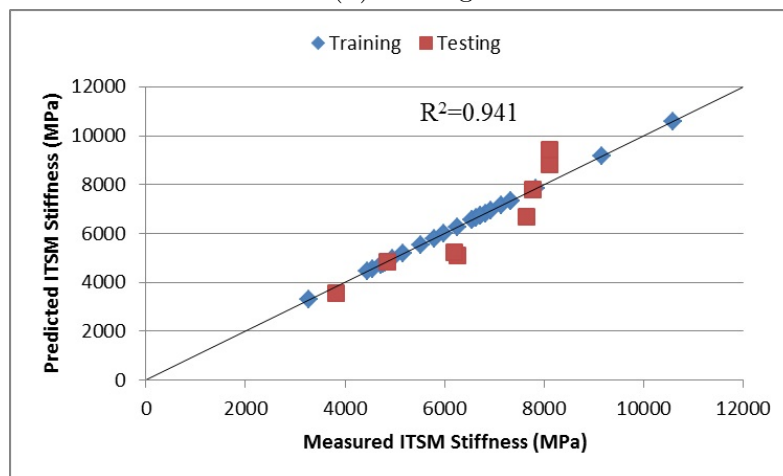
A sensitivity analysis between the input variables and the strain was conducted. The sensitivity analysis presented in the previous chapter for the five packing ratios was also applicable to this model. There is a need to add the effect of other added parameters (binder content, testing temperature, and the number of gyrations) although their impact on the performance of the mixtures are well known to investigate whether the ANN can predict by including the other variables. The analysis performed in the same way presented in the previous chapter which is to build a new ANN model for each input parameter. However, the sensitivity analysis for the five packing ratios was studied with respect to the strain. Therefore, each variable, binder content, testing temperature, and compaction effort will be used individually with the five packing ratios to investigate which of the input variables is negatively affecting the ANN model. Table 5.5 shows the performance of the sensitivity analysis models. It can be seen in the table that the compaction effort had the poorest performance compared to others in terms of  $R^2$  and  $RMSE$ . The analysis was then performed by excluding the compaction effort and including all the input data. The results (in Figure 5.14) showed improvement in the model



(a) Training



(b) Testing



(c) Training and Testing

Figure 5.13: Results of the ANN Prediction Model for ITSM Stiffness

prediction compared to the original model that was presented in Figure 5.12. To ensure that the compaction effort is negatively affecting the performance, it was decided to show how it behaves with each variable (binder content and testing temperature) separately and the five packing ratios. The results, presented in Table 5.5, showed poorer performance when combining binder content with compaction effort than combining testing temperature with compaction effort. However in all cases and whatever the values of performance parameters are, the final judge will depend on the measured and predicted plot for each one of them. Figures 5.14, 5.15, and 5.16 showed the predicted results of the testing phase for the three models. Although the combination of testing temperature and binder content with the compaction effort had reasonable performance, there were some poorly predicted strains which are shown in Figures 5.15, and 5.16. Therefore, it was evident that the compaction effort affected the model negatively. In fact, it was not very clear how the compaction effort can affect the permanent deformation in some cases as shown in a previous section.

Table 5.5: ANN Sensitivity Analysis for the Different Variables

Input Parameter	ANN Model	$R^2$		$RMSE$	
		Training	Testing	Training	Testing
Binder Content	6-5-15-5-1	1	0.9831	0.00303	0.8969
Compaction Effort	6-5-15-5-1	1	0.6757	0.003	2.41
Testing Temperature	6-5-15-5-1	1	0.9894	0.00211	1.1898
Binder Content and Testing Temperature	7-5-15-5-1	1	0.9636	0.0025	1.409
Binder Content and Compaction Effort	7-5-15-5-1	1	0.8673	0.0031	1.483
Testing Temperature and Compaction Effort	7-5-15-5-1	1	0.964	0.0027	1.047



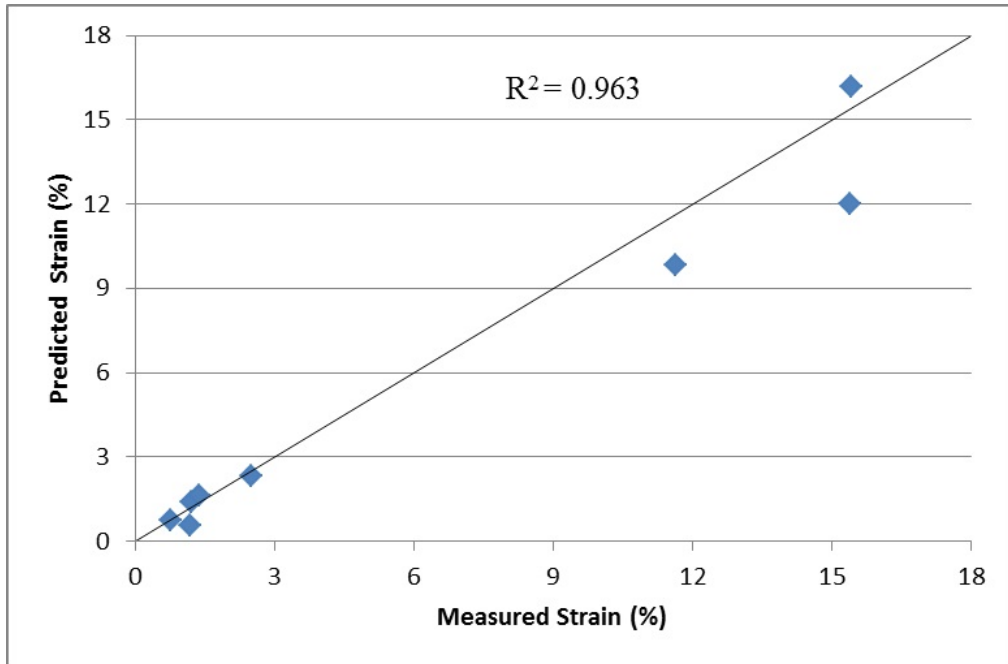


Figure 5.14: ANN Sensitivity Model for Packing Ratios, Binder Content, and Testing Temperature

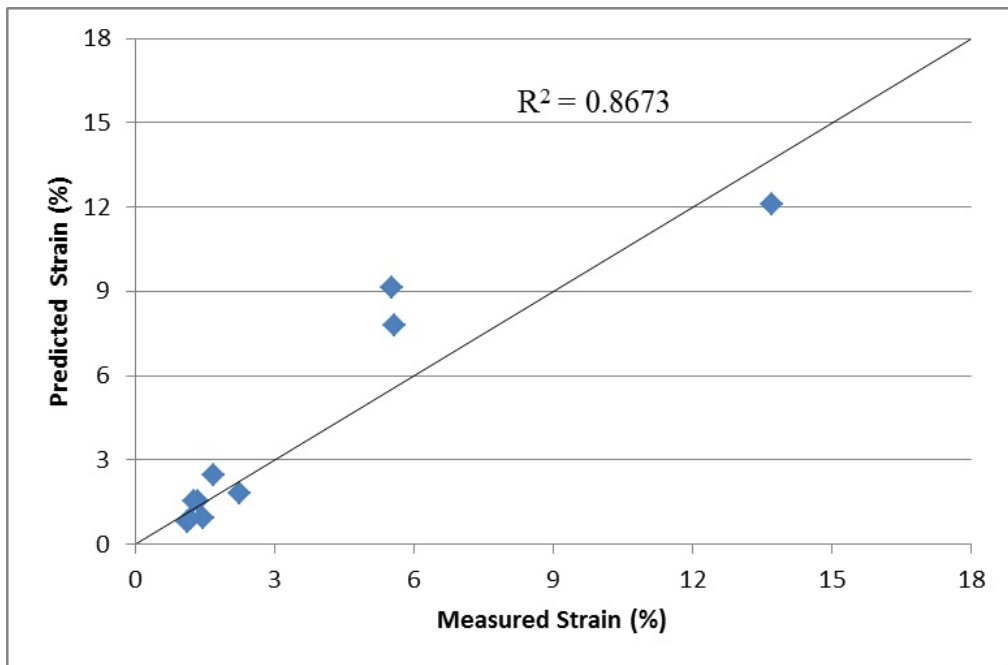


Figure 5.15: ANN Sensitivity Model for Packing Ratios, Binder Content, and Compaction Effort

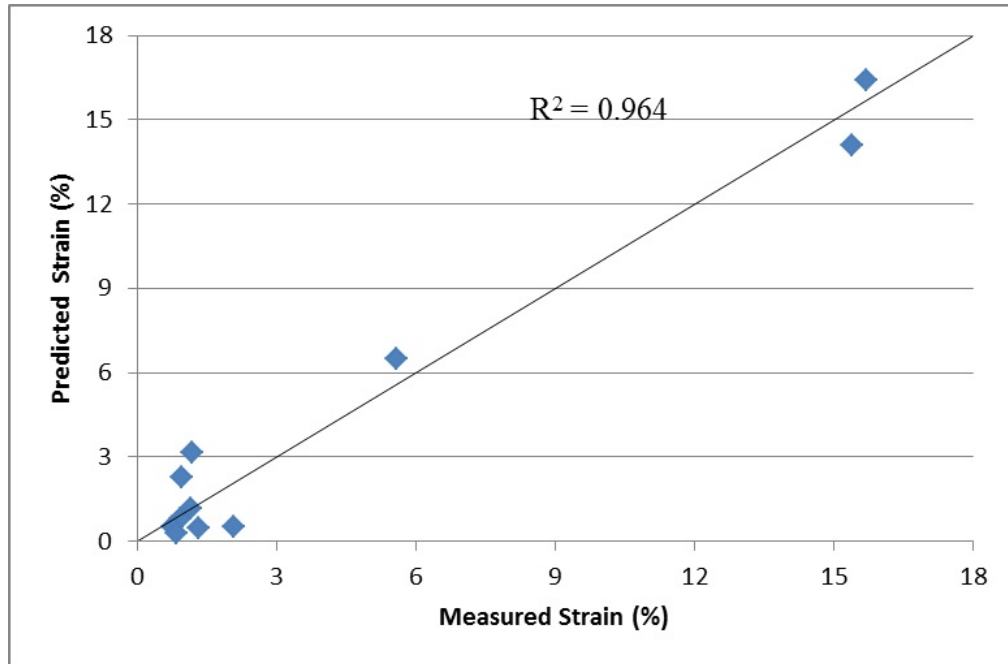


Figure 5.16: ANN Sensitivity Model for Packing Ratios, Testing Temperature, and Compaction Effort

### 5.7.2 Adaptive Neuro-Fuzzy Inference System ANFIS

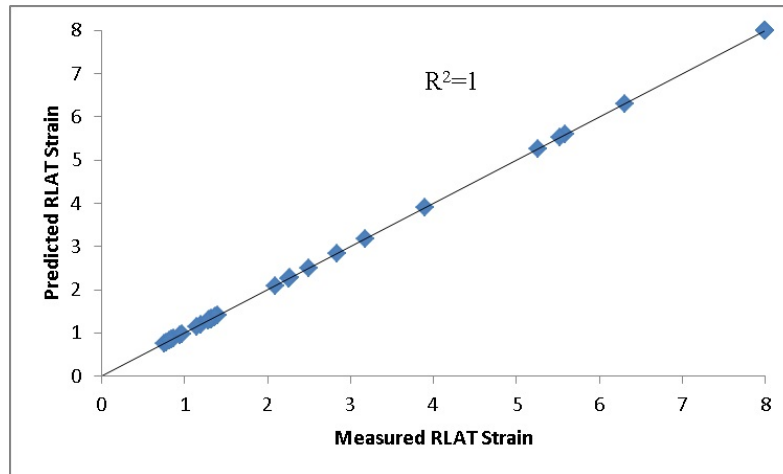
ANFIS was also used to train and test the data presented in this chapter aiming to develop a more precise prediction. In contrast to previously, ANFIS did not precisely predict the permanent strain and stiffness. Although the performance of the permanent strain is good based on the  $R^2$  and  $RMSE$  values (Table 5.6), the model did not predict the strain as well as with ANN (model results are shown in Figure 5.17). Several trials have been conducted to build the model, using the same model construction parameters as previously, but it was noticed that the mixtures with high values of strain (i.e. larger than 8%) negatively affect the model. Therefore, each mixture with high strain was assumed to have 8% strain for model construction consideration. In fact the mixtures in the RLAT test that reached this level of strain were badly deformed and any higher strain achieved was due to the

collapse of the mixture under the applied stress. So any value of predicted strain in Figure 5.17 close to 8% is considered as highly deformed. The Mixtures permanent strains predicted in Figure 5.17b were chosen to cover variation in all the input variables. The model under-predicted the permanent strain for most of the test data and after several trials, it was found that including more data in the testing phase reduces the efficiency of the model. The reason behind the non-precise results of ANFIS might be because of the small amount of the new variables data which did not allow the model to train itself on a broad range of data, especially as ANFIS treats the inputs as membership functions and produces rules based on that. A way to overcome and improve the results of the ANFIS model could be through choosing a different shape of the MFs and increasing their number, and selecting a linear membership function for the output, but all of these new parameters need high computational effort and long duration of processing.

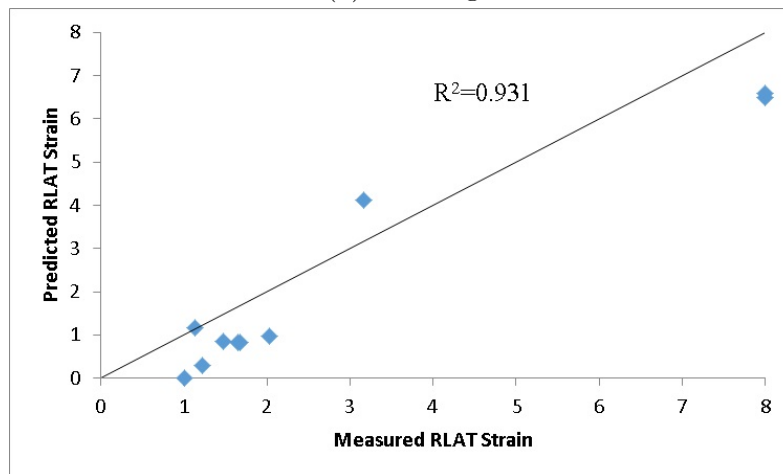
Table 5.6: Performance of Permanent Strain ANFIS Model for the Different Variables

	Training	Testing	All Data
<i>RMSE</i>	5.3E-05	0.998	0.442
<i>R</i> <sup>2</sup>	1	0.931	0.98

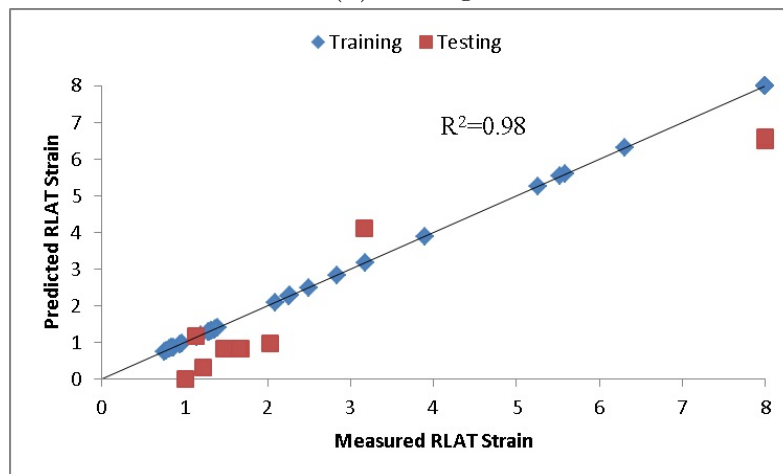
ANFIS was also not able to produce a good model for the stiffness when the new variables were added; after several trials with ANFIS the performance of the stiffness model was reduced and it seems that the network does not have enough data to produce the right rules for estimating the stiffness. Therefore, it was decided to rely on the ANN model for the use of stiffness prediction when using different variables.



(a) Training



(b) Testing



(c) Training and Testing

Figure 5.17: Results of the ANFIS Prediction Model for RLAT Strain

## 5.8 Conclusions

Aggregate particles play an important role in the performance of asphalt mixtures. The establishment of the effect of aggregate packing ratios on the stiffness of asphalt mixtures was presented earlier in this chapter, followed by the impact of other variables. The conclusions of this chapter can be summarised as follows:

- Several aggregate gradations including SMA and porous asphalt were used to study the effect of aggregate packing ratios on the ITSM stiffness of asphalt mixtures. Three ratios were used to build a regression analysis and model. The regression model of the aggregate packing ratios was compared with a previously established model and found to have lower root mean squared error (*RMSE*). An artificial neural network was also used for this purpose, and it helped to predict more precisely with larger  $R^2$  and smaller error (*RMSE*). Therefore, aggregate packing ratios were found to be a good tool to predict stiffness.
- Different variables were used to study their impact on the performance of asphalt mixtures in the light of aggregate packing ratios for six gradations. These variables were binder content, testing temperature, and compaction effort. The tests carried out were RLAT and ITSM
- Binder content showed a fascinating effect on asphalt mixtures regarding permanent strain and stiffness. Mix 7 and 13 were not greatly affected by the change of binder content due to the good interaction between particles. Mix

3 and 6 showed a large difference in performance as the binder content was increased. Meanwhile Mix 4 performed poorly at all binder contents due to the poor interaction of particles, and Mix 1 showed a gradual deterioration in their performance.

- Temperature effects were also evaluated, and it was found that at relatively low temperature the packing of aggregate does not greatly affect the performance of mixtures due to the high viscosity of bitumen. As the temperature increased, packing ratio effects started to appear. Some of the mixtures that have good aggregate interaction performed better than others. At higher temperatures, 50 °C, all the mixtures behaved poorly due to the relatively low viscosity of the binder; only Mix 13 performed well due to its good aggregate packing interlock. The 40 °C testing temperature was considered to be the most appropriate temperature to allow a good comparison between the mixtures' aggregate packing ratios. This variable shows explanation presented in Chapter 2 that when binder has high stiffness, it will be dominant in resisting the load and this is shown at 30 °C. While at 50 °C the binder has less stiffness and aggregate is maintaining the load, therefore high deformation occurred. At 40 °C it was considered as a balance stage where the two components (binder and aggregate) are contributing in resisting the applied load.
- Three compaction levels were used in the gyratory compactor. Due to their particle arrangements, some of the mixtures had poor performance at relatively high gyration number due to high contact pressure between particles

which may resulted in particle breakdown. Other mixtures reached optimum compaction level at 200 gyrations and no improvement in the performance was recorded at higher compaction effort.

- Prediction modelling was performed using Artificial Neural Network (ANN) and Adaptive Neuro-Fuzzy Inference System (ANFIS) aiming to make permanent strain and stiffness prediction. The input variables were the five packing ratios, binder content, testing temperature, and the number of gyrations. Both techniques showed poor ability for prediction for some of the mixtures; sensitivity analysis showed negative impact of the compaction effort on the model. The inability of the techniques to precisely predict the performance is expected to be due to the limited amount of data supplied to them, especially in using these three important variables.

Table 5.7 summarises the findings of this chapter in brief.

Table 5.7: Brief Summary of the Different Variables Results

Variable	Values considered	Effect of changing the variable on strain
<b>Binder Content</b>	4.1%	<ul style="list-style-type: none"> <li>- Mix 7 and 13 did not change</li> <li>- Mix 3 and 6 had higher strain when binder content increased from 5.1% to 6.1%</li> <li>- Mix 4 always poor</li> <li>- Mix 1 has a gradual increase in strain as binder content increases.</li> </ul>
	5.1%	
	6.1%	
<b>Temperature C °</b>	30	<ul style="list-style-type: none"> <li>- At 30 C °there was no clear effect on strain.</li> <li>- At 50 C °all mixtures behaved poor except Mix 13</li> <li>- At 40 C °there was clear difference in results between mixtures to allow understanding of aggregate packing effect.</li> </ul>
	40	
	50	
<b>Compaction Level (number of gyrations)</b>	100	Performance improved when compaction level increased from 100 to 200 gyrations. While at 300 gyrations, mixture performed poorly.
	200	
	300	



# Chapter 6

## Rut Depth Prediction

### 6.1 Introduction

The main form of permanent deformation in asphalt mixtures is rutting. Many studies have investigated the mechanism of rutting formation and how to optimise material proportions to avoid it. Permanent deformation is a key issue in asphalt pavement design especially in places with high temperatures, and it can be determined by using triaxial testing (Brown and Bell, 1977; Haas and Papagianakis, 1986; Monismith et al., 1977). Rutting needs to be predicted to avoid major deformation to the pavement.

Several prediction methods were introduced in Chapter 2, and others will be presented in the next section. The non-linear properties and behaviour of asphalt mixtures make the process of prediction complicated. The non-linearity needs advanced tools for estimating material properties and analysing the distribution of stresses throughout the pavement. A simple linear viscous approach will be in-

troduced in this chapter by using a multilayer linear elastic computer program (BISAR). This chapter aims to predict the rut depth generated in laboratory tests and then apply the method to predict field rutting.

## **6.2 Formulation of Theoretical Model**

The two most commonly used approaches for predicting asphalt mixture rutting, as presented in Chapter 2, are the layer-strain method and the viscoelastic approach. The layer-strain method can predict the life until rutting failure in asphalt mixtures by assuming a linear or non-linear relationship between the elastic stress field and vertical permanent deformation in each selected layer. This approach is only dependent on the elastic properties of the mixture and does not directly use the material viscosity (Khazada, 2000). Prediction models based on the viscoelastic approach invariably include a time-dependant response to the wheel load (Khazada, 2000). This type of rutting prediction model assumes that the ruts accumulate mainly from the shear flow of the pavement material. The viscoelastic approach is, unlike the layer-strain approach, purely dependent on the viscous characteristics of the asphalt and independent of the elastic properties. The viscoelastic properties of asphalt mixtures are, typically, measured from confined or unconfined creep testing. The method of linear viscoelastic asphalt material simulation and rutting prediction of asphalt concrete mixtures has been investigated by several researchers, (Battiato et al., 1977; Collop et al., 1995; Monismith and Secor, 1962; Moavenzadeh and Carnaghi, 1966; Nunn, 1986; Pagen, 1972; Thrower, 1977). The

asphalt mixtures are assumed to behave as linear viscoelastic materials in this type of model, and this is considered as the main drawback of the approach. In reality, asphalt mixtures behave non-linearly at high temperatures and stress levels. However, the implementation of the non-linear properties of asphalt mixtures in modelling demands a more advanced tool to be utilised. The aim is to develop a practical and usable method by modifying the simple linear viscous multi-layer model, to enable the prediction of wheel track rut depth. The modified approach incorporates the non-linear properties of the asphalt mixture into the analysis. The principle of linear viscous analysis is analogous to linear elastic, except that elastic parameter (Young's modulus) is replaced by the equivalent viscous parameter (viscosity)(Thrower, 1977). A study made by Collop et al. (1995) used this approach and showed how it has beneficial features regarding the accurate distribution of permanent deformation through the layers, effect of vehicle speed (loading time) and dynamic loads, and the effect of temperature by using different values of viscosity in layers near the surface. The accuracy of this approach mainly depends on the estimate of the viscous properties of the asphalt mixtures. Therefore, the next sections will show a method of determining these parameters and how to apply them in linear viscous analysis to make asphalt concrete mixture predictions based on data obtained from the Repeated Load Axial Test (RLAT) presented in Chapters 4 and 5.

## **6.3 Material and Testing Programme**

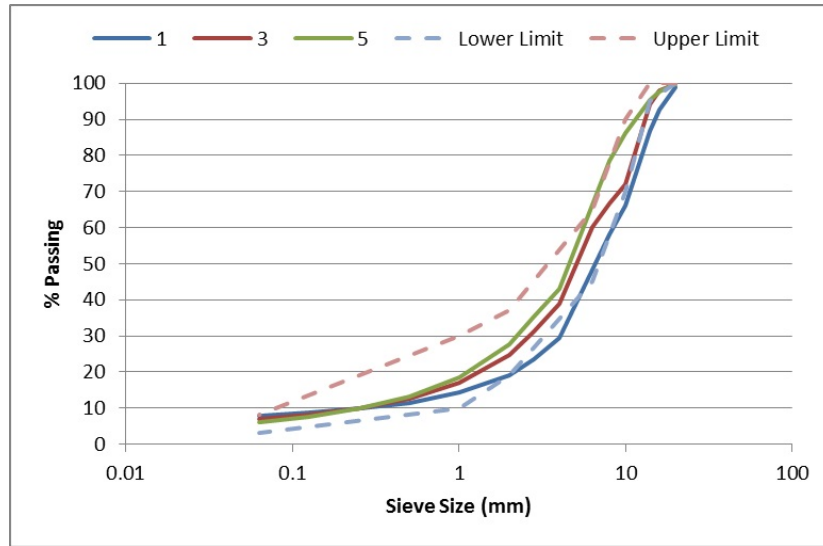
### **6.3.1 Material**

Six different aggregate gradations have been chosen, from those previously presented in Chapters 4 and 5, within the limits of 14 mm maximum aggregate size Asphalt Concrete according to EN (2005). The selected mixtures were chosen to cover range of possible variations. The aggregate used was granite; the aggregate blend for each gradation was mixed with a 5.1% binder content of 40/60 penetration grade at 160 °C. The aggregate gradation details are shown in Figure 6.1. The aggregate and binder were heated up and mixed at the required temperatures (mentioned in Chapter 4) and then compacted by roller compactor at  $150 \pm 5$  °C with target air voids of 5% to make a slab of  $306 \times 306 \times 50$  mm. The slabs were then tested in a wheel tracker machine and core subsequently taken from areas outside the wheel path.

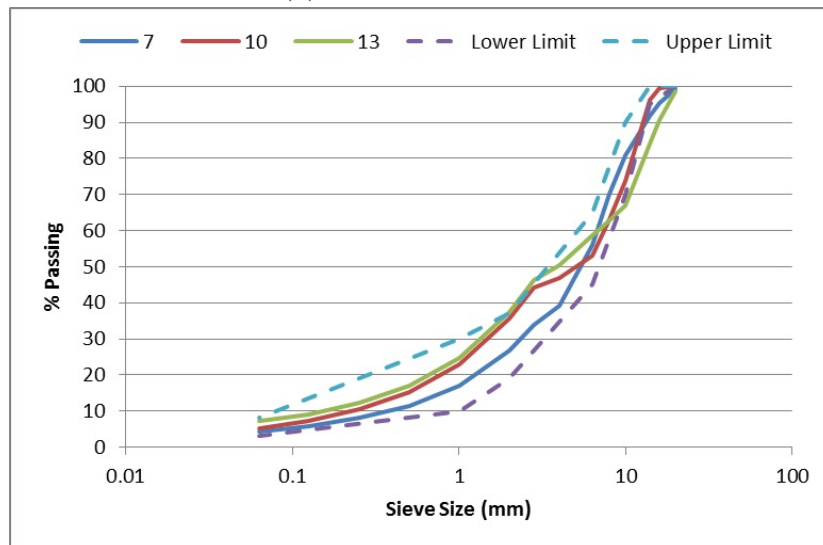
### **6.3.2 Testing Programme**

#### **Wheel Tracking Test**

Each slab was tested in the wheel tracker according to EN (2003). The temperature used was 40 °C and the load applied was 690 N; the test duration was 20000 passes (10000 cycles); Figure 6.2 shows wheel track testing machine.



(a) Mix 1, 3, and 5



(b) Mix 7, 10, and 13

Figure 6.1: Aggregate Gradations for Asphalt Mixtures

### Repeated Load Axial Test (RLAT)

The RLAT (or dynamic creep) test simply consists of a vertical stress repeatedly applied to the cores that were taken from the outer region of rut line in the slab. The core dimensions were 100 mm diameter by 50 mm height. The test applies a stress for 1 second to the sample followed by a 1 second rest period. In this study,



Figure 6.2: Wheel Tracking Machine

the cores from each slab were tested under a stress level of 300 kPa and at 40 °C for 5000 cycles (10000 seconds). The test procedure was performed according to British Standards Standard (1996), and testing machine is shown in Figure 6.3



Figure 6.3: RLAT Testing Machine

## 6.4 Methodology

The method used to predict asphalt concrete wheel track rut depth in this chapter is based on using the strain-dependent properties of the asphalt mixture in a multi-layer linear viscous analysis. The methodology can be summarised as follows:

1. Produce the laboratory rut depth curve by testing the slab samples in the wheel tracking machine.
2. Four cores are then taken from the tested slab (from regions outside the rut line as shown in Figure 6.4) and tested in the RLAT under a value of stress (300 kPa) close to that applied during wheel tracking.

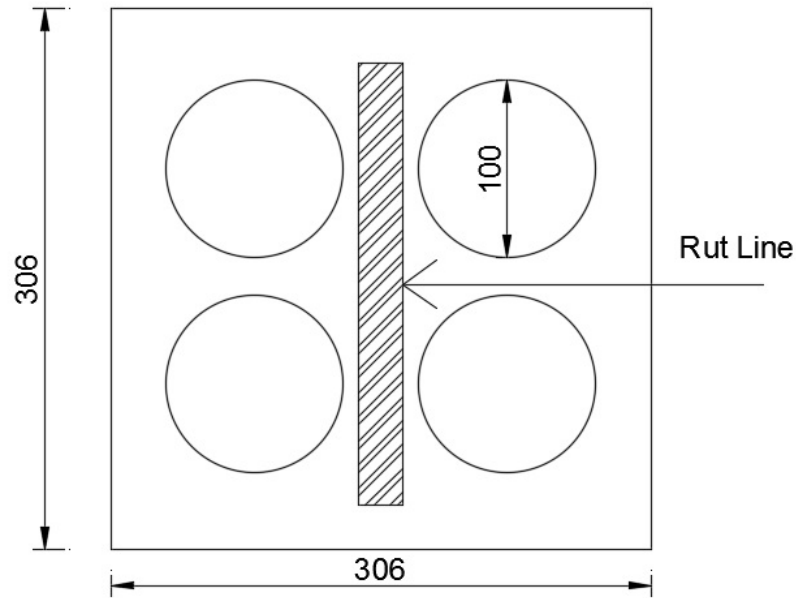


Figure 6.4: Schematic diagram of slab coring (dimensions in mm)

3. Calculate the strain rate ( $\dot{\epsilon}$ ) for each RLAT cycle by using the following equation:

$$\dot{\epsilon} = \frac{\epsilon_2 - \epsilon_1}{t_2 - t_1} \quad (6.1)$$

where  $t_2$  and  $t_1$  are the time (in seconds = number of cycles) corresponding to strains ( $\epsilon_2 - \epsilon_1$ )

4. Determine the viscosity ( $\eta$ ) of the mixture, as a function of strain. Viscosity is computed by dividing the stress ( $\sigma$ ) in MPa by the strain rate ( $\dot{\epsilon}$ ) (Nunn, 1986)

$$\eta = \frac{\sigma}{\dot{\epsilon}} \quad (6.2)$$

A plot of mixture viscosity vs strain is then produced and used to establish the viscous material properties for rutting prediction. A typical plot representing



a mixture showing all three stages of creep (primary, secondary, and tertiary) is shown in Figure 6.5).

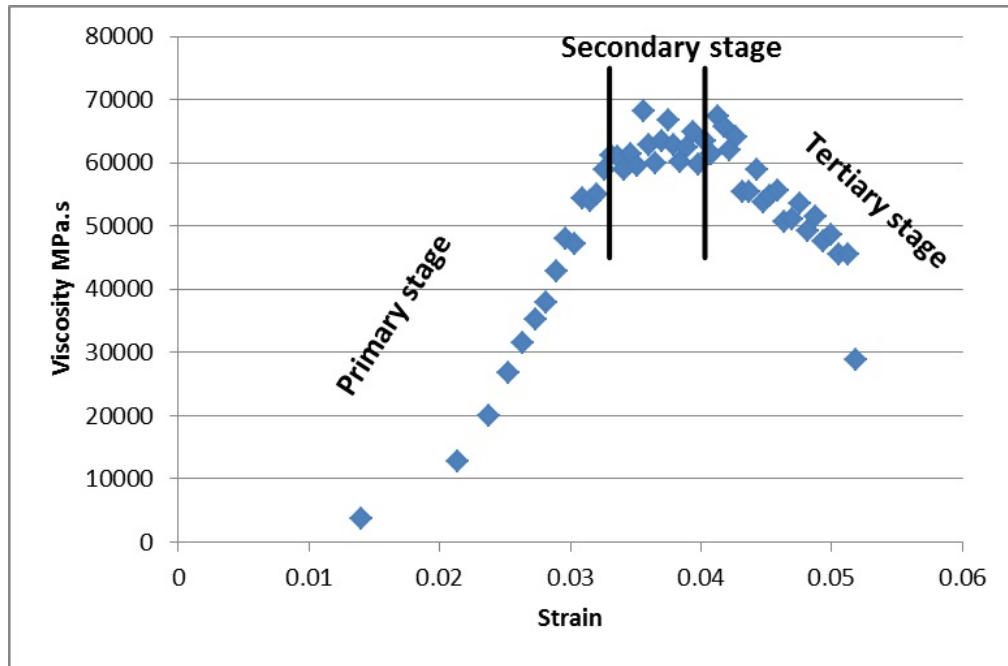


Figure 6.5: Typical Plot of Viscosity vs Strain for an asphalt mixture

5. After that, an initial material viscosity is determined from the viscosity-strain curve by extrapolating to zero strain. This initial value is then used in the first deformation analysis increment.
6. The asphalt slab is then modelled in BISAR as three layers with thicknesses of 10, 20 and 20 mm, in order to model the wheel tracking test, see Figure 6.6.

The load input data to BISAR is as follows:

- Vertical stress (kPa): 300. This value corresponds to the stress in the wheel tracking test.

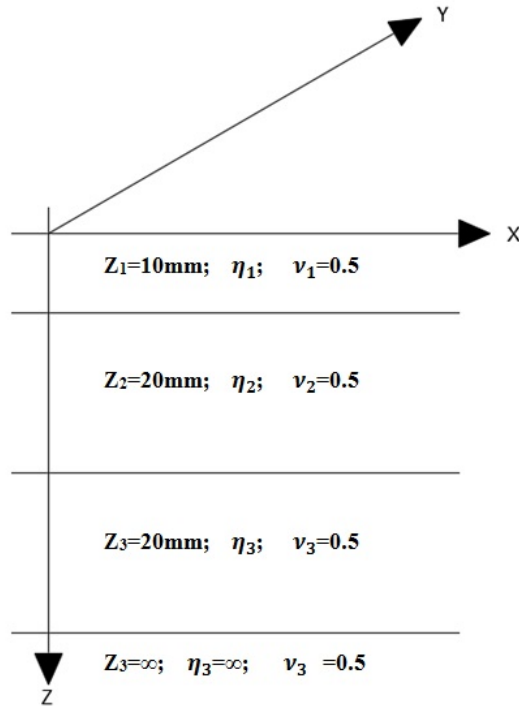


Figure 6.6: Slab Model Layers divided in BISAR

- Radius (m): 0.0250. This is the tire width in the wheel tracking test.
7. The three layers of asphalt are assigned viscosity values. A final very stiff bottom layer is added (effectively  $\infty$  viscosity). All the four layers are assumed to be incompressible (Poissons ratio of 0.5) to ensure that the deformation is due to viscous flow not densification, and full friction between layers is adopted.
  8. The analysis is then performed and the strain rate (strain/second = strain/-cycle) in the middle of each layer under the centre of the load is used in further calculations.
  9. A surface deformation increment of 0.1 mm is applied and the layer strains

and the number of cycles to cause this increment are determined.

10. The new layer strains require new corresponding viscosities from the strain viscosity curve (Figure 6.5) established earlier in the process giving new viscosities for each layer; these are used in BISAR for the following deformation increment.
11. Continue this loop until a specified deformation is reached.

No adjustment was made to the loading time because it was similar in both cases (RLAT and wheel track). In the RLAT the stress was applied for 1 second and in the wheel tracking test the rate of loading was 26.5 cycles/minute and each cycle consisted of two passes. To clarify the above methodology, see the flow chart in Figure 6.7.

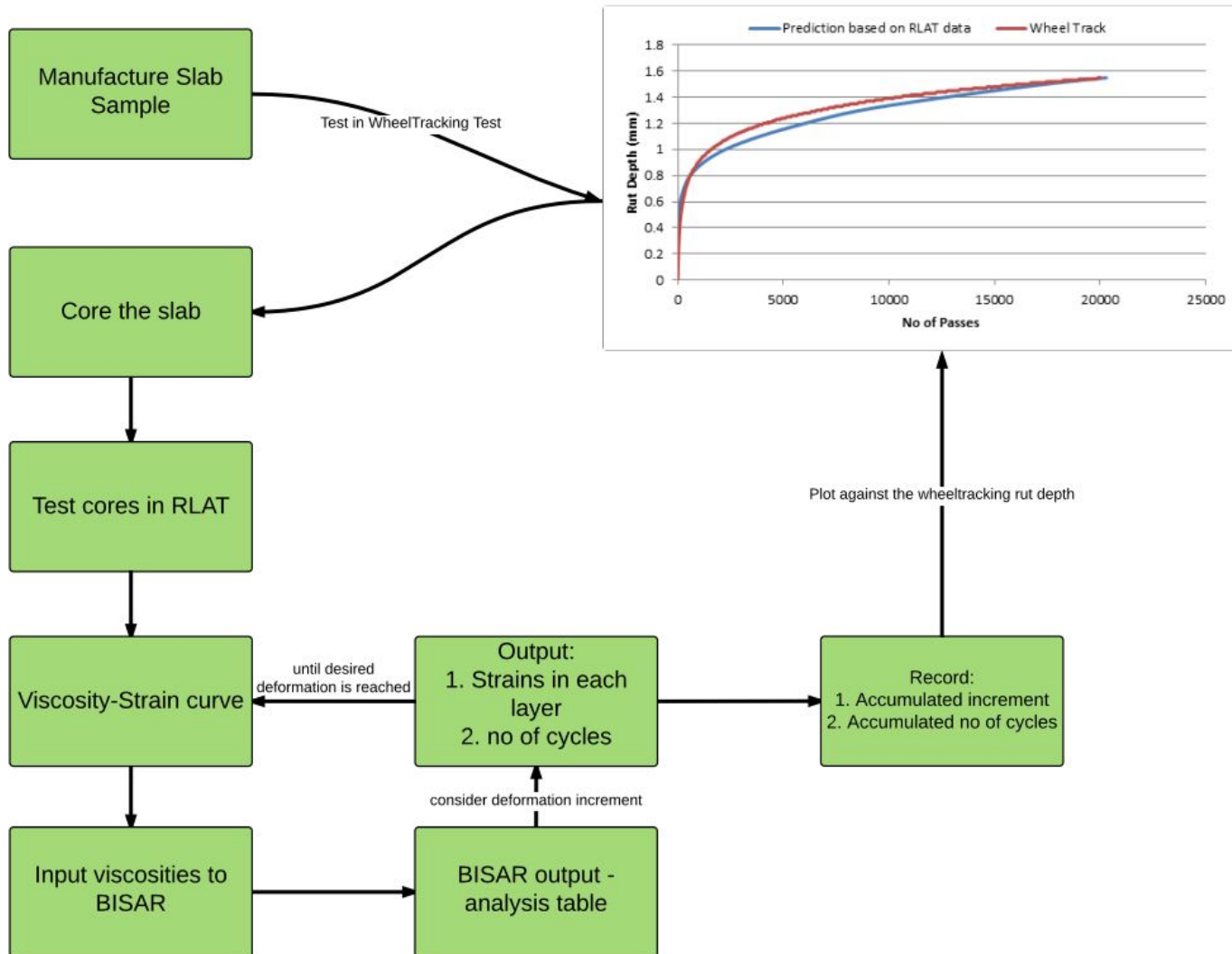


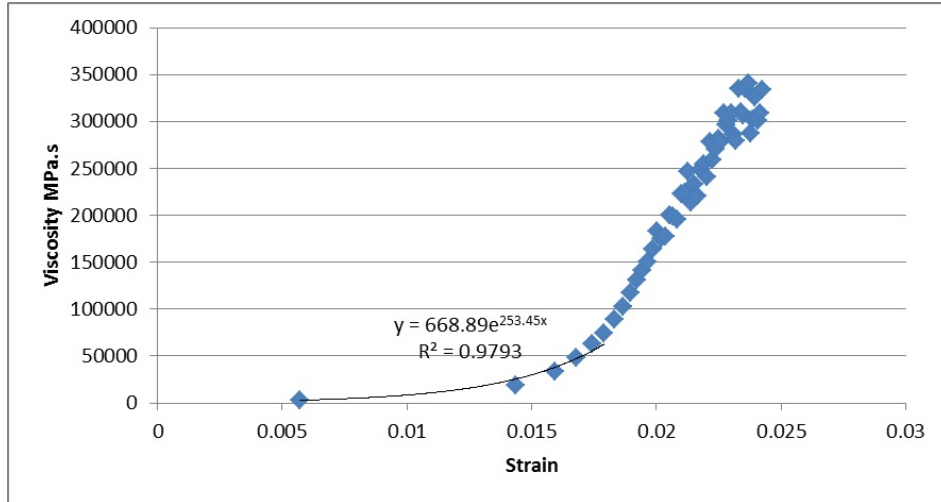
Figure 6.7: Methodology Flow Chart

## 6.5 Analysis of Results

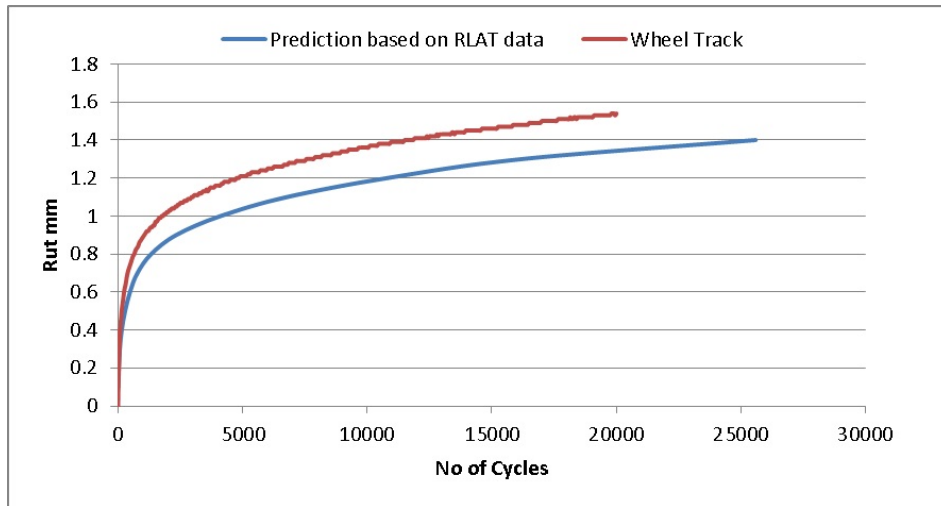
Six slabs were manufactured for six different gradations. The slabs were all tested in the wheel tracking test, and four cores were taken from each slab. This section presents (in Figures 6.8 - 6.13) the results of the prediction process and compares these prediction results to the wheel tracking rut depth. The viscosity-strain curves will also be shown for each mix, and a trend line is fitted to the primary stage of each. The best option found was an exponential curve, and it has been used to estimate the values of viscosity where strain is lower than the first point on the curve. After the first data point, linear interpolation was assumed between each two points.

The prediction based on RLAT data for Mix 3 and 5 showed, in Figures 6.9 and 6.10 respectively, an underestimation compared to the real wheel track curve by about 0.4 mm.

All these results were based on the properties of material determined at 40 °C in RLAT tests modelling the same conditions in the wheel track test. Although the stress distribution in the wheel track test is complex and the assumption in BISAR that the model has an infinite width is incorrect, nevertheless the RLAT test provides a reliable and convenient approach to characterising the properties of the asphaltic materials. The reasonable agreement between the predicted and measured deformations confirm the argument that the permanent deformation can be predicted from the viscous properties of the material.



(a)

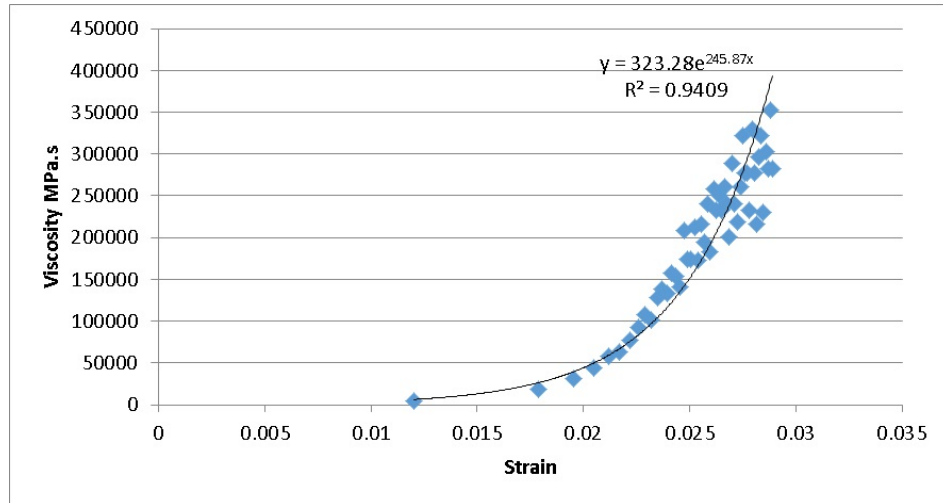


(b)

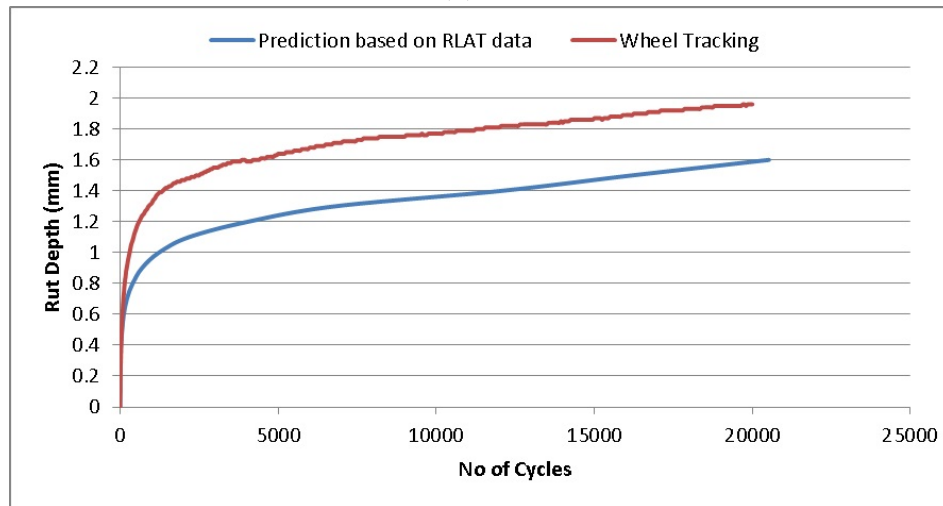
Figure 6.8: (a) Viscosity-Strain Curve. (b) Rut Depth Prediction. For Mix 1

### 6.5.1 Temperature

As the linear viscous analysis showed good agreement with the experimental data at 40 °C, it was decided to investigate the validity of the method at other temperatures. Two temperatures were selected, 30 °C and 50 °C. The whole process and experimental work were performed again at 30 °C for all six mixtures and repeated at 50 °C for one of the mixtures only because the others were expected to fail in



(a)

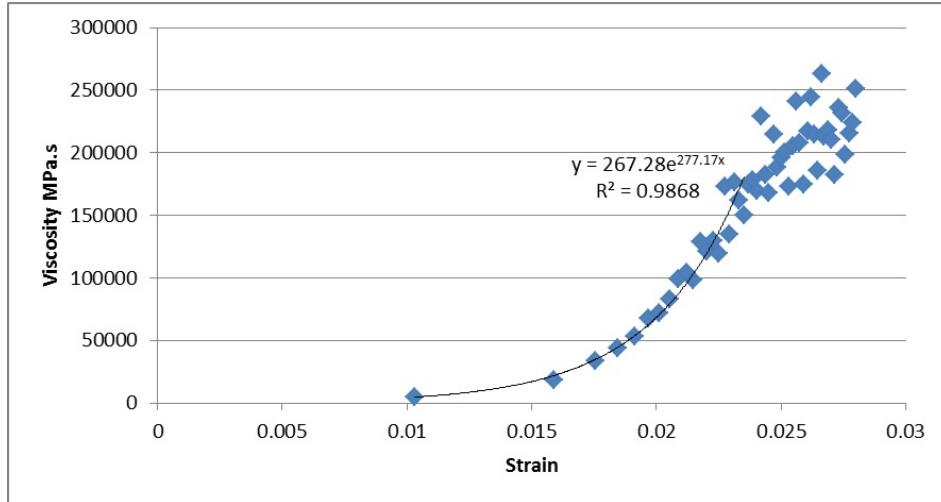


(b)

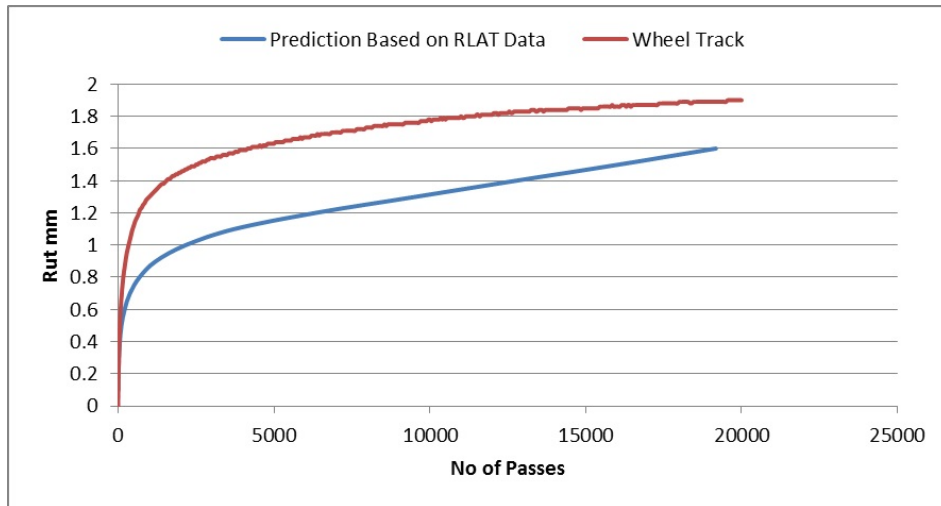
Figure 6.9: (a) Viscosity-Strain Curve. (b) Rut Depth Prediction. For Mix 3 the RLAT test at 50 °C under 300 kPa stress.

### Prediction at 30 °C

Six asphalt mixture slabs were manufactured and tested in the wheel tracking machine at 30 °C under the same load of 690 N, and a frequency of  $26.5 \pm 1.0$  load cycles/minute. The slabs were then cored in the region outside the rut line, and cores were tested in the RLAT at 30 °C. The results of predictions at 30 °C are



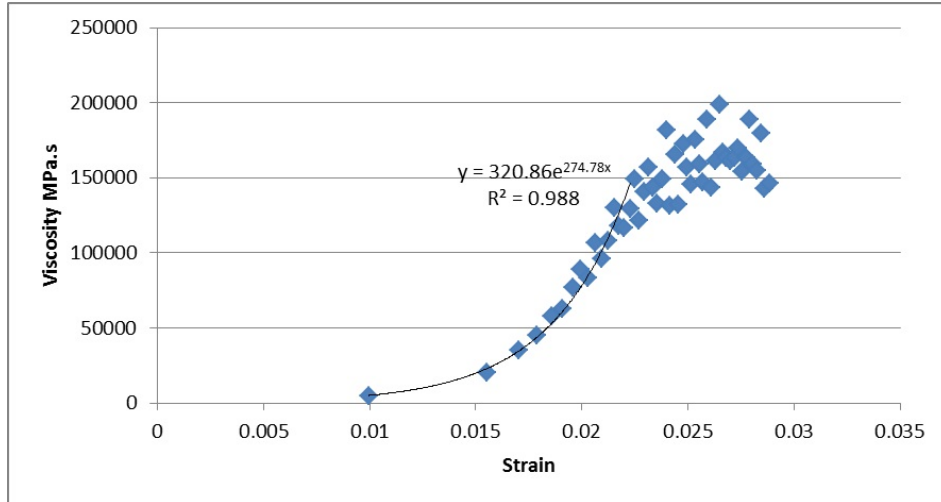
(a)



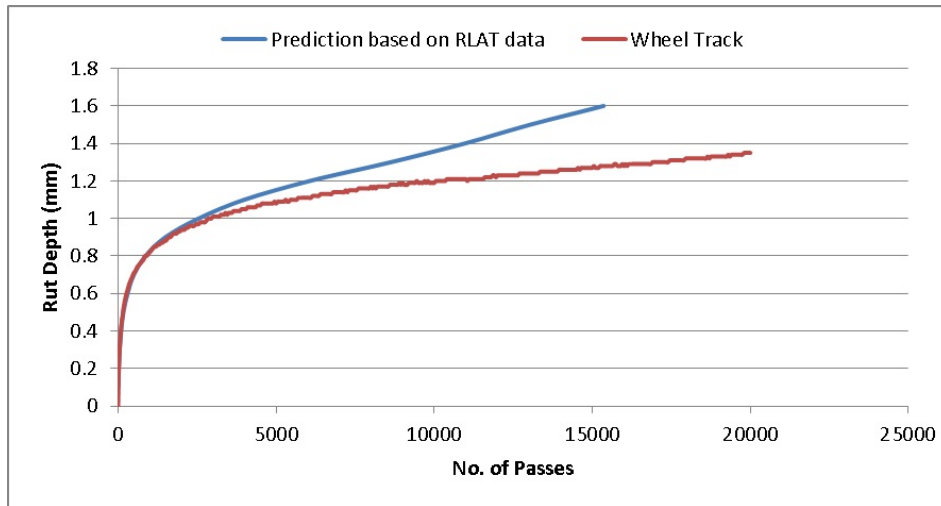
(b)

Figure 6.10: (a) Viscosity-Strain Curve. (b) Rut Depth Prediction. For Mix 5 shown in Figures 6.14 - 6.19, and it can be seen from the figures that, as expected, the values of viscosity are higher than those determined at 40 °C, and also there is less data scatter than found previously. These two points helped to generate a good set of predictions of wheel tracking rut depth at 30 °C. Mix 1, 3, and 7 are the most affected by the change in viscosity values compared to results at 40 °C, and it can be seen from the results that their predictions were all reasonably good.





(a)

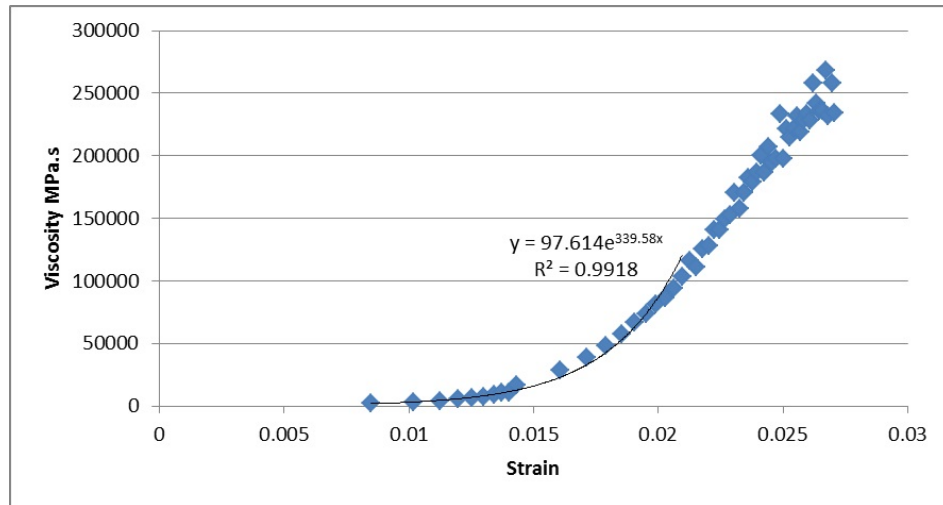


(b)

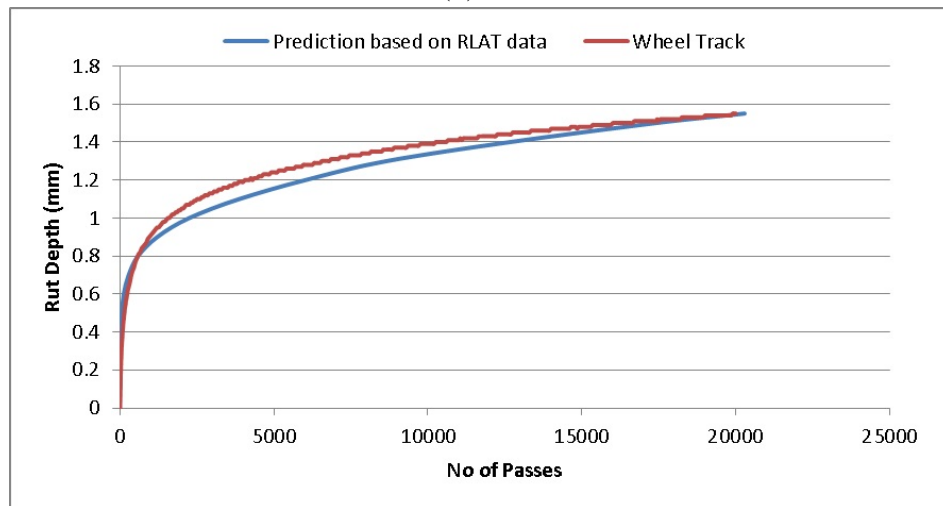
Figure 6.11: (a) Viscosity-Strain Curve. (b) Rut Depth Prediction. For Mix 7

### Prediction at 50 °C

The higher testing temperature was also examined aiming to validate the methodology. The samples were expected to approach collapse under the 300 kPa dynamic stress in the RLAT at 50 °C. Therefore, only one of the mixtures was selected. The selected Mixture was Mix 13 because it is expected to have good aggregate interlock as presented in Chapters 4 and 5. Consequently, one slab was manufactured

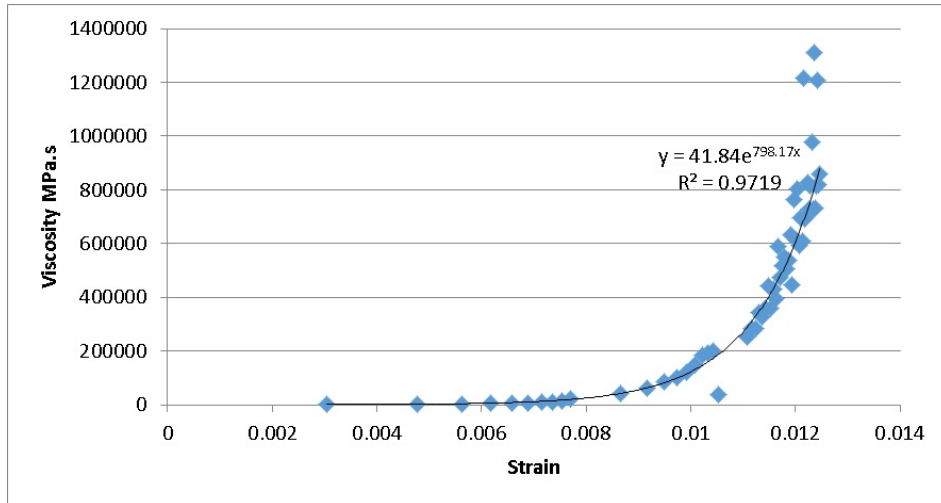


(a)

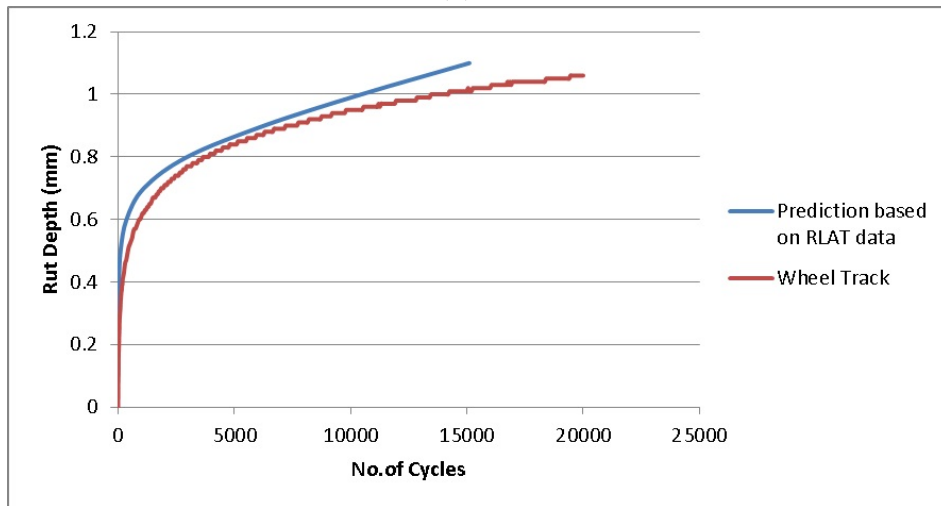


(b)

Figure 6.12: (a) Viscosity-Strain Curve. (b) Rut Depth Prediction. For Mix 10 and tested in the wheel tracking machine at 50 °C and cores were taken from the outer region and tested in the RLAT at the same temperature (50 °C). As expected, the mixture had high strain values in the RLAT, resulting in small values of viscosity. Figure 6.20 shows the viscosity-strain curve having a decrease in viscosity values at high strains, signifying the high temperatures the mixture behaviour lies in areas where linear viscous does not work, and the aggregate is more dominant in maintaining the applied load, therefore, it is clear that this has resulted in an

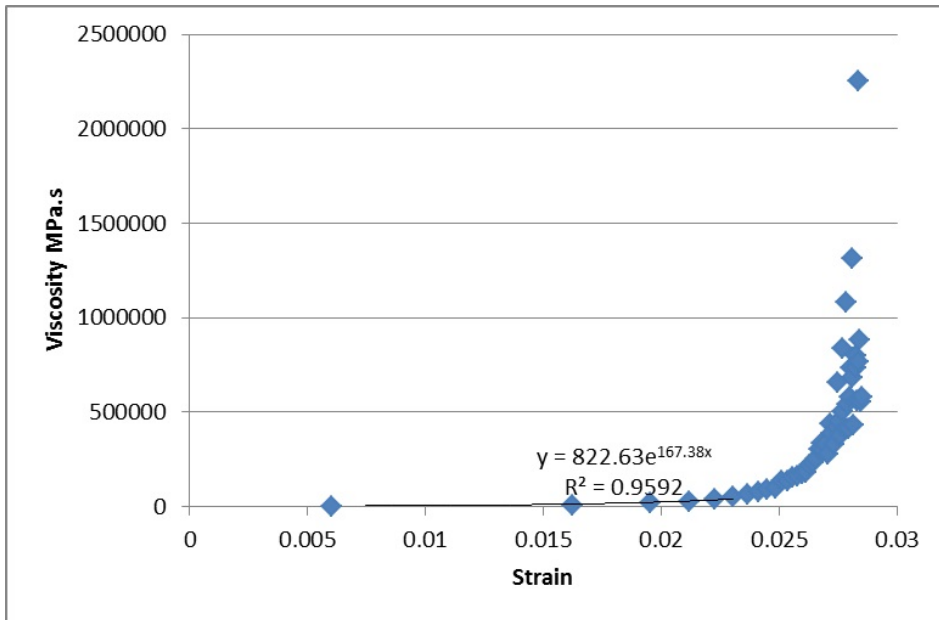


(a)

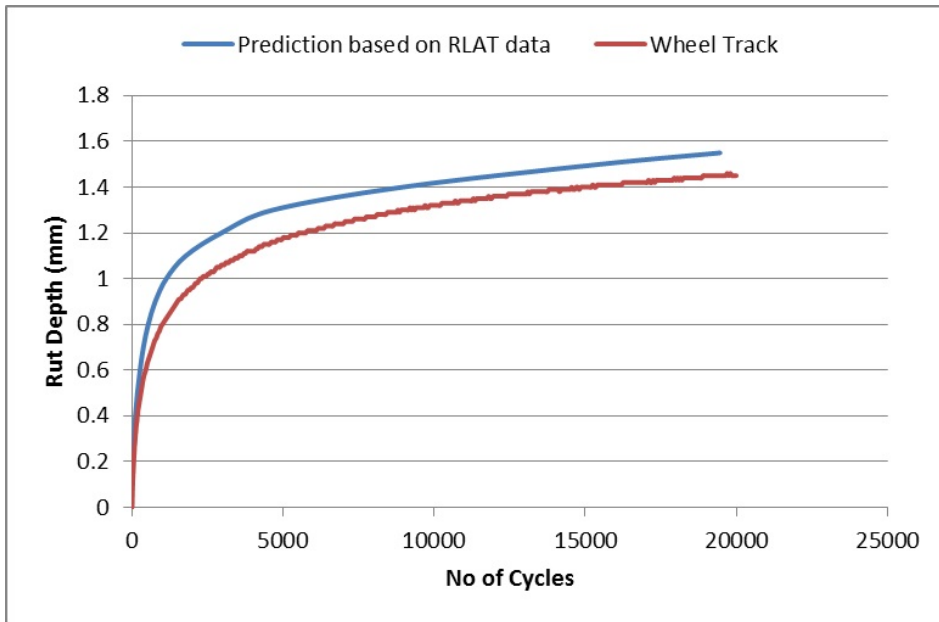


(b)

Figure 6.13: (a) Viscosity-Strain Curve. (b) Rut Depth Prediction. For Mix 13 unrealistically high rut prediction.

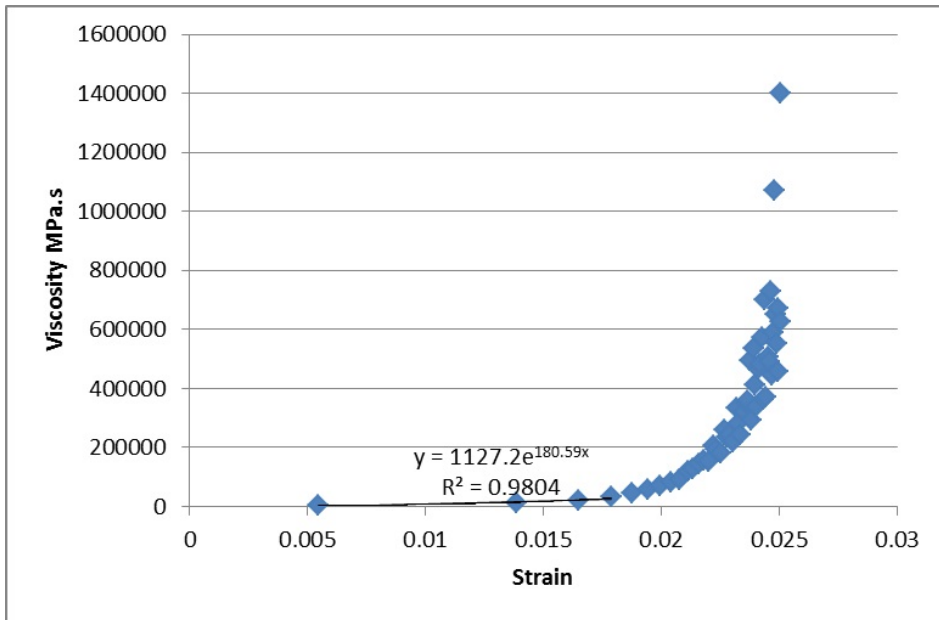


(a)

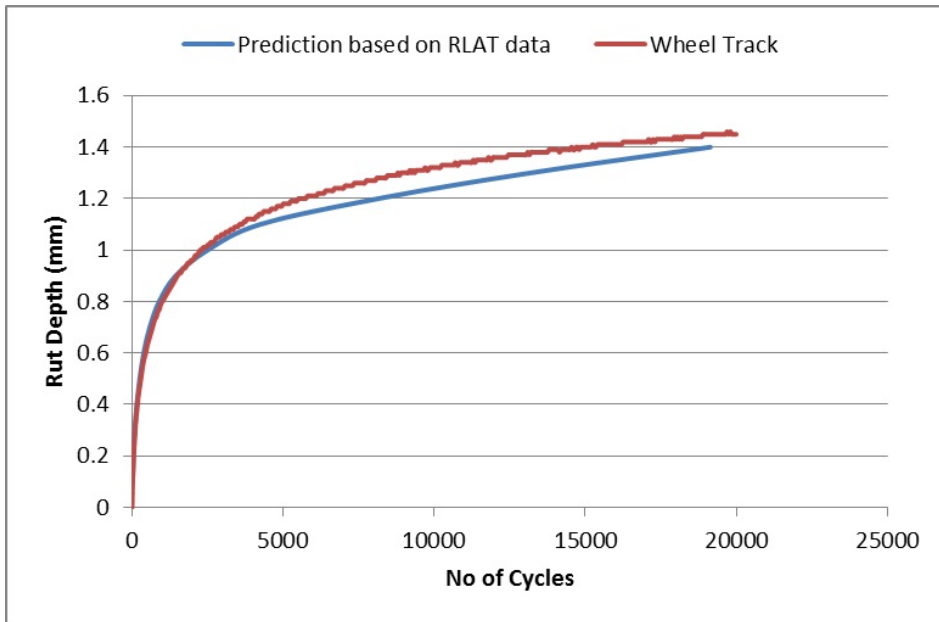


(b)

Figure 6.14: (a) Viscosity-Strain Curve. (b) Rut Depth Prediction. For Mix 1 at 30 °C

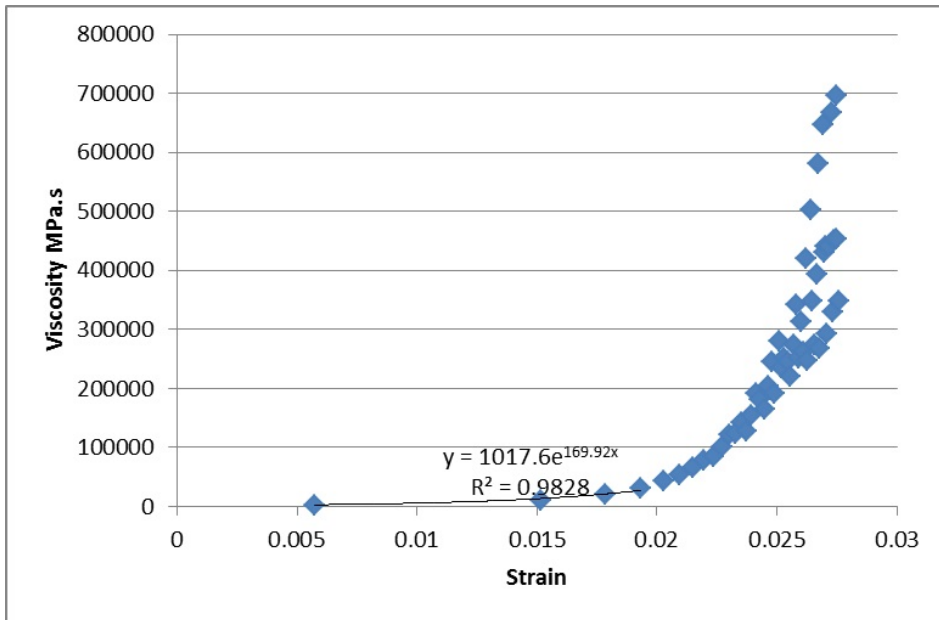


(a)

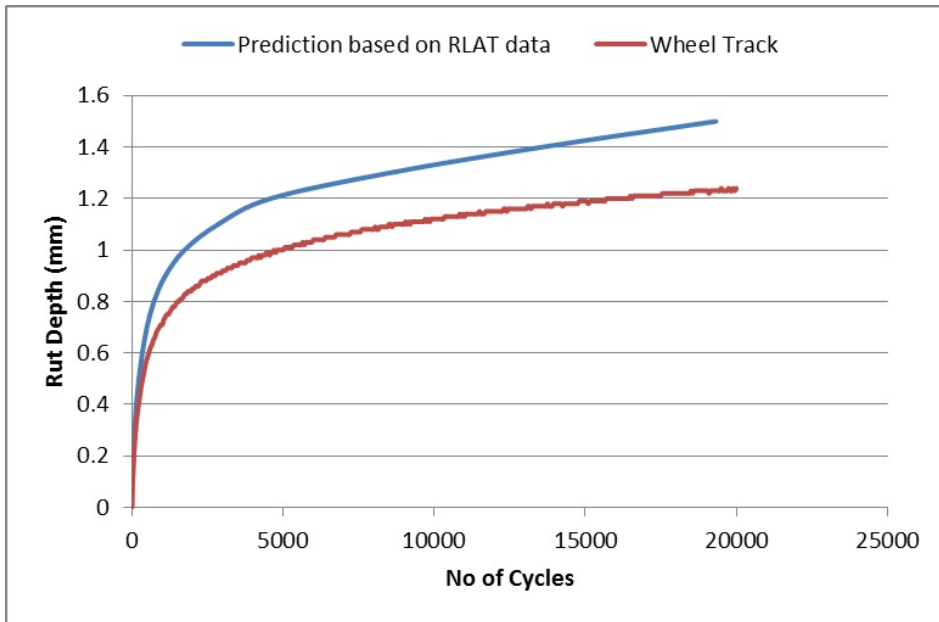


(b)

Figure 6.15: (a) Viscosity-Strain Curve. (b) Rut Depth Prediction. For Mix 3 at 30 °C

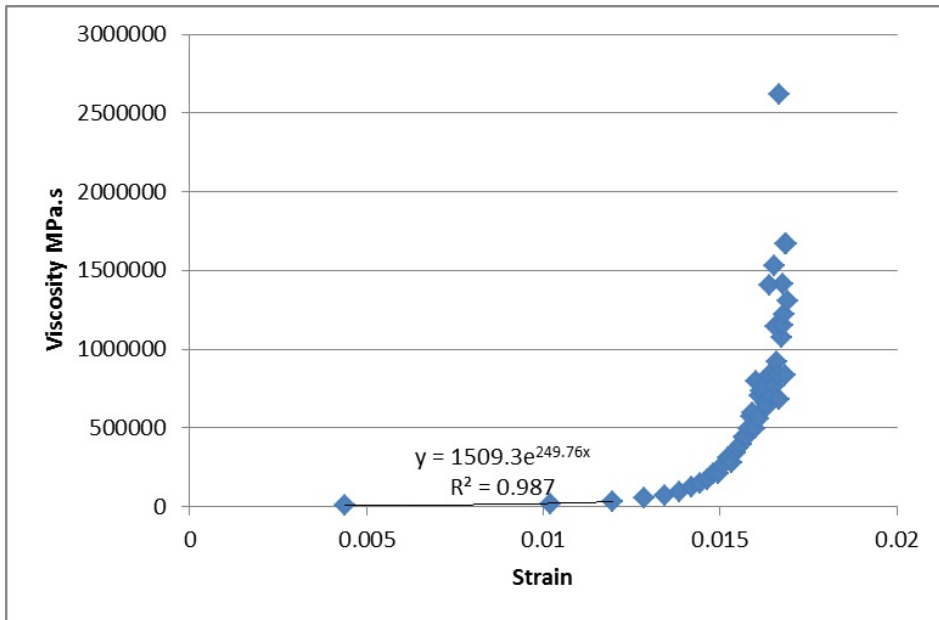


(a)

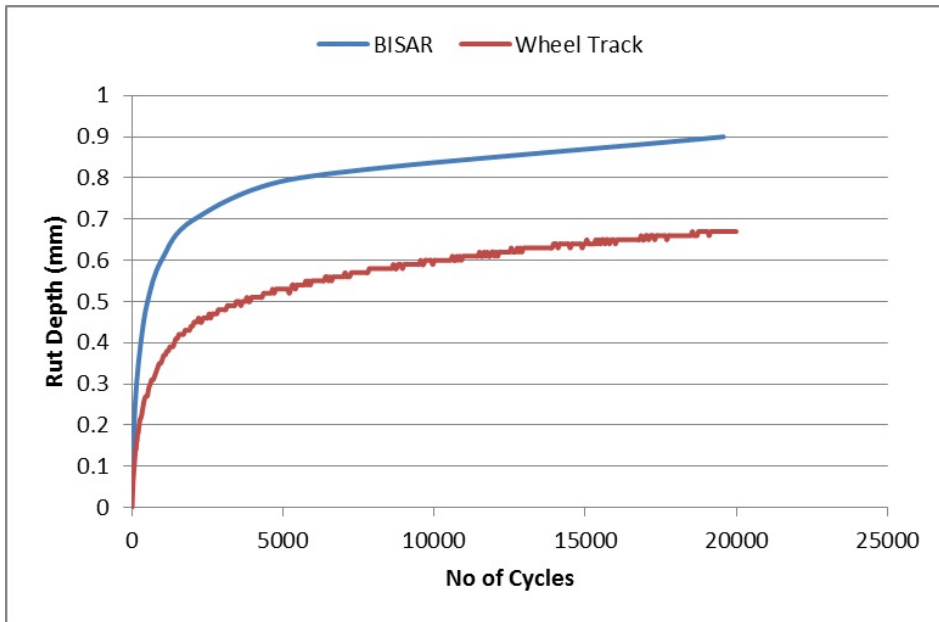


(b)

Figure 6.16: (a) Viscosity-Strain Curve. (b) Rut Depth Prediction. For Mix 5 at 30 °C

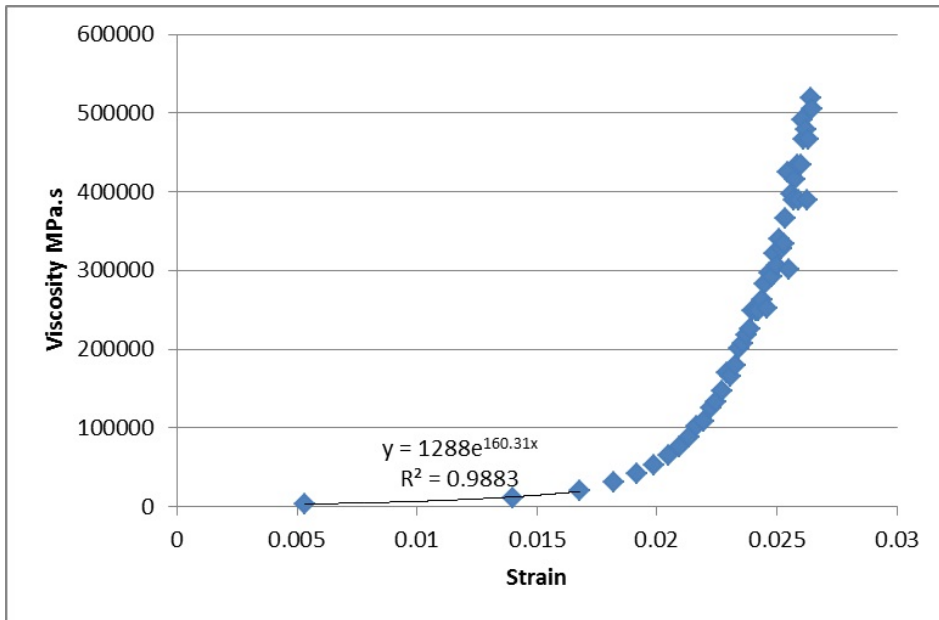


(a)

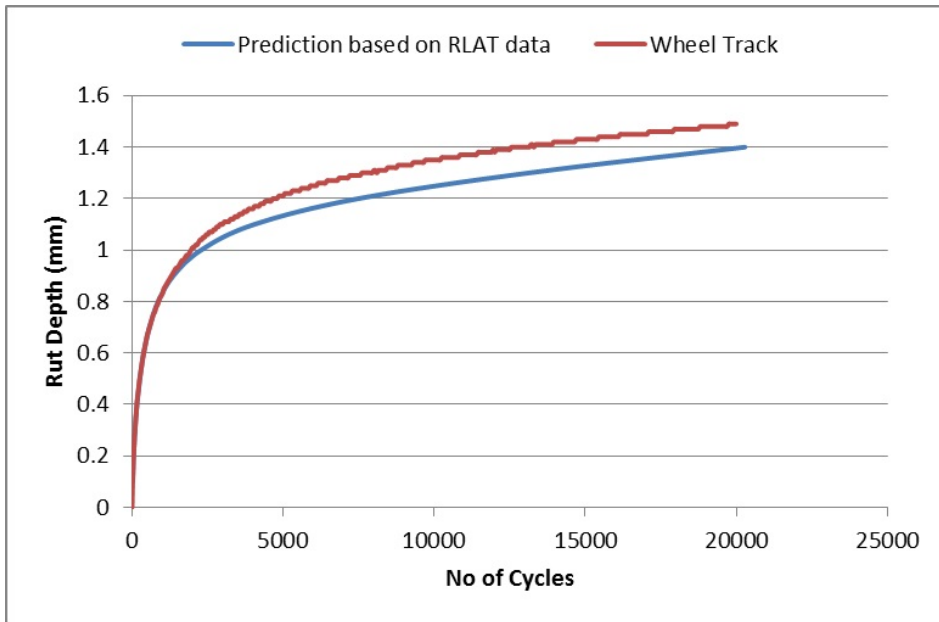


(b)

Figure 6.17: (a) Viscosity-Strain Curve. (b) Rut Depth Prediction. For Mix 7 at 30 °C



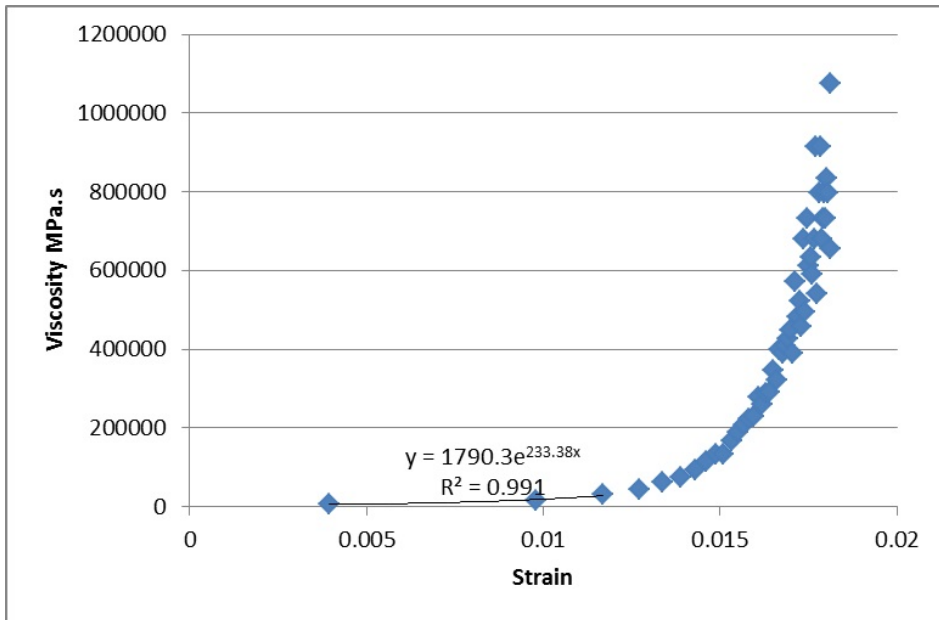
(a)



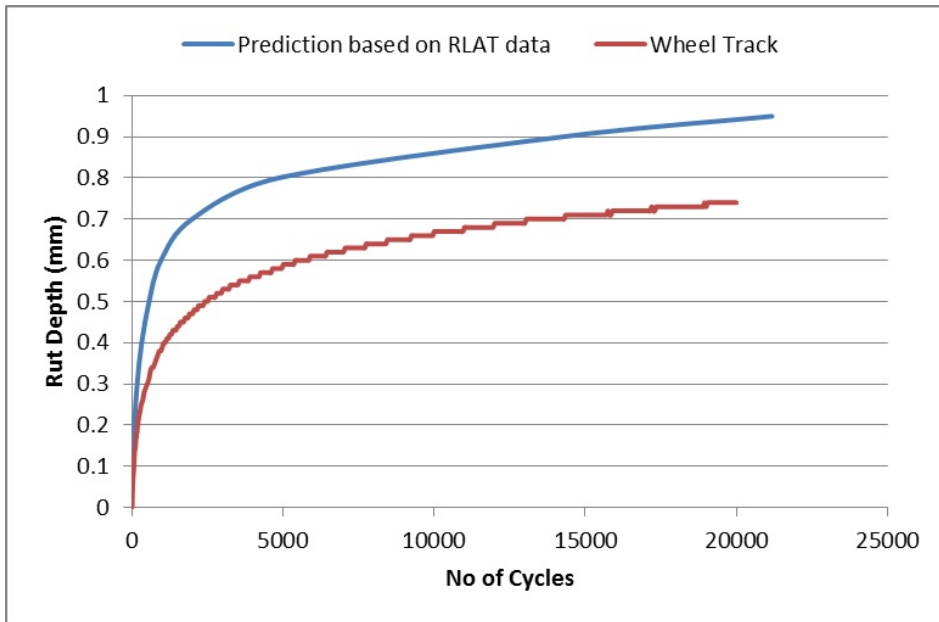
(b)

Figure 6.18: (a) Viscosity-Strain Curve. (b) Rut Depth Prediction. For Mix 10 at 30 °C



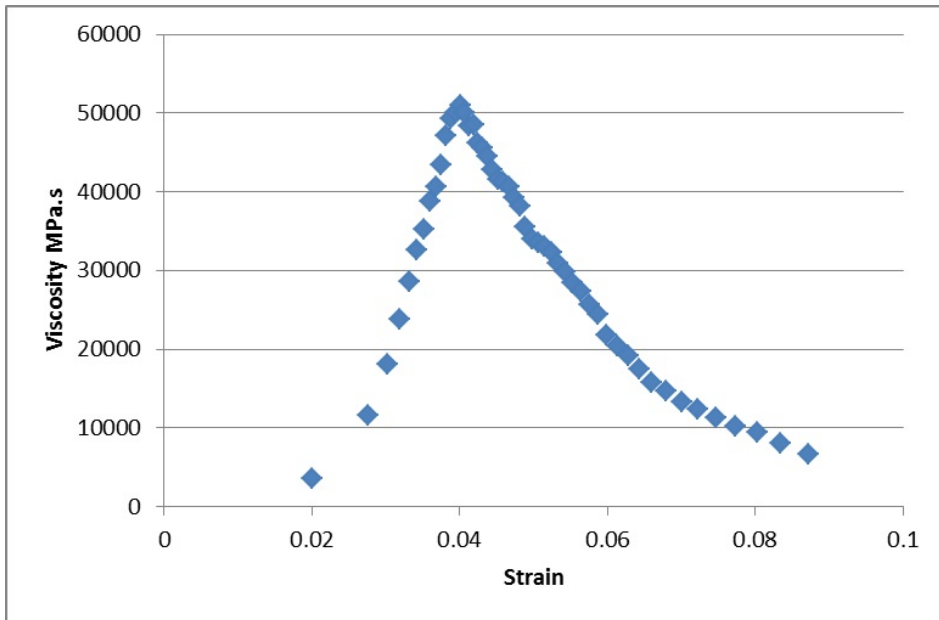


(a)

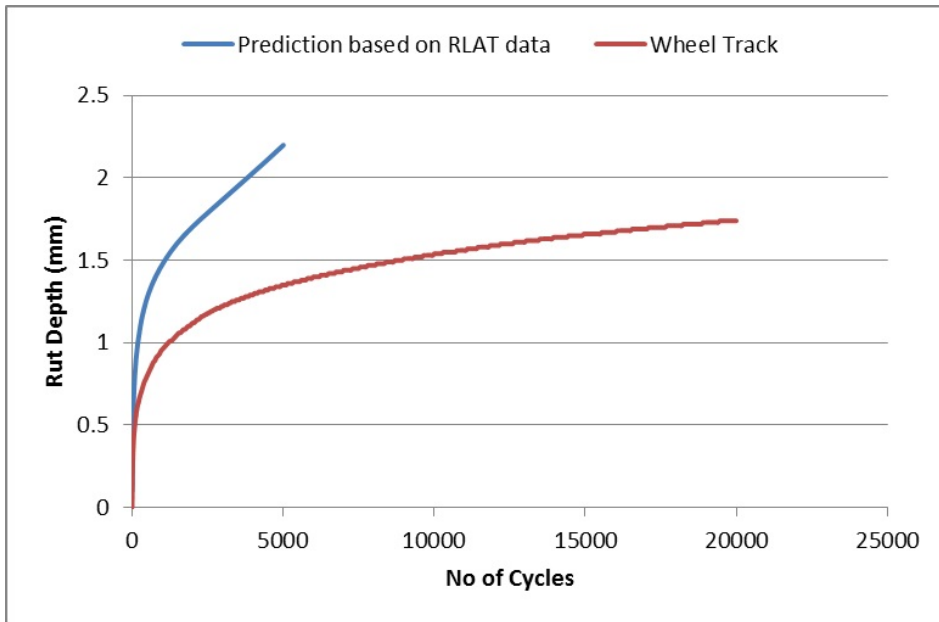


(b)

Figure 6.19: (a) Viscosity-Strain Curve. (b) Rut Depth Prediction. For Mix 13 at 30 °C



(a)



(b)

Figure 6.20: (a) Viscosity-Strain Curve. (b) Rut Depth Prediction. For Mix 13 at 50 °C

## **6.6 Field Rut Depth Prediction**

### **6.6.1 Data Collection**

The above analysis has also been applied to real road rut depths to check its validity further. Field data were obtained from Aecom related to a particular rutted road in the UK. The asphaltic layer consisted of three sublayers: 40 mm thickness of 0/10 mm Stone Mastic Asphalt (SMA) surface course, 50 mm thickness of 0/20 mm Dense Bitumen Macadam (DBM) binder course, and 135 mm thickness of 0/32 mm Hot Rolled Asphalt (HRA) base layer. It was noted that rutting to depths of 10-60 mm had taken place within two years of constructing the pavement, so a site investigation was performed, and cores were taken from outside the rutting area, and the cores showed the above thicknesses of each sublayer. The cores were then tested in the RLAT to measure the permanent deformation in each layer and the results were made available to this research. They were tested at 40 °C under a stress of 100 kPa for 3600 cycles according to Standard (1996).

### **6.6.2 Use of Field Data**

The field data report shows an assessment of the three layers to predict which layer is more susceptible to rutting by using an analytical tool called Permanent Deformation Program (PDP). PDP is based on the approach described in Chapter 2 by Nunn (1986) and it incorporates the RLAT data, initial penetration grade and softening point of binder used in each asphalt layer, and the traffic loading. The RLAT data from two core locations were utilised for the three sublayers. Viscosity-

strain curves were produced for all the asphalt layers, although none reached a viscosity peak. This is because of the relatively low stress applied (100 kPa) and the lower number of cycles compared to the data in the previous section. An exponential function was fitted to the viscosity-strain curves to allow an initial viscosity to be estimated, as shown in Figure 6.22. The pavement was then modelled in BISAR in three layers with the real thicknesses and a standard wheel load of 40 kN on a radius of 150 mm. The same process as presented in section 6.4 was applied but with extrapolation using the exponential function and 1 mm deformation increments.

Two issues were considered in performing the analysis: the loading time (speed of the vehicle), and temperature. For the loading time, a previously developed model by Brown (1973) was used to relate the loading time to vehicle speed and rut depth:

$$\log(t) = 0.5d - 0.2 - 0.94 \log(v) \quad (6.3)$$

where:  $t$  = loading time (sec);  $d$  = pavement depth (m); and  $v$  = vehicle speed (km/h). The RLAT loading time of 1 second was used in the above equation with the real depth to obtain an equivalent vehicle speed of 0.81 km/hr in the BISAR prediction. The prediction results were compared with a PDP prediction at 1 km/hr. Concerning temperature, an approximate estimate was made to convert the results from 40 to 26 °C (stated by Aecom as the effective field temperature). The temperature shift factor evaluation was based on previous RLAT data at 30, 40, and 50 °C; the initial parts of the 30 and 50 °C RLAT curves were shifted with respect to 40 °C by factors of 1.6 and 0.7 respectively, as shown in Figure

6.21. Extrapolation was made to 26 °C based on these factors assuming linear behaviour. The extrapolated shift factor for results from 26 °C to 40 °C was found to be 1.84. Therefore, all the predicted rut depths in BISAR were multiplied by a factor of 0.54 ( $\frac{1}{1.84}$ ) to convert the predicted data from 40 to 26 °C.

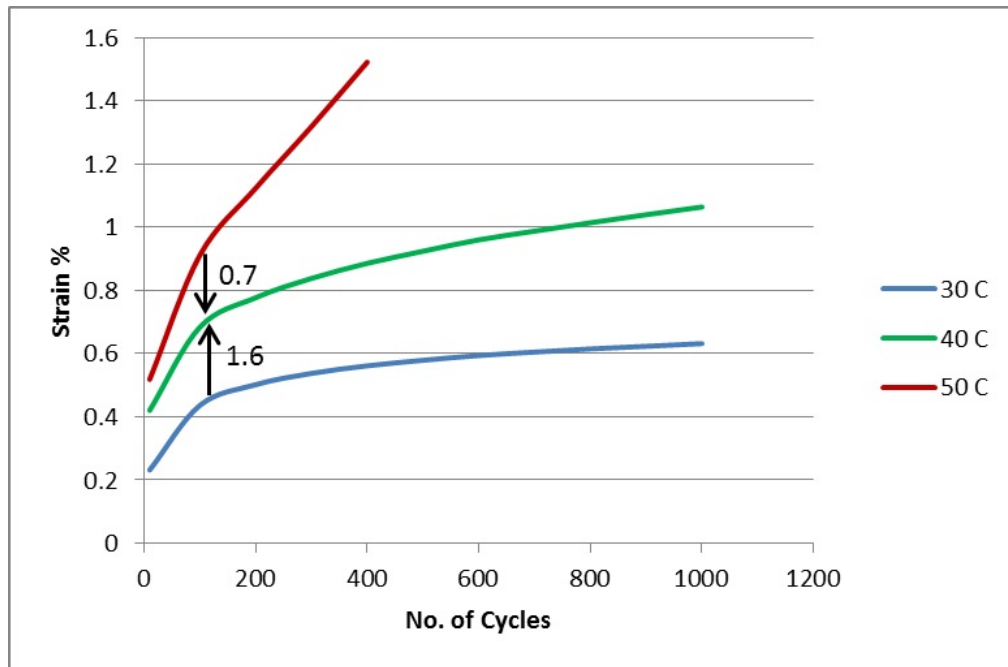
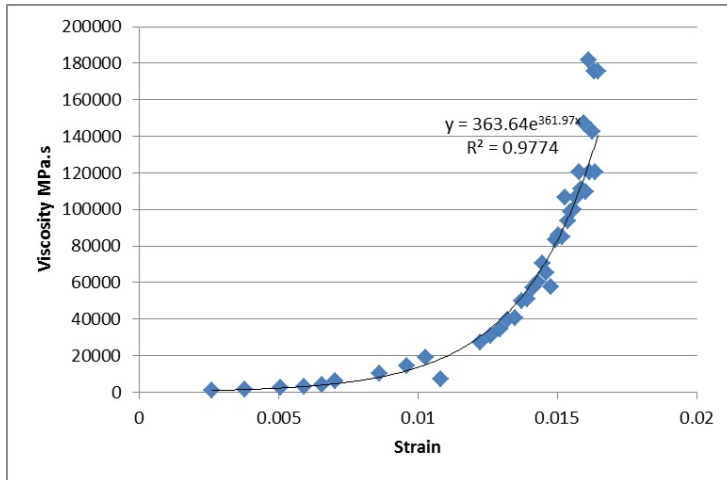


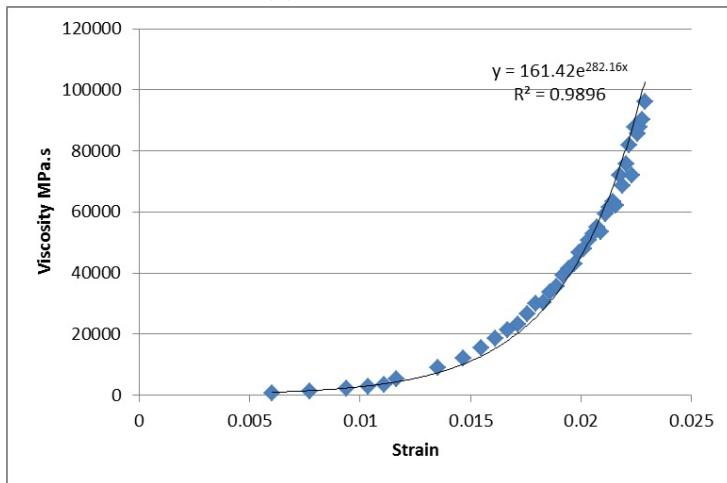
Figure 6.21: Shifting RLAT data to 40 °C

### 6.6.3 Prediction Results and Discussion

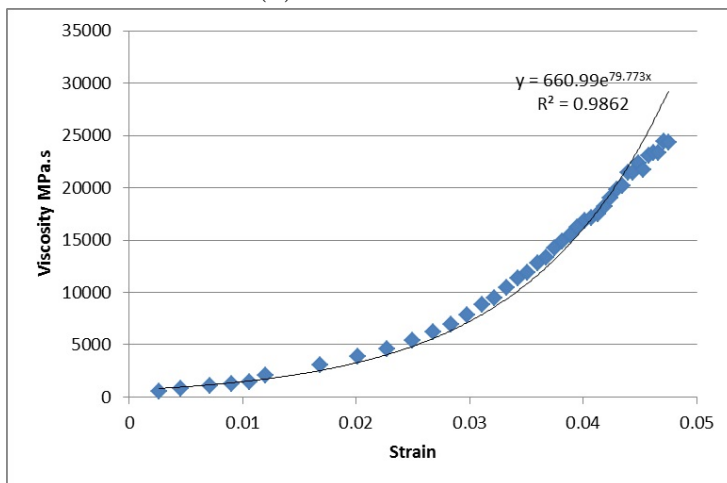
The prediction process was performed for 2 locations in the field, taken from a region outside rut line. The prediction of the rut is shown in Figure 6.23 and compared with the PDP prediction after considering the temperature shift factor. By way of comparison the field rut depth was measured to be 10-60 mm after two years of construction. The form of loading is entirely different in the BISAR and PDP analyses compared to a real load application. The actual wheel load includes



(a) Surface Layer



(b) Binder Course



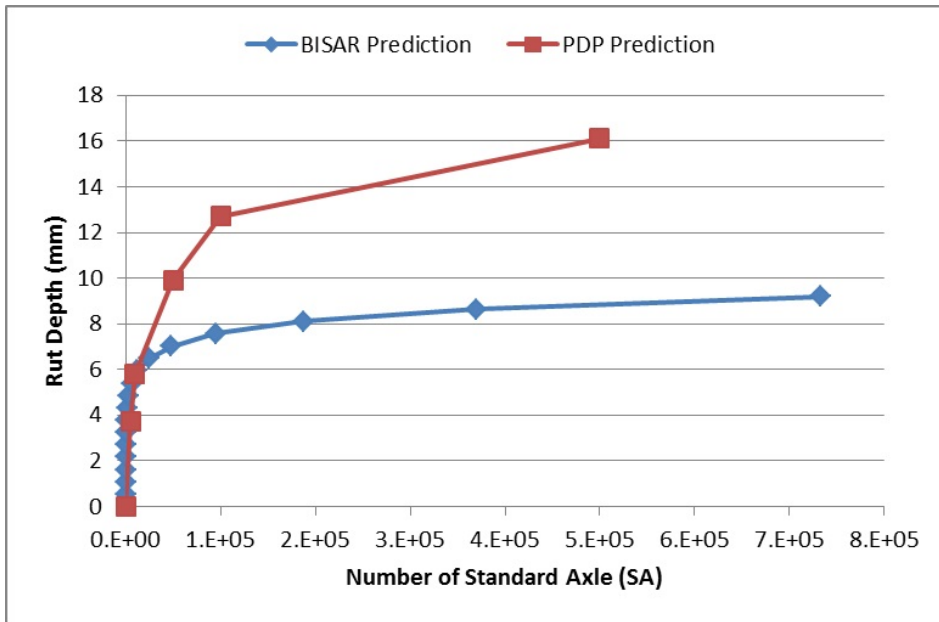
(c) Base Layer

Figure 6.22: Viscosity-Strain curve of Core 4 in Field

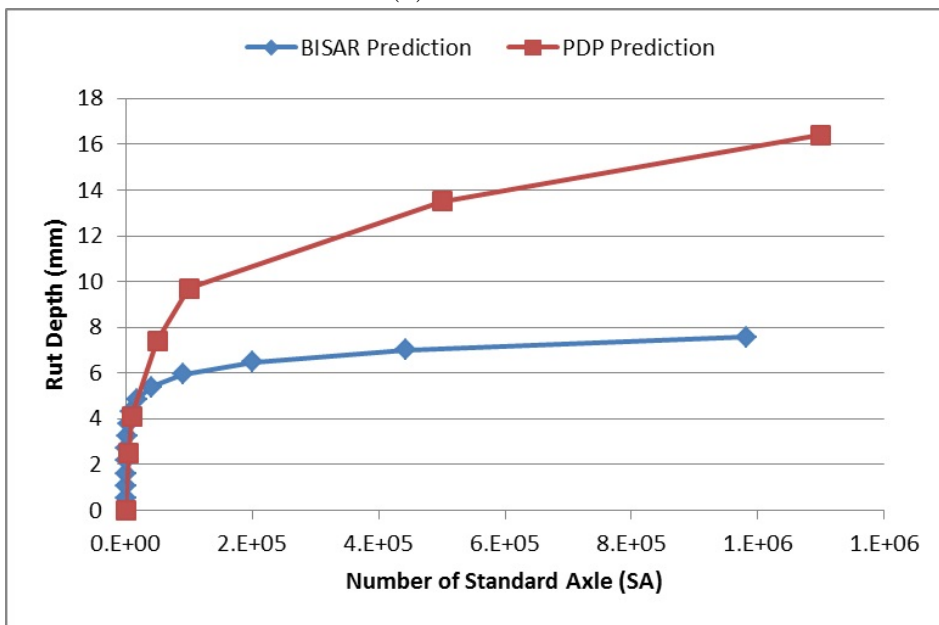
the rotational principle stress effects while BISAR and PDP do not. This has a very definite effect on unbound material and may also have an impact on asphalt mixtures, however it did not show effects on the prediction of wheel track prediction results presented earlier. The BISAR prediction matched PDP regarding the shape of the rut curve (the two stages primary and secondary); however, the process clearly underestimated the total rut depth.

The reason for this underestimation is that the viscosity-strain curve never reached a peak; and the fitted exponential function assumes that the viscosity keeps increasing. This produced very stiff layers of asphalt which then require a high number of Standard Axle (SA) to develop a 1 mm deformation. This is clearly shown in Figure 6.23 where the BISAR curves end in a very flat trend.

To overcome this problem, it was planned to fit a Gaussian function to the RLAT data to generate the peak of the viscosity-strain curve. Matlab 2015 was used to fit the RLAT data to the Gaussian function, but unfortunately, it has been found that the function could not be fitted to the data with any confidence. The reason is that the RLAT test was performed under a stress of 100 kPa and a duration of 3600 load applications; these parameters do not allow the sample to reach the tertiary stage; therefore, the function was not able to identify the peak. A trial was performed to estimate the strain value which corresponded to the peak viscosity for each layer but it was found that it was difficult to estimate it accurately and poor prediction was obtained.



(a) Core 2



(b) Core 4

Figure 6.23: Field Prediction Results

#### 6.6.4 Limitations and Specific Data Required

From the above discussion, it was noted that the data supplied was not enough to make a precise prediction. It is believed that to obtain an improved prediction



compared to the field, the RLAT data should fulfil specific requirements. Firstly, the sample should be left in the RLAT until high deformation is reached; this will allow the sample to reach the tertiary stage, and consequently the peak will be detected, allowing Gaussian function fitting. Secondly, the temperature used in the RLAT should be the ‘design’ temperature in the field to avoid the assumption of linear viscous behaviour in determining the shift factor and to obtain more precise prediction. Ideally, the loading time in the RLAT should be consistent with the design speed for the road; however in most test equipment it is accepted that this may not be practical and so an adjustment may therefore be required. These suggestions for RLAT testing are recommended to be considered if the method in this chapter is to be used to predict a field rut accurately.

## 6.7 Conclusions

The main type of permanent deformation in asphalt mixtures is rutting. Rutting appears in asphalt layers due to many reasons, such as very slow movement of a heavy vehicle, mixture properties and high temperature during loading. This chapter introduced an approach to predict rutting in asphalt mixtures, and several conclusions can be drawn:

- A linear viscous method was introduced aiming to predict the permanent deformation of the asphalt mixture. The method was based on using a multilayer linear computer program (BISAR) and inputting viscous parameters rather than elastic parameters. The information used to input to the program

was the nonlinear properties of the mixtures derived from RLAT test data, specifically the viscosity of the asphalt mixtures as a function of strain.

- Six asphalt concrete slabs with different aggregate gradations were manufactured for this purpose and were tested in the wheel tracking test to generate the rut depth. After that samples were cored from outside the rut line and tested in the RLAT at the same loading stress, loading time, and testing temperature.
- Three temperatures were used 30, 40, and 50 °C to verify that the approach is applicable. The approach shows good ability to predict the wheel tracking rut depth at 30 and 40 °C for all the mixtures. At 50 °C, only one dense sample was manufactured, and as expected the approach gave a poorer prediction than at other temperatures (because the analysis lies in areas where linear viscous does not work) due to the uncertainty inherent in the tertiary stage of deformation.
- Field data were also analysed, and asphalt layers were simulated in BISAR. Cores were taken from outside the rut line in the field and tested in the RLAT but at a different temperature than the weighted average field temperature, a low stress level and a low number of cycles. The prediction of field rut depth was relatively poor and, the reason was mainly due to having insufficient RLAT data to determine the non-linear properties. It is recommended that if this approach is to be used to predict real rutting, then specific requirements for RLAT test conditions need to be met.

- Finally, the effect of aggregate packing ratios was studied for the samples cored from each slab at different aggregate gradations and the results showed good agreement with the theory developed in Chapter 4.

# Chapter 7

## Conclusions and Recommendations

### 7.1 Introduction

One of the major forms of distress in asphalt pavement is permanent deformation. Permanent deformation is highly affected by the distribution of aggregate particles in the mixture. This research has focused on the effect of aggregate gradation on permanent deformation and stiffness of asphalt mixture by incorporating the theory of aggregate packing. A Surface course layer with 14 mm maximum aggregate size was selected to examine the effect of aggregate packing on the permanent deformation and stiffness. More than 20 asphalt mixtures with different aggregate gradations were manufactured for this purpose. The repeated load axial test (RLAT) was used to evaluate the performance of the mixtures in terms of permanent deformation and the indirect tensile stiffness modulus (ITSM) test for stiffness

evaluation.

Rutting depth was predicted by using a linear viscous approach. For this purpose wheel tracking tests were performed, for six mixtures, giving a measured rut depth and cores were taken from each slab and tested in the RLAT. By using the BISAR programme, the rut depth was predicted by introducing an approach to consider the non linear properties of the material.

## 7.2 Conclusions

The main conclusions of this thesis can be summarised in two areas:

### 7.2.1 Aggregate Packing

- It was shown that Bailey ratios are not adequate to evaluate the interaction of aggregate particles in the asphalt mixture. Therefore, three more ratios were introduced to define the whole aggregate gradation of each mixture. It was found that these three ratios combined with the two Bailey ratios provide a good understanding of the performance of the mixture.
- It was explained in theory what each ratio in the mixture represents. For example,  $CA$  ratio represents how the coarse particles are supported by the interceptors, and  $C_f/F_c$  represents how the coarse particles of the fine fraction support the fine particles of the coarse fraction. According to these ratios, the mixtures were determined to be either voided, to have too much fine material, too much coarse, to have coarse material but not supported by the fines, fine

materials but with no coarse material to carry the load, etc.

- To prove the applicability of these ratios in understanding the performance of the mixture, two mixtures were selected and images were taken for them in three locations top, middle, and bottom of the sample. It was shown that the ratios were applicable to the mixture and could estimate its performance. They showed whether the coarse aggregate particles were floating in a matrix of interceptors, or if they were well supported by other particles.
- The ANN and ANFIS techniques were found to be suitable tools to use these ratios to predict the permanent deformation (from RLAT) and stiffness modulus (from ITSM). Models were constructed in Matlab by feeding them the properties of each mixture (the five ratios) as input and data from the RLAT and ITSM tests as output.
- More variables were added to the models related to testing parameters. These variables were binder content, testing temperature, and compaction effort. The five packing ratios were able to explain why the changes in these variables affected the performance of the asphalt mixture. Mixtures with good aggregate interlock as recognized by the packing ratios were not hugely affected by changes in binder content. The effect of the packing ratios did not appear at relatively low temperature and they started to be more influential when temperature was increased. The increase in compaction effort produced no change in the performance of some mixtures because they have reached optimum compaction at a certain level. Other mixtures had poor performance

at higher compaction effort due to the high contact pressure developed between coarse particles and this may have led to particle breakdown, although there is no clear evidence on this.

- Models were also constructed for these new variables by using the ANN and ANFIS techniques to predict the permanent deformation and stiffness modulus. The ANN approach showed better prediction results in estimating the performance when these variables were used as input parameters.

### **7.2.2 Rut Depth Prediction**

Conclusions are drawn from the prediction of rut depth by using a linear viscous approach:

- The linear viscous approach and the implementation of viscosity presented in Chapter 6 is considered as a good approach to predict wheel track rut depth. The approach is based on data from RLAT tests on cores taken from tested asphalt slabs from regions outside the rut line.
- The prediction was performed at a testing temperature of 40 °C for six mixtures, and results showed good agreement with the measured rut line. After that the same procedure was repeated at 30 °C testing temperature and it also showed good agreement with the laboratory tested slabs. A final prediction set at 50 °C was performed but this showed poor prediction because the behaviour of asphalt mixtures lies in outside the areas of linear viscous

approach work. The high strain in RLAT test is mainly because the aggregate is more dominant than binder.

- The approach could be used for field rut prediction if appropriate data were supplied. Field data were provided by Aecom and were also analysed in BISAR. The predicted results were compared with PDP (another prediction programme) results and they were found to give lower rut depths. The concern about the data was that the RLAT test was not performed at the same average temperature as assumed in the field, and the load duration was different from the design speed in the field. Finally, the RLAT test was stopped before reaching the tertiary stage, and this could lead to inaccurate prediction results because the start point of the tertiary stage is difficult to estimate. The difficulty of estimating the start point of the tertiary stage is because there is no previous data that could be a base to predict the behaviour. The samples used in the lab cannot be used for this purpose because they are not under the same conditions of material preparation and testing (stress applied, compaction, aggregate gradation, binder content, volumetric properties, etc).

### **7.3 Recommendations for Future Work**

The effect of aggregate gradation on the performance of asphalt mixtures has been investigated in this thesis. The aggregate packing ratios presented in this research showed good ability to describe the performance of the mixture and to characterise the mixture properties. However, there are some issues that need to be investigated



in future work, summarised as:

- i. The effect of aggregate angularity on particle packing is a very important aspect to examine. In this research only one type of aggregate was used (one angularity) to establish the the use of packing ratios. Other types of aggregate could also be used and this will tacitly affect the angularity, shape and strength of the aggregate. However, in theory the packing ratios give the same understanding on any other type of aggregate because they are related to the arrangement of particles.

It is very recommended to meet industrial needs by implementing RAP to the aggregate and check if the packing ratios are also applicable.

- ii. This research focused on the prediction of permanent deformation in asphalt mixtures, therefore rutting related tests were carried out and stiffness modulus. It is strongly recommended to investigate how these packing ratios affect the cracking characteristics by performing fatigue tests. In fatigue tests there are big differences in the number of cycles taken to reach failure and the reason behind this is often not clear. The packing ratios may give improved understanding of this.
- iii. Although asphalt concrete mixtures, stone mastic asphalt, and porous asphalt were used to validate the use of packing ratios in understanding the performance of the mixture, it would be beneficial to investigate other mixtures such as hot rolled asphalt (HRA).

- iv. The Discrete Element Method (DEM) is an efficient tool to study the arrangement of particles in a mixture. Different arrangements could be assumed and different aggregate angularity could be used to study the behaviour of the mixture and compare it with laboratory results.
- v. The compaction used in this study was only by means of the gyratory compactor. It would be worth using other types of compaction and see if the aggregate is packed differently by other compaction methods.

Regarding the prediction of rutting in an asphalt pavement the approach showed good correlation with the measured rut depth in the laboratory. However there are some issues that need to be investigated in future work, summarised as follows:

- i. The use of BISAR is a time consuming process because each deformation increment needs a separate run. Therefore investigations are recommended using the equations of the Method of Equivalent Thicknesses (MET), implementing them into a spreadsheet to ease the process.
- ii. At high temperatures the approach is less precise due to the plastic deformation of the sample and the linear viscous approach is not valid. This needs extra investigations in terms of the optimal stress in RLAT testing to use and the use of the finite element method may be helpful.
- iii. The field data was not very well predicted due to reasons listed in Chapter 6. It is strongly recommended to either perform a large scale rutting test (if available) and use the linear viscous approach to predict the rut depth or use

real rut data from the field and take cores from the same road. Then test the cores in the RLAT under the same field conditions in terms of average annual temperature and loading time, ensuring that the sample reaches the tertiary stage in the RLAT test.

# References

- Ahmed, M. A. & Attia, M. I. (2013). Impact of aggregate gradation and type on hot mix asphalt rutting in egypt. *International Journal of Engineering Research and Application (IJERA)*, 3:2249–2258.
- Al-Qadi, I. L., Xie, W., & Elseifi, M. A. (2008). Frequency determination from vehicular loading time pulse to predict appropriate complex modulus in mepdg. *Journal of the Association of Asphalt Paving Technologists*, 77.
- Albayati, A. (2006). Permanent deformation prediction of asphalt concrete under repeated loading. *University of Baghdad, Iraq*, 129.
- Alshamsi, K. S. (2006). *Development of a mix design methodology for asphalt mixtures with analytically formulated aggregate structures*. PhD thesis, University of Birmingham, United Kingdom.
- Antes, P. W., van Dommelen, A. E., Houben, L. J., Molenaar, A. A., & Parajuli, U. (2003). Stress dependent behavior of asphalt mixtures at high temperatures. *Asphalt Paving Technology*, 72:173–195.

- Asphalt Institute, S. (1996). Superpave series no. 2 (sp-2). *Asphalt Institute, Lexington, KY.*
- Avizo (2014). Users guide: modular and object-oriented software system. *AVIZO Fire.*
- Barksdale, R. D. (1971). Compressive stress pulse times in flexible pavements for use in dynamic testing. *Highway research record*, (345).
- Barksdale, R. D. (1972). Laboratory evaluation of rutting in base course materials. In: *Presented at the Third International Conference on the Structural Design of Asphalt Pavements, Grosvenor House, Park Lane, London, England, Sept. 11-15, 1972.*, volume 1.
- Battiato, G., Ronca, G., & Verga, C. (1977). Moving loads on a viscoelastic double layer: Prediction of recoverable and permanent deformations. In: *Volume I of proceedings of 4th International Conference on Structural Design of Asphalt Pavements, Ann Arbor, Michigan, August 22-26, 1977.*, number Proceeding.
- Bianchini, A. & Bandini, P. (2010). Prediction of pavement performance through neuro-fuzzy reasoning. *Computer-Aided Civil and Infrastructure Engineering*, 25(1):39–54.
- Bolk, H. & Van de Loo, P. (1979). The creep test: a routine method for the design of stable asphalt mixes. *Amsterdam: Koninklijke/Shell-Laboratories.*
- Brown, A. & Sparks, J. (1958). Viscoelastic properties of a penetration grade

- paving asphalt at winter temperature. In: *Proceedings of the Association of asphalt Paving Technologists*, volume 27, pages 35–51.
- Brown, E. & Foo, K. Y. (1994). Comparison of unconfined-and confined-creep tests for hot mix asphalt. *Journal of materials in civil engineering*, 6(2):307–326.
- Brown, S. (1973). Determination of young's modulus for bituminous materials in pavement design. *Highway Research Record*, (431).
- Brown, S. (1976). Laboratory testing for use in the prediction of rutting in asphalt pavements. *Transportation Research Record*, (616).
- Brown, S. (1978). Material characteristics for analytical pavement design. *Developments in highway pavement engineering*, 1:41–92.
- Brown, S. & Bell, C. (1977). The validity of design procedures for the permanent deformation of asphalt pavements. In: *Volume I of proceedings of 4th International Conference on Structural Design of Asphalt Pavements, Ann Arbor, Michigan, August 22-26, 1977.*, number Proceeding.
- Brown, S. & Bell, C. (1979). The prediction of permanent deformation in asphalt pavements. In: *Association of Asphalt Paving Technologists Proceedings*, volume 48.
- Brown, S. & Cooper, K. (1984). The mechanical properties of bituminous materials for road bases and base courses. *Journal of the Association of Asphalt Paving Technologists*, 53(4):10–15.

- Brown, S. & Snaith, M. (1974). The permanent deformation characteristics of a dense bitumen macadam subjected to repeated loading. In: *Association of Asphalt Paving Technologists Proc*, volume 43.
- Burmister, D. (1943). The theory of stresses and displacements in layered systems and applications of the design of airport runways, paper presented at the annual meeting, highway res. Board, Natl. Res. Council., Washington, DC.
- Cai, W. (2013). *Discrete Element Modelling of constant strain rate and creep tests on a graded asphalt mixture*. PhD thesis, University of Nottingham.
- Ceylan, H., Gopalakrishnan, K., & Kim, S. (2008). Advanced approaches to hot-mix asphalt dynamic modulus prediction. *Canadian Journal of Civil Engineering*, 35(7):699–707.
- Ceylan, H., Gopalakrishnan, K., & Kim, S. (2009). Looking to the future: the next-generation hot mix asphalt dynamic modulus prediction models. *International Journal of Pavement Engineering*, 10(5):341–352.
- Chattopadhyay, S. (2006). Soft computing techniques in combating the complexity of the atmosphere-a review. *arXiv preprint nlin/0608052*.
- Cheung, C. & Cebon, D. (1997a). Deformation mechanisms of pure bitumen. *Journal of Materials in Civil Engineering*, 9(3):117–129.
- Cheung, C. & Cebon, D. (1997b). Experimental study of pure bitumens in tension, compression, and shear. *Journal of Rheology (1978-present)*, 41(1):45–74.

- Cheung, C. & Cebon, D. (1997c). Thin film deformation behavior of power-law creeping materials. *Journal of engineering mechanics*, 123(11):1138–1152.
- Cheung, C. Y. (1995). *Mechanical behaviour of bitumens and bituminous mixes*. PhD thesis, University of Cambridge.
- Collop, A., Cebon, D., & Hardy, M. (1995). Viscoelastic approach to rutting in flexible pavements. *Journal of Transportation Engineering*, 121(1):82–93.
- Croney, D. & Croney, P. (1991). *The design and performance of road pavements*.
- Demircan, E., Harendra, S., & Vipulanandan, C. (2010). Artificial neural network and nonlinear models for gelling time and maximum curing temperature rise in polymer grouts. *Journal of Materials in Civil Engineering*, 23(4):372–377.
- Denneman, E., Verhaeghe, B., & Sadzik, E. (2007). Aggregate packing characteristics of good and poor performing asphalt mixes. Proceedings of the 26th Southern African Transport Conference 2007.
- Eisenmann, J., Lempe, U., & Leykauf, G. (1977). Method for the structural design of asphalt pavements. In: *Volume I of proceedings of 4th International Conference on Structural Design of Asphalt Pavements, Ann Arbor, Michigan, August 22-26, 1977.*, number Proceeding.
- EN, B. (2003). 12697: Bituminous mixtures. test methods for hot mix asphalt. wheel tracking. *British Standards*.



- EN, B. (2004). 12697: Bituminous mixtures. test methods for hot mix asphalt. laboratory mixing. *British Standards*.
- EN, B. (2005). 4987: Coated macadam (asphalt concrete) for roads and other paved areas. specification for constituent materials and for mixtures. *British Standards*.
- EN, B. (2007a). 1426: Bitumen and bituminous bindersdetermination of needle penetration. *British Standards*.
- EN, B. (2007b). 1427: Bitumen and bituminous bindersdetermination of the softening pointring and ball method. *British Standards*.
- Far, M., Underwood, B., Ranjithan, S., Kim, Y., & Jackson, N. (2009). Application of artificial neural networks for estimating dynamic modulus of asphalt concrete. *Transportation Research Record: Journal of the Transportation Research Board*, (2127):173–186.
- Fuller, W. B. & Thompson, S. E. (1907). The laws of proportioning concrete. *Transactions of the American Society of Civil Engineers*, 59(2):67–143.
- Gandhi, T., Xiao, F., & Amirghanian, S. N. (2009). Estimating indirect tensile strength of mixtures containing anti-stripping agents using an artificial neural network approach. *International Journal of Pavement Research and Technology*, 2(1):1.
- Gardner, L. & Skok, E. (1967). Use of viscoelastic concepts to evaluate laboratoty test results and field performance of some minnesota asphalt mixtures. In: *Intl Conf Struct Design Asphalt Pvmts*.

- Gaskins, F. H., Brodnyan, J. G., Philippoff, W., & Thelen, E. (1960). The rheology of asphalt. ii. flow characteristics of asphalt. *Transactions of The Society of Rheology (1957-1977)*, 4(1):265–278.
- Gershenson, C. (2003). Artificial neural networks for beginners. *arXiv preprint cs/0308031*.
- Gibb, J. M. (1996). *Evaluation of resistance to permanent deformation in the design of bituminous paving mixtures*. PhD thesis, University of Nottingham.
- Golalipour, A., Jamshidi, E., Niazi, Y., Afsharikia, Z., & Khadem, M. (2012). Effect of aggregate gradation on rutting of asphalt pavements. *Procedia-Social and Behavioral Sciences*, 53:440–449.
- Gopalakrishnan, K. & Ceylan, H. Adaptive neuro-fuzzy inference system-based backcalculation approach to airport pavement structural analysis. In: *Material Design, Construction, Maintenance, and Testing of Pavements*.
- Graham, A. et al. (1980). An instrumented triaxial cell for cyclic loading of clays.
- Guarin, A. (2009). *Interstitial component characterization to evaluate asphalt mixture performance*. PhD thesis, University of Florida.
- Haas, R. & Papagianakis, A. (1986). Understanding pavement rutting.
- Hall, M. (1972). Mechanical properties of solid polymers. in ward. wiley-interscience. 1971. pp. 375. price£ 7.00. *British Polymer Journal*, 4(4):367–367.

- Hills, J. (1973). Creep of asphalt mixes. *Journal of the Institute of Petroleum*, 59(570):247–262.
- Hills, J. F., Brian, D., & Loo, P. (1974). The correlation of rutting and creep tests on asphalt mixes. Technical report.
- Hofstra, A. & Klopm, A. (1972). Permanent deformation of flexible pavements under simulated road traffic conditions. In: *Presented at the Third International Conference on the Structural Design of Asphalt Pavements, Grosvenor House, Park Lane, London, England, Sept. 11-15, 1972.*, volume 1.
- Huschek, S. (1977). Evaluation of rutting due to viscous flow in asphalt pavements. In: *Volume I of proceedings of 4th International Conference on Structural Design of Asphalt Pavements, Ann Arbor, Michigan, August 22-26, 1977.*, number Proceeding.
- Isola, R. (2008). *Packing of granular materials*. University of Nottingham.
- Jang, J.-S. R. (1993). Anfis: adaptive-network-based fuzzy inference system. *Systems, Man and Cybernetics, IEEE Transactions on*, 23(3):665–685.
- Jongepier, R., Kuilman, B., Schmidt, R., Puzinauskas, V., & Rostler, F. (1969). Characteristics of the rheology of bitumens. In: *Association of Asphalt Paving Technologists Proc.*
- Juang, C. H. & Chen, C. J. (1999). Cpt-based liquefaction evaluation using artificial neural networks. *Computer-Aided Civil and Infrastructure Engineering*, 14(3):221–229.

- Kandhal, P. & Cooley Jr, L. (2001). The restricted zone in the superpave aggregate gradation specification, nchrp report 464. *Transportation Research Board, National Research Council, Washington, DC.*
- Kandhal, P. & Mallick, R. (2001). Effect of mix gradation on rutting potential of dense-graded asphalt mixtures. *Transportation Research Record: Journal of the Transportation Research Board*, (1767):146–151.
- Kandil, K. A. (2013). Modeling marshall stability and flow for hot mix asphalt using artificial intelligence techniques. *Nature and Science*, 11(6):106–112.
- Khanzada, S. (2000). *Permanent Deformation in Bituminous Mixtures*. PhD thesis, Civil Engineering, The University of Nottingham.
- Khosla, N. P. & Sadasivam, S. (2005). Determination of optimum gradation for resistance to permeability, rutting and fatigue cracking. Technical report.
- Kim, S. (2006). *Identification and Assessment of the Dominant Aggregate Size Range of Asphalt Mixture*. PhD thesis, University of Florida.
- Kim, S., Roque, R., Guarin, A., & Birgisson, B. (2006). Identification and assessment of the dominant aggregate size range (dasr) of asphalt mixture (with discussion). *Journal of the Association of Asphalt Paving Technologists*, 75.
- Kutay, M. E., Arambula, E., Gibson, N., & Youtcheff, J. (2010). Three-dimensional image processing methods to identify and characterise aggregates in compacted asphalt mixtures. *International Journal of Pavement Engineering*, 11(6):511–528.

- Kutner, M. H., Nachtsheim, C., & Neter, J. (2004). *Applied linear regression models*. McGraw-Hill/Irwin.
- Lacroix, A., Kim, Y., & Ranjithan, S. (2008). Backcalculation of dynamic modulus from resilient modulus of asphalt concrete with an artificial neural network. *Transportation Research Record: Journal of the Transportation Research Board*, (2057):107–113.
- Lambe, T. & Whitman, R. (1969). *Soil mechanics*, 553 pp.
- Lee, Y. W. (2006). *Discrete element modelling of idealised asphalt mixture*. PhD thesis, University of Nottingham.
- Lira Miranda, B. F. (2012). *Gradation-based framework for asphalt mixtures*. Master's thesis, School of Architecture and Built Environment.
- Loulizi, A., Al-Qadi, I., Lahouar, S., & Freeman, T. (2002). Measurement of vertical compressive stress pulse in flexible pavements: representation for dynamic loading tests. *Transportation Research Record: Journal of the Transportation Research Board*, (1816):125–136.
- Lu, Y. (1998). *Temperature dependent visco-elastoplastic evaluation of flexible pavements*. PhD thesis, London South Bank University.
- Mallick, R. B. & El-Korchi, T. (2013). *Pavement engineering: principles and practice*. CRC Press.

- Mamat, R. (2008). *Evaluation of marshall properties of asphalt mixtures with aggregate gradations designed using the bailey method*. PhD thesis, Universiti Teknologi Malaysia, Faculty of Civil Engineering.
- McLean, D. & Monismith, C. (1974). Estimation of permanent deformation in asphalt concrete layers due to repeated traffic loading. *Transportation research record*, (510).
- Mehran, K. (2008). Takagi-sugeno fuzzy modeling for process control. *Industrial Automation, Robotics and Artificial Intelligence (EEE8005), School of Electrical, Electronic and Computer Engineering, Newcastle University*.
- Meyer, F. & Haas, R. (1977). A working design subsystem for permanent deformation in asphalt pavement. In: *Volume I of proceedings of 4th International Conference on Structural Design of Asphalt Pavements, Ann Arbor, Michigan, August 22-26, 1977.*, number Proceeding.
- Mirzahosseini, M. R., Najjar, Y. M., HosseinAlavi, A., & HosseinGandomi, A. (2013). Ann-based prediction model for rutting propensity of asphalt mixtures. In: *Transportation Research Board 92nd Annual Meeting*, number 13-2180.
- Moavenzadeh, F. & Carnaghi, R. (1966). Viscoelastic response of sand asphalt beams on elastic foundations under repeated loading. *Proceedings of the Association of the Asphalt Pouring Technologists*, 35:514–528.
- Moavenzadeh, F. & Stander Jr, R. (1967). Effect of aging on flow properties of asphalts. *Highway Research Record*, (178).

- Moghaddam, T. B., Soltani, M., Karim, M. R., Shamshirband, S., Petković, D., & Baaaj, H. (2015). Estimation of the rutting performance of polyethylene terephthalate modified asphalt mixtures by adaptive neuro-fuzzy methodology. *Construction and Building Materials*, 96:550–555.
- Mohammad, L. N. & Shamsi, K. (2007). A look at the bailey method and locking point concept in superpave mixture design. *Practical Approaches to Hot-Mix Asphalt Mix Design and Production Quality Control Testing*, pages 24–32.
- Monismith, C., Inkabi, K., Freeme, C., & McLean, D. (1977). A subsystem to predict rutting in asphalt concrete pavement structures. In: *Volume I of proceedings of 4th International Conference on Structural Design of Asphalt Pavements, Ann Arbor, Michigan, August 22-26, 1977.*, number Proceeding.
- Monismith, C. L. & Secor, K. E. (1962). Viscoelastic behavior of asphalt concrete pavements. In: *International Conference on the Structural Design of Asphalt Pavements*, volume 203.
- Monismith, C. L. & Tayebali, A. (1988). Permanent deformation (rutting) considerations in asphalt concrete pavement sections. In: *Association of Asphalt Paving Technologists Technical Sessions, 1988, Williamsburg, Virginia, USA*, volume 57.
- Morris, J., Haas, R., Reilly, P., & Hignell, E. (1974). Permanent deformation in asphalt pavements can be predicted. In: *Proc. AAPT*, volume 43.
- Negnevitsky, M. (2005). *Artificial intelligence: a guide to intelligent systems*. Pearson Education.

- Nijboer, L. W. (1948). *Plasticity as a factor in the design of dense bituminous road carpets*. Elsevier Pub. Co.
- Nunn, M. (1986). Prediction of permanent deformation in bituminous pavement layers.
- Ossa, E., Deshpande, V., & Cebon, D. (2005). Phenomenological model for monotonic and cyclic behavior of pure bitumen. *Journal of materials in civil engineering*, 17(2):188–197.
- Ossa, E. A. (2005). *Deformation behaviour of bitumen and bituminous mixes*. PhD thesis, University of Cambridge.
- Ozgan, E. (2011). Artificial neural network based modelling of the marshall stability of asphalt concrete. *Expert Systems with Applications*, 38(5):6025–6030.
- Özgan, E., Korkmaz, I., & Emiroğlu, M. (2012). Adaptive neuro-fuzzy inference approach for prediction the stiffness modulus on asphalt concrete. *Advances in Engineering Software*, 45(1):100–104.
- Pagen, C. A. (1972). Dynamic structural properties of asphalt pavement mixtures. In: *Intl Conf Structural Design Proc*, volume 1.
- Pavement Interactive (2008). Pavement history.
- Peutz, M., Van Kempen, H., & Jones, A. (1968). Layered systems under normal surface loads. *Highway Research Record*, (228).



- Poel, V. & Der, C. (1954). A general system describing the visco-elastic properties of bitumens and its relation to routine test data. *Journal of applied chemistry*, 4(5):221–236.
- Pourtahmasb, M. S., Karim, M. R., & Shamshirband, S. (2015). Resilient modulus prediction of asphalt mixtures containing recycled concrete aggregate using an adaptive neuro-fuzzy methodology. *Construction and Building Materials*, 82:257–263.
- Powell, M. (1980). Computer-simulated random packing of spheres. *Powder Technology*, 25(1):45–52.
- Rabbira, G. (2002). *Permanent deformation properties of asphalt concrete mixtures*. PhD thesis, Doctoral thesis.
- Read, J. M. (1996). *Fatigue cracking of bituminous paving mixtures*. PhD thesis, University of Nottingham England.
- Romain, J. (1972). Rut depth prediction in asphalt pavements. In: *Presented at the Third International Conference on the Structural Design of Asphalt Pavements, Grosvenor House, Park Lane, London, England, Sept. 11-15, 1972.*, volume 1.
- Rumelhart, D. E., McClelland, J. L., Group, P. R., et al. (1986). Parallel distributed processing: Explorations in the microstructure of cognition, vol. 1-2. *Cambridge, MA*.
- Sánchez-Leal, F. J. (2007). Gradation chart for asphalt mixes: Development. *Journal of materials in civil engineering*, 19(2):185–197.

- Selvi, O. (2009). *Taffic Accident Predictions Based on Fuzzy Logic Approach for Safer Urban Environments, Case Study: Izmir Metropolitan Area*. PhD thesis, Graduate School of Engineering and Sciences, zmir Institute of Technology.
- Serin, S., Morova, N., Sargin, Ş., Terzi, S., & Saltan, M. (2013). Modeling Marshall stability of lightweight asphalt concretes fabricated using expanded clay aggregate with anfis.
- Shafabakhsh, G., Ani, O. J., & Talebsafa, M. (2015). Artificial neural network modeling (ann) for predicting rutting performance of nano-modified hot-mix asphalt mixtures containing steel slag aggregates. *Construction and Building Materials*, 85:136–143.
- Shafabakhsh, G. & Tanakizadeh, A. (2015). Investigation of loading features effects on resilient modulus of asphalt mixtures using adaptive neuro-fuzzy inference system. *Construction and Building Materials*, 76:256–263.
- Singh, D., Zaman, M., & Commuri, S. (2012). Artificial neural network modeling for dynamic modulus of hot mix asphalt using aggregate shape properties. *Journal of Materials in Civil Engineering*, 25(1):54–62.
- Sousa, J. B., Craus, J., & Monismith, C. L. (1991). Summary report on permanent deformation in asphalt concrete. Technical report.
- Sousa, J. B. & Weissman, S. L. (1994). Modeling permanent deformation of asphalt-aggregate mixes (with discussion). *Journal of the Association of Asphalt Paving Technologists*, 63.

- Standard, B. (1996). Method for determining resistance to permanent deformation of bituminous mixtures subject to unconfined dynamic loading. *Draft for development, DD*, 226(1).
- Suzuki, M. & Oshima, T. (1985). Comparison between the computer-simulated results and the model for estimating the co-ordination number in a three-component random mixture of spheres. *Powder technology*, 43(1):19–25.
- Swiertz, D., Mahmoud, E., & Bahia, H. Asphalt mixture compaction and aggregate structure analysis techniques: State of the art report. *RILEM Technical Committee*.
- Szpiro, G. (2003). *Kepler's conjecture: how some of the greatest minds in history helped solve one of the oldest math problems in the world*. John Wiley & Sons Hoboken.
- Tabatabaei, S. A., Khaledi, S., & Jahantabi, A. (2013). Modeling the deduct value of the pavement condition asphalt pavement by adaptive neuro fuzzy inference system. *International Journal of Pavement Research and Technology*, 6(1):59.
- Taherkhani, H. (2006). *Experimental Characterisation of the Compressive Permanent Deformation Behaviour in Asphaltic Mixtures*. University of Nottingham.
- Talbot, A. N. & Richart, F. E. (1923). The strength of concrete-its relation to the cement, aggregates and water. *Illinois Univ Eng Exp Sta Bulletin*.
- Tapkın, S., Çevik, A., & Uşar, Ü. (2010). Prediction of marshall test results for

- polypropylene modified dense bituminous mixtures using neural networks. *Expert Systems with Applications*, 37(6):4660–4670.
- Tapkin, S., Çevik, A., & Usar, Ü. (2012). Prediction of rutting potential of dense bituminous mixtures with polypropylene fibers via repeated creep testing by using neuro-fuzzy approach. *Periodica Polytechnica. Civil Engineering*, 56(2):253.
- Tarefder, R. A. & Zaman, M. (2005). Design of neural networks for pavement rutting. In: *Applied Research in Uncertainty Modeling and Analysis*, pages 193–213. Springer.
- Tayfur, G., Ozdemir, S., & Singh, V. P. (2003). Fuzzy logic algorithm for runoff-induced sediment transport from bare soil surfaces. *Advances in water resources*, 26(12):1249–1256.
- Thompson, G. (2006). Investigation of the bailey method for the design and analysis of dense-graded hmac using oregon aggregates. Technical report, Oregon Department of Transportation, Research Unit.
- Thrower, E. (1977). Methods of predicting deformation in road pavements. In: *Volume I of proceedings of 4th International Conference on Structural Design of Asphalt Pavements, Ann Arbor, Michigan, August 22-26, 1977.*, number Proceeding.
- Tory, E., Cochrane, N., & Waddell, S. (1968). Anisotropy in simulated random packing of equal spheres.

- Ullidtz, P., Battiato, G., Larsen, B., & Stubstad, R. (1987). Verification of the analytical-empirical method of pavement evaluation based on fwd testing. sixth international conference, structural design of asphalt pavements, volume i, proceedings, university of michigan, july 13-17, 1987, ann arbor, michigan. *Publication of: Michigan University, Ann Arbor.*
- Van der Poel, C. (1954). Representation of rheological properties of bitumens over a wide range of temperatures and loading times. In: *Proc of 2nd Int Congress on Rheology*, pages 331–337. Academic Press Inc., New York.
- Van der Poel, C. (1955). Time and temperature effects on the deformation of asphaltic bitumens and bitumen-mineral mixtures. *Society of Petroleum Engineers Journal*, pages 47–53.
- Vavrik, W. R. (2000). *Asphalt mixture design concepts to develop aggregate interlock*. PhD thesis, University of Illinois at Urbana-Champaign.
- Vavrik, W. R. (2002). *Bailey method for gradation selection in hot-mix asphalt mixture design*. Transportation Research Board, National Research Council.
- Vavrik, W. R., Pine, W. J., Huber, G., Carpenter, S. H., & Bailey, R. (2001). The bailey method of gradation evaluation: the influence of aggregate gradation and packing characteristics on voids in the mineral aggregate (with discussion). *Journal of the Association of Asphalt Paving Technologists*, 70.
- Wang, Z., Palade, V., & Xu, Y. (2006). Neuro-fuzzy ensemble approach for mi-

- croarray cancer gene expression data analysis. In: *Evolving Fuzzy Systems, 2006 International Symposium on*, pages 241–246. IEEE.
- Xiao, F. & Amirkhanian, S. N. (2009). Artificial neural network approach to estimating stiffness behavior of rubberized asphalt concrete containing reclaimed asphalt pavement. *Journal of Transportation Engineering*, 135(8):580–589.
- Xiao, F., Putman, B. J., & Amirkhanian, S. N. (2011). Viscosity prediction of crm binders using artificial neural network approach. *International Journal of Pavement Engineering*, 12(5):485–495.
- Yideti, T. F. (2014). Packing theory-based framework for performance evaluation of unbound granular materials.
- Yilmaz, M., Kok, B. V., Sengoz, B., Sengur, A., & Avci, E. (2011). Investigation of complex modulus of base and eva modified bitumen with adaptive-network-based fuzzy inference system. *Expert Systems with Applications*, 38(1):969–974.
- Zaman, M., Solanki, P., Ebrahimi, A., & White, L. (2010). Neural network modeling of resilient modulus using routine subgrade soil properties. *International Journal of Geomechanics*, 10(1):1–12.
- Zhou, F., Scullion, T., & Sun, L. (2004). Verification and modeling of three-stage permanent deformation behavior of asphalt mixes. *Journal of Transportation Engineering*, 130(4):486–494.

# Appendices

# Appendix A

## Matlab Code for ANN

```
1 % Note: open file for input and output
2 for m=1:1:20;% Make an iteration until arrive to the target of ...
    (R-sequ.)
3 % Solve an Input-Output Fitting problem with a Neural Network
4 % This script assumes these variables are defined:
5 %   Input - input data.
6 %   Output - target data.
7 inputs = Input;
8 targets = Output;
9
10 % Create a Fitting Network
11
12 hiddenLayerSize =[5 15 5];% number of hidden ...
    layersr=====
13 net = fitnet(hiddenLayerSize);
```



```

14 % Choose Input and Output Pre/Post-Processing Functions
15 net.inputs{1}.processFcns = {'removeconstantrows','mapminmax'};
16 net.outputs{2}.processFcns = {'removeconstantrows','mapminmax'};
17 % Setup Division of Data for Training, Validation, Testing
18 % For a list of all data division functions type: help nndivide
19 %[trainInd,valInd] =divideind(47,1:40,41:47);
20 %net.divideFcn = 'dividerand'; % Divide data randomly
21 net.divideMode = 'sample'; % Divide up every sample
22 net.divideParam.trainRatio = 75/100;% training data
23 net.divideParam.valRatio = 0/100; % validation data
24 net.divideParam.testRatio = 25/100;% testing data
25 % For help on training function 'trainlm' type: help trainlm
26 % For a list of all training functions type: help nntrain
27 net.trainFcn = 'trainlm'; % for training Levenberg-Marquardt ...
    was used
28 % Choose a Performance Function
29 % For a list of all performance functions type: help nnperformance
30 net.performFcn = 'mse'; % Mean squared error
31 % Choose Plot Functions
32 % For a list of all plot functions type: help nnplot
33 net.plotFcns = ...
    {'plotperform','plottrainstate','ploterrhist','plotregression', ...
    'plotfit'};
34
35 % Train the Network;
36 [net,tr] = train(net,inputs,targets);
37

```

```

38 % Test the Network;
39 outputs = net(inputs);
40 errors = gsubtract(targets, outputs);
41 performance = perform(net, targets, outputs);
42 %Recalculate Training, Validation and Test Performance
43 trainTargets = targets.* tr.trainMask{1};
44 valTargets = targets.* tr.valMask{1};
45 testTargets = targets .* tr.testMask{1};
46 trainPerformance = perform(net, trainTargets, outputs);
47 valPerformance = perform(net, valTargets, outputs);
48 testPerformance = perform(net, testTargets, outputs);
49
50 %View the Network
51 %view(net)
52
53 wb = formwb(net, net.b, net.iw, net.lw); %net.b= baise, net.IW= ...
    input weight, net.LW= layer weight.
54 [b, iw, lw] = separatewb(net, wb); %net.b= baise, net.IW= input ...
    weight, net.LW= layer weight.
55 %if regression(valTargets, outputs)>0.980 ;% the target of ...
    R-square is 0.95
56 if regression(targets, outputs)>0.95;% the target of R-square is ...
    0.95
57     break;
58 end;
59
60 R(m, 1)=regression(targets, outputs);

```

```

61
62 m;
63 end;
64
65 % Plots
66 % Uncomment these lines to enable various plots;
67 %figure, plotperform(tr);
68 %figure, plottrainstate(tr);
69 %figure, plotfit(net,inputs,targets);
70 %figure, plotregression(targets,outputs);
71 %figure, ploterrhist(errors);
72 %performance = perform(net,targets,outputs)
73 %Rs=regression(targets,outputs)
74 MAX=max(R(:,1));
75 %-----
76 for I=1:length(Input);
77 DATA(I,1)=Output(1,I);%experementals values
78 DATA(I,2)=outputs(1,I);%modelled valeues
79 end;
80 m;
81 %sim(train(net,inputs,targets),SAMPLE)

```

# Appendix B

## Weights and Biases for ANN and ANFIS

### B.1 ANN

Table B.1: Strain ANN Weights for Packing Ratios Model

Input Layer																			
Node 1	Node 2	Node 3	Node 4	Node 5															
0.994	-0.738	-0.676	-0.523	1.158															
-0.059	1.144	1.357	-0.362	-0.047															
-1.138	-0.150	0.155	1.028	-1.122															
-0.916	-0.663	0.368	-0.972	1.062															
-0.621	0.037	-1.700	-0.724	-0.757															
Hidden Layer 1					Hidden Layer 2														
Node 1	Node 2	Node 3	Node 4	Node 5	Node 1	Node 2	Node 3	Node 4	Node 5	Node 6	Node 7	Node 8	Node 9	Node 10	Node 11	Node 12	Node 13	Node 14	Node 15
-0.862	1.262	1.647	0.754	-0.527															
-0.818	0.031	1.247	-1.585	-1.041															
1.389	-0.925	1.469	-0.518	-0.302															
0.385	-0.068	1.132	0.278	2.067															
-0.922	-1.473	0.798	0.538	-1.617															
-0.914	-1.118	1.428	-0.117	1.166	0.421	-0.004	-0.752	-0.166	0.967	0.260	-0.213	0.098	0.496	0.415	0.464	-0.083	-0.484	-0.495	0.511
1.258	0.249	0.566	-1.306	-1.352	-0.382	0.407	0.267	-0.263	-0.754	-0.017	0.416	0.422	0.384	0.180	0.579	-0.333	-0.056	-0.292	-0.533
0.154	-2.422	-0.218	0.330	-0.058	0.033	0.573	-0.130	0.519	0.211	-0.506	0.758	-0.036	0.531	0.113	-0.360	0.026	-0.525	-0.515	-0.551
1.215	0.446	0.394	-1.909	-0.502	-0.500	-0.199	-0.324	0.352	-0.488	0.526	0.106	0.468	-0.615	0.609	-0.213	-0.025	0.357	0.011	0.455
1.297	-1.389	0.753	1.046	0.610	0.470	0.374	0.474	-0.424	-0.710	0.055	0.596	0.528	0.631	-0.006	0.130	0.553	0.065	-0.373	0.436
0.830	-1.092	-1.647	1.051	0.271															
0.110	1.197	1.143	0.050	1.694															
-0.425	1.913	-0.125	1.171	0.349															
-0.026	-1.937	0.895	0.393	1.051															
0.266	-1.408	1.726	-0.775	0.018															
Hidden Layer 3																			
Node 1	Node 2	Node 3	Node 4	Node 5															
-0.490	0.652	-0.587	0.598	1.203															

Table B.2: Strain ANN Biases for Packing Ratios model

<b>Hidden Layer 1</b>	<b>Hidden Layer 2</b>	<b>Hidden Layer 3</b>	<b>Output</b>
	2.37638		
	2.04729		
	-1.9271		
	-1.3882		
	1.0983		
-1.9819	0.94191	-1.3624	
1.14645	-0.4652	0.77298	
0.09008	-0.0483	-0.0013	-0.2909
-0.9305	0.33398	-0.7264	
-1.883	0.759	1.53198	
	1.04442		
	-1.5182		
	-1.7146		
	-2.0597		
	2.43689		

Table B.3: Strain ANN Weights for Packing Ratios and Different Variables Model

Input Layer																						
Node 1	Node 2	Node 3	Node 4	Node 5	Node 6	Node 7	Node 8															
-1.238	1.893	0.922	1.135	0.540	-0.634	-2.087	-0.404															
0.035	-3.484	0.914	2.102	-1.416	-0.007	-1.703	0.391															
-1.810	1.426	-1.560	-1.054	-0.225	-0.981	-1.705	1.306															
0.808	0.265	-0.971	0.561	-2.164	-0.277	-1.272	1.852															
1.783	-1.255	-0.100	-0.170	0.431	1.417	0.575	-1.080															
Hidden Layer 1					Hidden Layer 2																	
Node 1	Node 2	Node 3	Node 4	Node 5	Node 1	Node 2	Node 3	Node 4	Node 5	Node 6	Node 7	Node 8	Node 9	Node 10	Node 11	Node 12	Node 13	Node 14	Node 15			
0.272	-1.667	0.454	0.247	2.618																		
-0.569	1.038	-1.139	-1.526	1.362																		
-0.726	0.045	1.457	-0.495	1.842																		
-0.164	2.662	1.196	-0.724	-0.616																		
0.764	-1.193	-0.807	-1.164	-1.025																		
-0.388	1.849	1.265	0.442	-2.262	0.553	0.578	0.765	-0.264	0.221	0.758	0.878	-0.953	-1.405	-0.201	-0.743	0.233	-0.237	1.047	1.023			
1.791	0.607	0.348	2.162	0.070	1.293	-0.176	-0.190	-1.118	-0.381	0.287	-0.041	-0.177	-0.965	1.104	-0.267	-0.057	-0.072	0.398	0.148			
0.117	-1.025	0.150	1.287	-2.136	0.297	-0.143	0.735	-0.196	-0.441	-0.244	0.680	-0.207	-0.395	-0.970	-0.280	0.698	0.344	0.181	0.737			
-0.811	2.408	0.680	0.543	1.832	0.352	-0.364	-0.038	-0.399	-0.134	-1.570	-0.090	0.456	-1.675	-1.086	0.732	-0.482	-1.230	-0.384	0.098			
-1.481	0.236	0.739	1.203	-1.720	1.378	-0.665	-0.645	1.010	0.712	-1.435	1.884	0.203	-0.393	-0.646	0.530	0.054	-0.529	-0.492	-0.773			
-0.545	1.163	-0.807	-1.610	-0.603																		
0.117	-0.104	1.435	-1.664	1.023																		
-1.685	-1.124	1.333	-0.940	0.077																		
0.349	0.969	-1.220	1.338	1.135																		
0.834	-1.138	0.407	-1.198	1.435																		

Hidden Layer 3				
Node 1	Node 2	Node 3	Node 4	Node 5
-0.431	1.048	0.377	0.799	-0.985

Table B.4: Strain ANN Biases for Packing Ratios and Different Variables Model

Hidden Layer 1	Hidden Layer 2	Hidden Layer 3	Output
	-2.204828683		
	1.996538052		
	2.547200511		
	1.096737045		
	-1.654271435		
1.646346289	-0.335848112	-0.930364867	
0.20308558	0.274961926	-0.871561486	
1.304789094	-0.669505259	0.13940708	0.119534105
-0.749363942	0.642136285	0.705837222	
0.228394626	-1.31742977	1.351610711	
	-1.647498124		
	1.413512651		
	-1.80336181		
	2.330028779		
	2.852786317		



Table B.5: Stiffness ANN Weights for Packing Ratios and Different Variables Model

Input Layer																					
Node 1	Node 2	Node 3	Node 4	Node 5	Node 6	Node 7															
-1.556	-0.537	-1.137	-0.666	-0.149	-1.019	0.836															
1.983	1.541	-1.672	-1.204	0.176	0.768	-3.168															
0.837	1.224	1.502	0.501	-2.350	-0.476	1.803															
0.528	1.572	-1.209	-1.921	-2.025	-2.157	-0.684															
0.736	0.881	-2.021	1.915	-0.702	-0.081	2.413															
Hidden Layer 1					Hidden Layer 2																
Node 1	Node 2	Node 3	Node 4	Node 5	Node 1	Node 2	Node 3	Node 4	Node 5	Node 6	Node 7	Node 8	Node 9	Node 10	Node 11	Node 12	Node 13	Node 14	Node 15		
-0.785	1.764	1.782	1.023	-1.384																	
-0.360	-1.719	1.376	0.633	-0.017																	
-0.490	0.540	-1.507	-0.891	-1.841																	
1.425	0.017	-1.140	-0.937	1.566																	
-0.535	-0.814	1.317	-1.667	0.458																	
0.548	0.324	2.649	-0.873	-0.990	0.665	-0.746	1.667	-0.269	-1.164	-0.381	-0.747	0.250	-0.717	0.278	-0.429	1.066	-0.046	0.428	-0.212		
-0.124	-0.418	-1.842	1.186	-1.059	-0.975	0.089	0.870	0.759	-0.786	-0.064	-0.846	-0.653	-0.711	-0.547	-1.139	-1.340	-0.841	-0.287	0.088		
-0.584	1.128	-1.148	2.059	-0.479	1.295	-0.214	0.396	-0.918	-0.053	-0.023	0.777	-0.412	-1.039	-0.050	-0.873	-0.538	-0.286	-1.004	0.046		
-1.174	-0.742	1.055	0.973	1.499	-0.020	0.136	-0.477	-0.254	-0.661	-1.065	-0.406	0.136	-0.313	0.739	0.868	1.195	-0.463	0.568	0.849		
-1.477	-1.079	-0.257	1.359	-0.631	2.000	0.146	0.051	-1.462	-0.180	0.428	-0.424	-0.124	0.451	-0.258	-0.166	1.210	0.630	-0.144	-0.781		
-0.395	0.002	-0.757	2.257	1.223																	
-0.778	0.321	-2.013	1.511	-1.402																	
0.239	-1.287	0.630	1.977	-0.383																	
-1.642	-1.185	0.888	0.208	0.695																	
-0.806	-1.417	-1.081	-0.560	-0.789																	
Hidden Layer 3																					
Node 1	Node 2	Node 3	Node 4	Node 5																	
-0.962	0.793	0.974	2.901	0.598																	

Table B.6: Stiffness ANN Biases for Packing Ratios and Different Variables Model

Hidden Layer 1	Hidden Layer 2	Hidden Layer 3	Output
	2.005129325		
	1.909145178		
	1.448832689		
	-1.616056382		
	1.040353516		
3.272547626	-0.503922928	1.415190474	
-0.398990876	0.382909162	1.516667144	
0.872407675	0.200275279	0.329679	1.001297533
-0.103649955	-0.469313444	-1.044456973	
-0.357595449	-0.784737872	1.69291865	
	-1.215335232		
	-1.419585325		
	1.762101314		
	-2.245452956		
	-2.352290962		

## B.2 ANFIS

Source codes, Functions and System files for All Packing Ratios Model

```

1 [System]
2 Name='final'
3 Type='sugeno'
4 Version=2.0
5 NumInputs=5
6 NumOutputs=1
7 NumRules=243
8 AndMethod='prod'
9 OrMethod='probor'
10 ImpMethod='prod'
11 AggMethod='sum'

```

```
12 DefuzzMethod='wtaver'  
13  
14 [Input1]  
15 Name='input1'  
16 Range=[0.369916312 2.007203154]  
17 NumMFs=3  
18 MF1='in1mf1':'trimf',[-0.2369503675 0.369669062227676 ...  
    0.975750739624839]  
19 MF2='in1mf2':'trimf',[0.370247991640055 0.976465116872959 ...  
    1.58286489367843]  
20 MF3='in1mf3':'trimf',[0.976576627028935 1.58357904614528 ...  
    2.1905163505]  
21  
22 [Input2]  
23 Name='input2'  
24 Range=[0.271508028 0.48759609]  
25 NumMFs=3  
26 MF1='in2mf1':'trimf',[0.163463997 0.271359429541806 ...  
    0.379273989174918]  
27 MF2='in2mf2':'trimf',[0.277411557641705 0.378909673888802 ...  
    0.48051820077889]  
28 MF3='in2mf3':'trimf',[0.380136819880285 0.487102303346997 ...  
    0.595640121]  
29  
30 [Input3]  
31 Name='input3'  
32 Range=[0.348764403 2.168343026]
```

```

33 NumMFs=3
34 MF1='in3mf1':'trimf',[-0.5610249085 0.348693368779104 ...
    1.2582076455365]
35 MF2='in3mf2':'trimf',[0.349636659981002 1.25846769090146 ...
    2.1683371743299]
36 MF3='in3mf3':'trimf',[1.25851721156848 2.16832803662236 ...
    3.0781323375]
37
38 [Input4]
39 Name='input4'
40 Range=[0.262146124 1.300702499]
41 NumMFs=3
42 MF1='in4mf1':'trimf',[-0.2571320635 0.262538635668114 ...
    0.781575066815497]
43 MF2='in4mf2':'trimf',[0.264040284988717 0.781843941384744 ...
    1.30070536050123]
44 MF3='in4mf3':'trimf',[0.781538489611184 1.30072961721663 ...
    1.8199806865]
45
46 [Input5]
47 Name='input5'
48 Range=[0.2143015 0.5404065]
49 NumMFs=3
50 MF1='in5mf1':'trimf',[0.051249 0.214912477748511 0.37826640099706]
51 MF2='in5mf2':'trimf',[0.214792548759294 0.378510640381034 ...
    0.540533881967115]
52 MF3='in5mf3':'trimf',[0.379355243737009 0.540952162632522 0.703459]

```

```
53
54 [Output1]
55 Name='output '
56 Range=[0.945216667 15.1]
57 NumMFs=243
58 MF1='outlmf1': 'constant', [-0.000628292076036838]
59 MF2='outlmf2': 'constant', [2.46136407852949]
60 MF3='outlmf3': 'constant', [0.837860604309635]
61 MF4='outlmf4': 'constant', [0.0649302944159856]
62 MF5='outlmf5': 'constant', [0.639836428490079]
63 MF6='outlmf6': 'constant', [0.293059506169673]
64 MF7='outlmf7': 'constant', [0.0221254533710595]
65 MF8='outlmf8': 'constant', [0.0212012967117338]
66 MF9='outlmf9': 'constant', [0]
67 MF10='outlmf10': 'constant', [-0.0154891238643098]
68 MF11='outlmf11': 'constant', [0.398893501071379]
69 MF12='outlmf12': 'constant', [0.347342540909675]
70 MF13='outlmf13': 'constant', [1.05514875965356]
71 MF14='outlmf14': 'constant', [-1.40467518870887]
72 MF15='outlmf15': 'constant', [0.121490416170112]
73 MF16='outlmf16': 'constant', [-0.0998029558784106]
74 MF17='outlmf17': 'constant', [0.603708247691]
75 MF18='outlmf18': 'constant', [0]
76 MF19='outlmf19': 'constant', [0]
77 MF20='outlmf20': 'constant', [0]
78 MF21='outlmf21': 'constant', [0]
79 MF22='outlmf22': 'constant', [-0.198414937754411]
```

80 MF23='outlmf23': 'constant', [1.74458915610732]  
81 MF24='outlmf24': 'constant', [3.49700731783121e-08]  
82 MF25='outlmf25': 'constant', [-0.246350961922909]  
83 MF26='outlmf26': 'constant', [0.37000023214352]  
84 MF27='outlmf27': 'constant', [0.00634061374954542]  
85 MF28='outlmf28': 'constant', [-0.00103707334545574]  
86 MF29='outlmf29': 'constant', [4.8305002187799]  
87 MF30='outlmf30': 'constant', [0.615903610992692]  
88 MF31='outlmf31': 'constant', [0.0885139831256964]  
89 MF32='outlmf32': 'constant', [5.36213992659359]  
90 MF33='outlmf33': 'constant', [-0.935252128916187]  
91 MF34='outlmf34': 'constant', [0.0308071071178912]  
92 MF35='outlmf35': 'constant', [0.0295203270140624]  
93 MF36='outlmf36': 'constant', [0]  
94 MF37='outlmf37': 'constant', [-0.025566703952891]  
95 MF38='outlmf38': 'constant', [-2.18650251835102]  
96 MF39='outlmf39': 'constant', [-4.16398931415117]  
97 MF40='outlmf40': 'constant', [2.39197894815522]  
98 MF41='outlmf41': 'constant', [-0.0148037712507594]  
99 MF42='outlmf42': 'constant', [-1.5244922631668]  
100 MF43='outlmf43': 'constant', [0.544885689729886]  
101 MF44='outlmf44': 'constant', [1.76259081711547]  
102 MF45='outlmf45': 'constant', [0]  
103 MF46='outlmf46': 'constant', [0]  
104 MF47='outlmf47': 'constant', [0]  
105 MF48='outlmf48': 'constant', [0]  
106 MF49='outlmf49': 'constant', [0.101671380257337]

107 MF50='outlmf50': 'constant', [3.55673892480193]  
108 MF51='outlmf51': 'constant', [1.17881906466633e-07]  
109 MF52='outlmf52': 'constant', [-0.0802857061215568]  
110 MF53='outlmf53': 'constant', [1.47938278505216]  
111 MF54='outlmf54': 'constant', [0.0213738082038617]  
112 MF55='outlmf55': 'constant', [0]  
113 MF56='outlmf56': 'constant', [3.96752659160645]  
114 MF57='outlmf57': 'constant', [6.78155964998761]  
115 MF58='outlmf58': 'constant', [0]  
116 MF59='outlmf59': 'constant', [-1.14657658480498]  
117 MF60='outlmf60': 'constant', [-3.92341486268316]  
118 MF61='outlmf61': 'constant', [0]  
119 MF62='outlmf62': 'constant', [0]  
120 MF63='outlmf63': 'constant', [0]  
121 MF64='outlmf64': 'constant', [0]  
122 MF65='outlmf65': 'constant', [-6.57356206357714]  
123 MF66='outlmf66': 'constant', [-5.7460317369295]  
124 MF67='outlmf67': 'constant', [0]  
125 MF68='outlmf68': 'constant', [-4.01429853993282]  
126 MF69='outlmf69': 'constant', [-4.07920607546454]  
127 MF70='outlmf70': 'constant', [0]  
128 MF71='outlmf71': 'constant', [0]  
129 MF72='outlmf72': 'constant', [0]  
130 MF73='outlmf73': 'constant', [0]  
131 MF74='outlmf74': 'constant', [0]  
132 MF75='outlmf75': 'constant', [0]  
133 MF76='outlmf76': 'constant', [0]

134 MF77='outlmf77': 'constant', [0]  
135 MF78='outlmf78': 'constant', [0]  
136 MF79='outlmf79': 'constant', [0]  
137 MF80='outlmf80': 'constant', [0]  
138 MF81='outlmf81': 'constant', [0]  
139 MF82='outlmf82': 'constant', [0.956934794258858]  
140 MF83='outlmf83': 'constant', [4.58185940568531]  
141 MF84='outlmf84': 'constant', [1.29263108328575]  
142 MF85='outlmf85': 'constant', [0.241532551027591]  
143 MF86='outlmf86': 'constant', [1.34911698746698]  
144 MF87='outlmf87': 'constant', [0.452125120758185]  
145 MF88='outlmf88': 'constant', [0.0780658348461269]  
146 MF89='outlmf89': 'constant', [0.0748051079416907]  
147 MF90='outlmf90': 'constant', [0]  
148 MF91='outlmf91': 'constant', [0.0638979399499979]  
149 MF92='outlmf92': 'constant', [1.29119739183135]  
150 MF93='outlmf93': 'constant', [0.53587167435224]  
151 MF94='outlmf94': 'constant', [4.48015533263991]  
152 MF95='outlmf95': 'constant', [2.23846420138341]  
153 MF96='outlmf96': 'constant', [0.187432476767759]  
154 MF97='outlmf97': 'constant', [0.749610430874522]  
155 MF98='outlmf98': 'constant', [0.952731529900271]  
156 MF99='outlmf99': 'constant', [0]  
157 MF100='outlmf100': 'constant', [0]  
158 MF101='outlmf101': 'constant', [0]  
159 MF102='outlmf102': 'constant', [0]  
160 MF103='outlmf103': 'constant', [-0.542092673476708]



161 MF104='outlmf104': 'constant', [0.100170255845813]  
162 MF105='outlmf105': 'constant', [0]  
163 MF106='outlmf106': 'constant', [-0.456536977937207]  
164 MF107='outlmf107': 'constant', [-0.335867811039835]  
165 MF108='outlmf108': 'constant', [0]  
166 MF109='outlmf109': 'constant', [-4.78399500126833]  
167 MF110='outlmf110': 'constant', [1.74302425313201]  
168 MF111='outlmf111': 'constant', [4.86397281464326]  
169 MF112='outlmf112': 'constant', [-3.67168475815058]  
170 MF113='outlmf113': 'constant', [0.0849420948151548]  
171 MF114='outlmf114': 'constant', [2.95613709957768]  
172 MF115='outlmf115': 'constant', [0.108697548298319]  
173 MF116='outlmf116': 'constant', [0.104157367296493]  
174 MF117='outlmf117': 'constant', [0]  
175 MF118='outlmf118': 'constant', [-1.21304788851612]  
176 MF119='outlmf119': 'constant', [-0.240470895414756]  
177 MF120='outlmf120': 'constant', [0.056982493551563]  
178 MF121='outlmf121': 'constant', [7.07222708527024]  
179 MF122='outlmf122': 'constant', [4.50657184450894]  
180 MF123='outlmf123': 'constant', [0.636790170068476]  
181 MF124='outlmf124': 'constant', [2.19606114778872]  
182 MF125='outlmf125': 'constant', [2.50333470501633]  
183 MF126='outlmf126': 'constant', [0]  
184 MF127='outlmf127': 'constant', [0]  
185 MF128='outlmf128': 'constant', [0]  
186 MF129='outlmf129': 'constant', [0]  
187 MF130='outlmf130': 'constant', [-0.181768274996029]

188 MF131='outlmf131': 'constant', [0.925479375160748]  
189 MF132='outlmf132': 'constant', [0]  
190 MF133='outlmf133': 'constant', [-0.194466147938767]  
191 MF134='outlmf134': 'constant', [-0.0123602594258481]  
192 MF135='outlmf135': 'constant', [0]  
193 MF136='outlmf136': 'constant', [-1.23592614035461]  
194 MF137='outlmf137': 'constant', [26.5890316567072]  
195 MF138='outlmf138': 'constant', [11.6336437612259]  
196 MF139='outlmf139': 'constant', [-1.01721916870219]  
197 MF140='outlmf140': 'constant', [6.27499146655773]  
198 MF141='outlmf141': 'constant', [2.13363924284419]  
199 MF142='outlmf142': 'constant', [0]  
200 MF143='outlmf143': 'constant', [0]  
201 MF144='outlmf144': 'constant', [0]  
202 MF145='outlmf145': 'constant', [-0.307709317964186]  
203 MF146='outlmf146': 'constant', [-1.86060286032728]  
204 MF147='outlmf147': 'constant', [-1.59834780445102]  
205 MF148='outlmf148': 'constant', [-0.253257703998624]  
206 MF149='outlmf149': 'constant', [-1.27959831303417]  
207 MF150='outlmf150': 'constant', [-1.1432152397776]  
208 MF151='outlmf151': 'constant', [0]  
209 MF152='outlmf152': 'constant', [0]  
210 MF153='outlmf153': 'constant', [0]  
211 MF154='outlmf154': 'constant', [0]  
212 MF155='outlmf155': 'constant', [0]  
213 MF156='outlmf156': 'constant', [0]  
214 MF157='outlmf157': 'constant', [0]

215 MF158='outlmf158': 'constant', [0]  
216 MF159='outlmf159': 'constant', [0]  
217 MF160='outlmf160': 'constant', [0]  
218 MF161='outlmf161': 'constant', [0]  
219 MF162='outlmf162': 'constant', [0]  
220 MF163='outlmf163': 'constant', [19.2552081138974]  
221 MF164='outlmf164': 'constant', [15.3660220003553]  
222 MF165='outlmf165': 'constant', [0]  
223 MF166='outlmf166': 'constant', [4.76911744383185]  
224 MF167='outlmf167': 'constant', [3.7993653645862]  
225 MF168='outlmf168': 'constant', [0]  
226 MF169='outlmf169': 'constant', [0]  
227 MF170='outlmf170': 'constant', [0]  
228 MF171='outlmf171': 'constant', [0]  
229 MF172='outlmf172': 'constant', [1.96705044400533]  
230 MF173='outlmf173': 'constant', [1.56907809906657]  
231 MF174='outlmf174': 'constant', [0]  
232 MF175='outlmf175': 'constant', [0.452669110469853]  
233 MF176='outlmf176': 'constant', [0.351672444178518]  
234 MF177='outlmf177': 'constant', [0]  
235 MF178='outlmf178': 'constant', [0]  
236 MF179='outlmf179': 'constant', [0]  
237 MF180='outlmf180': 'constant', [0]  
238 MF181='outlmf181': 'constant', [0]  
239 MF182='outlmf182': 'constant', [0]  
240 MF183='outlmf183': 'constant', [0]  
241 MF184='outlmf184': 'constant', [0]

242 MF185='outlmf185': 'constant', [0]  
243 MF186='outlmf186': 'constant', [0]  
244 MF187='outlmf187': 'constant', [0]  
245 MF188='outlmf188': 'constant', [0]  
246 MF189='outlmf189': 'constant', [0]  
247 MF190='outlmf190': 'constant', [-0.705090260204011]  
248 MF191='outlmf191': 'constant', [-1.9216483265055]  
249 MF192='outlmf192': 'constant', [0]  
250 MF193='outlmf193': 'constant', [1.32437179828769]  
251 MF194='outlmf194': 'constant', [-1.59061930053277]  
252 MF195='outlmf195': 'constant', [0]  
253 MF196='outlmf196': 'constant', [0.199332608476822]  
254 MF197='outlmf197': 'constant', [0]  
255 MF198='outlmf198': 'constant', [0]  
256 MF199='outlmf199': 'constant', [-0.176368224937162]  
257 MF200='outlmf200': 'constant', [-0.479297431696797]  
258 MF201='outlmf201': 'constant', [0]  
259 MF202='outlmf202': 'constant', [1.76570771210859]  
260 MF203='outlmf203': 'constant', [-0.407567865819005]  
261 MF204='outlmf204': 'constant', [0]  
262 MF205='outlmf205': 'constant', [0.200378812987847]  
263 MF206='outlmf206': 'constant', [0]  
264 MF207='outlmf207': 'constant', [0]  
265 MF208='outlmf208': 'constant', [0]  
266 MF209='outlmf209': 'constant', [0]  
267 MF210='outlmf210': 'constant', [0]  
268 MF211='outlmf211': 'constant', [0]

269 MF212='outlmf212': 'constant', [0]  
270 MF213='outlmf213': 'constant', [0]  
271 MF214='outlmf214': 'constant', [0]  
272 MF215='outlmf215': 'constant', [0]  
273 MF216='outlmf216': 'constant', [0]  
274 MF217='outlmf217': 'constant', [-0.182254519312782]  
275 MF218='outlmf218': 'constant', [-0.497011438490831]  
276 MF219='outlmf219': 'constant', [0]  
277 MF220='outlmf220': 'constant', [0.00295275999992829]  
278 MF221='outlmf221': 'constant', [-0.409061306971833]  
279 MF222='outlmf222': 'constant', [0]  
280 MF223='outlmf223': 'constant', [0.0159355611569387]  
281 MF224='outlmf224': 'constant', [0]  
282 MF225='outlmf225': 'constant', [0]  
283 MF226='outlmf226': 'constant', [-0.045376023697578]  
284 MF227='outlmf227': 'constant', [-0.12374125424139]  
285 MF228='outlmf228': 'constant', [0]  
286 MF229='outlmf229': 'constant', [0.116412310532877]  
287 MF230='outlmf230': 'constant', [-0.101844254007229]  
288 MF231='outlmf231': 'constant', [0]  
289 MF232='outlmf232': 'constant', [0.0160191995334607]  
290 MF233='outlmf233': 'constant', [0]  
291 MF234='outlmf234': 'constant', [0]  
292 MF235='outlmf235': 'constant', [0]  
293 MF236='outlmf236': 'constant', [0]  
294 MF237='outlmf237': 'constant', [0]  
295 MF238='outlmf238': 'constant', [0]

```
296 MF239='outlmf239': 'constant', [0]
297 MF240='outlmf240': 'constant', [0]
298 MF241='outlmf241': 'constant', [0]
299 MF242='outlmf242': 'constant', [0]
300 MF243='outlmf243': 'constant', [0]
```

```
301
```

```
302 [Rules]
```

```
303 1 1 1 1 1, 1 (1) : 1
```

```
304 1 1 1 1 2, 2 (1) : 1
```

```
305 1 1 1 1 3, 3 (1) : 1
```

```
306 1 1 1 2 1, 4 (1) : 1
```

```
307 1 1 1 2 2, 5 (1) : 1
```

```
308 1 1 1 2 3, 6 (1) : 1
```

```
309 1 1 1 3 1, 7 (1) : 1
```

```
310 1 1 1 3 2, 8 (1) : 1
```

```
311 1 1 1 3 3, 9 (1) : 1
```

```
312 1 1 2 1 1, 10 (1) : 1
```

```
313 1 1 2 1 2, 11 (1) : 1
```

```
314 1 1 2 1 3, 12 (1) : 1
```

```
315 1 1 2 2 1, 13 (1) : 1
```

```
316 1 1 2 2 2, 14 (1) : 1
```

```
317 1 1 2 2 3, 15 (1) : 1
```

```
318 1 1 2 3 1, 16 (1) : 1
```

```
319 1 1 2 3 2, 17 (1) : 1
```

```
320 1 1 2 3 3, 18 (1) : 1
```

```
321 1 1 3 1 1, 19 (1) : 1
```

```
322 1 1 3 1 2, 20 (1) : 1
```

323 1 1 3 1 3, 21 (1) : 1  
324 1 1 3 2 1, 22 (1) : 1  
325 1 1 3 2 2, 23 (1) : 1  
326 1 1 3 2 3, 24 (1) : 1  
327 1 1 3 3 1, 25 (1) : 1  
328 1 1 3 3 2, 26 (1) : 1  
329 1 1 3 3 3, 27 (1) : 1  
330 1 2 1 1 1, 28 (1) : 1  
331 1 2 1 1 2, 29 (1) : 1  
332 1 2 1 1 3, 30 (1) : 1  
333 1 2 1 2 1, 31 (1) : 1  
334 1 2 1 2 2, 32 (1) : 1  
335 1 2 1 2 3, 33 (1) : 1  
336 1 2 1 3 1, 34 (1) : 1  
337 1 2 1 3 2, 35 (1) : 1  
338 1 2 1 3 3, 36 (1) : 1  
339 1 2 2 1 1, 37 (1) : 1  
340 1 2 2 1 2, 38 (1) : 1  
341 1 2 2 1 3, 39 (1) : 1  
342 1 2 2 2 1, 40 (1) : 1  
343 1 2 2 2 2, 41 (1) : 1  
344 1 2 2 2 3, 42 (1) : 1  
345 1 2 2 3 1, 43 (1) : 1  
346 1 2 2 3 2, 44 (1) : 1  
347 1 2 2 3 3, 45 (1) : 1  
348 1 2 3 1 1, 46 (1) : 1  
349 1 2 3 1 2, 47 (1) : 1

350 1 2 3 1 3, 48 (1) : 1  
351 1 2 3 2 1, 49 (1) : 1  
352 1 2 3 2 2, 50 (1) : 1  
353 1 2 3 2 3, 51 (1) : 1  
354 1 2 3 3 1, 52 (1) : 1  
355 1 2 3 3 2, 53 (1) : 1  
356 1 2 3 3 3, 54 (1) : 1  
357 1 3 1 1 1, 55 (1) : 1  
358 1 3 1 1 2, 56 (1) : 1  
359 1 3 1 1 3, 57 (1) : 1  
360 1 3 1 2 1, 58 (1) : 1  
361 1 3 1 2 2, 59 (1) : 1  
362 1 3 1 2 3, 60 (1) : 1  
363 1 3 1 3 1, 61 (1) : 1  
364 1 3 1 3 2, 62 (1) : 1  
365 1 3 1 3 3, 63 (1) : 1  
366 1 3 2 1 1, 64 (1) : 1  
367 1 3 2 1 2, 65 (1) : 1  
368 1 3 2 1 3, 66 (1) : 1  
369 1 3 2 2 1, 67 (1) : 1  
370 1 3 2 2 2, 68 (1) : 1  
371 1 3 2 2 3, 69 (1) : 1  
372 1 3 2 3 1, 70 (1) : 1  
373 1 3 2 3 2, 71 (1) : 1  
374 1 3 2 3 3, 72 (1) : 1  
375 1 3 3 1 1, 73 (1) : 1  
376 1 3 3 1 2, 74 (1) : 1



377 1 3 3 1 3, 75 (1) : 1  
378 1 3 3 2 1, 76 (1) : 1  
379 1 3 3 2 2, 77 (1) : 1  
380 1 3 3 2 3, 78 (1) : 1  
381 1 3 3 3 1, 79 (1) : 1  
382 1 3 3 3 2, 80 (1) : 1  
383 1 3 3 3 3, 81 (1) : 1  
384 2 1 1 1 1, 82 (1) : 1  
385 2 1 1 1 2, 83 (1) : 1  
386 2 1 1 1 3, 84 (1) : 1  
387 2 1 1 2 1, 85 (1) : 1  
388 2 1 1 2 2, 86 (1) : 1  
389 2 1 1 2 3, 87 (1) : 1  
390 2 1 1 3 1, 88 (1) : 1  
391 2 1 1 3 2, 89 (1) : 1  
392 2 1 1 3 3, 90 (1) : 1  
393 2 1 2 1 1, 91 (1) : 1  
394 2 1 2 1 2, 92 (1) : 1  
395 2 1 2 1 3, 93 (1) : 1  
396 2 1 2 2 1, 94 (1) : 1  
397 2 1 2 2 2, 95 (1) : 1  
398 2 1 2 2 3, 96 (1) : 1  
399 2 1 2 3 1, 97 (1) : 1  
400 2 1 2 3 2, 98 (1) : 1  
401 2 1 2 3 3, 99 (1) : 1  
402 2 1 3 1 1, 100 (1) : 1  
403 2 1 3 1 2, 101 (1) : 1

404 2 1 3 1 3, 102 (1) : 1  
405 2 1 3 2 1, 103 (1) : 1  
406 2 1 3 2 2, 104 (1) : 1  
407 2 1 3 2 3, 105 (1) : 1  
408 2 1 3 3 1, 106 (1) : 1  
409 2 1 3 3 2, 107 (1) : 1  
410 2 1 3 3 3, 108 (1) : 1  
411 2 2 1 1 1, 109 (1) : 1  
412 2 2 1 1 2, 110 (1) : 1  
413 2 2 1 1 3, 111 (1) : 1  
414 2 2 1 2 1, 112 (1) : 1  
415 2 2 1 2 2, 113 (1) : 1  
416 2 2 1 2 3, 114 (1) : 1  
417 2 2 1 3 1, 115 (1) : 1  
418 2 2 1 3 2, 116 (1) : 1  
419 2 2 1 3 3, 117 (1) : 1  
420 2 2 2 1 1, 118 (1) : 1  
421 2 2 2 1 2, 119 (1) : 1  
422 2 2 2 1 3, 120 (1) : 1  
423 2 2 2 2 1, 121 (1) : 1  
424 2 2 2 2 2, 122 (1) : 1  
425 2 2 2 2 3, 123 (1) : 1  
426 2 2 2 3 1, 124 (1) : 1  
427 2 2 2 3 2, 125 (1) : 1  
428 2 2 2 3 3, 126 (1) : 1  
429 2 2 3 1 1, 127 (1) : 1  
430 2 2 3 1 2, 128 (1) : 1

431 2 2 3 1 3, 129 (1) : 1  
432 2 2 3 2 1, 130 (1) : 1  
433 2 2 3 2 2, 131 (1) : 1  
434 2 2 3 2 3, 132 (1) : 1  
435 2 2 3 3 1, 133 (1) : 1  
436 2 2 3 3 2, 134 (1) : 1  
437 2 2 3 3 3, 135 (1) : 1  
438 2 3 1 1 1, 136 (1) : 1  
439 2 3 1 1 2, 137 (1) : 1  
440 2 3 1 1 3, 138 (1) : 1  
441 2 3 1 2 1, 139 (1) : 1  
442 2 3 1 2 2, 140 (1) : 1  
443 2 3 1 2 3, 141 (1) : 1  
444 2 3 1 3 1, 142 (1) : 1  
445 2 3 1 3 2, 143 (1) : 1  
446 2 3 1 3 3, 144 (1) : 1  
447 2 3 2 1 1, 145 (1) : 1  
448 2 3 2 1 2, 146 (1) : 1  
449 2 3 2 1 3, 147 (1) : 1  
450 2 3 2 2 1, 148 (1) : 1  
451 2 3 2 2 2, 149 (1) : 1  
452 2 3 2 2 3, 150 (1) : 1  
453 2 3 2 3 1, 151 (1) : 1  
454 2 3 2 3 2, 152 (1) : 1  
455 2 3 2 3 3, 153 (1) : 1  
456 2 3 3 1 1, 154 (1) : 1  
457 2 3 3 1 2, 155 (1) : 1

458 2 3 3 1 3, 156 (1) : 1  
459 2 3 3 2 1, 157 (1) : 1  
460 2 3 3 2 2, 158 (1) : 1  
461 2 3 3 2 3, 159 (1) : 1  
462 2 3 3 3 1, 160 (1) : 1  
463 2 3 3 3 2, 161 (1) : 1  
464 2 3 3 3 3, 162 (1) : 1  
465 3 1 1 1 1, 163 (1) : 1  
466 3 1 1 1 2, 164 (1) : 1  
467 3 1 1 1 3, 165 (1) : 1  
468 3 1 1 2 1, 166 (1) : 1  
469 3 1 1 2 2, 167 (1) : 1  
470 3 1 1 2 3, 168 (1) : 1  
471 3 1 1 3 1, 169 (1) : 1  
472 3 1 1 3 2, 170 (1) : 1  
473 3 1 1 3 3, 171 (1) : 1  
474 3 1 2 1 1, 172 (1) : 1  
475 3 1 2 1 2, 173 (1) : 1  
476 3 1 2 1 3, 174 (1) : 1  
477 3 1 2 2 1, 175 (1) : 1  
478 3 1 2 2 2, 176 (1) : 1  
479 3 1 2 2 3, 177 (1) : 1  
480 3 1 2 3 1, 178 (1) : 1  
481 3 1 2 3 2, 179 (1) : 1  
482 3 1 2 3 3, 180 (1) : 1  
483 3 1 3 1 1, 181 (1) : 1  
484 3 1 3 1 2, 182 (1) : 1

485 3 1 3 1 3, 183 (1) : 1  
486 3 1 3 2 1, 184 (1) : 1  
487 3 1 3 2 2, 185 (1) : 1  
488 3 1 3 2 3, 186 (1) : 1  
489 3 1 3 3 1, 187 (1) : 1  
490 3 1 3 3 2, 188 (1) : 1  
491 3 1 3 3 3, 189 (1) : 1  
492 3 2 1 1 1, 190 (1) : 1  
493 3 2 1 1 2, 191 (1) : 1  
494 3 2 1 1 3, 192 (1) : 1  
495 3 2 1 2 1, 193 (1) : 1  
496 3 2 1 2 2, 194 (1) : 1  
497 3 2 1 2 3, 195 (1) : 1  
498 3 2 1 3 1, 196 (1) : 1  
499 3 2 1 3 2, 197 (1) : 1  
500 3 2 1 3 3, 198 (1) : 1  
501 3 2 2 1 1, 199 (1) : 1  
502 3 2 2 1 2, 200 (1) : 1  
503 3 2 2 1 3, 201 (1) : 1  
504 3 2 2 2 1, 202 (1) : 1  
505 3 2 2 2 2, 203 (1) : 1  
506 3 2 2 2 3, 204 (1) : 1  
507 3 2 2 3 1, 205 (1) : 1  
508 3 2 2 3 2, 206 (1) : 1  
509 3 2 2 3 3, 207 (1) : 1  
510 3 2 3 1 1, 208 (1) : 1  
511 3 2 3 1 2, 209 (1) : 1

512 3 2 3 1 3, 210 (1) : 1  
513 3 2 3 2 1, 211 (1) : 1  
514 3 2 3 2 2, 212 (1) : 1  
515 3 2 3 2 3, 213 (1) : 1  
516 3 2 3 3 1, 214 (1) : 1  
517 3 2 3 3 2, 215 (1) : 1  
518 3 2 3 3 3, 216 (1) : 1  
519 3 3 1 1 1, 217 (1) : 1  
520 3 3 1 1 2, 218 (1) : 1  
521 3 3 1 1 3, 219 (1) : 1  
522 3 3 1 2 1, 220 (1) : 1  
523 3 3 1 2 2, 221 (1) : 1  
524 3 3 1 2 3, 222 (1) : 1  
525 3 3 1 3 1, 223 (1) : 1  
526 3 3 1 3 2, 224 (1) : 1  
527 3 3 1 3 3, 225 (1) : 1  
528 3 3 2 1 1, 226 (1) : 1  
529 3 3 2 1 2, 227 (1) : 1  
530 3 3 2 1 3, 228 (1) : 1  
531 3 3 2 2 1, 229 (1) : 1  
532 3 3 2 2 2, 230 (1) : 1  
533 3 3 2 2 3, 231 (1) : 1  
534 3 3 2 3 1, 232 (1) : 1  
535 3 3 2 3 2, 233 (1) : 1  
536 3 3 2 3 3, 234 (1) : 1  
537 3 3 3 1 1, 235 (1) : 1  
538 3 3 3 1 2, 236 (1) : 1

539 3 3 3 1 3, 237 (1) : 1

540 3 3 3 2 1, 238 (1) : 1

541 3 3 3 2 2, 239 (1) : 1

542 3 3 3 2 3, 240 (1) : 1

543 3 3 3 3 1, 241 (1) : 1

544 3 3 3 3 2, 242 (1) : 1

545 3 3 3 3 3, 243 (1) : 1